ASSESSMENT OF PLASTIC ZONE THICKNESS AND CONVERGENCES FOR TUNNELS EXCAVATED IN WEAK TO FAIR QUALITY ROCKS IN TURKEY

A THESIS SUBMITTED TO
THE GRADUATE SCHOOL OF NATURAL AND APPLIED SCIENCES
OF
MIDDLE EAST TECHNICAL UNIVERSITY

BY

ÖZGÜR SATICI

IN PARTIAL FULFILLMENT OF THE REQUIREMENTS
FOR
THE DEGREE OF DOCTOR OF PHILOSOPHY
IN
GEOLOGICAL ENGINEERING

MAY 2018

Approval of the thesis:

ASSESSMENT OF PLASTIC ZONE THICKNESS AND CONVERGENCES FOR TUNNELS EXCAVATED IN WEAK TO FAIR QUALITY ROCKS IN TURKEY

submitted by **ÖZGÜR SATICI** in partial fulfillment of the requirements for the degree of **Doctor of Philosophy in Geological Engineering Department, Middle East Technical University** by,

Prof. Dr. Halil KALIPÇILAR
Dean, Graduate School of **Natural and Applied Sciences** _____

Prof. Dr. Erdin BOZKURT
Head of Department, **Geological Engineering** _____

Prof. Dr. Tamer TOPAL
Supervisor, **Geological Engineering Dept., METU** _____

Examining Committee Members:

Prof. Dr. Nurkan KARAHANOĞLU
Geological Engineering Dept., METU _____

Prof. Dr. Tamer TOPAL
Geological Engineering Dept., METU _____

Prof. Dr. Bahtiyar ÜNVER
Mining Engineering Dept., Hacettepe University _____

Prof. Dr. Erdal ÇOKÇA
Civil Engineering Dept., METU _____

Assoc. Prof. Dr. Mutluhan AKIN
Geological Eng. Dept., Nevşehir Hacı Bektaş Veli University _____

Date: 21.05.2018

I hereby declare that all information in this document has been obtained and presented in accordance with academic rules and ethical conduct. I also declare that, as required by these rules and conduct, I have fully cited and referenced all material and results that are not original to this work.

Name, Last Name: Özgür SATICI

Signature :

ABSTRACT

ASSESSMENT OF PLASTIC ZONE THICKNESS AND CONVERGENCES FOR TUNNELS EXCAVATED IN WEAK TO FAIR QUALITY ROCKS IN TURKEY

Satıcı, Özgür
Ph.D., Department of Geological Engineering
Supervisor: Prof. Dr. Tamer Topal

June 2018, 238 pages

Most of the ancient civilization structures were constructed under the ground, such as underground dwellings, transportation systems or storage facilities. In our modern era, underground constructions are still keeping their importance. Yet, every underground excavation requires prediction of rock mass behavior prior to excavation. Besides, this also means the prediction of convergences and plastic zone thicknesses after an excavation. In this thesis, development of convergences and plastic zone thickness during tunnel excavations were evaluated especially for weak to fair quality rock masses using actual field measurements, statistical and numerical analyses. Plastic zone thicknesses in relation with tunnel convergences were also identified. Decision tree method was selected as the best convergence estimation method, which is first in this kind and convenient for the determination of the relation between one dependent variable and multiple independent variables where there is not any linear relation within. As a result, a useful and user friendly convergence estimation model was generated. Moreover, the relation of convergences with plastic zone thickness was also revealed by the help of empirical equations, by using finite element analysis. Moreover, a new empirical equation was also identified for the prediction of tunnel wall closures. This equation is proved to be working well in the specified similar tunnel sections especially if three or more tunnel wall convergences are known and can be used for the estimation of unmeasured convergences for that section.

Keywords: Convergence, Decision Tree Analysis, Finite Element Method, Plastic Zone, Tunnel Excavation

ÖZ

TÜRKİYE'DE ZAYIF VE ORTA KALİTE KAYALARDAKİ TÜNELLERİN KAZILARI İÇİN PLASTİK ZON VE DEFORMASYONLARIN TAHMİNİNE İLİŞKİN DEĞERLENDİRME

Satıcı, Özgür
Doktora, Jeoloji Mühendisliği Bölümü
Danışman: Prof. Dr. Tamer Topal

Haziran 2018, 238 sayfa

Eski medeniyetlere ait bir çok yapı yeraltında inşaa edilmiştir. Bunlardan bazıları yeraltı şehirleri, ulaştırma sistemleri veya depolama alanlarıdır. Modern çağda ise yeraltı yapıları halen önemini korumaktadır. Ancak her yeraltı yapısı, kaya kütle davranışlarının kazı öncesi, tünel yakınsamalarının ve plastik bölge kalınlıklarının ise kazı sonrası tahmin edilmesini gerektirir. Bu tez çalışmasında herhangi bir tünel kazı aynasının kazı öncesi deformasyonlarının ve plastik zon kalınlığının tahminine ilişkin bir yöntemin; gerçek saha verileri, istatistiksel ve nümerik metotlarla ortaya konulması hedeflenmiştir. Bu amaçla karayolu tünel kazılarında deformasyonların ve plastik zon kalınlıklarının gelişimi, özellikle zayıf ve orta kalite kaya kütlelerinde değerlendirilerek plastik zon kalınlıkları ile tünel yakınsaklıkları arasındaki ilişki ortaya konulmuştur. İstatistiksel ve sayısal yöntemler kullanılarak çeşitli tünel kazılarına ait deformasyon ve kaya kütlesi jeoteknik verileri toplanmış ve istatistiksel olarak modellenmiştir. Tüm bu değerlendirmeler için bu alanda ilk kez kullanılan ve özellikle aralarında doğrusal bir ilişki bulunmayan bir bağımlı değişkenin birden fazla bağımsız değişkenle olan ilişkisini açıklamakta faydalı olan karar ağacı yöntemi en uygun yöntem olarak seçilerek kullanılmıştır. Sonuç olarak, kullanışlı ve kullanıcı dostu bir deformasyon tahmin modeli oluşturulmuş ve ayrıca, elde edilen ampirik denklemlerle deformasyonların plastik zon kalınlığı ile olan ilişkisi sonlu elemanlar analizi ile ortaya konulmuştur. Ayrıca, ilgili tünel enkesitinin birbirine benzer olduğu tünel kesimlerinde, kapanmaların öngörülmesi için yeni bir ampirik denklem de tanımlanmıştır. Bu denklem, özellikle üç veya daha fazla noktada tünel duvarı deformasyon miktarı bilindiğinde, deformasyon miktarları araştırılan tünel bölümü için ölçülmemiş deformasyonların tahminine yönelik bir yöntem olarak kullanılabilir.

Anahtar Kelimeler: Deformasyon, Karar Ağacı Analizi, Sonlu Elemanlar Yöntemi, Plastik Zon, Tünel Kazısı

… to my mom who devotes her life to me,

… to my father who I suffer the lack of him in years

… to my spouse who shares her life with me

… and to my beloved children, who gave me the chance of fatherhood and all of these successes

ACKNOWLEDGMENTS

Firstly, I would like to express my sincere gratitude to my supervisor Prof. Dr. Tamer TOPAL for the continuous support of my Ph.D. study and related research, for his patience, motivation, and immense knowledge. His guidance helped me in all the time of research and writing of this thesis. Besides my supervisor, I would like to thank the rest of my Ph.D. monitoring thesis committee members, namely, Prof. Dr. Bahtiyar UNVER, Prof. Dr. Nurkan KARAHANOGLU for their insightful comments and encouragement, but also for the compelling questions which incented me to widen my research from various perspectives. I would also thank to dear jury members, Prof. Dr. Erdal ÇOKÇA and Doç. Dr. Mutluhan AKIN, for their kind support and attention on reading and evaluating my thesis. My sincere thanks also go to Prof. Dr. Levent TUTLUOGLU for his classes, which broaden my knowledge and force me to do more, during the doctoral study course period.

I would also like to thank to my experienced colleagues dear Ahmet Öztürk and Mehmet Tokgöz who teach me more than a profession but teaching me how to be a better person, in last 20 years. Besides, my special thanks also go to my fellows Canser Demirci, Gökhan Macit, İbrahim Anacali, Osman Altınordu, Serkan Güner, Serkan Yılmaz, Şenda Sarialioglu, Sina Kiziroglu, Tuncay Çelebi, Dr. Tülin Solak, Veysel Yılmaz, and Yavuz Ergintav for their patience and support to me during my studies. This study could not be completed without the technical support of; Ahmet Artunç, Altug Onaran, D. Gaye Oral, Emrullah Kasım, Ercument Karahan, Eyup Sengul, Faruk Turkoz, Feyzullah Ozel, Dr. Özgür Dolgun, Dr. H. Tolga Bilge, Huseyin Maral, M. Kemal Akman, Serhan Ergin, U. Kanat Aydın and Zafer Başesgioğlu.

Last but not the least, I would like to thank to my whole family for supporting me during the thesis study and spiritually my life in general.

TABLE OF CONTENTS

LIST OF TABLES

TABLES

LIST OF FIGURES

FIGURES

LIST OF ABBREVIATIONS

a: Hoek–Brown parameter of the material

ANN: Artificial neural network

ANOVA: Analysis of variance

***B*:** Tunnel width

***BANSJI*:** Back analysis of non-linear strain for jointed rock mass in incremental

***c*:** Cohesion

***CC*:** Cohesive component

***CCM*:** Convergence confinement method

CHAID: Chi-square automatic interaction detection analysis

C&RT: Classification and regression tree analysis

CV: Resultant total convergence value of the excavation wall at point x,y

***δ*:** Radial convergence

***Δ*:** Deformation measured in tunnel or cavern (related to dimension of excavation span)

***D*:** Zone of arching

***D_f*:** Disturbance factor

***DBAP*:** Direct back analysis program

***DBBA*:** Displacement based back-analysis method

***DDA*:** Discontinuous deformation analysis

Def.: Deformation

***DEM*:** Discrete element methods

***Δ_h*:** Horizontal component of deformation

***Δ_v*:** Vertical component of deformation

***EB*:** Elastic Brittle

***EDZ*:** Excavation damaged zone

***EdZ*:** Excavation disturbed zone

***E_i*:** Elasticity modulus of intact rock

E_j**:** Elasticity modulus of jointed rock mass

E_{rm}**:** Elasticity modulus of rock mass or deformation modulus

***EPP*:** Elastic perfectly plastic

ϕ: Internal friction angle of intact rock

ϕ_{rm}**:** Internal friction angle of rock mass

***FC*:** Frictional component

***FEM*:** Finite element method

***FDM*:** Finite difference method

γ: Rock mass density

GCV: Generalized cross-validation

GPa: Gigapascal

GPR: Ground penetrating radar

***GRC*:** Ground reaction curve

***GSI*:** Geological strength index

GSI_r**:** Residual value of geological strength index

***H or h*:** Overburden thickness of a tunnel (from roof to ground surface)

$H_{t\ or}$ ***HEIGHT*:** Vertical dimension or clearance of a tunnel

***I-N-DBAP*:** In homogeneous non-linear direct back analysis program

I_{s50}**:** Point load index for 50 mm size samples

J_a**:** Rating for joint alteration, discontinuity filling (of least favorable set or discontinuity)

J_f**:** Joint factor

J_n**:** Rating for number of joint sets

J_r**:** Rating for joint surface roughness (of least favorable set or discontinuity)

J_w**:** Rating for water softening, inflow and pressure effects

JNCI: Japanese nuclear cycle development institute

C_c**:** Convergence constant

k_0**:** Horizontal to vertical stress ratio

K_p**:** Passive earth pressure of the material

***LDP*:** Longitudinal deformation profile

m_b**:** Hoek–Brown parameter of the rock material

MAE: Mean absolute error

MARS: Multivariate adaptive regression spinal

Max: Maximum

MCC: Mean convergence coefficient

***Min*:** Minimum

***MLP*:** Multi-layer perceptron analysis

mm: Millimeters

MPa: Megapascal

MSE: Mean squared error

***MVR*:** Multi variable regression

***NATM*:** New Austrian Tunneling Method

v**:** Poisson's ratio

P_0**:** Initial stress

P_i**:** Internal pressure or support pressure

P^{cr}_i**:** Critical internal pressure

p_s**:** Increasing support pressure

Q**:** Rock mass quality index

Q_c**:** Rock mass quality rating (normalized by $\sigma_c/100$)

Q_t**:** Rock mass quality rating (Q or Q_0, normalized by $I_{50}/4$, for strongly anisotropic rock types)

q_u**:** Unconfined compressive strength

R^2**:** Coefficient of determination

***RBF*:** Radial basis function

R^*_{EPP}**:** Plastic radius of the corresponding EPP rock mass

***RMR*:** Rock mass rating index

RMSE: Root mean square error

R_{pl}**:** Extent of the plastic region

R^*_{SS}**:** Plastic radius of the SS rock mass

***RQD*:** Rock quality designation index

RQD_0**:** RQD oriented in the loading or measurement direction

R_t**:** Tunnel radius

***s*:** Hoek–Brown parameter of the rock material

***SCR*:** Solid core recovery

***Sigma$_{cm}$*:** Rock mass compression strength based on compression failure of the intact portions

***Sigma$_{tm}$*:** Rock mass compression strength based on tensile failure of the intact portions

***SPAN*:** Horizontal dimension of a tunnel

***SRF*:** Rating for faulting, strength/stress ratios, squeezing, swelling

SRM: Rock class rating index of the surrounding rock mass

***SS*:** Strain softening

SSE: Sum of the squared errors

SVM: Support vector machine

SVR: Support vector regression

Stand. Dev.: Standard deviation

σ_0: Field stress

σ_c: Unconfined or uniaxial compression strength of rock mass (sometimes used for intact rock)

σ_{ci}: Uniaxial or unconfined compressive strength of intact rock

σ_{cj}: Uniaxial compressive strength of jointed rock mass

σ_h: Horizontal component of stress (relevant to problem considered)

σ_t: Uniaxial tensile strength of rock mass

σ_v: Vertical principal stress

τ : Shear resistance

TBM: Tunnel boring machine

***TCR*:** Total core recovery

***UCS*:** Uniaxial compressive strength

***U_r, u_r*:** Radial displacement

Y: Mean convergence or deformation of tunnel wall

Y': Normalized mean deformation

CHAPTER 1

INTRODUCTION

Developing and upgrading existing transportation infrastructures, such as high-speed railways, highways and urban transit lines require construction of long, large-diameter tunnels. The well-known typical example of this kind is the high-speed railway Alpine Base Tunnel in Switzerland; the 57-km long Gotthard and 42-km long Lotschberg tunnels. Besides, several large metro tunneling projects have been completed in Europe recently (Kavvadas 2005). Turkey, which is an important crossing point for Europe and Asia, is another tunnel construction country, because of its geographical location. According to current data, total length of tunnels which have excavated and under construction in Turkey is almost 1000 km[1] and increasing up day by day. This length consists of mainly dam site and highway tunnels. Most of them were constructed in the last 30 years. That means tunneling will be a growing area in Turkish construction industry. Other ongoing underground excavation works which are not reckoned in this study will also increase the total length of the tunnels.

However, owing to the nature of the geology, all underground excavations are challenging operations. Geology of earth is chaotic. Nobody can exactly determine what will happen in next 10 meters ahead of the tunnel excavation face and vicinity of the excavation area. There will always be damaged-zone (plastic zone, disturbance zone) that occurs around an excavation area with advance of the tunnel face. These disturbances may stem from various reasons such as; selected excavation technique (Sato et al. 2000, Martino and Chandler 2004), contractor's and construction crew's expertise degree, geological and geotechnical conditions of the media (Martino and

[1] According to General Directorate of Turkish Highways and General Directorate of Turkish State Hydraulic Works data

Chandler 2004, Kwon et al. 2009, Kim et al. 2012) and selected tunnel design methodology. Therefore, plastic zone and its effects around an excavation have been studied by many researchers previously (Lunardi 2000, Sato et al. 2000, Bizjak and Petkovsek 2004, Martino and Chandler 2004, Hao and Azzam 2005, Palmstrom and Einar 2006, Blumling et al. 2007, Cai et al. 2007, Lia et al. 2008, Kwon et al. 2009, Pellet et al. 2009, Ramulu et al. 2009, Wu et al. 2009, Basarir et al. 2010, Alejano et al. 2012, Kim et al. 2012, Leia et al. 2017, Yi et al. 2017).

After an advance of the tunnel face, convergence develops naturally through an excavation space. This behavior of the ground is regarded as a reaction to stress changes or to new stress conditions in the media. Convergence movements start ahead of the face excavation. It is accepted that these convergences start nearly up to 2 times tunnel diameters ahead of the face. Then, it propagates through the periphery of an excavation and induces by the application of supporting. This zone is named as a plastic zone or excavation damaged zone (Kontogianni et al. 2006). Owing to the plastic zone around an excavated area, tunnel perimeter converges through the excavated space. These convergence movements through the excavated space named as deformation or displacement in underground excavation works. The prediction of displacements prior to advance of the tunnel face is an important issue in underground excavation works.

Determining plastic zone thickness and convergences are both safety end economical issues in underground excavations. Misestimation of these two issues will not only threat the workers' safety but also consume time and money. Hence, several researches have tried to predict tunnel convergences before excavation of the face by different manners (Lunardi 2000, Hoek 2001, Barton 2002, Kim and Chung 2002, Kontogianni and Stiros 2002, Kontogianni and Stathis 2003, Bizjak and Petkovsek 2004, Martino and Chandler 2004, Kontogianni and Stiros 2005, Kontogianni et al. 2006, Zhang et al. 2006, Hammah et al. 2008, Mahdevari and Torabi 2012, Sharifzadeh et al. 2012, Fattahi et al. 2014, Perras and Diederichs 2015).

Tunnel convergence, its eventual consequences and general tunnel excavation methodology is given below and shown in Figure 1.1. There are three types of excavation lines in highway tunnel constructions:

- The first one is the “construction line” which is formed naturally after an excavation. If this line is anticipated accurately there will be no problem occurred during the construction. This irregular line is also the point where the immediate deformations occur within the tunnel and cannot be measured by conventional monitoring methods. This thickness is expected to be converging through to the “supported section line” at amount of “*c*”.

- The second is the “supported section line”. This imaginary line is the starting location of the support-system. At this point generally “welded wire mesh” which is the primary supporting element, is installed. After that, other supporting elements are applied if necessary. In practice, there is no monitoring equipment established till the installation of last supporting element and after a while. In a well-designed tunnel, this section is allowed and expected to be converged through the point of "final lining section" at amount of "a".

- Thickness of “c” and “a” depends on the rock mass conditions.

- The last is the starting location of “final lining”. When the final lining is completed it is expected to furnish that ultimate tunnel clearance and occurrence of any more deformations are not expected beyond this point.

Therefore, any miscalculation about these imaginary lines causes construction and cost problems. For these reasons, accurate prediction of displacements and conditions ahead of the excavation face are essential issues for safe, fast and economical tunnel construction. Moreover, displacements directly affect the excavation method and support design. Misjudgment of tunnel displacements may create serious consequences and may end up with the collapse of the excavated area.

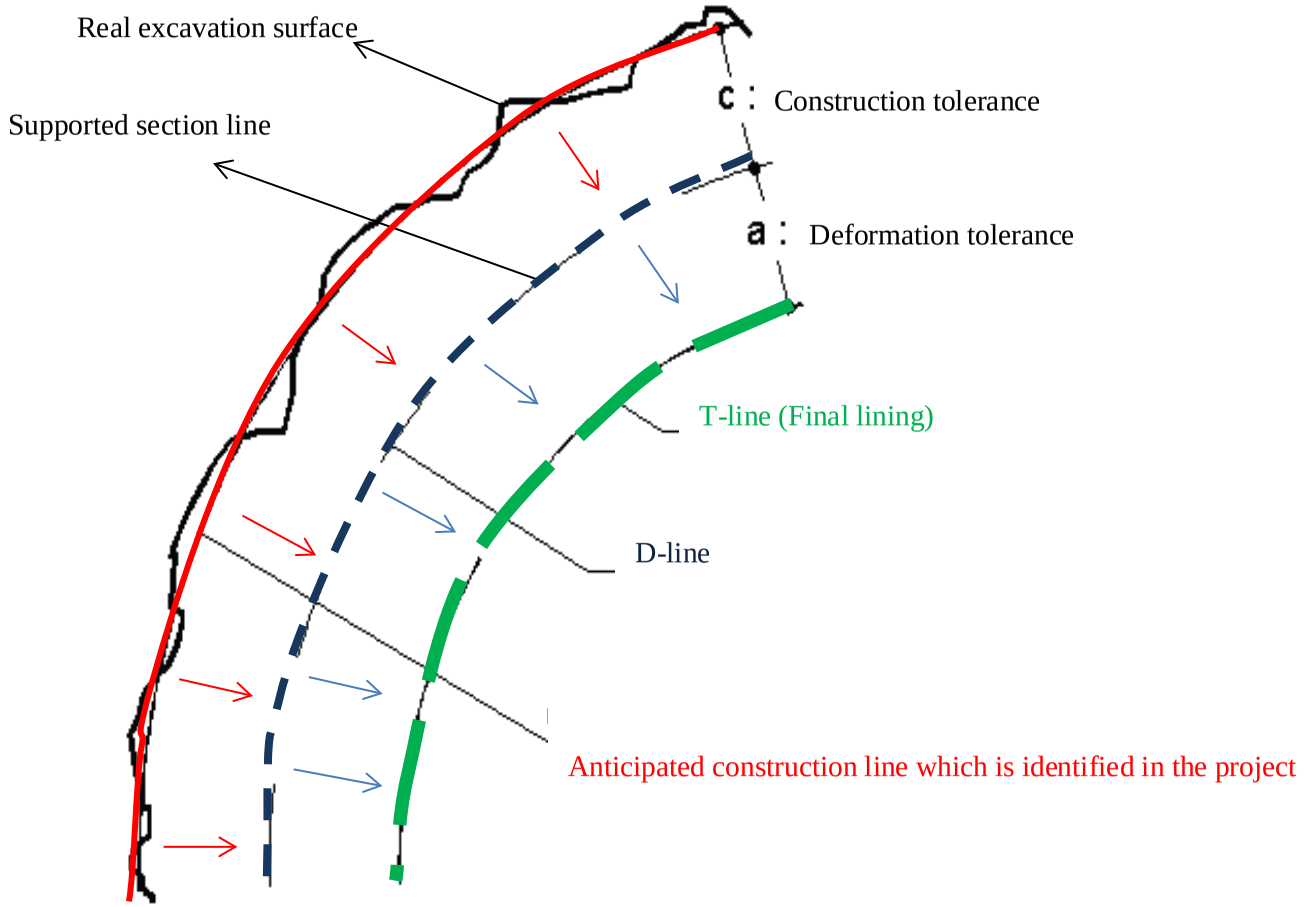

Figure 1.1. Schematic diagram of tunnel convergence, its eventual consequences and general tunnel excavation methodology in practice.

In practice, misjudgements come out in two forms to the engineers:

- If the displacements are underestimated, the amount of convergences ($c + a$) will be more than anticipated and final lining may face with danger of destruction owing to exceeding convergences, because underestimated convergences will not finalize at the “final lining section” and will breach the required tunnel clearance. Moreover, reshaping of excavation may be necessary due to the excessive forces, which directly affect the excavation surface and cost. This situation demands an additional supporting and re-excavation of the converged section of the tunnel that has same meaning with time and money.

- On the contrary, in case of overestimation of displacements more than the real situation, tunnel section will be excavated larger than required to allow the deformations come through to excavated space to furnish required clearance when it is finalized. However, owing to the better rock mass properties, which are not identified properly, expected convergences will not be formed. Therefore larger tunnel cross section will be obtained and final clearance will be higher than the required. So, excessive excavation space needs to be refilled with concrete fillings to furnish required tunnel clearance after the final lining. It is clear that this means additional cost.

Misjudgment of the deformations and damaged zone can be explained clearly with an imaginary scenario. In the first case let us assume that plastic zone thickness and amount of convergences are predicted more than what it has to be. In this case ground arch effect is created around the tunnel perimeter and excavation stability is established. Yet, applied rock bolt length is more than required. That means “overdesign” of the tunnel. In the second case; damaged zone thickness and amount of convergences have been predicted less than what it has to be. That means applied bolt length is less than required. In this case; underestimation of the damaged zone thickness and convergences in the tunnel cause unstable ground conditions and undesirable consequences.

The first scenario only affects the excavation economy. However, in the second scenario; owing to the misestimation of convergences and damaged zone thickness, applied rock bolts will be shorter than required. As a result, ground arch condition will not be established around the excavation and excessive convergences on the walls will deform the excavation geometry and results in yielding of supporting elements. In this case, progressive failure of the surrounding rock mass in the tunnel may not be realized rapidly by the contractor.

In most of the cases, contractor may think some part of tunnel is stabilized, but after a certain period of time “from a few days up to a few months”, convergences may be in large scales (Kontogianni and Stathis, 2003). Once it has noticed, it will be too late to remediate. At this time, yielded supporting elements must be disassembled, excavated area must be re-excavated to obtain required clearance and geometry and stronger support system must be installed. The cost of remediation cannot be predicted. This situation does not mean only wasting of sources, but also time, and it will risk machinery and the workers’ safety, too.

As it can be clearly seen from brief explanations above; proper prediction of deformations and damaged zone thicknesses is of vital importance for all underground excavations.

1.1. Description of the Problem

Rock masses are under significant stresses owing to their own weights and previous tectonic activities, yet these stresses are in the equilibrium state in nature. These equilibrium states of the rock masses are deteriorated by underground excavations and rock masses seek to form a new equilibrium. Thus, excavation wall converges through the excavation cavity and as a result excavated area become narrower. This shrinking continues up to a specific zone behind the excavation wall. In literature, this zone is named as plastic zone, damaged zone or yield zone (Sato et al. 2000, Bizjak and Petkovsek 2004, Martino and Chandler 2004, Hao and Azzam 2005, Kontogianni et al. 2006, Blumling et al. 2007, Lia et al. 2008, Pellet et al. 2009, Ramulu et al. 2009, Wu et al. 2009, Basarir et al. 2010, Adoko et al. 2013, Fattahi et al. 2014, Perras and Diederichs 2015, Siren et al. 2015, Leia et al. 2017, Yi et al. 2017), where the rock mass geomechanical properties and stress conditions change.

Commonly, excavations are done by three main methods; mechanical excavations, drill & blast and tunnel boring machines. Estimation of yield zone when TBM method is used will be out of the scope of this study. Depending on the rock type, yield zone or plastic zone occur in mechanical or drill & blast type excavations, especially in weak and fair rock conditions. Magnitude of convergences and rock mass properties have direct effect on the plastic zone thickness, support type and pattern. Correct estimation of the plastic zone thickness and the amount of convergences in underground excavations are required to prevent work accidents and excessive project costs before they occurred. Misestimation of convergences is not only a threat for safety but also the reason of consuming sources unnecessarily.

If that is so, the question is; “How the actual convergence value and plastic zone thickness around the tunnel section could be determined accurately?” The maximum convergence value can be obtained from about one and a half tunnel diameter behind the face, yet this is a rather prior assumption that at the face position, about 20-30% of total convergences have already occurred (Kim and Chung 2002, Kontogianni and Stiros 2002, Bizjak and Petkovsek 2004,).

For example, Kim and Chung (2002) have been stated the existence of unmeasurable convergences because of the delay of monitoring instrumentation installation and it was obtained as more than 28% prior to first monitoring activity. As the initial convergences have developed immediately before the next excavation section, 30% of total convergences cannot be measured by using geodetic or other monitoring techniques. Some researchers claim that this amount reaches up to a level of 60-80% (Kavvadas 2005). Then, another question comes out; "Which of the geodetic measurements represent the actual deformation degree for the ground?"

Besides, there is a measurement deficit between excavation period and the first geodetic monitoring reading that can be defined as a time gap for blasting of rocks or mechanical excavation with the installation of first geodetic survey points and its reading. Deformations occurred in this time gap cannot be measured by conventional monitoring methods. Buried monitoring devices like rod extensometers should be used for measuring the deformations in this time gap. Using extensometers ahead of the excavation face may be easy and undoubted way to learn plastic zone thickness. On the other hand, this also means spending time and money. There are some rare examples about using extensometers in underground excavations but these are mostly used in nuclear repository sites, and by its very nature of the repository sites host rocks are massive, and do not contain any discontinuities. As these monitoring techniques are not commonly used in underground excavations, deformations cannot be measured until the installation of monitoring stations on the walls, and this usually takes a few hours to a few days (Kontogianni and Stiros 2002).

There are some studies in highway tunnels about determination of plastic zone thickness and estimation of convergences. Yet, these studies were done for only unstable zones or for just in only one tunnel (Dalgic 2002, Kim and Chung 2002, Kontoginni and Stiros 2002, Kontogianni and Stathis 2003, Bizjak and Petkovsek 2004, Fakhimi et al. 2004, Kontogianni and Stiros 2005, Kontogianni et al. 2006, Hao and Azzam 2005, Kavvadas 2005, Golshania et al. 2007, Lia et al. 2008, Kwon et al. 2009, Pellet et al. 2009, Mahdevari and Torabi 2012, Mahdevari et al. 2013, Adoko et al. 2013, Fattahi et al. 2014, Rahimi et al. 2014, Lin et al. 2015, Perras and Diederichs 2015, Lei et al. 2017, Verma et al. 2018).

Consequently unless any special instability problems have not occurred, buried convergence monitoring devices, which give the opportunity to read convergences accurately and before the face excavation, do not preferred too much in practice.

1.2. Purpose and Scope

Moving from this point on, it is aimed to create a statistical estimation model for determining convergences for tunnels prior to the face excavation and predicting thickness of the yield zone accurately by using previous tunnel convergence monitoring data, rock mass properties with the help of appropriate statistical modelling and numerical methods. Therefore, putting forth of new approaches for horseshoe-shaped highway tunnels, which are cheap and user friendly about determination of convergences and plastic zone thickness, it will be a very useful tool both for contractors and engineers.

For this to be possible, tunnel convergence measurements data were collected from tunnel excavation sites. Input data was collected from 6 highway tunnels from various regions of Turkey and 5 highway tunnels were selected for validation and the prediction results were compared by. Weak to fair rock masses, which have GSI values between 25 and 65, and showing strain-softening behavior was our main target. To specify related rock mass geotechnical parameters, site investigation data for each tunnel route and their laboratory experiment data were reviewed for statistical and numerical models. After words, geotechnical properties of the rocks were interpreted and used for correct estimation model for the determination of convergences. By using independent parameters (such as; *RMR*, *Q*, *RQD*, σ_c, E_i, E_{rm}, *c*, ϕ, *h* etc.) and dependency degree of actual convergence monitoring data with rock mass properties and by trying various statistical techniques, the most effective statistical model was created.

To understand whether the statistical prediction model is effective or not, it was validated with ongoing tunnel excavation data. After validation, numerical models were generated with new tunnel excavation data for cross-validation.

Then, the convergence measurements data were compared with the results of numerical models in terms of convergences. After getting reasonable results regarding the convergences, plastic zone thicknesses were determined by using convergence measurement and statistical prediction model outcomes.

1.3. Methodology

This study can be divided into three main sections; literature survey and data collection, creation of statistical prediction model, and validation of the findings. At first, previous studies were researched in terms of rock mass strength parameters, convergences and plastic zone thicknesses. Then, essential geological, geotechnical and convergence data for this study were collected from completed tunnel excavation sites. After that, these data were interpreted in terms of their appropriateness. Afterwards, various statistical modelling methods were used to find out the most suitable one and then several statistical models were created to see which has the highest explanation capacity for our case. Amongst all, four most suitable modelling techniques (MVR, ANN, CHAID and C&RT) were selected to use in this study. And then, findings of the statistical modelling were compared with previous studies to understand the suitableness of our result. And then, the most eligible statistical model was selected to use for validation.

After getting coherent results with the previous researchers' findings, selected statistical modelling results were validated with ongoing tunnel excavations. For this aim, new geological, geotechnical and convergence data were obtained from ongoing tunnel excavation sites. These data were interpreted in terms of suitability for this study. After that, site-obtained geological and geotechnical data were put to our proposed statistical estimation model whether to see how the estimated convergences are coherent with the model. Thereafter, statistical model convergence predictions were compared with these new ongoing tunnel excavation convergence values. All of the processes above were repeated till finding the best model with appropriate results for our purpose. So, by doing all these operations the first part of our study, which is creation of statistical modelling for tunnel convergences, had been completed.

Afterwards, numerical models were generated for the prediction of plastic zone thickness. For this aim, tunnel excavation site data which are collected for validation of statistical modelling was used again. For the most critical and representative cross sections, numerical models were created and run. After this, numerically obtained convergence results were compared with real convergence monitoring values. Both of the convergence results (measured and modelled) were verified with each other. This means that the established numerical model is run properly and reliably for measurement of plastic zone thickness. After that, plastic zone thicknesses were measured on the model. A convergence versus plastic zone thickness graph was drawn to understand the existence of any relation with plastic zone thickness and convergences. Then, a new prediction model equation has been created for the plastic zone thickness by this way. The proposed methodology is explained below briefly in Figure 1.2 as a flowchart and detailed version of this flowchart is given in Appendix A in Figure A.1.

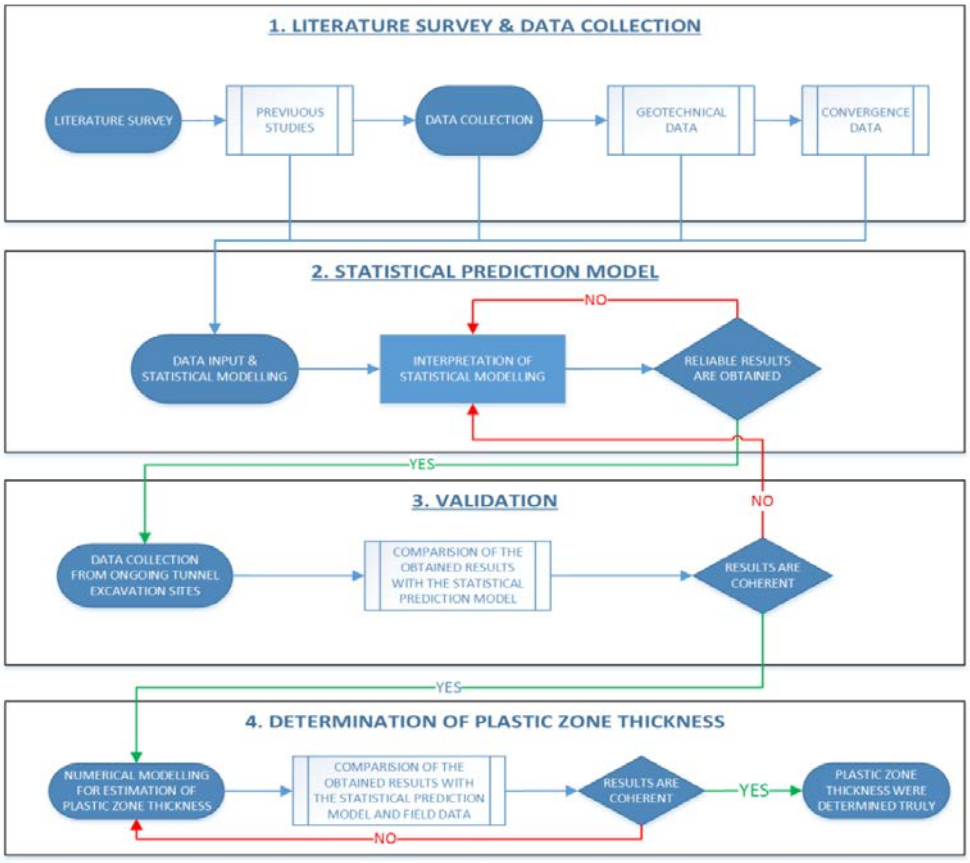

Figure 1.2. Simplified flowchart for the methodology of this study

1.4. Definitions

Many researchers have been investigated the rock mass behavior, plastic zone, creep and some other concepts in underground excavations in different manners and have used different terms to describe the similar phenomena. As an inherent result of this, some differences have been formed in terms of definitions between the researches. Because of this, before passing through to the literature survey section, it is essential to explain some of the main definitions which are used in this study. Therefore, in this section some well-known definitions are given here to furnish a meaning integrity in this study.

Convergence: Convergences, deformation and displacement concepts are used for definition of movement of a certain points through excavation space inside a tunnel wall after an excavation. In other words, convergence in a tunnel can be defined as the amount of closure in tunnel diameter, resulting with redistribution of stresses and new deformations in rock mass. Most of the time, it commences with driving of the face and develops due to loss in stress-strain equilibrium state of any rock mass around the excavation (Adoko et al. 2013). Therefore, convergences occur in underground excavations due to the face advance of the tunnel. This behavior of the excavated ground is regarded as a reaction to stress changes (Kontogianni et al. 2006). In this context, all these terms are used for identification of the same concept, in this study.

Creep: Creep term is very similar to displacement concept and most of the time it is too hard to distinguish them. Namely, in underground excavation process, convergence movements commence ahead of the excavated section. Then, it continues around the periphery of the excavated tunnel and induces by application of ground-support system along a distance up to two or three times of the tunnel diameter. In some special cases, convergences behave like as if it has finished, yet it does not. In these cases, convergences continue slowly and called as “creep" or time dependent effect” of the ground (Kontogianni et al. 2006). In another definitions creep was defined as a viscous behavior of excavated rock mass.

This behavior has another effect on rocks that may lead to excessive time-dependent strain (Kontogianni and Stiros 2005). Similarly, creep is also defined as time-dependent behavior of rock mass material (Mahdevari and Torabi, 2012).

Damaged or Plastic Zone: No matter which excavation technique is used, some parts behind the excavation face and tunnel wall will be affected and the rock mass loose its original structure. There are various reasons which cause development of this zone. These are; excavation method, blasting quality, expertise of the crew, rock mass properties, stress distribution, excavation size and geometry, back-pressure by rock supports and swelling or slaking with groundwater reaction. Therefore, it is clear that a large number of factors can influence the degree of disturbance in the rock mass surrounding an excavation, and that it may never be possible to quantify these factors precisely (Fattahi et al. 2014).

So, as it is natural, the excavation crushed parts will be developed behind the excavation face and tunnel wall. There are various definitions of these terms in the literature. While some of the researchers have used only “plastic zone” term for crushed area behind the excavation wall, the others have divided this zone into several parts, and named differently. Even if the crushed zone surrounding the tunnel excavation wall has been explained by several terms by different researchers, all of them have preferred similar definitions for almost the same sections. Amongst these, definitions which are used in this study are given below briefly;

- Plastic zone or yield zone: This is the most general definition of crushed zone and some of the researchers have preferred “plastic zone” term instead of “damage zone”. Yield zone is divided into several subsections and named this way by several researchers (Martino and Chandler 2004, Blumling et al. 2007, Fattahi et al. 2014, Perras and Diederichs 2015, Siren et al. 2015). These are; construction damage zone, highly damaged zone, excavation damaged zone, excavation disturbed or influenced zone.

- Construction damaged zone (CDZ): This zone is defined as very outer section of tunnel excavation wall and it is directly influenced by the excavation itself (Perras and Diederichs 2015).

- Highly damage zone (HDZ): There is inevitable damage occuring after an excavation and this is purely the result of geometry, structure, and/or induced stress changes (independent of excavation method). Place of this type of damage, which is typically observed as interconnected macro-fractures, is referred to as highly damaged zone (Perras and Diederichs 2015).

- Excavation damaged zone (EDZ): It was defined as a hydro-mechanical and geochemical modification zone, which induces significant changes in flow and transport properties of rock. These changes can include one or more orders of magnitude increase in effective hydraulic conductivity (Blumling et al. 2007). Measurable and permanent changes in mechanical and hydraulic-transport properties of rock that surrounds the excavation is also defined as excavation damaged zone (Martino and Chandler 2004). In another study, it is defined as a rock zone where the rock properties and conditions have been changed due to the processes related to an excavation. This zone affects the behavior of rock mass surrounding the construction, which reduces the stability and safety factor, and increases the probability of failure of the structure (Fattahi et al. 2014).

- Excavation disturbed zone (EdZ): It was defined as a zone of minor changes in hydro-mechanical and geochemical modifications, without major changes in flow and transport properties. Within the EdZ there are no negative effects on the long-term safety (Blumling et al. 2007). Excavation disturbed zone is usually used to distinguish furthest zone around opening where reversible changes caused by stress redistribution have occurred. Boundary of this zone is hard to define as stress redistributions can reach far from the excavation (Siren et al. 2015). EdZ can also be named as outer damage zone or zone of disturbance (stress-disturbed rock zone) where in-situ stresses are affected

from the excavation merely and no certain damages may be measured in this zone. Unless proper support installation is not applied, these zones can easily become an EDZ (Martino and Chandler, 2004). Due to its easily confusable letter structure of EdZ and EDZ, Perras and Diederichs (2015) used term EIZ (excavation influence zone) instead of EdZ. According to their definition; there is a stress and/or strain influence zone which is beyond the excavation damaged zone that involves only elastic change named as "EIZ".

Squeezing rock: If ratio of rock mass strength to in-situ stress is below 0.2, then squeezing rock may occur and it becomes a problem that may cause instability issues both for tunnel and its face (Hoek 2001). According to Barton; if H, depth of an excavation, is more than "$350xQ^{1/3}$" squeezing condition may occur (Barton 2002). In the literature, another definition of squeezing rock is given as reduction in cross-sectional area of an opening owing to the large deformations (Barton 2002, Yassaghi and Salari-Rad 2005).

Related to squeezing and deformation rate, magnitude of convergences in underground excavations depend largely upon geological conditions, in-situ stress relative to rock mass strength, groundwater flow and pore fluid pressure, as well as the rock mass properties. However, tunnel size, excavation method, supporting techniques and their sequences adopted in tunneling can increase the potential of squeezing rock conditions. Delay in support installation will further increase the squeezing conditions of the excavated rock masses (Yassaghi and Salari-Rad 2005). With regard to the squeezing conditions, it is thought that, at some high depths, rock mass is subjected to a great initial stresses and stress redistributions resulting with squeezing conditions. Squeezing rock conditions create irreversible deviatoric creep strains.

Once it has formed, this creep strains rate increases constantly and eventually secondary and tertiary creep stages are developed. These behaviors are usually observed in weak, altered rocks, in deep excavations (Sterpi and Gioda 2009). It should be kept in mind that almost all of the former studies, which concern about

these zones, were done mostly in the nuclear repository sites. Therefore, host rocks in those areas were massive and highly strong.

For this reason, in those areas the determination of that zone was easier. However, in nature transition of these zones is gradational and distinguishing them by in-situ measurements can be difficult especially in weak and fair rock mass conditions (Perras and Diederichs 2015). In this study, we will concern with excavation damage zone and highly damaged zones where the rock mass properties change in plastic manner. The following figures (Figure 1.3, 1.4, 1.5) are given for detailed understanding of the subject. All of them belong to researchers whose studies (Fattahi et al. 2014, Perras and Diederichs 2015, Siren et al. 2015) are used in this thesis and definitions are given above.

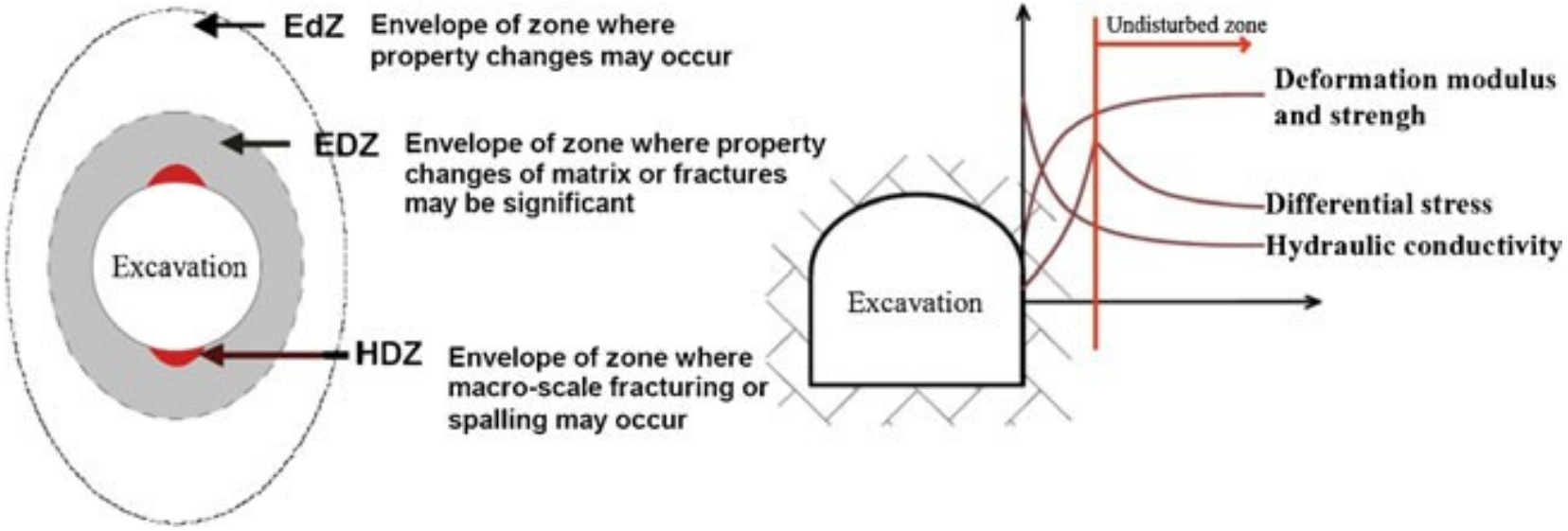

Figure 1.3. The definitions of EdZ, EDZ, HDZ (Fattahi et al. 2014).

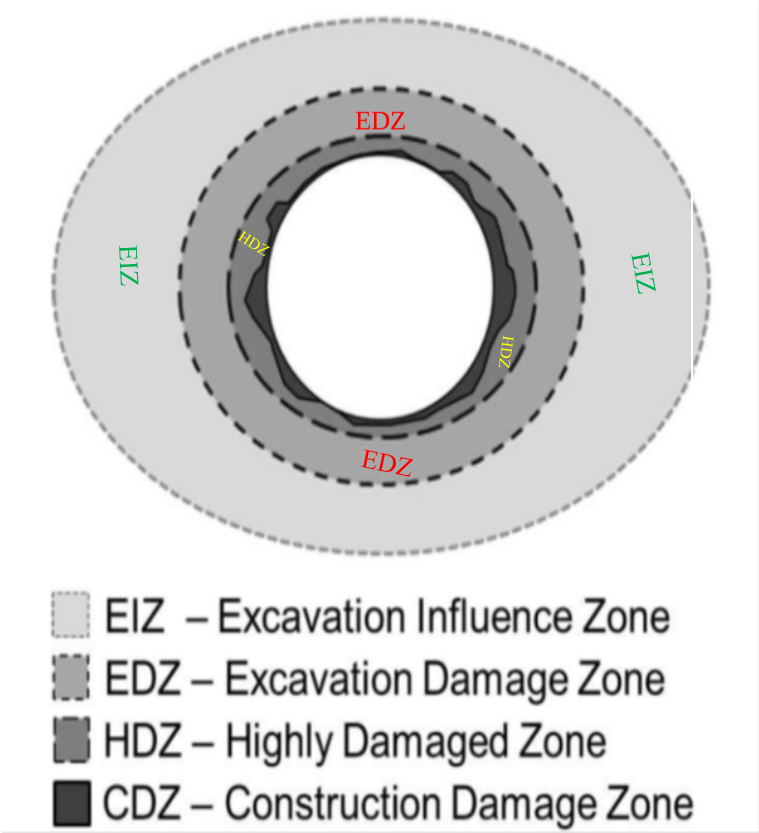

Figure 1.4. The excavation damage zones (HDZ, EDZ, EIZ) and the construction damage zone (CDZ) in tunnel. Note that the EIZ is referred to as the excavation disturbed zone (EdZ) and is renamed due to potential confusion with the lowercase “d” and the uppercase “D” of the EdZ and EDZ, respectively (Perras and Diederichs 2015).

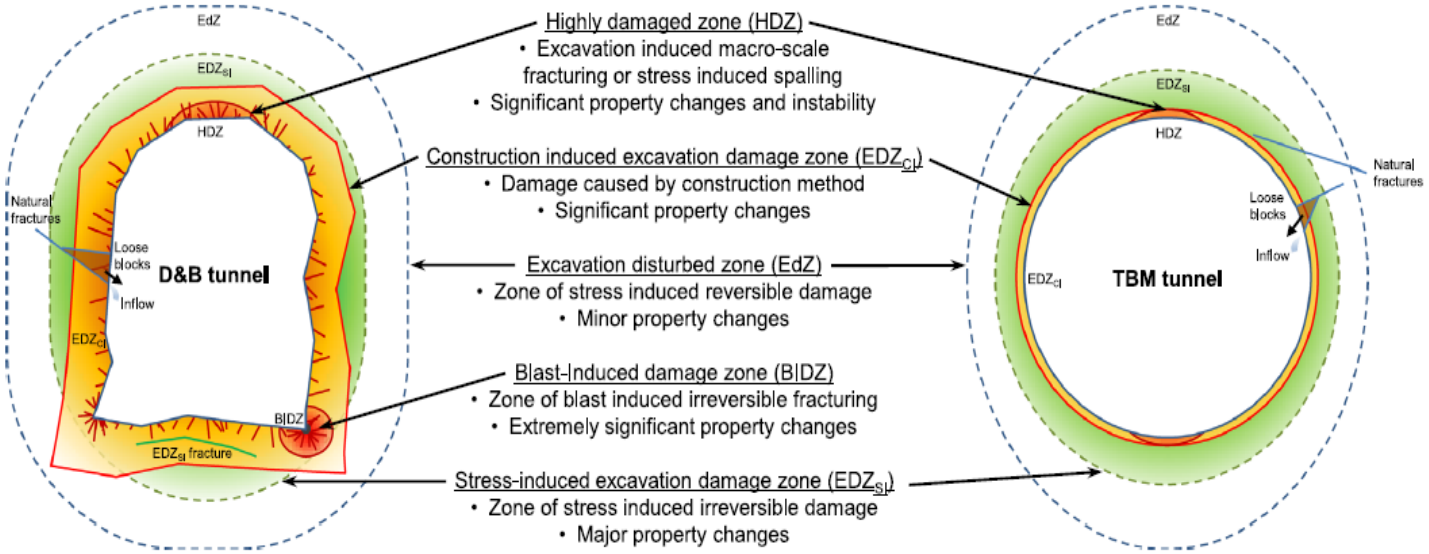

Figure 1.5. Description of damage zones in underground excavations (Siren et al. 2015).

CHAPTER 2

LITERATURE SURVEY

2.1 Literature Survey About Rock Mass Strength Behaviors, Convergences and Plastic Zone Thickness of Tunnels

In this section, all of the previous researchers' studies about rock mass strength behaviors under stresses, prediction of tunnel convergences and determination of plastic zone thickness are given in detail.

2.1.1 Rock mass strength parameters and its post-failure behaviors

Owing to the importance of this subject, plastic zone thickness and convergences on the tunnel excavation wall have been studied by many researchers. For accurate prediction of the convergences and plastic zone thickness, rock mass' post-failure behavior and strength parameters have to be understood clearly. Some of the previous studies about rock mass post-failure behavior and strength parameters are briefly given in this section. Different quality rock masses, which show post-failure behavior, under various stress conditions were explained by Alejano et al. (2009). The authors are in the opinion that, correct failure model selection and prediction of rock masses' post-failure behavior are the key issues in analyzing tunnel stability, especially when using convergence-confinement method and numerical modeling. For this aim; three different quality rock masses were modeled; good, average and poor. By this way, different post-failure behaviors namely "elastic perfectly plastic (EPP), elastic brittle (EB) and strain softening (SS)" were modeled along with the corresponding ground reaction curves, and rock mass parameters were calculated.

They showed that elastic perfectly plastic model is suitable only for poor quality rock masses. In practice, it would theoretically be representative for behavior of the soft rock masses (Alejano et al. 2009).

Elastic brittle plastic (EBP) models include peak and residual strength criteria. They have emphasized superiority of elastic brittle plastic models in representing good quality rock masses. Besides, as there are no significant differences between peak and residual strength values for poor quality rock masses, there should also be no great differences in results for elastic perfectly plastic model and brittle plastic or elastic brittle plastic rock models for poor quality rock masses (Alejano et al. 2009).

Another objective of their study was the identification of actual post failure behavior of a tunnel rock. They proposed that actual post failure behavior of a tunnel rock must, in all cases, lie somewhere in between two extremities represented by the elastic perfectly plastic and elastic brittle models. For this reason, they are on the opinion that strain softening models are the best behavior model for rocks lie between GSI values 40 and 60 (Alejano et al. 2009). They have proposed some new empirical equations for these three approaches. However, at the end of their studies they could not have found any clear equation for their approaches. They have highlighted that variable dilatancy model did not give significantly different results. The authors proposed that calculation of an accurate and precise softening parameter is challenging process, and still very hard to determine the correct one. They have also implied that plastic zone remains constant in all models for each tunnels described. Therefore, the authors explain that variability observed in final displacements could only be due to the post-failure strain behavior of the rock masses.

Deformation modulus and importance of post failure behavior of various types of rock masses were explained with some case studies in Hoek and Brown (1997) study. Post-failure behavior characteristics of the rock mass are required if numerical modelling will be used. According to the authors, progressive failures of rock masses are modeled only by using this approach (Hoek and Brown 1997).

The authors also explained elastic perfectly plastic, strain softening and elastic brittle rock masses behaviors in their study. These examples were chosen from real excavation cases and were explained by showing their design parameters.

In existence of very good quality hard rock masses, the authors believed that these rock masses behave in an elastic brittle manner (GSI > 75). As shown in the Figure 2.1a, a sudden strength drop occurs if the strength of the rock mass is exceeded. GSI value of average quality rock masses is reduced to lower than its in-situ value. This characterizes the broken rock mass for average quality rock masses. The authors claimed that this reduction of the rock mass corresponds to the strain softening behavior as illustrated in Figure 2.1b (25 < GSI < 75). According to this figure they have assumed that post failure deformation occurs at a constant stress level, defined by compressive strength of the broken rock mass. The last behavior type was explained as a progressive failure. This type of failure can be seen in very poor quality rock mass. It is assumed that this type of rocks behave perfectly plastic (GSI < 25). That is to say; after yielded at constant stress level, no more stress change is associated with ongoing failure. Yet, the rock continues to deform. This type of failure is illustrated in Figure 2.1c (Hoek and Brown 1997).

The phenomenon of strain softening was also discussed by Sterpi (1999). Subject of softening was evaluated with two different approaches; structural softening and material softening. Structural softening was defined as; leads to criterion for detecting the onset localization, which depends on current values of stress components. An analytical example was discussed and solved to explain this situation. In this example, strain-softening behavior of the rock mass was shown for elastic perfectly plastic material in presence of a non-associated flow rule. The second approach is material softening. In this approach, it is assumed that initiation of softening depends on accumulated plastic strains. Some applications of this approach were also discussed in this study.

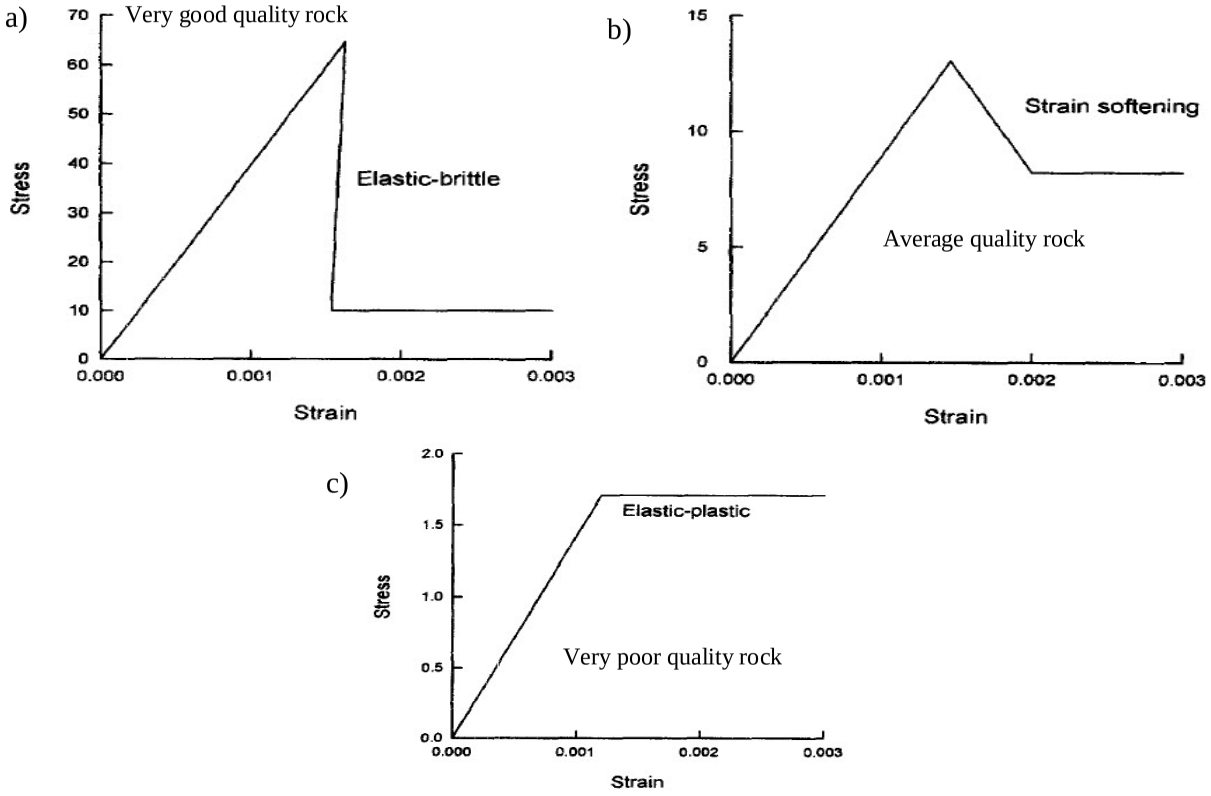

Figure 2.1. Suggested post-failure characteristics for different quality rock masses (Hoek and Brown 1997).

To explain and evaluate these approaches, macro scale models were prepared and tested. Besides, analytical calculations were done, two and three-dimensional numerical models were done. In these numerical models, frictional and cohesive shear strength parameters were gradually reduced in the softening zone. This softening procedure was continued until reaching their residual values that characterize the so-called “fully softened” or “ultimate state”. During this process, local elastic modulus of the material was reduced as well. At the end of the study, the author compared the experimental, analytical and numerical results to evaluate the effectiveness of the approach (Sterpi 1999).

Significant influence of post-peak behavior of rock masses on design stage of underground excavation, and upon the excavation stability is explained by Cai et al. (2007). The authors’ main point is; current GSI system is for the estimation of peak strength parameters of jointed rock masses. However, it is claimed that there are no guidelines given by the GSI or by any other system, for estimation of rock masses’ residual strengths that give consistent results. It is highlighted that several attempts have been made to estimate residual strength of jointed rock masses and reduction of GSI to its residual value. Yet, current reduction methods lead to inconsistent results for different rock masses.

The suggested method is based on observation of actual rock mass failure processes which are obtained from laboratory and in-situ tests, as well as on understanding of rock fracturing process from numerical simulation. Some known rock mechanics test data (strength of rock masses and especially for intact rocks) were used to obtain residual strength parameters of the rock mass. By using these, data residual GSI value for design was obtained. This method extends current GSI system in estimation of rock masses’ residual strength parameters. That is to say by using this method, peak GSI value in current GSI system is adjusted to its residual GSI_r in this study (Cai et al. 2007).

The proposed method for estimation of rock mass residual strength was validated using in-situ "block shear test data" from three large-scale cavern construction sites and data from back-analysis of rock slopes. When it is compared, a good agreement between field tests or back analyzed data with the proposed residual GSI calculation method was found. The proposed method for residual strength estimation extends the GSI system and adds quantitative means to determine complete set of rock mass properties needed for design (Cai et al. 2007). The residual GSI_r value can then be empirically expressed as a function of the peak GSI value as;

$$GSI_r = GSI.e^{-0,134.GSI} \quad [1]$$

An exact solution was not given by this equation for residual GSI value but it was accepted as an admissible approach for residual GSI value.

Barton (2002) has also researched rock mass parameters under specific stress conditions. In his study; he has proposed three different rock and soil interactions for discontinuity surfaces. One algorithm is direct rock to rock contact. In this case there is no fillings between two rock surfaces. The second case is rock to rock contact with thin fillings. In this case, there is thin soil layer that exist, between two rock surfaces. The third case is rock to rock contact with thick fillings. In this case, there is thick soil layer that exists between two rock surfaces. In the third case, it is accepted that there is no rock contact occurs when it is sheared (Figure 2.2).

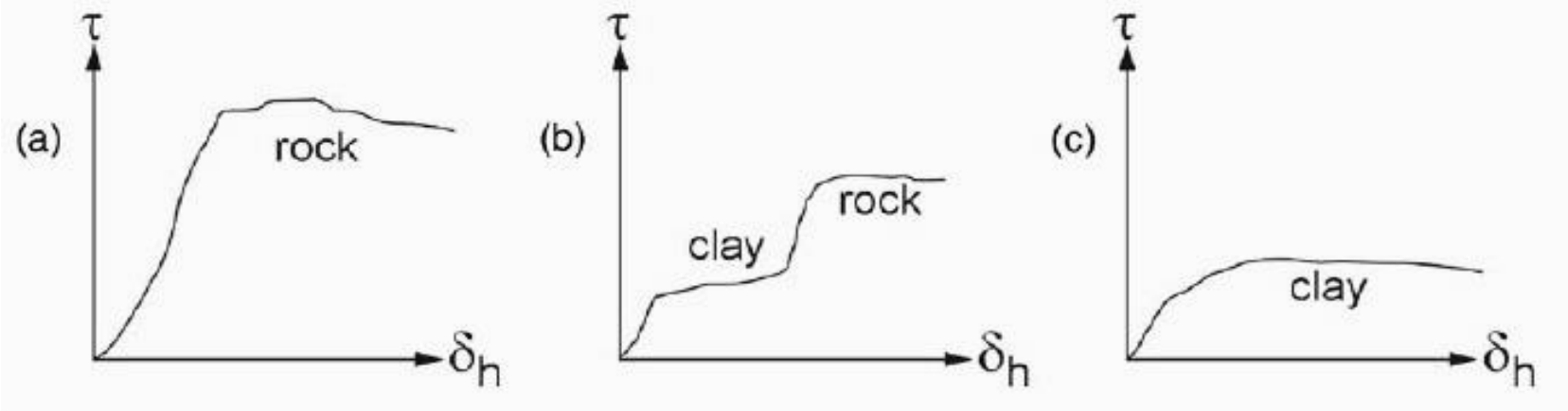

Figure 2.2. Inter-block frictional behavior, an extract from the J_r and J_a rating tables (Q chart). a) Rock wall contact, b) Rock wall contact when sheared (thin fillings), c) No rock wall contact when sheared (thick fillings) (Barton 2002).

Frictional Component "*FC*" term for a rock mass or in another words, rock mass "ϕ" value (as a unit of °) was defined in this study, as follow:

$$"FC = tan^{-1}\left(\frac{J_r}{J_a} x J_w\right)" \qquad [2]$$

The above figure can be assumed as the summary of the equation 2. It is logical to assume that the relation of J_r and J_a ratings to joints or discontinuities. Because the most affecting result from a particular loading direction will be get from a sensitive anisotropic joint properties. As defined, Jr and Ja will tend to give the minimum frictional component FC. In this equation FC should be applied only to the least favorable joint set or filled discontinuity. This approach should not be used in isotropic models without caution (Barton 2002).

Besides frictional component, *Cohesive Component* "*CC*" of the rock mass or in another words, rock mass "C_{rm}" value (as a unit of MPa) was defined in this study, as follow;

$$CC = \frac{RQD}{J_n} X \frac{1}{SRF} X \frac{\sigma_c}{100} \qquad [3]$$

The author suggested replacing $\sigma_c/100$ with $I_{50}/4$ in highly anisotropic rocks which are having high ratios of σ_c/I_{50} to obtain more accurate results. The potential anisotropy of CC could be improved further by selecting RQD_0, i.e. RQD in the loading direction. Yet, "*C*" and "ϕ" are the most difficult parameters to assess or measure in rock mechanics. They are usually anisotropic and stress-dependent properties. It should not be expected to have certain values of these two parameters from any rock mass classification systems. Instead of this, an interval should be defined for these values in conformity with the anisotropy.

The other important parameters for numerical design, σ_{cm} (rock mass compression strength based on compression failure of the intact portions) and σ_{tm} (rock mass compression strength based on tensile failure of the intact portions) were also defined in this study. However; since there are no solid data available, these are remained as estimation (Barton 2002).

$\sigma_{cm} = 5\gamma Q_c^{1/3}$ (MPa) where γ is the rock density in t/m^3 unit and [4]

$Q_c = Q x \sigma_c/100$ [5]

$\sigma_{tm} = 5\gamma Q_t^{1/3}$ (MPa) where $Q_t = \sigma_0 x I_{50}/4$ [6]

Similar to Barton's study, Ramamurthy (2004) has also worked on rock mass parameters especially for jointed rock mass. According to this study, when rock mass uniaxial compressive strength and modulus ratio are estimated from RMR, Q or GSI the results are not satisfactory. Because changes in quality of rock mass does not significantly change the modulus ratio. For this reason, the author suggests to use the *joint factor* (J_f). RMR, Q and GSI are linked to joint factor in this study. For this aim, strength and modulus values of the rock mass are obtained from all of the rock classification systems with using previous equations and results are then evaluated (Ramamurthy 2004). The author has proposed new approaches for rock mass uniaxial compressive strength value, and for rock mass elasticity modulus value. Both of the parameters are derived from RMR, Q and GSI values which are given below:

$$\sigma_{cj}/\sigma_{ci} = \exp[RMR - 100/25] \quad [7]$$

$$\sigma_{cj}/\sigma_{ci} = \exp[0.6 log Q - 2] \quad [8]$$

$$E_j/E_i = \exp[(RMR - 100)/17.4] \quad [9]$$

$$E_j/E_i = \exp[0.8625 log Q - 2.875] \quad [10]$$

On the basis of the GSI, the following equation should be adopted to estimate the uniaxial compressive strength of rock mass for GSI > 25 in case of an undisturbed rock mass,

$$\sigma_{cj}/\sigma_{ci} = \exp[(GSI - 100)/9] \quad [11]$$

The other well-known study about rock mass strength parameter is Hoek et al. (2002) criterion. In this study, Mohr-Coulomb failure criterion parameters were determined as equivalent angles of friction and cohesive strengths for each rock mass and stress range. According to this study C_{rm} and ϕ_{rm} values were identified as shown in the following equations;

$$\phi' = sin^{-1}\left\{\frac{6am_b(s+m_b\sigma'_{3n})^{a-1}}{2(1+a)(2+a)+6am_b(s+m_b\sigma'_{3n})^{a-1}}\right\} \quad [12]$$

$$c' = \frac{\sigma_{ci}\left|(1+2a)s+(1-a)m_b\sigma'_{3n}\right|(s+m_b\sigma'_{3n})^{a-1}}{(1+a)(2+a)\sqrt{1+\left(6am_b\left(s+m_b\sigma'_{3n}\right)^{a-1}\right)/(1+a)(2+a)}} \quad [13]$$

In literature lots of works can be found about prediction of rock mass deformation modulus (Fakhimi et al. 2004, Rahimi et al. 2014). Amongst these well-known equation of Hoek and Diederich's (2006) study for E_{rm} is given here in Equation [14];

$$E_{rm} = E_i\left(0.02 + \frac{1-{}^{D_f}/_2}{1+e^{\{(60+15D-GSI)/11\}}}\right) \quad [14]$$

2.1.2 Determination and prediction of tunnel convergences

Monitoring of convergences is one of the main philosophies of underground structures. Effectiveness of monitoring equipment have made convergence monitoring system is an integral part of decision making process that consist of design, construction, supervision and maintenance parts (Kavvadas 2005).

According to NATM, controlled ground deformation should be permitted inside an excavation (Rabcewicz 1964). Therefore, contemporary tunnel designs and construction techniques have significantly benefited from convergence measurements. Controlled deformation make partial release of stress and allows using less stiff, less-expensive support system. To achieve this aim; accurate, systematic and continuous monitoring of tunnel and convergences should be done during an excavation (Kontogianni and Stathis 2003). Perception of deformation pattern around underground excavations will also give a clue about face advance behavior. Additionally, large amount of convergence monitoring data permit estimation of real displacements and reveals deformed tunnel profile sections (Kontogianni and Stathis 2003). Hence, correct interpretation of deformations and rock mass behavior will let us design economic and safer environments in underground excavations. This will not only give us economy and safety, but also expedite the excavation. The researchers who are aware of importance of this subject, studied deformations previously, in many different ways (Dalgic 2002, Kim and Chung 2002, Kontogianni and Stathis 2003, Kavvadas 2005, Kontogianni and Stiros 2002, Bizjak and Petkovsek 2004, Schubert et al. 2004, Kontogianni and Stiros 2005, Sharan 2005, Li et al. 2006, Hsiao et al. 2009, Mahdevari and Torabi 2012, Sharifzadeh et al. 2012, Adoko et al. 2013, Mahdevari et al. 2013, Lin et al. 2015).

Kontogianni and Stathis (2003) has stated that detailed geodetic recording of tunnel closure time-history and ground behavior of underground opening for different stages of excavation sequence is sometimes an early warning tool to modify the excavation method and by this way large deformations can be avoided. For instance; if high deformation area exists, a swell-type closure pattern can be observed along the tunnel axis.

In these areas, deformations do not gradually develop at each section. On the contrary, it develops on certain sections and then propagated bilaterally along a distance of several tens of meters and affects the neighbor sections. Some parts of weak-rock tunnels can follow this pattern of convergence.

This is a major threat for tunnel construction and stability. Contractor possibly thinks that some parts of tunnel have already stabilized, but after a certain time “from a few days to a few months,” convergences can reach higher levels and threat excavation stability.

In most of the weak rock tunnels, if there is a long delay on ring closure and supporting, extreme unexpected deformations can occur even after full support installation. On this account, monitoring is crucial for proper support system selection and provides cost-effective solutions for stable underground excavations (Kontogianni and Stathis 2003).

In another study, time and deformation propagation relation is explained in detail (Kontogianni and Stiros 2005). According to this study, deformation propagation along the tunnel axis results in an induced deformation. It has been stated that this kind of deformation occurs under certain circumstances, and it seems to have a clear time and space-controlled pattern. Namely, if there is existence of weak rocks in close approximation of any excavation section, this section may behave like a stress source. After excavation of this section, it induces new stress occurrence. Therefore, new deformations probably propagate from the previously excavated and supported weak rock sections. This behavior is named as a rejuvenated deformation, which is stems from nearby weak rock excavations, hydrological effects, swelling rocks and gradual failure of supported shell under imposed stresses. If rejuvenated deformation exists, after the first period of deformation and stabilization, stresses build-up at critical levels and their propagation to the surrounding ground may induce a new phase of deformation at several neighboring sections, occasionally leading to necking and failure of the tunnel along distances. This deformation type should not be confused with creep behavior of the ground (Kontogianni and Stiros 2005).

Barton, who is one of the inventors of Q system which is a kind of rock mass classification system for underground excavation, has published the relation between the Q values and deformations in tunnel. The rock mass quality Q-value was originally developed to assist for empirical design of underground excavations and support. Yet, owing to wider use of Q-system, new areas of use are explained in Barton (2002). Tunnel convergence measurements and Q-value data have been collected by Barton for many years.

In fact, that is not the original purpose of developing a rock mass classification system. Nevermore, a collection of Q/SPAN versus deformation data was published by the help of the collected data. And, the simple equation is obtained;

$$\Delta = \frac{SPAN}{Q} \qquad [15]$$

Here; SPAN is expressed in "meters", and Δ is in "mm". On the basis of the equation 15 following two equations were obtained;

$$\Delta_v = \frac{SPAN}{100Q}\sqrt{\frac{\sigma_v}{\sigma_c}} \qquad [16]$$

$$\Delta_h = \frac{HEIGHT}{100Q}\sqrt{\frac{\sigma_h}{\sigma_c}} \qquad [17]$$

In these equations; *"SPAN and HEIGHT"* are horizontal and vertical dimensions of a tunnel or cavern in meter, respectively, and Δ_v is vertical component of deformation, and Δ_h (assume half of horizontal convergence) is horizontal component of deformation both in millimeter, while rock stresses and rock strengths are in terms of MPa.

After finding these two parameters which are very crucial for any tunnel design, Barton (2002) has also suggested an approximation for "k_0" value.

This value is used widely in tunnel design and is defined as horizontal to vertical stress ratio. k_0 value directly affects ground deformations. Yet, it is so hard to measure it correctly. Following equation is an empirical approximation for this value

$$k_0 = \left(\frac{SPAN}{HEIGHT}\right)^2 \left(\frac{\Delta_h}{\Delta_v}\right)^2 \quad [18]$$

Importance of convergence monitoring in underground excavations is also emphasized in Kavvadas (2005) study. Selection of proper excavation method and suitable support system, ensuring safety of workers and structures located at ground surface during tunnel excavation, and construction quality are counted as the importance of deformation monitoring in his study. Several types of extensometers, geodetic surveying tools and laser scanners were used to investigate the plastic zone thickness and convergence measurements. According to his findings; significant portion of ground deformation could not be recorded owing to time gap between installation of first monitoring device and deformation measurement, an appreciable part of deformation occurs before monitoring device installation. Therefore, all monitoring instruments that are placed on tunnel walls or installed in the ground behind the tunnel face, should be put in place as soon as possible to reduce data losses. However in most of the cases, monitoring devices are placed at least 10 m far from the excavation face. This distance can be accepted reasonable to prevent interference with construction of temporary support (sprayed concrete, steel sets, etc.). Yet, when monitoring device is placed at this distance, 60-80% of immediate deformation has already occurred (Kavvadas 2005).

Similar to Kavvadas (2005) study, Kim and Chung (2002) have also pointed out the importance of deformations in underground excavations. They have tried to predict tunnel deformations by using previously occurred and recorded data in the same tunnel. For this aim, actual measurements from 4 highway tunnels in Korea were used to generate a statistical prediction model. The statistical prediction model results were compared with finite element models. When the statistical prediction model results compared with the finite element models, it was found that 20-30% of total displacement could not be measured due to delay in monitoring device installation.

This result is quite similar to Bizjak and Petkovsek's (2004) study. In both, deformation results were only input parameter for prediction model. Although geological and geotechnical characteristics of rock mass are very important for the deformations around the tunnel excavation, they were not taken into account in both studies.

Convergence characteristics of different types of rock masses were assessed by using geodetic survey methods in Kontogianni and Stiros (2002) study. Soft and hard rock masses, which have GSI value within 15 to 65 were assessed in the selected tunnels having shallow overburden thickness (45 to 120 m). Selected GSI range describes strain softening rock mass behavior. Aim of the study was to make a prediction for vertical and horizontal convergence for the selected tunnel excavation and make a comparison between convergence prediction techniques. For this purpose two convergence prediction methods were used; finite element modeling and empirical prediction method. In the study, a commercial software named as Phase2 was used for finite element modeling, and empirical predictions were achieved by using Hoek's characteristic line theory. Result of the study indicated the compliance of suggested prediction methods with tunnel convergences collected from 4 tunnels. Maximum convergence value obtained from about one-half of the tunnel diameters ahead of the excavation face is one of the finding of this study. In fact, statement of "*after an excavation, 30% of total convergences occur instantaneously and cannot be measured easily*" is a priori assumption about the excavation face. That is to say; since convergences have advanced before an excavation, 30% of the total convergences cannot be measured by geodetic surveys or other monitoring techniques. This result is in compliance with the similar studies described above. Deformation rate obtained from the numerical analysis is 30% greater than the geodetic survey results of the study and this also proves their theory. Additionally, tunnel wall closure cannot be measured directly by using geodetic survey methods. Vital amount of tunnel wall closure completed between excavation of faces and the first geodetic measurement. Namely, to measure wall closure, there should be enough span between the excavation face and the nearest measuring point. Otherwise, optical measuring equipment gets damaged from an excavation operation.

In this way, tunnel wall closures can only be measured in a few hours to a usually few days after the excavation. Therefore, buried measuring devices like extensometers should be used to measure the deformations behind the face in this time interval. However, practically it is very rare to see the application of extensometers or any other kind of similar measurement devices in underground excavations, except for the geodetic measurements. Hence, deformation predictions and numerical analysis are very useful tools for underground excavations (Kontogianni and Stiros 2002).

In Bizjak and Petkovsek's (2004) study, back analysis technique was used to evaluate field convergence monitoring data. For this aim, numerical studies were performed by using finite difference method to calculate propagation of stresses around the most expensive tunnel (Golovec) ever built in Slovenia, which is the first three-lane, double-tube highway tunnel. Golovec tunnel's dimensions are 520 m in length, 10.5 m in height, 14.1 m in width respectively with overburden up to 80 m. Its cross section is 148 m^2. Instability issue in the entrance region was increased the construction cost. The tunnel was excavated in Carboniferous-aged soft rocks, mainly consisting of siltstone, claystone, sandstone and tectonic clay with some trusted faults. Spatial distribution of rock displacements was analyzed by numerical modeling (FDM), with selecting Mohr–Coulomb criteria in strain softening constitutive modeling procedure. 3D displacement monitoring technique, which is supported by suitable software showing graphical time evolution of recorded displacements and their intermediate or final values on cross section, was used for standard lining-deformation measuring procedure. Time dependent estimation of final convergences through the first measured convergence data was achieved by means of artificial neural networks. Geodetic monitoring results have shown integrity between calculated and measured data, when they are compared with numerical studies and back calculations.

According to Bizjak and Petkovsek's study' it was stated that; before reading the first convergence data and shortly after the excavation of any section 30-35% of rock deformation has already occurred ahead of the excavation face and in its close vicinity. Vertical direction was found as major displacement component of tunnel walls. Fast fulfillment of invert construction is found as major factor, which prevents convergences. If the distance between the active excavation face and invert section is 80 m or more, great deformations are unavoidable even if the excavation is driven in favorable rock mass conditions.

After construction of invert, displacements can stop in 10 or 14 days in poor rock mass conditions and this period can be decreased to a few days in better quality rocks. Support installation time, its rigidity, and constructor's working accuracy and quick reaction to the changing geologic conditions are found as major factors affecting the radius of relaxed zone around the tunnel.

The other study for the prediction of tunnel convergence is Mahdevari and Torabi (2012) study. In this study, various statistical estimation approaches were used to predict convergences at Ghomroud water conveyance tunnel in Iran. Aim of the study was to reveal relationship between the selected rock parameters and convergences of the tunnel. For this aim, real convergence monitoring data, geomechanical and geological parameters obtained through site investigation and laboratory tests were introduced as an input to artificial neural network. The host rocks in the tunnel section has been named as metamorphic and sedimentary, which can be classified as weak to fair quality according to rock mass classifications. In order to predict tunnel convergences, two different Artificial Neural Network (ANN) approaches were used; Multi-Layer Perceptron (MLP) and Radial Basis Function (RBF) analysis. Besides, Multi-Variable Regression (MVR) analysis was also used to predict convergences in the study. Yet, the findings of MVR were not satisfactory when compared with the real field measurements. However, ANN based prediction model results that uses MLP has shown its estimation approach in acceptable range in terms of correlation (Figure 2.3). So, the study showed that ANN has great superiority when compared with MVR.

A parametric study is also carried out to estimate the effect of input geomechanical parameters on tunnel convergences. It is observed that *C, Φ, E* and *UCS* parameters are the most effective factors and σ_t is the least effective one on predicting tunnel convergences. Nevertheless, parametric study results have revealed meaningful effect of all input geomechanical parameters upon output. So, all selected input parameters can be used for the prediction of tunnel convergences (Figure 2.4) (Mahdevari and Torabi 2012).

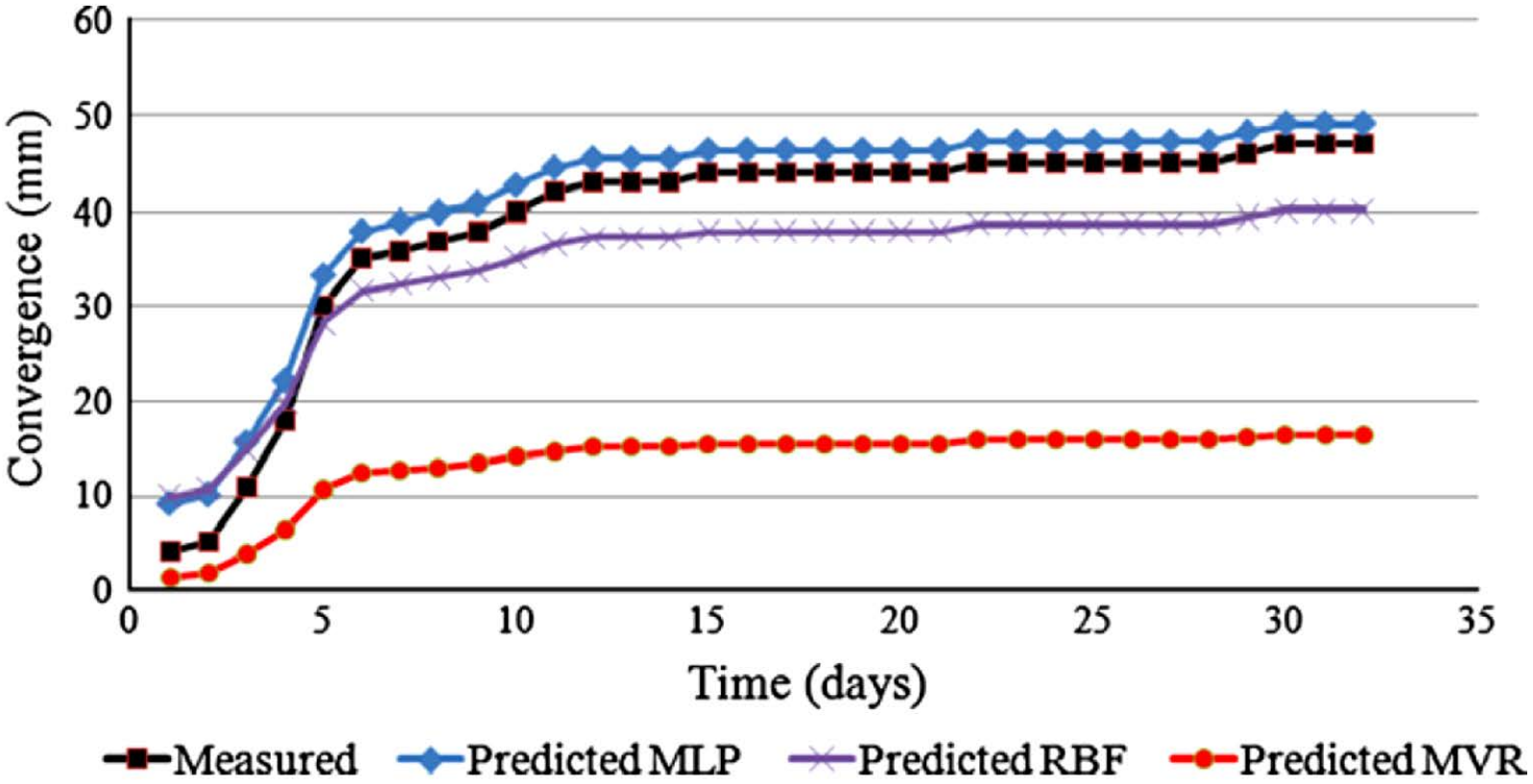

Figure 2.3. The comparison of the measured and different calculated time histories of tunnel convergence curve (Mahdevari and Torabi 2012).

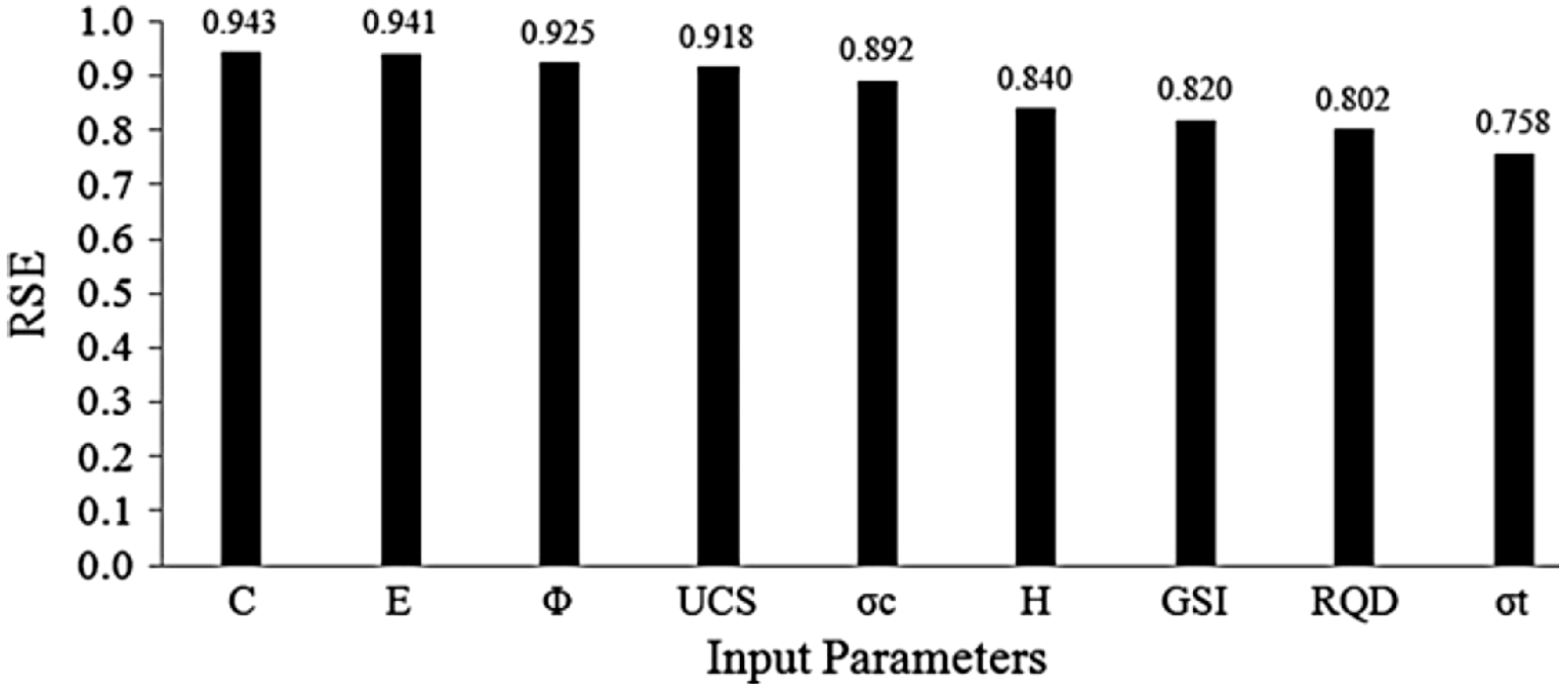

Figure 2.4. Relative effects of each input parameter on the tunnel convergence (Mahdevari and Torabi 2012).

By using MVR analysis, following relationship is established, between dependent variable “convergences” and independent variables “geomechanical parameters”;

$$d = 20.75 - (0.016xH) - (0.58xRQD) + (0.668xE) + (0.530x\phi) - (0.538xUCS) + (1.861x\sigma_c) + (1.872x\sigma_t) + (4.98xC) + (0.049xGSI) \quad [19]$$

where *d* is convergence expressed in millimeters and *H, RQD, E,* and Φ are height of overburden in meters, rock quality designation in percent, Young’s modulus in GPa and angle of internal friction in degree, respectively. Furthermore, *UCS,* σ_c, σ_t and *C* are uniaxial compressive strength of the intact rock, uniaxial compressive strength of rock mass, uniaxial tensile strength of rock mass and cohesion, respectively. All are expressed in MPa. The last parameter, *GSI*, is well-known Geological Strength Index value which has no unit.

Sharifzadeh et al. (2012) study is another good example to predict convergences by using previous data with combination of back analysis and numerical models. Stability problems and solutions for Shibli tunnels, located at 25 km away from Tabriz, were explained in this study. The tunnel was designed in accordance with sequential excavation method. During the excavation of southern tunnel, collapse problem has occurred in some sections of initial 800 m. Therefore, support system and excavation sequences had to be changed. Nevertheless, owing to the high costs required to change designed support system, excavation order was modified merely to overcome this issue. Initially, top heading and bench excavation procedure was modified based on the size of tunnel, uniaxial compressive strength of the rock mass material and vertical in-situ stress ratio. Then, with help of two-dimensional explicit finite difference method (Flac2d), back analysis procedure was applied to collapsed zones to find out correct design parameters of disturbed rock mass. Direct approach of displacement-based back analysis method was used to grasp optimized rock mass parameters. The applied method is based on optimization of mechanical properties of the rock mass by trial and error. After that, excavation order has been revised in accordance with back analysis and precisely designed new excavation procedure is applied.

By using optimized rock mass parameters, modified sequential excavation design is applied successfully without occurrence of any further collapses throughout the rest of the Shibli tunnels (Sharifzadeh et al. 2012).

One recent research about estimation of tunnel convergences was performed by Adoko et al. (2013). In this study two different approaches, Multivariate Adaptive Regression Spline (MARS), which is a nonlinear and nonparametric regression technique that uses piecewise linear segments (splines) to represent nonlinear behaviors between input and output variables of a system (Friedman 1991) and Artificial Neural Networks (ANN), were used to predict convergences of a high-speed railway tunnel in weak rocks located in Hunan province (China). Limitations of ANN's were stated and superiorities of MARS were highlighted in terms of explaining nonlinear multidimensional relationships among the factors influencing the tunnel convergences.

The class index of surrounding rock mass, angle of internal friction, cohesion, Young's modulus, rock density, tunnel overburden, distance between monitoring stations, tunnel heading face and elapsed monitoring time were chosen as input parameters. For the selected approaches, 80% of all raw data was chosen as training datasets, while the rest was kept for testing purposes. MARS approach results revealed the most effective parameters in estimation of tunnel convergences, these are; rock class rating index of the surrounding rock mass (SRM), elapsed monitoring time (T), internal friction angle (ϕ) and cohesion (c). Performance of the two models was evaluated by comparing the predicted convergences with the measured data using several performance indices. As a result, it has been observed that both models show good agreement with the field monitoring data (Figure 2.5).

However, ANN models have shown a little bit better prediction performances when compared with MARS prediction capability (Figure 2.6). Nevertheless, MARS estimation technique was found computationally more efficient at finding the optimal model, and able to provide a contribution of each variable to the tunnel convergence through the ANOVA decomposition.

Additionally, the model outputs of MARS have been expressed in a more interpretable way since it uses a series of linear regressions defined in distinct intervals of the input variable space. So, it can be concluded that MARS can be used to predict the tunnel convergences as good as ANN method (Adoko et al. 2013).

Similarly, in Mahdevari et al. (2013), Support Vector Machine (SVM) model was designed to identify dependencies for tunnel convergences, and the geological and geotechnical conditions encountered to predict non-linear relationship between geotechnical properties of rock mass and monitoring results. For this aim, Amirkabir Tunnel which is located in Iran's Capital city Tehran was selected. Two different approaches, Multi-Variable Regression (MVR) and SVM regression, were applied both for comparison and prediction of convergences. A good agreement was obtained by using non-linear regression support vector machine algorithm (Figure 2.7). Yet, multi-variable regression model is not found to be capable to predict convergences (Figure 2.8).

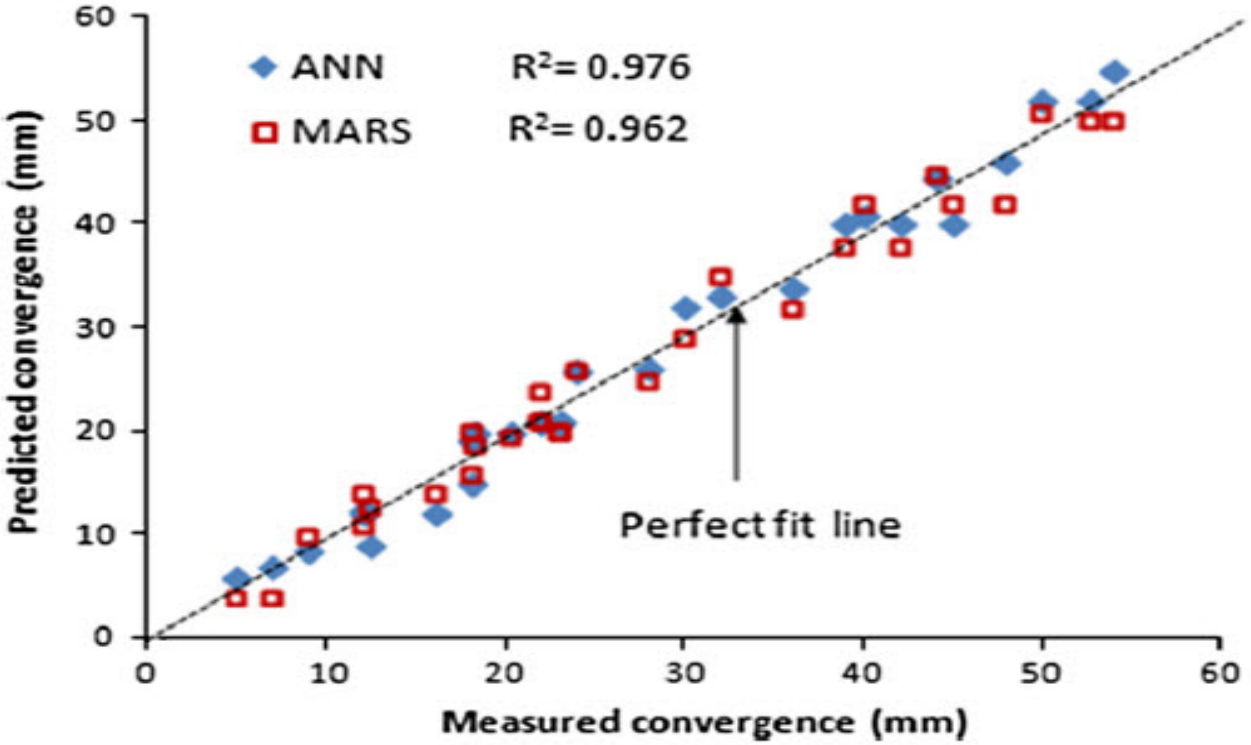

Figure 2.5. Comparison of ANN and MARS analysis prediction capability (Adoko et al. 2013).

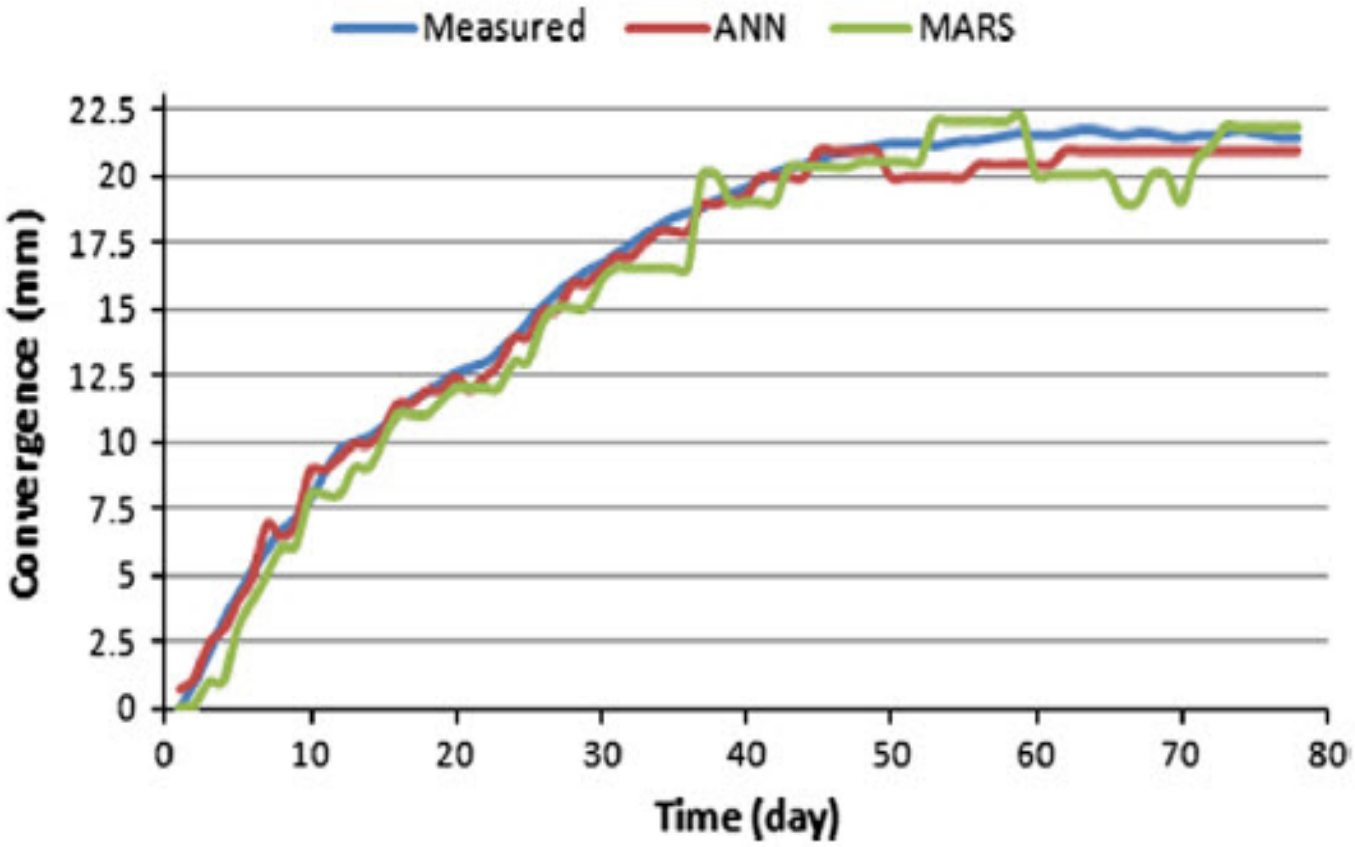

Figure 2.6. Predicted convergence trends at specified monitoring station (Adoko et al. 2013).

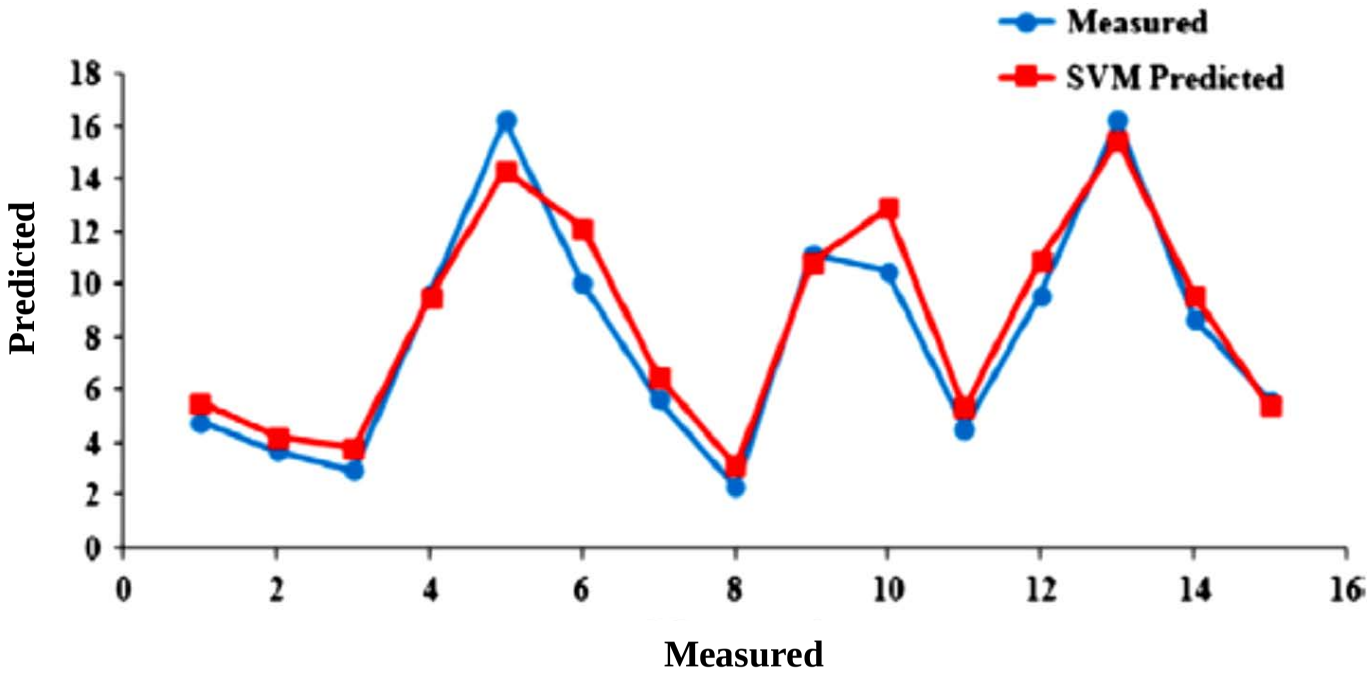

Figure 2.7. Predicted and measured convergences graph for SVM analysis (Mahdevari et al. 2013).

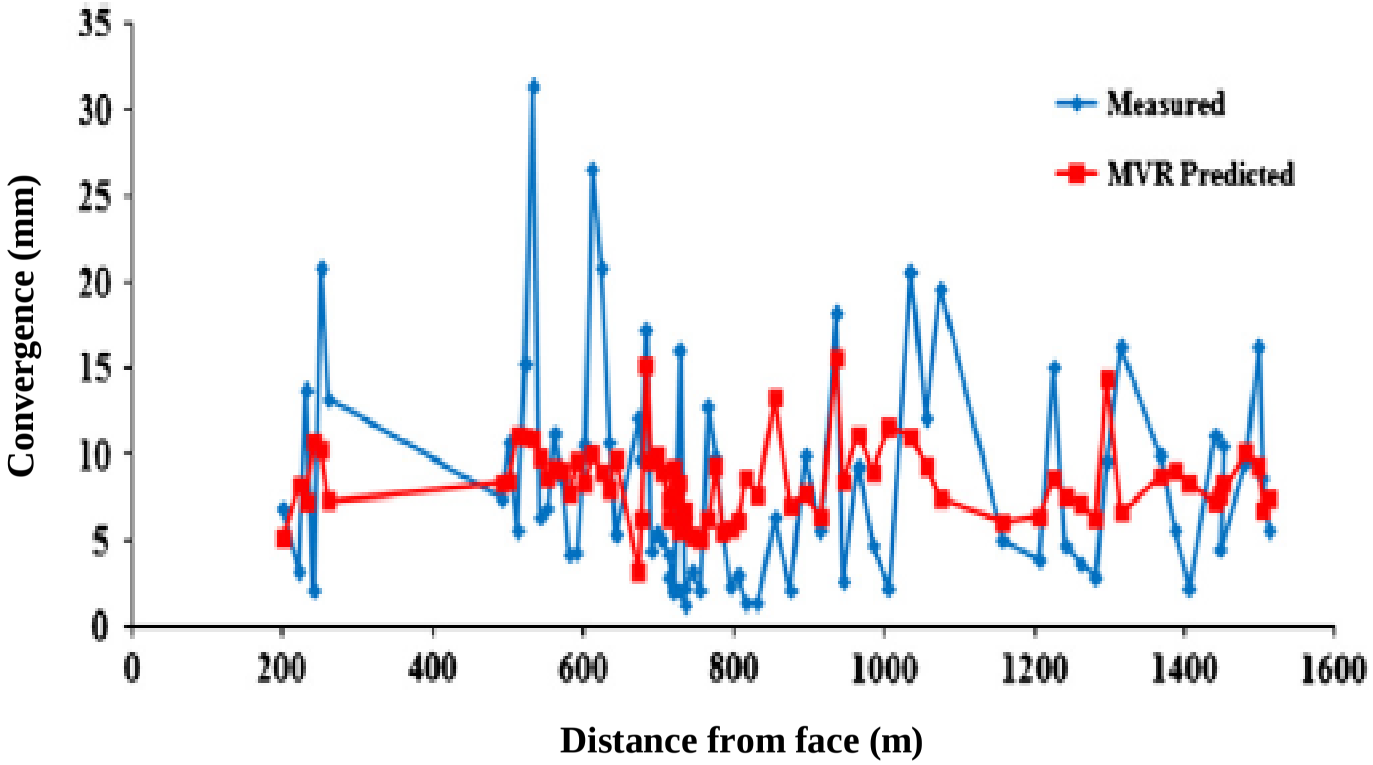

Figure 2.8. Predicted and measured convergences graph for MVR analysis (Mahdevari et al. 2013).

2.1.3. Determination and prediction of plastic zone thickness in tunnels

In literature, there are three well-known methods for determination of plastic zone thickness. These are empirical methods, field measurements and back-analysis technique. All of the three methods were given in detail in this section.

2.1.3.1. Empirical methods

Rate of convergence around excavation depends on in-situ stress conditions, post-failure behavior of host rock, selected excavation method and contractor's ability. As excavation methods and contractor experiences were not in the scope of this study, they will not be explained here in detail. Proper understanding of post-failure behavior and correct interpretation of previous convergences help us to estimate plastic zone thickness around an excavation. As mentioned previously in introduction part, accurate estimation of plastic zone thickness not only expedites the tunnel excavation, but will also ensure excavation stability. Besides, it will provide safe working conditions for machinery and workers. Some researchers have tried to demonstrate connection between post-failure behavior, convergence and plastic zone thickness, previously (Fenner 1938, Terzaghi 1946, Sato et al. 2000, Torres and Fairhurst 1999, Torres and Fairhurst 2000, Hoek 2001, Martino and Chandler 2004, Hao and Azzam 2005, Blumling et al. 2007, Golshania et al. 2007, Lee and Pietruszczak 2008, Kwon et al. 2009, Kim et al. 2012, Zhang et al. 2012, Xia et al. 2013, Siren et al. 2015, Leia et al. 2017, Yanga et al. 2017, Yi et al. 2017, Verma et al. 2018, Wanga et al. 2013).

Plastic zone concept was introduced first in the studies named "Untersuchungen zur erkenntnis des gebirgs druckes, by Fenner (1938), and "Rock defects and loads on tunnel supports" Terzaghi (1946). These two studies were the landmarks in tunneling literature and are depicted in Figure 2.9.

Fenner’s method was based upon development of “plastic zone” in the rock mass surrounding the tunnel. Creation a balance between initial loading and internal stress (“p_0” and “p_i”) conditions lay behind the root of Fenner's concept. This can only be achieved by using supporting elements.

Similarly, Terzaghi has defined the ground arch concept. According to his theory, different arching thicknesses depending on type of host rock have been defined. So, nine different rock categories according to depths and discontinuity conditions have been identified. Except for swelling grounds, ground arch thickness is no more than (2.1 to 4.5), $(B+H_t)^*$ and this was defined as the extreme case (Table 2.1) (Bieniawski 1990).

During several decades, so many studies have been made on this subject. Among them, Hoek's study has become the most known. He has combined tunnel convergence and plastic zone concepts (Hoek 2001). In this study, evolution of deformations in the rock mass was illustrated for an advancing tunnel excavation. According to this, displacements start about two tunnel diameters ahead of the face, reaches about one third of its final value at the tunnel face and reaches its final value at about two tunnel diameters behind the face (Figure 2.10). Depending on the amount of radial displacements and propagation speed, plastic zone will occur around the excavation, until changing stress conditions reach steady-state.

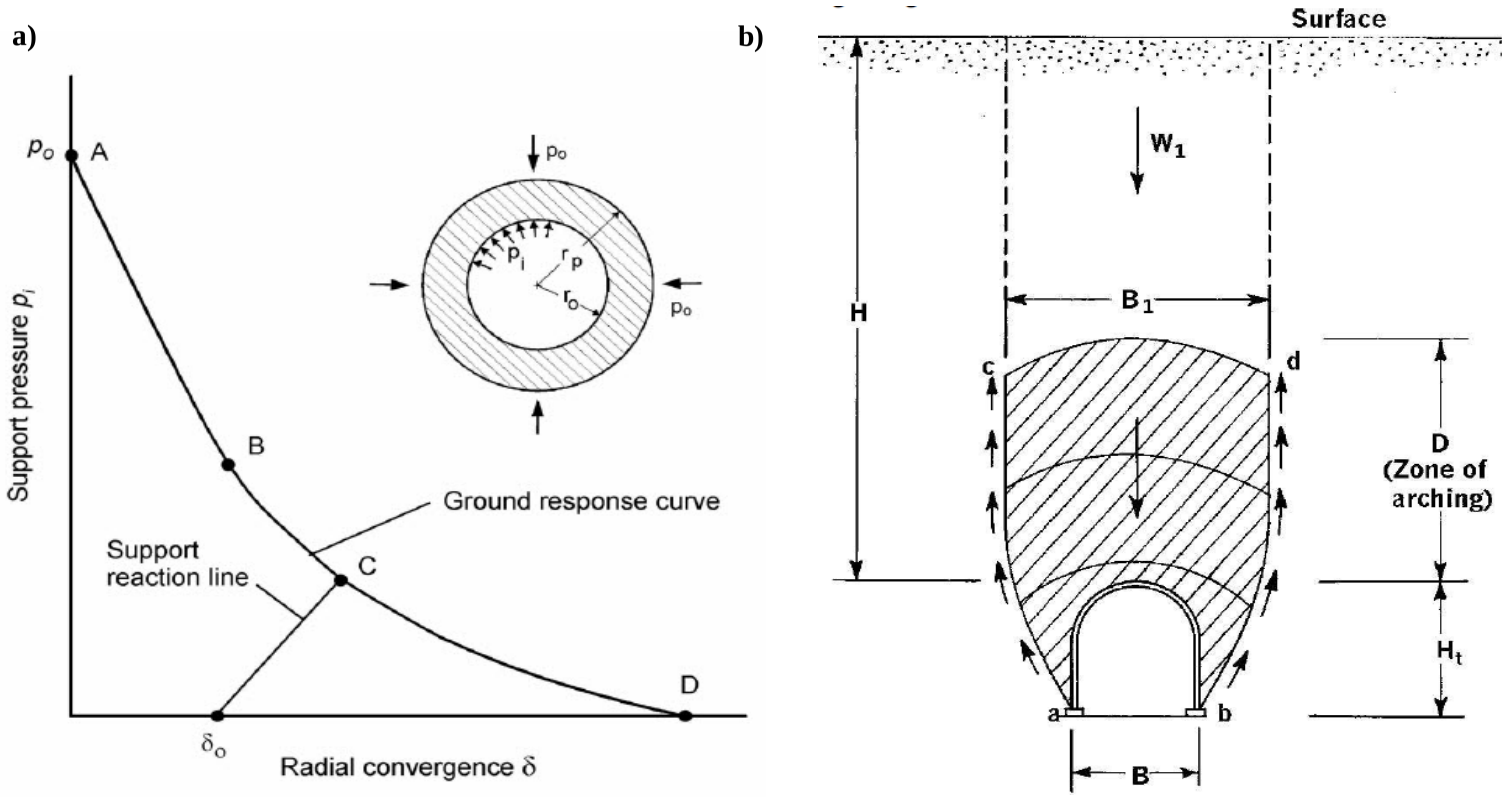

Figure 2.9. a) Fenner's plastic zone concept and b) Terzaghi's ground arch concept (Hoek 2001).

Table 2.1. Rock load classification for steel arch-supported tunnels (Rock load H_p in feet of rock on roof of support in tunnel with Width B and height H_t at a depth of more than $1.5(B+H_t)$)* (Terzaghi 1946)

Rock condition	**Rock load H_p in feet**	**Remarks**
1.Hard and intact	Zero	Light lining required only if spalling or popping occurs
2.Hard stratified or schistose**	0 to 0.5B	Light support, mainly for protection against spalls.
3.Massive, moderately jointed	0 to 0.25B	Load may change erratically from point to point
4.Moderately blocky and seamy	0.25B to 0.35 $(B+H_t)$	No side pressure
5.Very blocky and seamy	(0.35 to 1.10) $(B+H_t)$	Little or no side pressure
6.Completely crushed but chemically intact	1.10 $(B+H_t)$	Considerable side pressure. Softening effects of seepage towards bottom of tunnel requires either continuous support for lower ends of ribs or circular ribs.
7.Squeezing rock, moderate depth	(1.10 to 2.10) $(B+H_t)$	Heavy side pressure, invert struts required. Circular ribs are recommended.
8.Squeezing rock great depth	(2.10 to 4.50) $(B+H_t)$	
9.Swelling rock	Up to 250 feet, irrespective of the value of $(B+H_t)$	Circular ribs are required. In extreme cases use yielding support.

**The roof of the tunnel is assumed to be located below the water table. If it is located permanently above the water table, the values given for types 4 to 6 can be reduced by fifty percent.*

***Some of the most common rock formations contain layers of shale. In an unweathered state, real shales are no worse than other stratified rocks. However, the term shale is often applied to firmly compacted clay sediments which have not yet acquired the properties of rock. Such so-called shale may behave in a tunnel like squeezing or even swelling rock. If a rock formation consists of a sequence of horizontal layers of sandstone or limestone and of immature shale, the excavation of the tunnel is commonly associated with a gradual compression of the rock on both sides of the tunnel, involving a downward movement of the roof. Furthermore, the relatively low resistance against slippage at the boundaries between the so-called shale and the rock is likely to reduce very considerably the capacity of the rock located above the roof to bridge. Hence, in such formations, the roof pressure may be as heavy as in very blocky and seamy rock.*

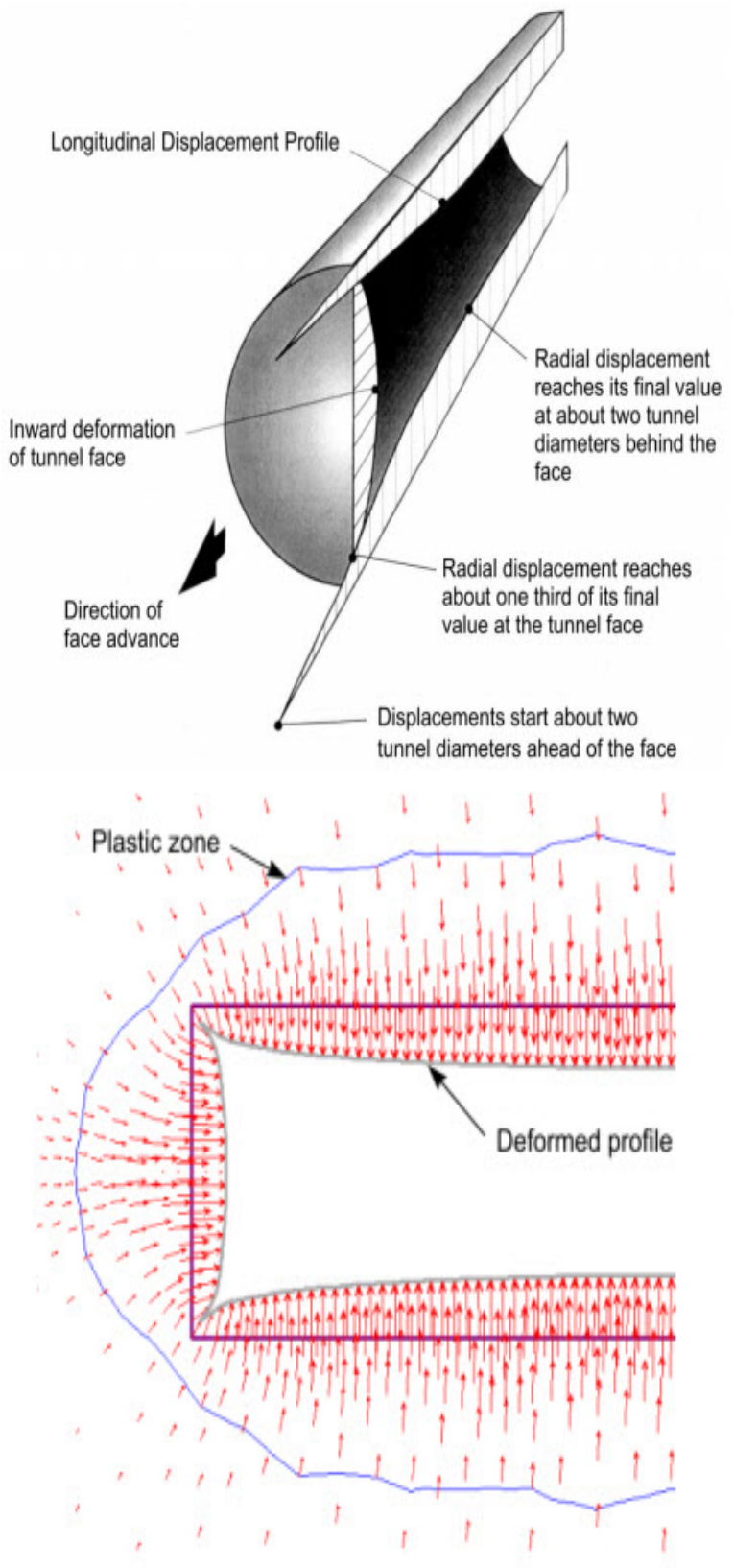

Figure 2.10. Development of plastic zone and radial displacements around a tunnel excavation (Hoek 2001).

To generate correct design and understand this phenomenon, empirical methods or analytical techniques can be used. Torres and Fairhurst (2000) study is one of the well-known studies, explaining convergence confinement method. In this study, three indispensables of CCM for proper support design, Longitudinal Deformation Profile (LDP), Ground Reaction Curve (GRC) and Support Characteristic Curve (SCC), were explained elaborately. LDP is the graphical representation of radial displacements that occur along the axis of an unsupported cylindrical excavation for sections located ahead and behind of the excavation face. LDP should be drawn in accordance with the measured geodetic monitoring data. SCC is similarly defined as the relationship between increasing support pressure (p_s) and radial displacement (u_r). This relationship depends on geometrical and mechanical characteristics of the support. Finally, GRC is defined as the relationship between decreasing internal pressure (p_i) and increasing radial displacement of the wall (u_r). This relationship depending on geotechnical properties of the rock mass can be obtained from elasto-plastic solutions of rock mass deformations around an excavation (Torres and Fairhurst 2000). In Torres and Fairhurst's (2000) study, plastic zone thickness was determined analytically for rock masses, which satisfies Hoek-Brown failure criterion. For internal pressure "$p_i<p^{cr}{}_i$", extent of the plastic zone (R_{pl}) was calculated with following equation;

$$R_{pl} = R_t exp\left[2\left(\sqrt{P_i^{cr} - \sqrt{P_i}}\right)\right] \qquad [20]$$

In this study; there is also a useful graph, showing relationship between radial displacements of the tunnel wall with radius of failed zone (Figure 2.11). This graph was generated for 1 m diameter circular excavations by using CCM and 3D explicit finite difference method together. By using 3D numerical analysis software, GRC was plotted for three different GSI values. After that, failed zone thicknesses calculated by numerical software were recorded and the graph was generated. This fictious study's aim was to validate the Equation 20 (plastic zone thickness) by using 3D numerical software. This study may be accepted as the first attempt to establish relations among rock mass classification, radial displacement, and plastic zone thickness (Torres and Fairhurst 2000).

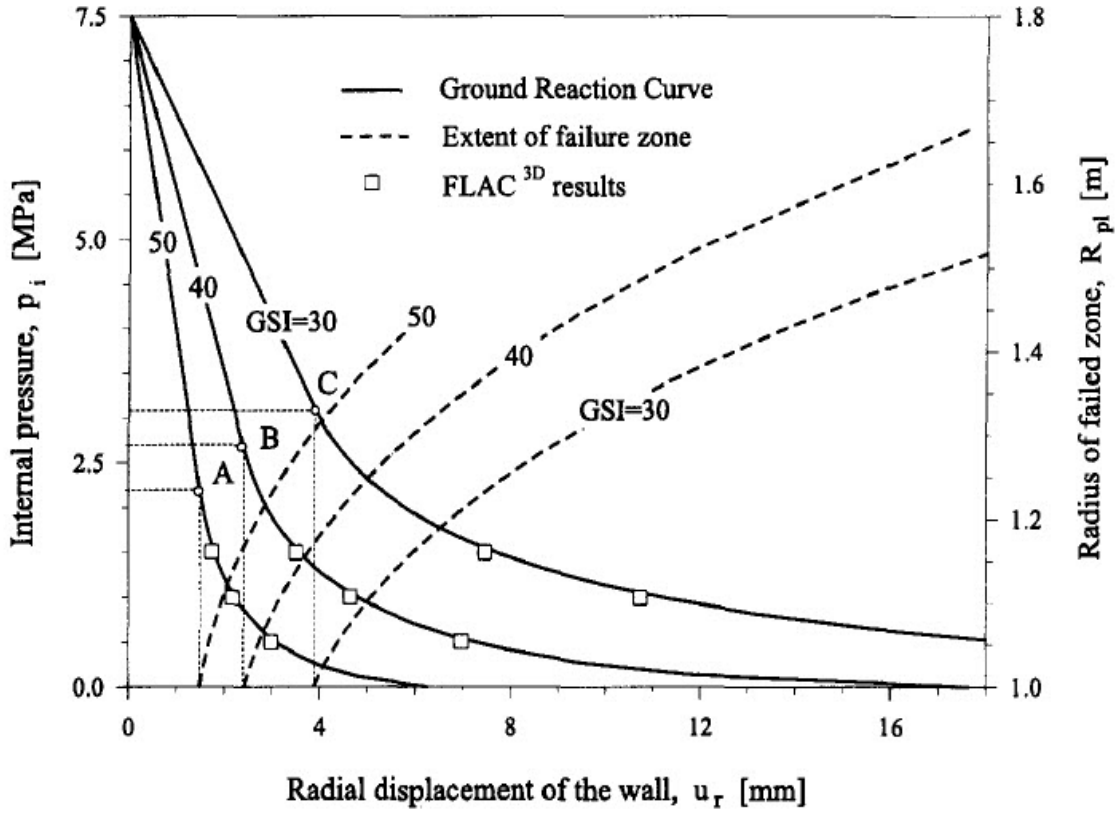

Figure 2.11. Ground reaction curves and extent of failure curves for a specified section in the model for GSI values of 50, 40 and 30. The points A, B and C represent the elastic limit in each GRC. The open squares in the diagram correspond to results obtained with FLAC3D (Torres and Fairhurst 2000).

2.1.3.2. Field measurement methods

The above mentioned studies were completely analytical. Fictitious data were produced to show how the results can change in case of using different GSI values. The authors have also suggested the use of different rock mass rating systems and discontinuity data sets to deepen the research.

Besides, plastic zone thickness in tunnels can be found also by using field measurements and back analysis techniques. A few main examples of in-situ measurements for determining plastic zone thickness have been applied either for unstable transportation tunnels or repository sites. Owing to the sensitivity and side effects of deposited material (mostly radioactive), most of the field measurement studies were applied for nuclear repository sites where assessments of the thickness of excavation damage zone (EDZ) or plastic zone is crucial. In these areas, increase in EDZ results with an increase in permeability potential of host rock. Consequently, an EDZ with a raised permeability could affect performance and safety of the repository sites, providing a preferential pathway for radionuclides to migrate (Kim et al. 2012).

The development of excavation damaged zone (EDZ) in the excavation of radioactive waste disposal site was investigated in Blumling et al. (2007). Excavation was held in the clay bearing geologic formations to prevent leakage of waste material. For this aim, four different clay-bearing formations were investigated. As known, clay formations are natural barriers against the leakage owing to the chemical, mineralogical composition and grain size of the units. However, owing to low geomechanical strength properties, clay formations show two different types of failure behavior; short-term and long-term. In this study, thickness of EDZ and long-term behavior of the excavation were investigated. Owing to the sensitivity of excavation area, rock mass properties in the excavation disturbed zone and excavation damaged zone were investigated separately. Hydraulic conductivity and saturation techniques were used to investigate EDZ. At first, mechanical properties of the host rock were investigated. Secondly, time dependent behavior of the clay formations was evaluated.

Time dependent geomechanical properties of clay bearing rock formations are very effective on underground excavation stability. Stability of the excavation, shear strength and deformation modulus values of the units decrease depending on the increase in water content. Results show that stress redistribution around a tunnel creates a significant damaged zone in plastic or stiff clays or claystones. There are some examples for this situation. These tunnels which have been fully supported were stable for a year, but then with increasing water content they have collapsed. Therefore, time dependent failure behavior of the clay formations can only be prevented by using adequate support. Another interesting result of the study is that clay formation has a tendency to seal its cracks after the excavation, but in limited extent. While soft clays are reacting very fast and seal the fractures (sealing), hard clays or claystones require much more time for the self-sealing processes. Nevertheless, observations indicate that reduction of transmissivity of the formation occurs in several orders of magnitude within a few years. (Blumling et al. 2007).

Influence of the excavation-damaged zone (EDZ) on the geomechanical performance of compressed air energy storage (CAES) in lined rock caverns was investigated by Kim et al. (2012). These rock caverns are mainly open in soluble rocks at shallow depths. Excavations were made for Korean pilot test program on Compressed Air Energy Storage (CAES). The authors mainly focused on the permeability characteristics of the EDZ, because raising permeability could affect the performance and safety of the repository, providing a preferential pathway for radionuclides to migrate. Permeability and *P*-*S* wave velocity measurements were done to determine the thickness of the EDZ and mechanical performance of the lining. Field data were evaluated with three-dimensional numerical analysis finite element software (Flac 3D). Results show that maximum EDZ thickness is no more than 1.0 m because of the strength of the host rock (Kim et al. 2012).

Characteristics of the excavation damaged zone (EDZ) in Kaeri Underground Research Tunnel (KURT) in Korea were researched by Kwon et al. (2009). To explore the EDZ, various in-situ and laboratory tests were carried out.

These are; rock core observation, goodman jack test, borehole radar, laboratory tests, theoretical prediction methods and sensitivity analysis. For in-situ tests, totally ten boreholes were drilled. Seven other boreholes were drilled at first to collect rock mass data before the excavation (excavation was done by drill & blast method) and to install some measuring devices. After the excavation three more boreholes were drilled, and same measurements were repeated to compare the former and latter results. In-situ studies were carried out at 8 m-long turning shelter, which is located about 60 m ahead from the main tunnel entrance. The rock mass was classified as hard rock with a total core recovery (TCR) of 100 and an RMR range from 40 to 60. The geologic formation of the study area is andesitic dykes cut through granite body with thick calcite veins. Besides, slightly weathered zone has been observed also around the joints. Rock core observations showed that, average RQD value obtained from the rock cores at 0-2 m depth where the blasting impact was significant, was 17% lower than the deeper regions. Goodman jack test showed that the deformation modules of the rock mass were influenced from blasting at depth of 1.5-2 m. A borehole radar reflection survey was carried out in a borehole, located at 5.5 m away from the access tunnel. However, satisfactory results were not obtained from the borehole radar surveys and they were not detected a reflection from the EDZ with the measured data. Thickness of the EDZ was predicted as 0.3 –2.3 m from empirical equations. However, the laboratory tests showed the EDZ size could be around 0.9–1.5 m. According to the obtained results, the elastic modules in the EDZ were decreased during excavation at about 56% (Kwon et al. 2009). By using obtained results, relationship between EDZ size and charge density, which is based upon previous data from blasting impact analysis, was suggested as follows;

$$S = 2.0xQ^{1.2} \qquad [21]$$

where, S is the EDZ depth (m) and Q is the linear charge density (kg/m). By using the blasting data at EDZ research area, where the charge density inside the perimeter holes was 0.22–0.37 kg/m, EDZ depth is predicted from the charge density as 0.3-0.6 m (Kwon et al. 2009).

A sensitivity analysis was also performed using the determined EDZ size and properties obtained from the laboratory and in situ tests. According to sensitivity analysis which was done with seven parameters; in-situ stress ratio, Young's modules, and EDZ size of the tunnel were found as the three main parameters, which are mostly affected from the excavation. Increase in the EDZ thickness, increases the displacements and principal stresses on roofs and walls. The principal stresses decrease with increase in depth of EDZ in the floor. Young's modulus of the rock also increased, when the maximum and minimum principal stresses increase. With increase in the horizontal to vertical stress ratio, the maximum and minimum principal stresses increase, too. Displacements, however, decrease on the roof and floor with an increase of the stress ratio (Kwon et al. 2009).

Geomechanical properties of deep disposal repository in crystalline rocks called as the "Underground Research Laboratory" (URL), which is situated in the Lac du Bonnet granite batholith in southeastern Manitoba Canada was researched in another study (Martino and Chandler 2004). The URL was developed to overcome issues related to deep disposal of used fuel from nuclear reactors. It has two major levels (240 and 420 levels) and two drilling stations (130 and 300 levels) accessed by a 443 m deep shaft. Upper part of the shaft from the surface to 255 m depth has rectangular in shape (2.8x4.9 m^2) and the lower part is circular in shape with 5 m in diameter. The shaft and majority of the tunnels were excavated by drilling and blasting. Including the shaft, raises and tunnels, the URL has approximately 2.5 km of underground passages available for experimental activities. Previous experiences showed that; while working in crystalline rocks, main reason of excavation damage zone is a combination of the effects of the excavation method and stress redistribution. Additionally, damage would be unavoidable around the openings when working in high stressed rock environments even if a low-energy excavation method was used. For this reason, extensive rock mechanics research was conducted, which includes understanding the character and extent of excavation damage zone.
The in-situ stress at the URL was determined by more than 1000 overcoring tests, approximately 80 hydraulic fracturing tests, as well as backcalculation of convergence measurements and instrument response calculations.

For determination and comparison of damage zone thickness, two types of experiments were conducted; Tunnel Sealing Experiment (TSX) and Blast Damage Assessment (BDA). The TSX consists of a 30-m-long tunnel with two keyed bulkheads separated by a 12-m-long sand-filled central chamber. Seismic tomography and seismic refraction methods were applied to the TSX experiment tunnel. After that by using borehole camera and core sampling, tunnel walls were observed to determine the depth of the EDZ. The Blast Damage Assessment (BDA) Project was conducted to examine the damage occurring around a drill and blast excavated tunnel on the 240 level of the URL. In DBA tunnel; dimension, orientation and in-situ stress direction were selected identical and the same excavation techniques were used with TSX to make reasonable comparison in terms of the character and extent of damage zones between the two tunnels.

At the end of these studies, two different excavation damage zones were defined (Figure 2.12). These are; zone of irreversible damage, which may involve inner and outer damage zones. And a zone of disturbance, where the in-situ stresses influenced from the excavation; no damage was measured in this zone. Studies showed that, the inner damage zone is affected from the excavation method and stress redistribution, but the outer damage zone is only affected from stress redistribution. In low stress environments; extent of the outer damage zone is lesser than the high stress environments, even if excavation shapes and orientations are the same.

As a summary it can be said that; in-situ stresses, tunnel shape and its orientation relative to the maximum stress, excavation method, subtle changes in rock fabric, application of thermal loads, changes in pore pressure and nearby excavations all affect development of the EDZ. The character of the EDZ was shown to vary significantly around the perimeter of an excavation cross-section. Therefore, proper design of the excavation geometry and orientation will play a major role to construct stable openings (Martino and Chandler 2004).

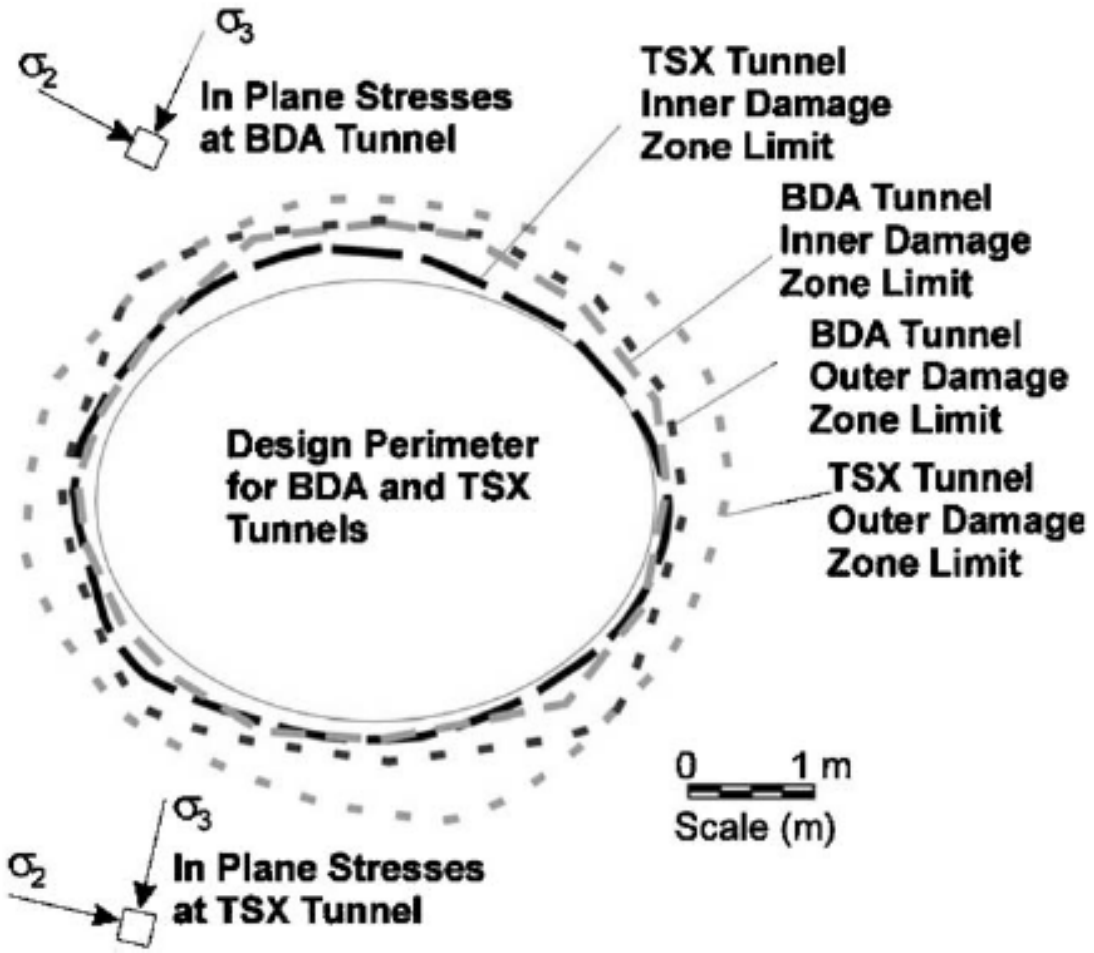

Figure 2.12. Comparison of the extent of the inner and outer damage zone around the TSX and BDA tunnels (Martino and Chandler 2004).

Another study was conducted by Japanese Nuclear Cycle Development Institute (JNCI). The JNCI has carried out a geoscientific research program to determine the geological characteristics of underground nuclear repository site after the excavation. Thus, an in-situ excavation disturbance experiment was performed in the Tono mine in Japan in accordance with this program. Main aim of the program was to safe disposing of high level radioactive wastes in deep geologic formations. Their objective was to determine the dependency of rock mass properties and thickness of the EDZ according to the excavation method. Excavation damage induced by blasting was considered as a primary factor, which causes changes in rock properties. Hence, the damage zone around an excavation was considered as dependency of the excavation method.

On this account, at first an excavation disturbance experiment was performed with mechanical excavation using a boom header in the soft Neogene sedimentary rocks. After that, mechanical excavation results were compared by the drill and blast method to understand the change in properties of rock mass and thickness of the EDZ, which was induced by excavation method. For this purpose; geological observation, rock mass displacement and vibration measurement were performed during the drift excavation.

Moreover, seismic refraction and tomographic surveys, borehole expansion test and hydraulic test were performed before and after the drift excavation. The research has shown that changes in rock properties and thickness of the EDZ particularly depend on the excavation method. Displacement monitoring and FEM based numerical analysis results indicated that the rock mass around the test drift behaves more elastic in machine excavation (EDZ thickness is no more than 0.5 m) when it is compared to blasting method (EDZ thickness is roughly 3.0 m) (Sato et al. 2000).

Another research about determination of EDZ is by Siren et al. (2015). In this study, two different kinds of EDZ were defined; construction-induced (EDZ_{CI}) and stress-induced (EDZ_{SI}) excavation damage zones.

Even if it is easy to distinguish between construction-induced damage zone and stress-induced damage zone in hard rock masses, description difficulties of these zones in softer rock masses have been highlighted. Therefore, two underground geological nuclear waste disposal laboratories excavated in hard rocks in Sweden, were used. The research and development have been continued between 2010 and 2013 with in-situ stress measurements. As rock mass strength, hydraulic conductivity and other rock mass properties are important for long term safety assessment of nuclear waste disposal, effects of drill-blast and TBM excavations to these parameters in excavation damage zone were researched. For this aim, besides the several known distinction methods, GPR based EDZ method, which is based on frequency analysis of reflected signals, was also used to distinguish the zone with increased rock damage. As the depth of the stress-induced damage is less than the depth of the construction-induced damage, GPR based EDZ method was found insufficient for distinction of these zones.

As a result of the study, it was found that while the construction-induced excavation damage zone is effective at whole tunnel perimeter, the stress-induced excavation damage zone is effective only at stress peaks. The effects of EDZ_{SI} can still be seen all-around the tunnel perimeter. However, these effects were not observed significantly in TBM excavation (Siren et al. 2015). As selected research area was nuclear repository site, it was a must to choose a hard and massive host rock. Therefore, no clear tangible result was observed for damage zone thickness.

Instead, some changes in hydraulic conductivity and rock mass properties with *p* and *s* wave velocity changes were reported. This study is another good example to highlight the effect of excavation method to the host rock and changing properties of rock mass around an excavation.

2.1.3.3. Back-analysis methods

Back analysis is one of the most practical methods in tunnel design applications. Deformability and ground strength parameters of excavated tunnel sections can be calculated from back-analyses (Jinga and Hudson 2002, Wu et al. 2004, Hisatake and Hieda 2008). In this method, measured ground deformations are used for generating criteria matching between observed and predicted responses. This method, if applied properly, gives more reliable values for ground parameters than the direct measurements, which are done by laboratory or standard field tests (Kavvadas 2005). Namely, even preliminary geological, geotechnical and geophysical studies have been applied to tunnel axis for defining complete geomechanical characterization of the ground, it is not always possible to explore every geotechnical and geomechanical characteristics of the rock mass. It is often not feasible to obtain complete characterization of the ground from the preliminary studies. For this reason, during construction of a tunnel itself or excavation of a pilot tunnel, it will only be possible to obtain complete evaluation for behavior of the rock mass. So, displacements and load results obtained from back-analysis which includes various numerical methods can be used to calibrate the initial estimations of geomechanical parameters of the ground. So, back-analysis can be defined as determination of the rock mass parameters that are used to reduce difference between in-situ monitoring and calculation results (Pierpaolo 2005).

Because of the reasons, which are explained above, previous deformation monitoring measurements, field studies, laboratory test results and rock mass geotechnical properties can be used in design stage of tunnels for the prediction of convergences and plastic zone thickness. There are many studies in literature about back analysis techniques in tunnel design (Sakurai and Takeuchi 1983, Kim and Chung 2002, Kontogianni and Stiros 2002, Sakurai et al. 2003, Bizjak and Petkovsek 2004, Pierpaolo 2005, Zhang et al. 2006, Sharifzadeh et al. 2012). Amongst them, back analysis techniques have been used in different manners, which are given below shortly.

Sakurai and Takeuchi (1983) used back-analysis application in tunnels as a method for interpretation of field monitoring data for the stability of tunnels. In the proposed formulation assumes excavation ground media is linear, isotropic and elastic. A case study was also presented at the end of this study in order to verify the applicability of the proposed method. In this study, back analyses procedure based on FEM used for determining the initial stresses and young modulus of the rock mass from displacement measurements

In Bizjak and Petkovsek (2004) study; back-analysis and numerical modeling method were applied to the most expensive tunnel in terms of construction per meter ever built in Slovenia. These studies were performed to calculate propagation of stresses around the tunnel with help of finite difference method. The spatial distribution of rock displacements was analyzed by using Mohr–Coulomb criterion in strain softening constitutive model. Time dependent development and prediction of final displacements through the first measured data were achieved by means of ANN. When compared with back analysis, good agreement was established between calculated and measured results in accordance with geodetic monitoring.

Prediction of tunnel displacements by using previously occurred and recorded displacements at the same tunnel was explained in Kim and Chung (2002) study. This study especially focused on evaluation of the unmeasured displacements developed at the initial stage of tunnel excavation which can't be measured. For this aim, estimated total displacements used to predict final displacements. Actual measurements in four highway tunnels in Korea were used for generation of a statistical prediction model and results were compared with displacements obtained from 3 dimensional FEM analyses of those tunnels. Totally, five types of support and excavation systems were determined and final convergences value was predicted for 1D face advance distance. Even if, it was difficult to find the displacements precisely behind the face, it was found as more than 28% of convergences are lost during measurement of convergences.

In Kontogianni and Stiros (2002), convergence of shallow tunnels (30–120 m overburden thickness) constructed in Greece in different types of rock masses (especially GSI ranging from 15 to 65) was assessed as a function of the GSI classification. Predictions of maximum vertical and horizontal convergences, during or shortly after tunnel excavation were made using (FEM). The results from FEM were found to be adequately and reliably predict the expected deformation during tunnel excavation. Predicted convergence from FEM and geodetically observed convergence were found to be in agreement, and the difference between the two values was found as up to 2 mm only.

A bunch series of back-analysis procedures were explained by Sakurai et al. (2003) study. In the study, input requirements for back-analysis models, identification of structures and flows of forward analysis versus back-analyses were discussed. These back-analysis procedures; Direct Back Analysis Program (DBAP), In Homogeneous Non-Linear Direct Back Analysis Program (I-N-DBAP) and Back Analysis of Non-linear Strain for Jointed Rock Mass in Incremental (BANSJI), were explained including application examples for shallow tunnels in soft grounds and for large underground caverns in hard discontinuous rock mass. Aim of this study was to show its limitations, area of use and procedures rather than the application of back-analysis technique itself.

In Pierpaolo (2005) study, it has been proposed a new efficient back-analysis technique for correct interpretation of convergence monitoring data, which are obtained from the tunnel construction. Some considerations concerning geomechanical parameters that are identified easily through correct interpretation of monitoring data were discussed. An example of back-analysis for a real case was presented in the study to illustrate the consistency of evaluation of the proposed procedure. Elastic modulus, poisson’s ratio, cohesion, internal friction angle and dilatancy values of the rock mass were used to predict some other parameters such as coefficient of the lateral earth pressure, rock mass residual strength parameters, which are very difficult to determine with preliminary investigations.

The given example emphasizes the importance of preliminary qualitative evaluation of initial back-analysis results to reliably steer calculation towards the final solution. Besides it was also draw attention to the parameters which are the greatest influence on the solution of this kind of a problem.

Zhang et al. (2006) tried to determine rock mass modulus (E) and horizontal in-situ stress value (P), which is perpendicular into the axis line of tunnel excavation in hard intact rock masses by using Displacement Based Back-Analysis Method (DBBA). Basic principles of the DBBA method were also provided. Given process is a kind of best-fit solution method for back-analysis applications, which compare measured displacements near the tunnel face during an excavation with those calculated using a three-dimensional finite element method. The use of this method is mainly suggested for determination of E and P values of rock masses that are virtually assumed isotropic, homogeneous and linear elastic.

In Sharifzadeh et al. (2012) study, stability problems and the solutions were evaluated for Shibli tunnel, in Iran with help of two-dimensional explicit finite difference software (Flac2d) and back analysis procedure. These procedures were applied for three-collapsed zones inside the tunnel to find correct design parameters of disturbed rock mass. Direct approach of displacement-based back analysis method, which is based on optimization of mechanical properties of rock mass by trial and error, was preferred to grasp an optimized identification of disturbed rock mass parameters. Through application of back analysis technique on three collapsed zones, the most probable rock mass strength parameters at the instances of collapses occurrence were identified. By using results obtained from the back analysis displacement values in the collapsed zones were assessed.

Taking into account the existing facilities and resources on the project site such as excavation machinery, steel frames, rolling system and also power and type of shotcreting equipment, three different SEM designs were suggested. This study revealed the importance of back-analysis method for both determining rock mass parameters and also the excavation sequence.

CHAPTER 3

DATA COLLECTION AND ANALYSIS

3.1. Data Collection Methodology

In this study, engineering characteristics of tunnel routes in terms of geology, engineering geology and geotechnical properties of the rock masses were determined by means of field and office studies. These studies include; literature surveys, geotechnical drillings and laboratory studies. In this context, geotechnical drilling and engineering geology studies were used to understand geology, and geotechnical properties of the rocks along the tunnel construction route. All of the data described above were collected from different tunnel excavation sites from various regions of Turkey. In this context two types of data were obtained; geotechnical properties and convergence measurements. While the geotechnical properties of the tunnel rock masses were collected from geotechnical drillings and site investigation, the convergence measurements were collected from the perimeter of the tunnel excavations.

As it is not possible to drill every section of the tunnel route, geotechnical data could only be get from limited drilling works. Therefore, it was not possible to have precise information about geology and geotechnical properties for all part of the tunnel rock mass. To obtain more reliable results, tunnel sections which are intersecting with geotechnical drilling data were selected both for the collection of geotechnical data and the prediction of convergences. Tunnel wall convergences were measured by optical measurement devices in three-dimensional space. Three out of five convergence monitoring points were selected for analysis. One of them was taken from the roof, one from the left shoulder and the other one was taken from the right shoulder.

The other two points, located on the lower left and right walls were ignored because no more displacements were observed in these points after the installation of supporting elements. At these points, all of the final convergence values were converted into a resultant vector values and the amount of the resultant vector was used in statistical models.

3.2. Geology and Geotechnical Properties of the Studied Tunnels

Different geological units and their interconnections with each other were tried to be identified by field and office studies for tunnel excavation sites. For geological-geomechanical description and convergence data collection, totally 9 tunnel sites in 142 tunnel sections were investigated in this thesis. Among these, 4 of them were only used for statistical modelling (Konak, Zonguldak1, Zonguldak2 and Puren tunnels), 2 of them were used both for statistical modelling and validation purposes (Tekir and Caglayan tunnels left and right tubes). Yet, this time while left tubes were selected for generation of statistical modelling, right tubes were used for validation. The rest 3 tunnels were only used for validation purpose (Eceabat1, Eceabat2 and Tirebolu2 tunnels). In this section general geological description of rocks along the tunnels, which are used for statistical modelling and validation, were given here briefly. Detailed geotechnical properties of the units, were also given in this section. As there are too many (112) geological cross-sections used in the statistical modelling part, it was avoided to give all of them in detail. Geotechnical properties of the units which are used for validation are not given here but explained in the validation section. Descriptive geological cross-sections of the validation tunnels were presented in Appendix B. Location of all tunnels which are considered in this study is shown in Figure 3.1.

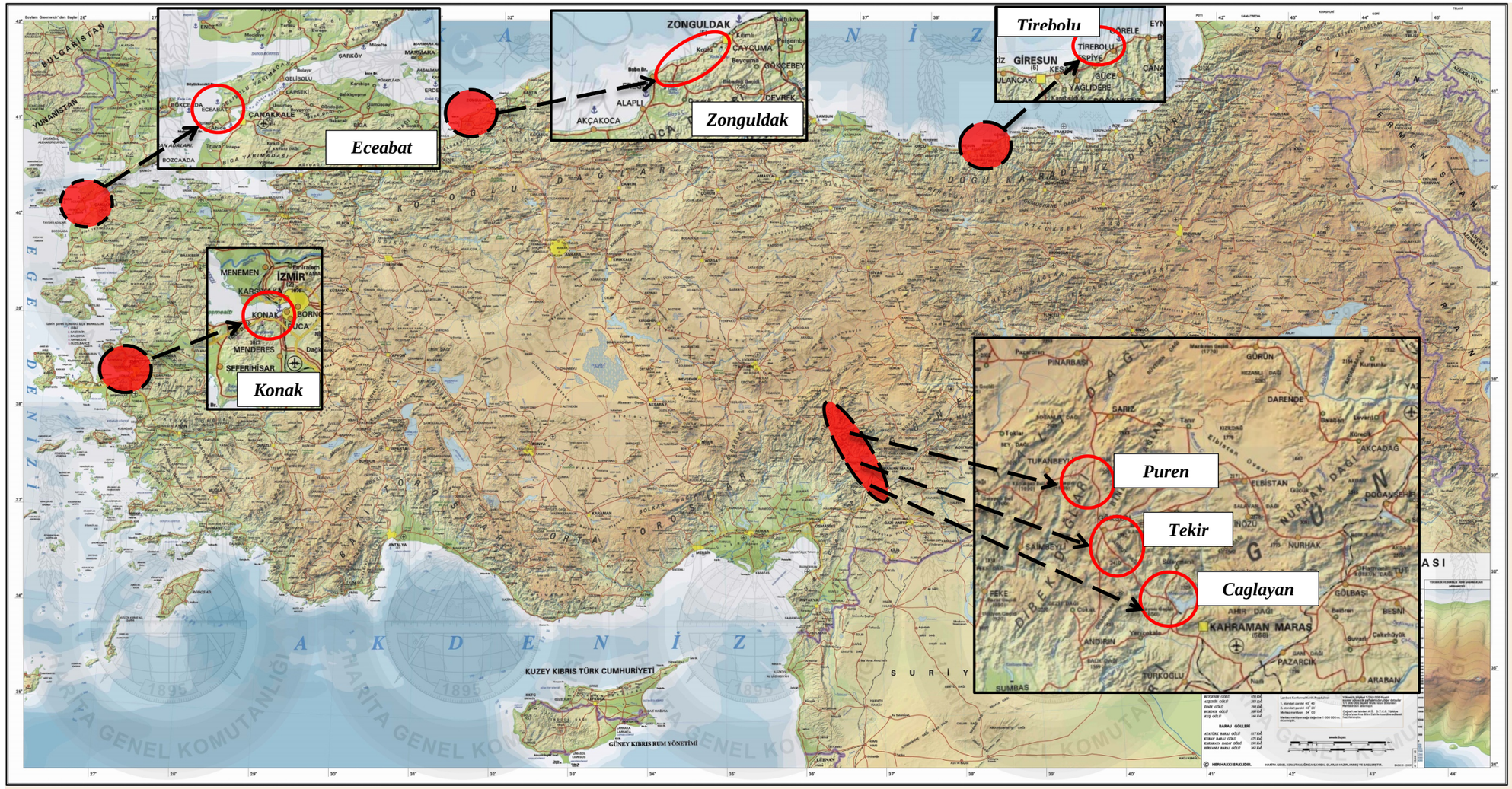

Figure 3.1. Location of the tunnels used in this study.

3.2.1 General geology of the Caglayan Tunnel

Caglayan Tunnel is located on the main highway between Kayseri and Kahramanmaras provinces. This route connects Central Anatolia to southern part of Turkey. The tunnel was designed as a double tube each has 2500 m in length. At the site investigation stage, twenty-two geotechnical drilling and field studies with rock mass classifications were performed along the tunnel route. According to site investigation studies; serpantinitic peridodite, weathered claystone-mudstone, sandstone interbedded conglomerate, sandstone-claystone intercalation, conglomerate-sandstone-claystone intercalation, claystone unit and residual soil were observed as main geological units in the study area.

3.2.2 General geology of the Eceabat T1 Tunnel

Eceabat T1 Tunnel is located in the Gallipoli Peninsula, which is in the north-western and European part of Turkey. The tunnel was designed as single tube which is 2515 m in length. At the site investigation stage, six geotechnical drilling and site studies with rock mass classifications were performed on the tunnel route. According to field investigation studies, sandstone and claystone units have been determined in the whole tunnel excavation area. Sandstone unit is partly intercalated with claystone and sand bands observed locally in some parts of it. Claystone unit is partly intercalated with sandstone, and fossil shells can also be seen.

3.2.3 General geology of the Eceabat T2 Tunnel

Eceabat T2 Tunnel is located in the Gallipoli Peninsula, which is in the north-western and European part of Turkey. The tunnel was designed as single tube which is 1430 m in length. At the site investigation stage, four geotechnical drilling and field studies with rock mass classifications were performed on the tunnel route.

According to the site investigation studies, sandy and sand intercalated and sand banded claystone units have been determined. In some parts of the tunnel alignment, these units grades into sand band, sand and gravel intercalated sandstone unit.

3.2.4. General geology of the Konak Tunnel

Konak tunnel is located on the south coast of İzmir. It was designed and constructed as an urban double tube tunnel with a length of 3290 m. Limited site investigation studies were performed, as the tunnel is placed in a densely populated residential district. Therefore, twenty-one geotechnical drilling and limited field studies with rock mass classifications were performed on the tunnel route. On the other hand, excavation material was regularly evaluated and face mapping was continuously recorded, and during the excavation stage rock mass classifications were cross-checked with the existing design criteria. According to these studies; andesite, conglomerate, andesitic tuff, tuff, weathered andesite, sandstone, claystone and siltstones were identified as main geological units in the study area.

3.2.5 General geology of the Puren Tunnel

Puren Tunnel is located on the main highway between Kayseri and Kahramanmaras provinces. This route connects Central Anatolia to southern part of Turkey. The tunnel was designed as a double tube each has 2808 m in length. Owing to the tunnel route's steep and abrupt morphology, only seven geotechnical drilling have been performed during the field investigation stage. Most of the engineering geology works were completed in the field with rock mass classifications on the tunnel route. According to the site investigation studies; clay-claystone intercalation, claystone, claystone-limestone intercalation and fault breccia were determined as main geological units along the tunnel route.

3.2.6 General geology of the Tekir Tunnel

Tekir Tunnel is located on the main highway between Kayseri and Kahramanmaras provinces. This route connects Central Anatolia to southern part of Turkey. The tunnel was designed as a double tube, each having 1154 m length. Tunnel route's steep topography causes the accessibility problems and this makes difficult to reach the geotechnical drilling points on top of the tunnel axis. Therefore, six geotechnical drilling have been performed during the site investigation stage. Most of the engineering geology works have been in the field with rock mass classifications on the tunnel route. According to the site investigation studies, conglomerate-sandstone intercalation and limestone were identified as main geological units along the tunnel axis.

3.2.7 General geology of the Tirebolu 2 Tunnel

Tirebolu 2 Tunnel is located on the north coast of Turkey, between Trabzon and Giresun provinces. The tunnel is part of one of the biggest projects of Turkey, so-called Black Sea Coastal Road. The tunnel was designed as a double tube each having 625 m length. At the site investigation stage, ten geotechnical drilling and field studies with rock mass classifications were performed along the tunnel route. Geotechnical drilling has been performed to reveal the engineering geology model and geomechanical properties of the host rock. Depending on the site investigation studies and geotechnical drilling results, most of the geological units of the Tirebolu 2 tunnel were characterized as volcanic rocks which are mainly tuff, tuffite, agglomerate, basalt and dacite.

3.2.8 General geology of the Zonguldak Eregli Road Left Tunnel 1 and 2

Zonguldak Eregli road is located on the north-east coast of Turkey which connects two coastal provinces of Black Sea Region; Bartın and Zonguldak to the Turkey's biggest city, Istanbul. The tunnels 1 and 2 were designed to be constructed next to an existing one as a single tube which are 344 m and 1445 m in length, respectively. So, both new tunnels will be at service only in one direction after the construction. Doubling up an existing tunnel comes with some benefits, such as the use of former tunnel data. However, construction of a new tunnel next to an existing one requires delicacy, as there is a risk of widening plastic zone thickness during the excavation of new tunnel. During the site investigation stage, three geotechnical drilling and field studies with rock mass classifications were performed on the left tunnel 1, and five for the left tunnel 2, respectively. Besides, excavation records of the former tunnels have also been used. According to the site investigation studies, thickly bedded massive limestone, thinly to thickly bedded conglomeratic sandstone, siltstone, claystone and limestone intercalation were identified as the geological units of the left tunnel 1. For the left tunnel 2; thinly bedded conglomeratic limestone, conglomerates-mudstone intercalation, thinly to thickly bedded limestone, sandstone geological units were observed. Descriptive brief information for all of the studied tunnels were given in Table 3.1.

3.2.9 Geotechnical properties of the tunnels used for statistical modelling

By using longitudinal profiles, geological cross-sections and geomechanical properties of the rock masses, tunnel routes were divided into sections which show similar rock mass characteristics. Data for 112 tunnel sections were used from 6 different tunnel excavation sites to generate statistical estimation model. After that, data for 30 tunnel sections were used to validate the statistical model from 5 different tunnel excavation sites. Geotechnical properties of these data and results of the validation are given in validation section. Intact rock geomechanical properties which are uniaxial compressive strength (σ_i), modulus of elasticity (E_i), RQD (Deere and Miller 1966), natural water content (γ_i) and poison ratio (ν), were

determined by using core samples obtained from geotechnical drilling with the help of laboratory studies. These data (σ_i, E_i, RQD, γ_i, ν) were used to obtain rock mass strength parameters. In order to prevent multicollinearity[1], these data were not taken into consideration directly in statistical modelling. After all, rock mass geotechnical properties such as cohesion, internal friction angle and deformation moduli were identified by using these data following Hoek et al. (2002) and Hoek and Diederichs (2006) approaches. As a result, RMR (Bieniawski 1989), Q (Barton 2002), C_{rm}, ϕ_{rm}, E_{rm} and H parameters were selected as independent variables. Detailed rock mass and tunnel section properties are given in Table 3.2 (Details of this table are given in Appendix C).

[1] Multicollinearity refers to a situation where a number of independent variables in a multiple regression model are closely correlated to one another. Multicollinearity can lead to skewed or misleading results when a researcher or analyst is attempting to determine how well each one of a number of individual independent variables can most effectively be utilized to predict or understand the dependent variable in a statistical model.

Table 3.1 Descriptive brief information for all of the studied tunnels

Tunnel Name	Length (m)	Single or Double Tube	Location in Turkey	Geological Units
Caglayan	2500	Double tube	Kayseri - Kahramanmaras	Serpantinitic peridodite, weathered claystone-mudstone, sandstone interbedded conglomerate, sandstone-claystone intercalation, conglomerate-sandstone-claystone intercalation, claystone unit and residual soil
Eceabat T1	2515	Single tube	Gallipoli Peninsula	Sandstone and claystone units, sandstone unit is partly intercalated with claystone and sand bands observed locally, claystone unit is partly intercalated with sandstone, and fossil shells can also be seen
Eceabat T2	1430	Single tube	Gallipoli Peninsula	Sandy and sand intercalated and sand banded claystone units have been determined, in some parts of the tunnel alignment, these units grades into sand band, sand and gravel intercalated sandstone unit
Konak	3290	Double tube	Izmir	Andesite, conglomerate, andesitic tuff, tuff, weathered andesite, sandstone, claystone and siltstones
Puren	2808	Double tube	Kayseri - Kahramanmaras	Clay-claystone intercalation, claystone, claystone-limestone intercalation and fault breccia
Tekir	1154	Double tube	Kayseri - Kahramanmaras	Conglomerate-sandstone intercalation and limestone
Tirebolu 2	625	Double tube	Trabzon – Giresun	Volcanic rocks which are mainly tuff, tuffite, agglomerate, basalt and dacite
Zonguldak Eregli T1	344	Single tube	Bartin – Zonguldak	Thickly bedded massive limestone, thinly to thickly bedded conglomeratic sandstone, siltstone, claystone and limestone intercalation
Zonguldak Eregli T2	1445	Single tube	Bartin – Zonguldak	Thinly bedded conglomeratic limestone, conglomerates-mudstone intercalation, thinly to thickly bedded limestone, sandstone

Table 3.2. Descriptive tunnel convergence data and geotechnical properties of the tunnels, which are used for generation of statistical modelling

Tunnel Section		Dependent Variables								H (m)	Inputs of Independent Variables					Independent Variables*				
	Km	RS-Y (mm)	RS-Y' (%)	R-Y (mm)	R-Y' (%)	LS-Y (mm)	LS-Y' (%)	$\bar{Y}$(mm)	$\bar{Y}'$(mm)		RQD	σ_i (MPa)	E_i (MPa)	γ_n (MN/m^3)	υ	RMR	Q	C_{rm} (MPa)	ϕ_{rm} (°)	E_{rm} (MPa)
KONAK TUNNEL	0+605	28.23	0.374	27.00	0.358	32.54	0.431	29.26	0.388	7.55	28.84	6.06	107.5	0.0203	0.3	34.66	0.12	0.018	32.56	4.65
	0+606	16.43	0.317	22.32	0.431	18.41	0.355	19.05	0.368	5.18	28.84	6.06	107.5	0.0203	0.3	34.66	0.12	0.015	35.28	4.65
	0+609	17.52	0.358	17.61	0.359	18.22	0.372	17.78	0.363	4.9	28.84	6.06	107.5	0.0203	0.3	34.66	0.12	0.014	35.68	4.65
	0+613	29.27	0.367	20.22	0.254	23.35	0.293	24.28	0.305	7.97	10.77	4.61	1285	0.0212	0.377	32.03	0.04	0.015	28.55	49.41
	0+614	21.68	0.364	20.25	0.340	24.88	0.417	22.27	0.374	5.96	10.77	4.61	1285	0.0212	0.377	32.03	0.04	0.012	30.61	49.41
	0+620	26.44	0.357	23.85	0.322	63.70	0.860	38.00	0.513	7.41	17.86	3.07	960	0.0218	0.392	32.75	0.07	0.012	26.59	38.1
	0+622	26.31	0.280	26.70	0.284	31.03	0.330	28.01	0.298	9.4	17.86	3.07	960	0.0218	0.392	32.75	0.07	0.014	24.96	38.1
	0+643	47.09	0.304	30.72	0.198	55.04	0.355	44.28	0.286	15.5	16.73	2.47	178.5	0.0214	0.37	32.54	0.07	0.017	20.2	7.02
	0+650	43.84	0.285	43.06	0.280	53.25	0.346	46.72	0.304	15.38	16.73	2.47	178.5	0.0214	0.37	32.54	0.07	0.017	20.25	7.02
	0+652	45.55	0.259	56.47	0.321	53.38	0.303	51.80	0.294	17.6	10.98	10.73	2180	0.0231	0.37	32.70	0.05	0.035	28.68	86.32
	0+655	59.21	0.355	64.16	0.384	37.43	0.224	53.60	0.321	16.69	16.73	2.47	178.5	0.0214	0.37	32.54	0.07	0.017	19.75	7.02
	0+660	67.74	0.414	65.19	0.398	37.13	0.227	56.69	0.347	16.36	10.98	10.73	2180	0.0231	0.37	32.70	0.05	0.034	29.2	86.32
	0+667	32.39	0.169	41.04	0.214	30.30	0.158	34.57	0.180	19.22	10.98	10.73	2180	0.0231	0.37	32.70	0.05	0.037	28.06	86.32
	0+754	11.58	0.034	7.21	0.021	17.15	0.050	11.98	0.035	34.02	16.02	10.18	1598	0.0229	0.368	33.27	0.18	0.083	36.31	64.9
	0+960	95.05	0.161	81.55	0.139	80.47	0.137	85.69	0.146	58.87	17.68	3.24	960	0.0221	0.3	32.75	0.10	0.041	14.24	38.08
	0+993	71.20	0.120	55.88	0.095	41.44	0.070	56.17	0.095	59.11	17.68	3.24	711	0.0221	0.3	32.75	0.10	0.041	14.22	28.2
	1+152	62.68	0.076	53.83	0.065	76.85	0.093	64.46	0.078	82.23	44.68	19.78	711	0.0212	0.3	38.76	0.25	0.153	30.22	37.94
	1+535	95.19	0.097	101.48	0.103	66.41	0.068	87.69	0.089	98.32	30.23	37.04	6000	0.0246	0.344	38.18	0.17	0.311	39.91	310.22
	1+730	44.64	0.049	42.76	0.047	36.29	0.040	41.23	0.045	91.69	26.18	27.82	4080	0.0243	0.364	49.57	4.36	0.386	46.52	420.06
	1+739	53.93	0.059	61.81	0.068	67.04	0.074	60.93	0.067	91.09	26.18	27.82	4080	0.0243	0.364	49.57	4.36	0.384	46.57	420.06
	1+958	50.45	0.080	30.95	0.049	29.31	0.047	36.90	0.059	62.97	38.91	56.75	9200	0.0252	0.309	47.20	2.59	0.383	53.24	812.23
	1+979	44.30	0.074	46.24	0.077	61.64	0.103	50.73	0.085	59.82	38.91	56.75	9200	0.0252	0.309	47.20	2.59	0.371	53.59	812.23
	2+175	86.47	0.237	50.69	0.139	25.81	0.071	54.32	0.149	36.56	33.04	38.69	6010	0.0241	0.337	38.80	0.18	0.174	49.09	321.21
	2+186	36.89	0.106	43.15	0.124	35.62	0.103	38.56	0.111	34.71	6.65	34.91	5880	0.0239	0.325	34.79	0.04	0.144	46.91	256.07
	2+186	93.69	0.272	51.58	0.150	63.04	0.183	69.44	0.202	34.39	6.65	34.91	5880	0.0239	0.325	34.79	0.04	0.143	46.98	256.07
	2+196	39.96	0.132	26.65	0.088	32.57	0.108	33.06	0.109	30.23	14.96	6.30	110	0.0218	0.3	32.72	0.08	0.064	34.66	4.36
	2+197	36.99	0.127	24.52	0.084	26.89	0.092	29.46	0.101	29.17	14.96	6.30	110	0.0211	0.3	32.72	0.08	0.062	35.18	4.36
TEKIR TUNNEL (Left Tube)	55+328	28.05	0.238	17.26	0.147	18.97	0.161	21.43	0.182	11.77	58.69	13.41	10550	0.0243	0.23	38.19	0.16	0.056	48.82	545.62
	55+333	11.00	0.084	15.84	0.121	16.43	0.126	14.42	0.110	13.06	48.23	15.11	12230	0.0246	0.23	36.41	0.13	0.06	48.02	576.65
	55+398	16.19	0.054	17.92	0.060	17.26	0.058	17.12	0.057	29.96	58.69	13.41	10550	0.0243	0.23	38.19	0.32	0.102	41.83	545.62
	55+403	27.93	0.116	16.67	0.069	16.03	0.067	20.21	0.084	24.01	48.23	15.11	12230	0.0246	0.23	36.41	0.27	0.089	43.49	576.65
	55+724	18.60	0.013	21.56	0.015	18.55	0.013	19.57	0.013	145.42	41.21	29.64	10680	0.0252	0.25	46.70	2.06	0.464	39.17	913.9
	55+729	20.93	0.014	24.84	0.017	19.31	0.013	21.69	0.015	146.43	41.21	29.64	10680	0.0252	0.25	46.70	2.06	0.466	39.11	913.9
	55+794	21.42	0.016	20.49	0.015	17.97	0.013	19.96	0.015	137.45	41.21	29.64	10680	0.0252	0.25	46.70	2.06	0.447	39.61	913.9
	55+799	19.90	0.014	22.23	0.015	24.29	0.017	22.14	0.015	146.07	41.21	29.64	10680	0.0252	0.25	46.70	2.06	0.465	39.13	913.9
	55+859	25.50	0.021	26.02	0.021	24.84	0.020	25.45	0.021	121.33	41.21	29.64	10680	0.0252	0.25	46.70	2.06	0.413	40.59	913.9
	55+864	19.75	0.018	13.93	0.013	18.81	0.017	17.50	0.016	111.25	41.21	29.64	10680	0.0252	0.25	46.70	2.06	0.391	41.27	913.9
	56+278	14.35	0.039	18.22	0.050	21.12	0.057	17.90	0.049	36.73	58.22	20.02	8340	0.0247	0.29	45.80	0.96	0.163	46.54	674.18

Table 3.2. continued

	56+283	14.53	0.046	20.32	0.064	13.38	0.042	16.08	0.051	31.7	58.22	20.02	8340	0.0247	0.29	45.80	0.96	0.149	47.64	674.18
	56+348	16.79	0.056	14.76	0.049	17.72	0.059	16.43	0.054	30.14	58.22	20.02	8340	0.0247	0.29	45.80	0.96	0.144	48.01	674.18
	56+353	20.05	0.068	18.57	0.063	20.81	0.070	19.81	0.067	29.57	58.22	20.02	8340	0.0247	0.29	45.80	0.96	0.143	48.16	674.18
	56+400	16.88	0.079	18.49	0.087	15.78	0.074	17.05	0.080	21.24	39.09	18.72	12800	0.0235	0.32	35.18	0.32	0.083	45.76	567.95
	56+418	16.43	0.150	18.97	0.173	14.87	0.135	16.76	0.152	10.99	29	14.23	8620	0.0240	0.24	33.05	0.24	0.047	47.39	346.65
	56+447	14.53	0.237	25.61	0.418	16.82	0.274	18.99	0.310	6.13	39.09	18.72	12800	0.0235	0.32	35.18	0.32	0.038	54.46	567.95
	56+453	15.68	0.272	14.76	0.256	15.94	0.277	15.46	0.268	5.76	29	14.23	8620	0.0240	0.24	33.05	0.24	0.031	51.92	346.65
ZON. ERG. TUN. 1	2+234	22.23	0.095	71.26	0.305	24.45	0.105	39.31	0.168	23.4	85	58.55	13595.25	0.0273	0.4895	66.27	2.13	0.537	60.32	3963.79
	2+243	23.62	0.091	36.25	0.139	33.12	0.127	31.00	0.119	26.1	85	58.55	13595.25	0.0273	0.4895	66.27	4.25	0.548	59.82	3963.79
	2+260	12.88	0.022	14.14	0.024	15.78	0.027	14.27	0.024	58.9	85	58.55	13595.25	0.0273	0.4895	66.27	4.25	0.684	55.54	3963.79
	2+426	12.88	0.015	13.15	0.015	16.76	0.019	14.27	0.016	87.7	69	43.61	9672.25	0.0261	0.4277	60.44	5.75	0.544	49.52	2008.81
	2+449	14.53	0.017	9.11	0.010	9.27	0.011	10.97	0.013	86.95	69	43.61	9672.25	0.0261	0.4277	60.44	5.75	0.542	49.58	2008.81
	2+469	14.07	0.019	17.15	0.024	16.67	0.023	15.96	0.022	72.9	69	43.61	9672.25	0.0261	0.4277	60.44	5.75	0.495	50.81	2008.81
	2+547	12.69	0.060	13.30	0.063	12.81	0.060	12.93	0.061	21.2	77.5	60.98	13049	0.0266	0.5485	58.00	1.29	0.338	59.52	2327.17
	2+561	8.83	0.067	8.77	0.067	9.49	0.072	9.03	0.069	13.1	77.5	60.98	13049	0.0266	0.5485	58.00	1.29	0.301	61.8	2327.17
ZON. ERG. TUN. 2	2+873	41.33	0.343	28.76	0.239	37.71	0.313	35.93	0.298	12.05	40	92.57	55558	0.0268	0.27	53.20	0.23	0.364	58.67	7256.21
	2+893	24.29	0.130	23.85	0.128	31.59	0.169	26.58	0.143	18.64	40	92.57	55558	0.0268	0.27	53.20	0.23	0.386	56.81	7256.21
	2+911	28.72	0.130	28.58	0.130	45.45	0.206	34.25	0.155	22.07	40	92.57	55558	0.0268	0.27	53.20	0.23	0.398	56.01	7256.21
	2+927	20.98	0.081	21.86	0.084	20.83	0.080	21.22	0.082	26	21.63	21.23	60570	0.0255	0.29	47.71	0.13	0.127	44.19	5525.11
	2+947	17.92	0.049	22.05	0.060	18.49	0.050	19.49	0.053	36.67	21.63	21.23	60570	0.0255	0.29	42.71	0.17	0.131	39.47	4047.85
	2+963	12.81	0.036	20.10	0.056	15.59	0.043	16.16	0.045	35.92	21.63	21.23	60570	0.0255	0.29	45.71	0.38	0.142	40.93	4865.66
	2+981	16.79	0.046	18.97	0.052	23.73	0.065	19.83	0.054	36.65	21.63	21.23	60570	0.0255	0.29	45.71	0.38	0.143	40.78	4865.66
	3+003	15.52	0.042	22.18	0.060	15.65	0.042	17.79	0.048	36.95	21.63	21.23	60570	0.0255	0.29	42.71	0.38	0.132	39.41	4047.85
	3+277	11.87	0.013	12.45	0.014	9.38	0.010	11.24	0.013	89.59	29.37	45.34	106045	0.0260	0.275	38.43	0.16	0.316	40.8	5555.35
	3+301	9.43	0.011	12.08	0.014	9.00	0.011	10.17	0.012	85.41	29.37	45.34	106045	0.0260	0.275	38.43	0.16	0.306	41.17	5555.35
	3+328	8.25	0.011	8.12	0.011	8.37	0.011	8.25	0.011	77.09	29.37	45.34	106045	0.0260	0.275	38.43	0.16	0.222	33.92	5555.35
	3+351	5.39	0.007	6.71	0.009	8.37	0.011	6.82	0.009	73.4	29.37	45.34	106045	0.0260	0.275	38.43	0.16	0.216	34.33	5555.35
	3+378	6.00	0.008	5.39	0.008	5.74	0.008	5.71	0.008	71.02	29.37	45.34	106045	0.0260	0.275	38.43	0.16	0.212	34.54	5555.35
	4+225	3.00	0.007	4.58	0.011	3.46	0.008	3.68	0.009	42.62	59.62	52.52	88220	0.0265	0.2667	56.04	3.93	0.378	46	13861.52
	4+242	3.74	0.012	5.10	0.016	3.00	0.009	3.95	0.012	32.17	59.62	52.52	88220	0.0265	0.2667	56.04	3.93	0.353	47.72	13861.52
	4+264	2.45	0.009	5.10	0.019	3.74	0.014	3.76	0.014	26.17	59.62	52.52	88220	0.0265	0.2667	56.04	3.93	0.338	48.9	13861.52
	4+298	3.00	0.022	3.00	0.022	3.46	0.025	3.15	0.023	13.94	59.62	52.52	88220	0.0265	0.2667	56.04	3.93	0.309	52.04	13861.52
CAGLAYAN TUNNEL (Left Tube)	48+788	6.78	0.021	7.14	0.022	6.08	0.019	6.67	0.021	32.407	43.36	22.03	14277.5	0.0239	0.2625	37.77	0.06	0.085	31.73	722.12
	48+839	17.23	0.045	20.20	0.053	19.13	0.050	18.85	0.049	38.439	11.05	37.64	18020	0.0244	0.205	37.74	0.01	0.123	34.21	909.97
	48+840	30.64	0.076	24.78	0.061	24.86	0.062	26.76	0.066	40.41	11.05	37.64	18020	0.0244	0.205	37.74	0.01	0.126	33.85	909.97
	48+903	15.84	0.034	15.84	0.034	19.54	0.042	17.08	0.037	46.673	11.05	37.64	18020	0.0244	0.205	37.74	0.01	0.135	32.8	909.97
	48+904	9.49	0.022	11.00	0.025	10.68	0.025	10.39	0.024	43.436	11.05	37.64	18020	0.0244	0.205	37.74	0.01	0.13	33.32	909.97
	49+044	33.42	0.057	29.43	0.050	29.43	0.050	30.76	0.052	58.993	13.83	15.67	8220	0.0236	0.278	37.58	0.05	0.098	25.06	411.62
	49+343	7.48	0.018	6.71	0.016	8.06	0.019	7.42	0.018	41.587	68.55	30.53	9976	0.0238	0.243	45.45	0.10	0.154	35.67	788.92
	49+345	20.66	0.052	17.23	0.043	18.19	0.046	18.70	0.047	39.69	68.55	30.53	9976	0.0238	0.243	45.45	0.10	0.152	36.01	788.92
	49+350	19.65	0.055	15.30	0.042	17.20	0.048	17.38	0.048	36.005	68.55	30.53	9976	0.0238	0.243	42.95	0.02	0.131	35.69	676.74
	49+357	26.57	0.081	24.54	0.075	22.23	0.068	24.44	0.074	32.855	68.55	30.53	9976	0.0238	0.243	42.95	0.02	0.126	36.34	676.74

Table 3.2. continued

	49+390	20.02	0.050	14.14	0.036	18.87	0.047	17.68	0.044	39.766	68.55	30.53	9976	0.0238	0.243	42.95	0.02	0.136	34.97	676.74
	49+400	18.06	0.055	15.59	0.047	16.03	0.049	16.56	0.050	32.999	68.55	30.53	9976	0.0238	0.243	42.95	0.02	0.126	36.31	676.74
	49+417	24.62	0.045	20.12	0.037	22.49	0.041	22.41	0.041	54.383	68.55	30.53	9976	0.0238	0.243	51.95	1.14	0.227	36.2	1200.25
	49+970	3.00	0.003	2.83	0.002	3.74	0.003	3.19	0.003	117.357	45.67	21.50	15240	0.0238	0.271	51.62	0.91	0.258	27.98	1794.29
	49+977	1.73	0.001	3.46	0.003	3.00	0.002	2.73	0.002	136.815	45.67	21.50	15240	0.0238	0.271	51.62	0.91	0.278	26.88	1794.29
	50+024	4.90	0.004	2.83	0.002	3.00	0.002	3.58	0.003	122.601	45.67	21.50	15240	0.0238	0.271	36.62	0.03	0.294	34.93	726.62
	50+777	18.81	0.021	18.60	0.021	19.72	0.022	19.05	0.021	90.399	30.25	52.27	26220	0.0214	0.24	45.30	0.50	0.336	44.44	2054.19
	50+825	12.21	0.015	12.69	0.015	10.05	0.012	11.65	0.014	82.124	30.25	52.27	26220	0.0214	0.24	45.30	0.50	0.318	45.16	2054.19
	50+880	16.03	0.022	16.79	0.023	14.04	0.019	15.62	0.021	72.673	3.94	20.25	4035	0.0223	0.19	30.94	0.01	0.095	22.71	148.35
	50+886	9.95	0.014	9.00	0.012	7.48	0.010	8.81	0.012	72.156	3.94	20.25	4035	0.0223	0.19	30.94	0.01	0.095	22.75	148.35
	50+886	12.88	0.018	10.77	0.015	14.76	0.020	12.81	0.018	72.224	3.94	20.25	4035	0.0223	0.19	30.94	0.01	0.095	22.75	148.35
	50+890	16.76	0.023	16.03	0.022	16.82	0.023	16.54	0.023	72.156	3.94	20.25	4035	0.0223	0.19	30.94	0.01	0.095	22.75	148.35
	50+906	7.07	0.010	8.31	0.012	10.05	0.014	8.48	0.012	69.656	3.94	20.25	4035	0.0223	0.19	30.94	0.01	0.093	22.98	148.35
	50+918	10.49	0.017	8.25	0.013	10.05	0.016	9.59	0.015	63.494	3.94	20.25	4035	0.0223	0.19	30.94	0.01	0.088	23.58	148.35
	51+148	24.10	0.054	25.00	0.056	27.39	0.062	25.50	0.058	44.254	31.44	44.93	24231.6	0.0245	0.228	40.71	0.05	0.226	50.31	1440.66
	51+166	7.55	0.015	10.49	0.021	12.21	0.025	10.08	0.020	49.621	31.44	44.93	24231.6	0.0245	0.228	40.71	0.05	0.243	49.48	1440.66
	51+195	21.12	0.064	13.19	0.040	13.89	0.042	16.07	0.049	32.929	31.44	44.93	24231.6	0.0245	0.228	40.71	0.02	0.188	52.38	1440.66
	51+242	5.48	0.017	6.16	0.019	7.35	0.023	6.33	0.020	32.422	32.8	33.18	11892.8	0.0252	0.234	39.67	0.03	0.165	49.72	667.15
PUREN TUNNEL	71+368	86.31	0.063	55.58	0.041	74.03	0.054	71.97	0.053	136.47	70.72	18.79	19331.5	0.0244	0.3	46.14	2.36	0.255	26.92	1595.54
	71+921	50.45	0.014	73.63	0.021	62.55	0.018	62.21	0.017	356.535	42.27	15.44	16801.33	0.0235	0.278	33.38	0.70	0.283	15.28	685.4
	71+925	53.82	0.015	47.89	0.013	77.54	0.022	59.75	0.017	360.253	42.27	15.44	16801.33	0.0235	0.278	33.38	0.70	0.285	15.22	685.4
	71+968	61.49	0.016	67.42	0.018	54.27	0.014	61.06	0.016	378.841	42.27	15.44	16801.33	0.0235	0.278	33.38	0.70	0.294	14.97	685.4
	71+983	28.51	0.007	56.96	0.015	71.53	0.019	52.34	0.014	381.349	42.27	15.44	16801.33	0.0235	0.278	33.38	0.70	0.295	14.93	685.4
	71+998	61.91	0.016	65.98	0.017	74.09	0.019	67.33	0.017	387.716	42.27	15.44	16801.33	0.0235	0.278	33.38	0.70	0.297	14.85	685.4
	71+999	63.38	0.016	64.57	0.017	45.09	0.012	57.68	0.015	387.716	42.27	15.44	16801.33	0.0235	0.278	33.38	0.70	0.297	14.85	685.4
	72+270	57.63	0.012	90.74	0.019	66.13	0.014	71.50	0.015	466.724	42.27	15.44	16801.33	0.0235	0.278	33.38	0.70	0.331	13.94	685.4
	72+985	67.54	0.018	63.06	0.016	81.32	0.021	70.64	0.018	384.206	72.84	31.57	35679.5	0.0258	0.27	49.92	2.43	0.831	29.79	3758.22
	73+512	61.61	0.083	37.59	0.050	36.80	0.049	45.33	0.061	74.506	72.84	31.57	35679.5	0.0258	0.27	56.92	2.73	0.334	35.33	5937.93
	73+513	68.91	0.092	32.71	0.044	34.19	0.046	45.27	0.061	74.506	72.84	31.57	35679.5	0.0258	0.27	56.92	2.73	0.334	35.33	5937.93
	73+560	22.49	0.040	43.52	0.077	55.94	0.099	40.65	0.072	56.237	72.84	31.57	35679.5	0.0258	0.27	60.92	2.73	0.376	38.43	7636.35
	73+572	61.08	0.113	11.49	0.021	46.28	0.086	39.62	0.074	53.823	72.84	31.57	35679.5	0.0258	0.27	60.92	2.73	0.373	38.71	7636.35
	73+593	48.28	0.099	37.78	0.077	32.71	0.067	39.59	0.081	48.88	72.84	31.57	35679.5	0.0258	0.27	55.92	1.82	0.279	37.91	5566.27

RS: Right Shoulder, R: Roof, LS: Left Shoulder, Y: Convergence value, Y': Normalized convergence value, $\bar{Y}$:Mean value of convergences, $\bar{Y}'$:Mean value of normalized convergences
***Calculation details of RMR and Q values were given in AppendixC**

CHAPTER 4

PREDICTION OF TUNNEL WALL CONVERGENCES

4.1. Determination of Statistical Modelling for Prediction of Convergences

As mentioned in the literature section, various statistical techniques, some of which are Multivariable Regression Analysis (MVR), Artificial Neural Networks (ANN), Multivariate Adaptive Regression Splines (MARS) and Support Vector Machine (SVM) methods have been used to estimate tunnel convergences by using similar independent parameters and applied to geotechnical and rock engineering problems (Adoko et al. 2013, Bizjak and Petkovsek 2004, Mahdevari and Torabi 2012, Mahdevari et al. 2013, Zhang and Goh 2013).

Among them, ANN has been compared with MVR in one of the studies and 60 data were used for testing and 43 of them had been used for estimation, respectively. ANN was found clearly more powerful in estimation of tunnel convergences (Bizjak and Petkovsek 2004, Mahdevari and Torabi 2012). Similarly in other study, SVM and MVR models were designed to identify dependencies of the tunnel convergences, and the geological and geotechnical conditions encountered for the prediction of non-linear relationship between geotechnical properties of rock mass and monitoring results (60 data points had been used for training and testing of the SVR, 15 of them was used for estimation). While MVR analysis was found insufficient at determination of tunnel convergences, SVM models have been found almost excellent explanation capacity with very high R^2 value (0,94). Yet, SVM have some limitations in application of geotechnical problems. The most important one is the data normalization process (Mahdevari et al. 2013).

It is very hard, and needs trial and error period. Like in our case, normalization of wide range of data will be reasonably hard.

Searching of the literature shows us the usage of MARS method as an alternative of above mentioned methods, but results still are not apprehensible for the end user. When ANN and MARS are compared, no clear superiority is determined between these two approaches (Adoko et al. 2013, Zhang and Goh 2013). In contradiction to ANN, MARS is found to be more effective in explaining tunnel convergences (Adoko et al. 2013). However, in both studies no clear solutions for the prediction of tunnel convergences are given for the end user.

Superiority of ANN has been shown by using limited number of data. In nature, it is very rare to encounter geological and geotechnical parameters, which shows linearly related structure. Besides, normalization of these parameters is not expected, either. For these reasons, it is very likely to expect superiority of ANN method to MVR, which does not have hypothetical limitations. Moreover, as explained previously, black-box algorithm and qualified output of ANN cannot give the required expected sufficient and detailed explanation to end user. So, this can be counted as the reason why ANN method is preferred commonly for explanation of relationship of tunnel convergences.

As a result, usage of MVR seems not suitable for the prediction of tunnel convergences because of its low explanation ratio (R^2). ANN method which is well-known and mostly used one, has some critics about its limitations, like its black-box structure. Moreover, developing a neural network model for data mining application is a very complex task, especially in solutions of geotechnical problems. It should be keep in mind that, building successful neural network is a combination of art & science, and software alone is not sufficient enough to solve all problems in the process (Nisbet et al. 2009). SVM and MARS methods have some limitations such as black-box structure and data normalization process and these two are not user friendly, either.

As can be seen from the above explanations ANN, MARS and SVM, have good explanation ratio but have some limitations either. So, the end users of these studies will have some difficulties in use and understanding besides field application of these methods will not be easy. However, ANN and MVR methods were used commonly for prediction of convergences in underground excavations and these two methods have been compared each other in many studies (Adoko et al. 2013, Bizjak and Petkovsek 2004, Mahdevari and Torabi 2012, Mahdevari et al. 2013, Zhang and Goh 2013).

Classification and regression tree (C&RT) and Chi-square automatic interaction detection (CHAID), which are the most apprehensible decision tree algorithms, were selected in this study. Decision tree algorithms have been used for solution of some geotechnical problems (Gandomi et al. 2013, Lee and Park 2013, Pham et al. 2016), but have never been applied before to this kind of problem. These algorithms are selected not only to overcome hypothetical limitations of geotechnical tunnel problems, but also to enlighten the potential interactive relationship within geomechanical parameters and tunnel convergences at comprehensible level. It should be kept in mind that there are no methods which are mutually exclusive to each other. One algorithm (statistical analysis technique), using to classify any datasets may not work well with others. Different algorithms may work better for different data sets (Nisbet et al. 2009; Rokach and Maimon 2010). MARS is another decision tree algorithm, but in our case its explaining capability (R^2) is not strong as CHAID and C&RT. Moreover the prediction results of CHAID and C&RT are apprehensible and user friendly. Besides, these two methods have never been used before in any geotechnical or rock mechanics application of underground structures. So, for furnishing the harmonization with literature ANN and MVR models were selected, which are mostly used in former studies, for comparison and to check the reliability of our results.

4.2. Description of "Decision Tree" (Regression Tree) Analysis

Decision tree is a kind of predictive modelling method used in statistics, especially in data mining applications. It consists of a tree type structure. In this structure; branches represent observations and leaves represent conclusions for the target born from observations. There are two types of tree structures. If the target variable takes a discrete set of values it's called as "classification trees". In these; tree structure leaves represent class labels and branches represent conjunction of features that lead to those class labels. If the target variable takes a continuous value (real numbers), this time it is called as "regression trees" (Breiman et al. 1984, Hastie et al. 2001, Quinlan 1986, Rokach and Maimon 2005, Rokach and Maimon 2008, Strobl et al. 2009). This regression tree explains a hierarchical group of relationships, which are organized into tree-like structure. The structure starts with one variable called root node and this root node splits into two to many branches. By this way, simple sequential question structures are generated (Rokach and Maimon 2010). The answers of these questions determine the next question. "if any, and if" based questions are asked and finalized with "ends". This generates network of questions and forms tree-like structures. Two popular algorithms exist in the literature which is C&RT and CHAID, standing for "classification and regression tree" and "chi-square automatic interaction detection", respectively (Nisbet et al. 2009). There are no big differences between each method, except for the using algorithms. While C&RT uses "Gini and "Twoing[1]", CHAID uses Chi-square algorithm.

[1] The splitting rule and the decision trees technique employ algorithms that are largely based on statistical and probability methods. Splitting procedure is the most important phase of classification tree training. The term "Gini" and "Twoing" is a kind of algorithm which enables the splitting rules in terms of misclassification cost, obtained the optimal balanced trees and the importance of independent variables. Gini index is an impurity-based criterion that measures the divergences between the probability distributions of the target attribute's values. The gini index may encounter problems when the domain of the target attribute is relatively wide. In this case it is possible to employ binary criterion called twoing criterion. When the target attribute is binary, the gini and twoing criteria are equivalent. For multi–class problems, the twoing criteria prefer attributes with evenly divided splits (Breiman et al., 1984).

The main disparity of CHAID is that it uses multiway splits instead of binary splits, where more than two splits can occur from a single parent node. Both CHAID and C&RT will construct trees, where each (nonterminal) node identifies a split condition to predict either a continuous or categorical response variable. Therefore, both algorithms can be applied to both classification and estimation (regression) problems (Brodley and Utgoff 1995; Nisbet et al. 2009; Murthy 1998; Rokach and Maimon 2005; Rokach and Maimon 2010).

4.2.1 C&RT

The name C&RT stands for Classification and Regression Tree (Breiman et al. 1984). In the C&RT structure, it constructs binary trees, where each internal node has exactly two outgoing edges. Each outgoing edges create splits and these splits are selected by using the "Twoing" criteria. As a result, these splits generate a tree type structure. The obtained tree is pruned by cost–complexity pruning method. When provided, C&RT can consider misclassification costs in the tree induction. It also enables to provide prior probability distribution. C&RT can create regression trees and when compared to CHAID, this is the superiority of it. Regression tree is a tree where their leaves predict a "real number" and not a class. In case of regression, C&RT looks for splits that minimize the prediction squared error (the least–squared deviation). The prediction in each leaf is based on the weighted mean for node (Brodley and Utgoff 1995; Kayri and Kayri 2015, Murthy 1998; Rokach and Maimon 2005; Rokach and Maimon 2010).

4.2.2 CHAID

The name CHAID stands for Chi-Square Automatic Interaction Detection analysis. CHAID was originally designed to handle nominal attributes only. For each input attribute a_i, CHAID finds the pair of values in V_i that is least significantly different with respect to the target attribute. The significant difference is measured by the p value obtained from a statistical test. The statistical test used depends on the type of target attribute. If the target attribute is continuous, an F test is used.

If it is nominal, then a Pearson chi–squared test is used. If it is ordinal, then a likelihood ratio test is used. For each selected pair, CHAID checks if the p value obtained is greater than a certain merge threshold. If the answer is positive, it merges the values and searches for an additional potential pair to be merged. The process is repeated until no significant pairs are found. The best input attribute to be used for splitting the current node is then selected, such that each child node is made of a group of homogeneous values of the selected attribute.

Note that no split is performed if the adjusted p value of the best input attribute is not less than a certain split threshold. CHAID handles missing values by treating them all as a single valid category. CHAID does not perform pruning.

4.3 Creation of the Statistical Model for Prediction of Convergences

Tunnel convergence monitoring is done by using optical measurement devices. In this system, optical reflection point is installed on the ground (tunnel excavation wall) and with the help of total station (GPS based), its relative movement is read. At each convergence monitoring point, relative ground movement is recorded in three dimensions by the monitoring device. However, this ground movement is recorded in UTM coordinate systems in three dimensions, and have to be converted into vectoral absolute numbers.

In this study, all of the field convergence measurement data have been converted into vectoral format, at first. After that, to evaluate these vectors (x, y, z directions), they were transformed into one resultant vector which has a magnitude value. Then, all of the dependent and independent variables which are given in Table 4.1 are evaluated together in terms of their interconnections. Several statistical modelling techniques are tried to find the most meaningful one. After deciding a modelling technique, all of the dependent and independent variables are uploaded to a model by using statistical software tool (IBM SPSS Modeler 17.0).

SPSS Modeler is based on nodes and streams. Nodes are the icons or shapes that represent individual operations on data. The nodes are linked together in a stream to represent the flow of data through each operation. Algorithms are represented by a special type of node known as a modeling node. There is a different modeling node for each algorithm that SPSS Modeler supplies. Modeling nodes are shown as a five-sided shape. Other types of nodes are source nodes, process nodes and output nodes. Source nodes are the ones that bring the data into the stream, and always appear at the beginning of the stream. Process nodes perform operations on individual data records and fields, and are usually found in the middle of the stream. Output nodes produce a variety of output for data, charts and model results, or they enable to export the results to another application, such as a database or a spreadsheet. Output nodes usually appear as the last node in a stream or a branch of a stream. When a stream is run that contains a modeling node, the resulting model is added to stream, and is represented by a special type of node known as a model nugget which has a shape that looks just like a gold nugget (Figure 4.1).

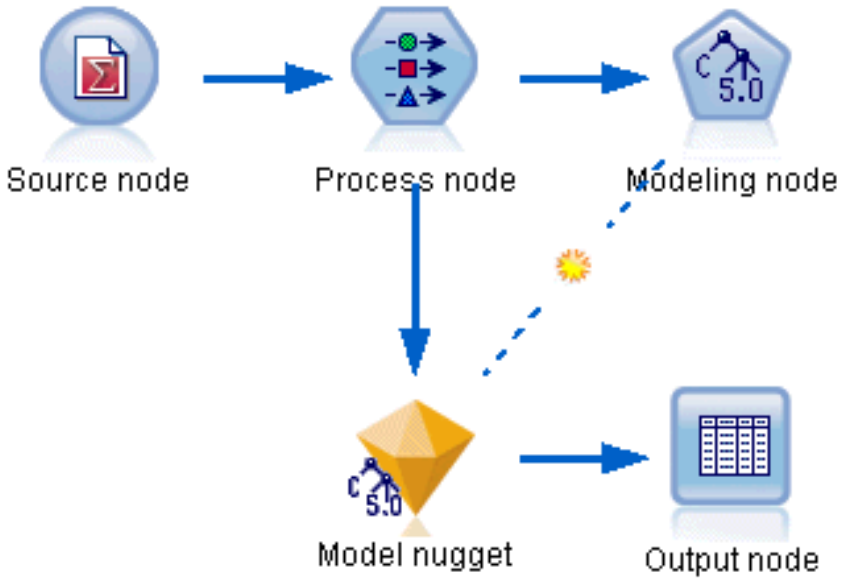

Figure 4.1. Working principle of IBM SPSS Modeler 17.0.

Provided that tunnel convergence is selected as dependent variable, *RMR*, *Q*, C_{rm}, ϕ_{rm}, E_{rm} and *H* parameters are selected as independent variables, as explained before. Then statistical estimation models are generated for left shoulder, roof and right shoulder, separately. As some of the intact rock geomechanical properties, which are uniaxial compressive strength, RQD and Poisson's ratio, are both inputs of RMR and Q, multicollinearity situation occurs. Therefore, two statistical estimation model are created for RMR and Q separately with other independent parameters at each estimation point. Hence, for each of the 3 convergence measurement points (LS, R, RS) 6 distinct models are generated by using a statistical software tool for 4 different statistical methods which are MVR, ANN, CHAID and C&RT. Generation of 6 distinct models for RMR and Q systems produces 12 decision tree models for CHAID and 12 more for C&RT. As can be predicted, this will make things harder and complicated to interpret. For this reason, right, left and roof convergence values are re-evaluated to simplify the models. As a result, it is observed that convergence values at 3 measurement points are consistent with each other. So, convergence values measured on left shoulder, roof and right shoulder are taken into account as mean values for these 3 measurement points. By this way of thinking, 12 decision tree models are converted into 2 for CHAID (1 for RMR and 1 for Q pairs) and 2 for C&RT models.

Overburden thickness, H is obtained as a most dominant independent parameter according to statistical analysis results. Besides, H is also affecting the other rock mass parameters, such as cohesion and internal friction angle of the rock mass, and deformation modulus, naturally. As the overburden thickness "H" is an important factor affecting the convergences, need for creation of another statistical model is emerged. To overcome this issue, relative amount of convergences within overburden thickness has to be calculated. By doing this, convergence values have been normalized and transformed into a unitless number.

For this reason, convergence values for the selected section are normalized by dividing to its overburden thickness. By this way, relative amount of convergences in overburden thickness is found by means of %, and convergences are converted into dimensionless dependent unit. Moreover, by doing this operation a universal estimation approach will have been obtained as because the suggested method will apply to all cases no matter what the overburden thickness is. Hence, the first statistical approach, which includes H as an independent parameter too, are applied again and this time 4 more statistical models are generated for normalized convergence values by putting out H. In this manner, while convergences in mm, represented as "***Y*** ", which are using as dependent variable, was transformed into percentage amount in overburden thickness and created as a new dependent variable, which is represented as " ***Y'*** ". Statistical description of all the data used in modelling is given in Table 4.1.

4.3.1 Results of the Statistical Modelling

Results of the statistical analysis are given in Table 4.2. It is clearly seen that, except for MVR method, the others have high R^2 value for our data set. In statistics, the coefficient of determination, denoted as R^2 or r^2, is the proportion of the variance in the dependent variable that is predictable from the independent variables. It provides a measure of how well observed outcomes are replicated by the model, based on the proportion of total variation of outcomes explained by the model. R^2 is a statistic that will give some information about the goodness of fit of a model. In regression, the R^2 coefficient of determination is a statistical measure of how well the regression line approximates the real data points. An R^2 of 1 indicates that the regression line perfectly fits the data (Glantz and Slinker 1990; Draper and Smith 1998; Devore 2011).

Therefore, when the R^2 values are considered, the best outcome highest R^2 value with lowest root mean squared error ($RMSE^2$), is obtained from C&RT model both for dependent variable *Y* and *Y'* (Table 4.2). *Y* and *Y'*. For both of the dependent variables, ANN and C&RT models give higher R^2 value. When the dependent variable Y is considered it reveals that C&RT method has higher R^2 value than the ANN. On the other hand, ANN and C&RT methods have almost the same R^2 values for the dependent variable *Y'*, and this value is bigger than *Y*'s R^2 and closer to 1. RMR based C&RT model structure has a little bit more R^2 value than ANN. Besides, both the RMR and Q based Y' models have the same R^2 and RMSE values. In fact, this is an expected situation, because there are no significant differences amongst each model.

As it has been stated before, different algorithms may work better than the other algorithms for different data sets; even so, findings of this study show that our ANN and C&RT models are consistent with the findings of former studies (Table 4.3) and verifies our suggested estimation method. Yet, use of ANN model in the field is not easy for the end user and the results are not comprehensible. So, decision tree structure is more reliable and easy to use. ANN model is not preferred in this study, but owing to its widely usage, the findings have been given here briefly (Figures 4.2 and 4.3).

[2] The root-mean-square error (RMSE) (or sometimes root-mean-squared error) is a frequently used measure of the differences between values (sample and population values) predicted by a model or an estimator and the values actually observed. The RMSE represents the sample standard deviation of the differences between predicted values and observed values. RMSE is a measure of accuracy, to compare forecasting errors of different models for a particular data and not between datasets, as it is scale-dependent (Hyndman and Koehler 2006).

Table 4.1. Statistical description of the independent model parameters

Types of Data	Symbol	Unit	Min.	Max.	Mean	Stand. Dev.
Measured	H	m	4,9	387,71	56,94	59,69
Empirical	RMR	No unit	30,94	66,27	42,55	9,19
Empirical	Q	No unit	0,0054	5,75	0,9744	1,4883
Empirical	C_{rm}	MPa	0,012	0,684	0,2066	0,1551
Empirical	ϕ_{rm}	Degree	14,22	61,8	38,79	11,08
Empirical	E_{rm}	MPa	4,36	13861,52	2113,16	3151,41
Meas. Mean Con.	Y	mm	2,73	71,97	23,28	15,73
Norm. Mean Con.	$Y' = \frac{Con.(mm)}{H(mm)} x100$	%	0,0019	0,5127	0,092	0,1123

Table 4.2 Results of the statistical analysis for the tunnel convergences

	Y (Measured mean convergences)				Y' (Normalized mean convergences)			
	Q-Based Model		RMR-Based Model		Q- Based Model		RMR- Based Model	
	R^2	RMSE	R^2	RMSE	R^2	RMSE	R^2	RMSE
CHAID	0.454	11.567	0.719	8.301	0.861	0.042	0.813	0.048
MVR	0.088	14.944	0.088	14.944	0.252	0.097	0.252	0.097
C&RT	0.870	5.633	0.793	7.113	0.933	0.029	0.933	0.029
ANN	0.616	9.707	0.388	12.244	0.933	0.029	0.921	0.031

Table 4.3. Findings of the previous studies about prediction of the tunnel convergences

Researchers	**Used Statistical Methods**			
	MVR		**ANN**	
Mahdevari and Torabi (2012)	R^2	RMSE	R^2	RMSE
	0,352	3,070	0,936	0,0842
	MARS		**ANN**	
Adoko et al. (2013)	R^2	RMSE	R^2	RMSE
	0,96	0,42	0,97	0,9581
	MVR		**SVM**	
Mahdevari et al. (2013)	R^2	RMSE	R^2	RMSE
	0,13	3,921	0,941	0,271

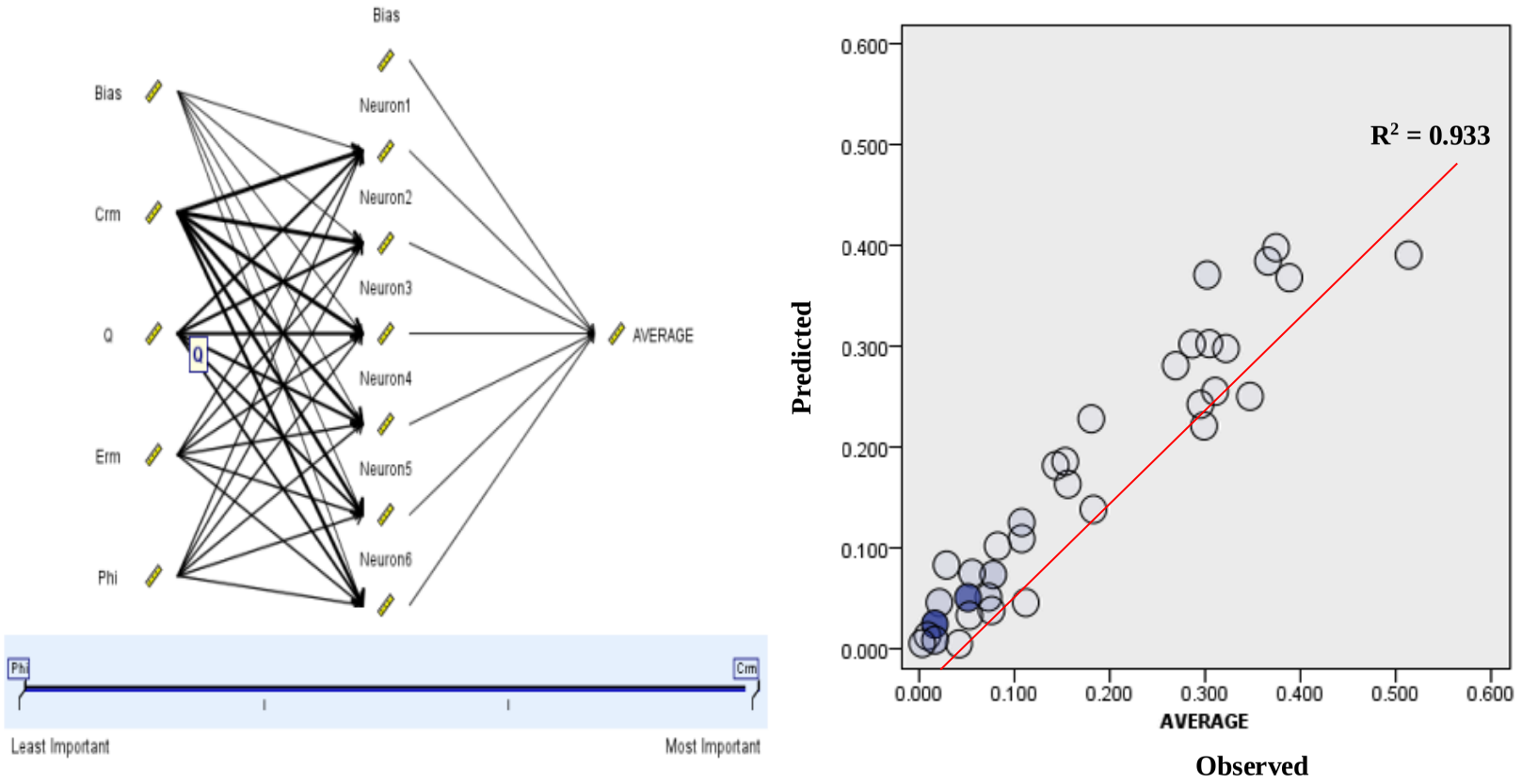

Figure 4.2. ANN structure for Q based model and comparison for predicted values to observed values in terms of averages of Y' values.

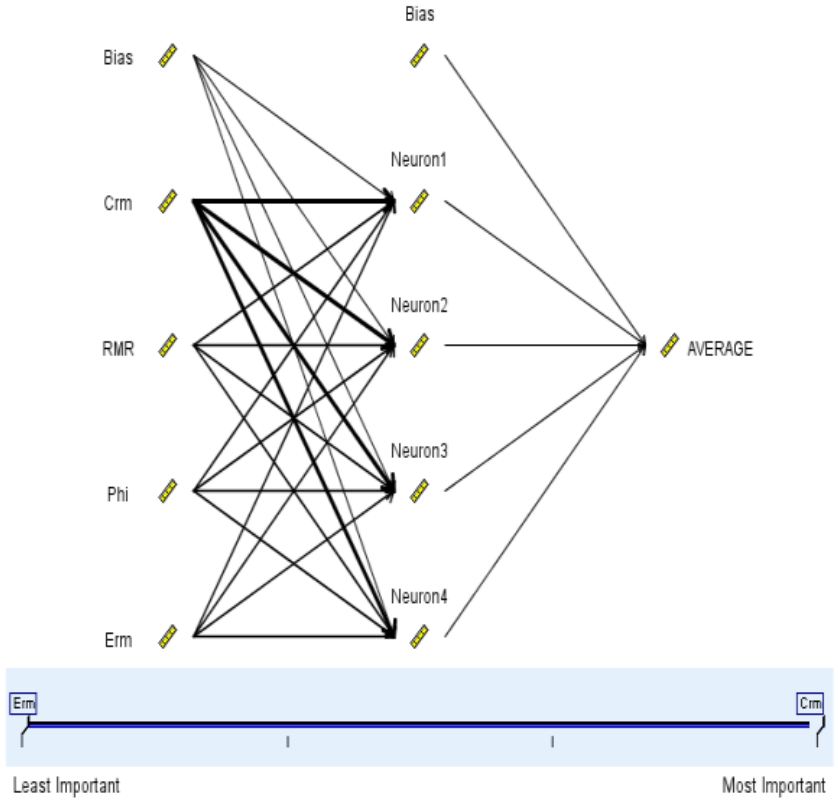

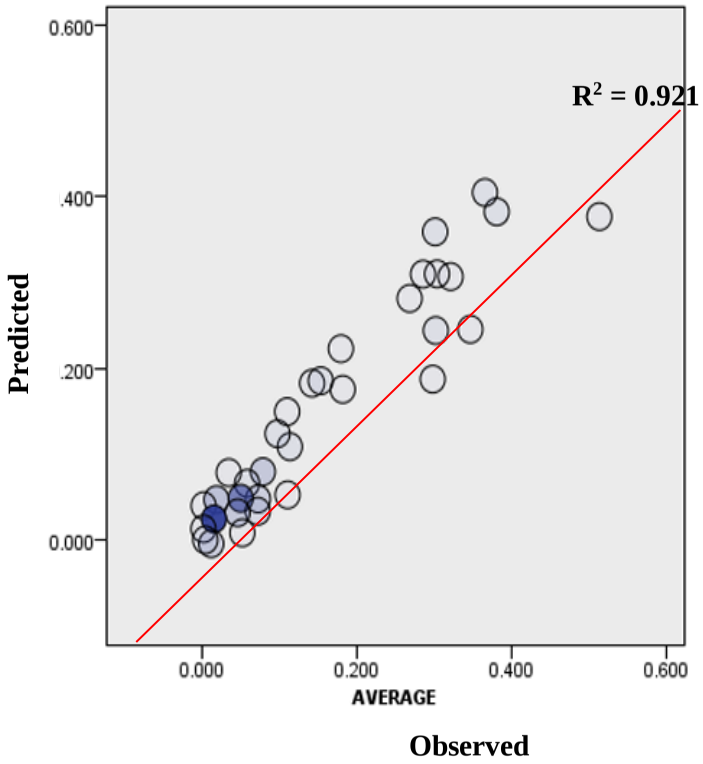

Figure 4.3. ANN structure for RMR based model and comparison for predicted values to observed values in terms of averages of Y' values.

For ANN modeling; multi-layer perceptron analysis was selected. A multilayer perceptron (MLP) is a class of feedforward artificial neural network. MLP consists of at least three layers of nodes. Except for the input nodes, each node is a neuron that uses a nonlinear activation function. MLP utilizes a supervised learning technique called backpropagation for training. Its multiple layers and non-linear activation distinguish MLP from a linear perceptron. It can distinguish data that is not linearly separable (Rosenblatt 1961, Cybenko 1989). For Q based Y' model structure, totally 6 neurons were generated and their interconnections between the independent variables were evaluated by the system. According to Q based ANN model rock mass internal friction angle was evaluated as a least effective parameter on convergences and cohesion of the rock mass was evaluated as the most effective one. How the other parameters affect the convergences and how to evaluate these effects could not be understand from the given ANN structure. Besides, predicted to observed Y' value graph is drawn (Figures 4.2 and 4.3) by the ANN model structure and there is almost a perfect fit is seen. However, the same input data are used for drawing of this graph. The same structural rules are valid for the RMR based Y' model. As can be seen, ANN model structure is not user friendly and comprehensible.

So, C&RT model was preferred for validation of the findings of this study and detailed results of C&RT model is shown in Figure 4.4 and 4.5. Similarity of two model structures (C&RT and ANN) and their consistency with the former studies can be compared by using Table 4.2 and 4.3.

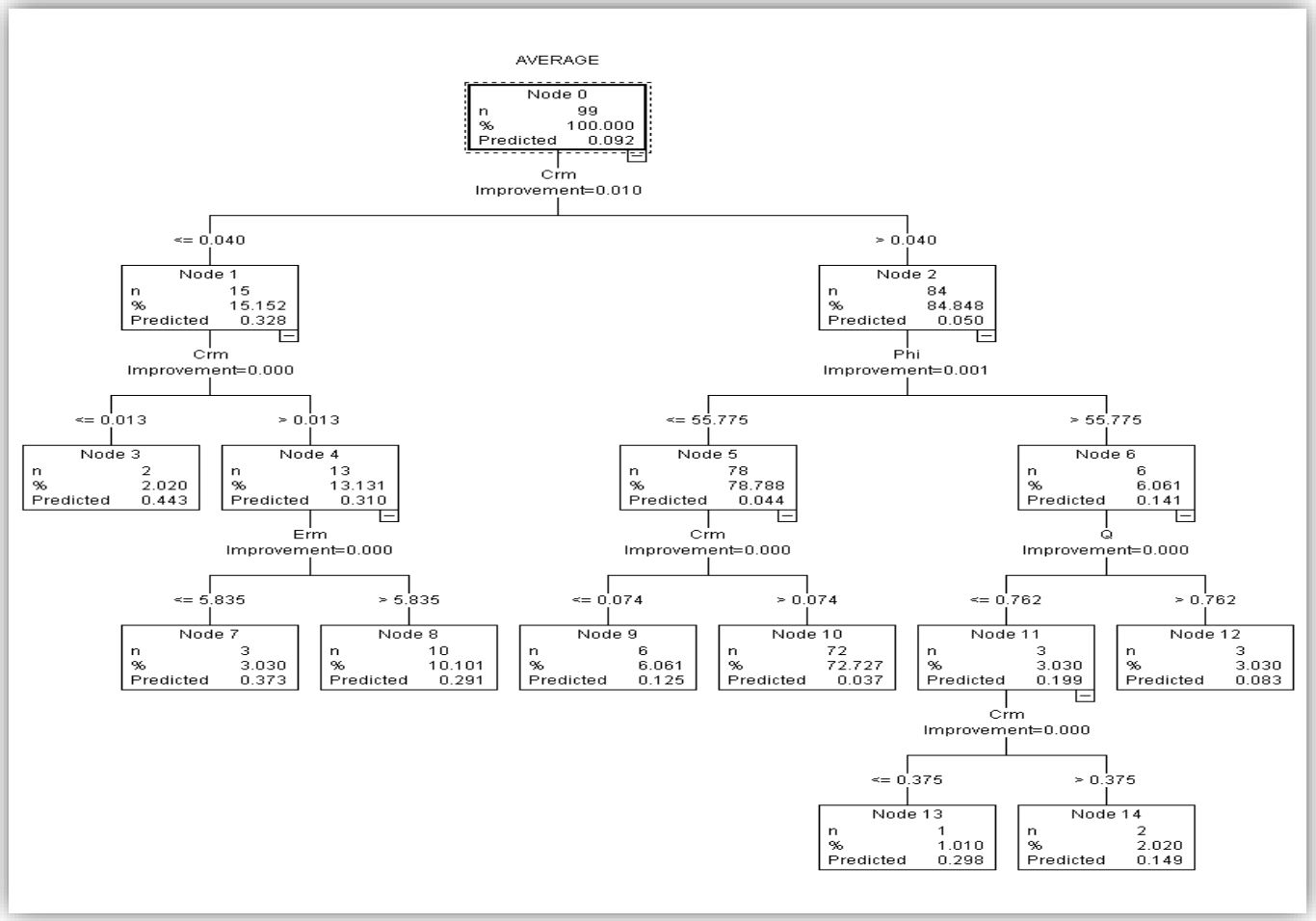

Figure 4.4. C&RT model structure and results for Q-Y' model

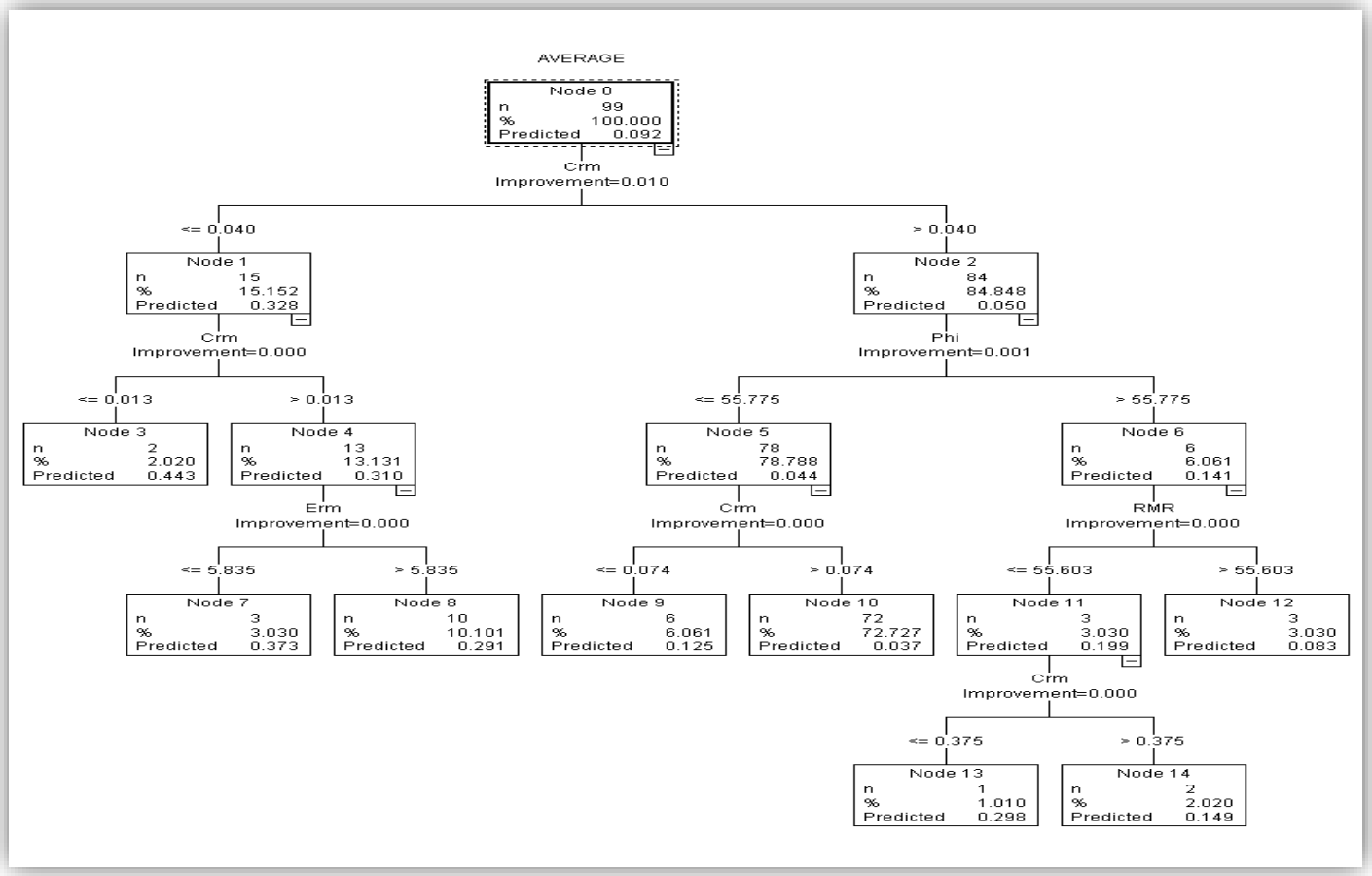

Figure 4.5. C&RT model structure and results for RMR-Y' model

According to Figures 4.4 and 4.5 there are 11 different paths generated by C&RT model structure. End user of this tree structure can use this model easily in the field. Namely, after the field studies, engineer will get the geotechnical properties of the rock mass. Besides, there will also be face excavation records. By using these two data RMR and Q ratings of the tunnel rock can be determined. So, all of the required parameters for the C&RT structure are ready to use, by this way. So, any suitable path well may be followed depending on an appropriate rock mass data. All of the alternative paths are given below both for Q and RMR based Y' model structures.

- In case of selection of Path 1; Crm $\leq$ 0.013 MPa, then predicted Y' value is 0.443
- In case of selection of Path 2; 0.013 < Crm $\leq$ 0.040 MPa and Erm $\leq$ 5.835 MPa, then predicted Y' value is 0.373
- In case of selection of Path 3; 0.013 < Crm $\leq$ 0.040 MPa and Erm > 5.835 MPa then predicted Y' value is 0.291
- In case of selection of Path 4; 0.040 < Crm $\leq$ 0.074 MPa, $\phi_{rm} \leq 55.775°$, then predicted Y' value is 0.125
- In case of selection of Path 5; Crm > 0.074 MPa, $\phi_{rm} \leq 55.775°$, then predicted Y' value is 0.037
- In case of selection of Path 6; 0.040 MPa < Crm $\leq$ 0.375 MPa, $\phi_{rm} > 55.775°$, Q $\leq$ 0.762, then predicted Y' value is 0.298
- In case of selection of Path 7; Crm > 0.375 MPa, $\phi_{rm} > 55.775°$, Q $\leq$ 0.762, then predicted Y' value is 0.149
- In case of selection of Path 8; Crm > 0.040 MPa, $\phi_{rm} > 55.775°$, Q > 0.762, then predicted Y' value is 0.083
- In case of selection of Path 9; 0.040 MPa < Crm $\leq$ 0.375 MPa, $\phi_{rm} > 55.775°$, RMR $\leq$ 55.603, then predicted Y' value is 0.298
- In case of selection of Path 10; Crm > 0.375 MPa, $\phi_{rm} > 55.775°$, RMR $\leq$ 55.603, then predicted Y' value is 0.149
- In case of selection of Path 11; Crm > 0.040 MPa, $\phi_{rm} > 55.775°$, RMR > 55.603, then predicted Y' value is 0.083

As can be seen from Figures 4.4 and 4.5 and the paths above, there are conditional nodes which are split into sub-branches, and new conditional nodes are created by this way. This procedure continues up till there will be no more conditional branches left. Each of the nodes contain number of data used for prediction and its prediction value. Prediction result gives the convergences as a percentage value for the related geotechnical data. As normalized convergence value has been selected for prediction of convergences, the obtained prediction results have to be transformed into a real convergence value by multiplying it with the related section's overburden thickness. It should be kept in mind that there is no precise number in nature, none of the geological structures are homogeneous. Therefore, specified geomechanical values for the rock masses should be accepted as an approach for the real value. Thus, all of the suggested estimation statistical models for the convergences should be used cautiously, because all of the geomechanical rock mass parameters are the input of statistical estimation models. The suggested ranges in our convergence estimation model should be accepted as a level for the maximum convergence of a related tunnel section, and it should be developed by adding up more convergence measurement data and rock mass data. Namely, in the tree structure of C&RT model (and many other decision tree structures) there are leaves and conjunctions (branches) whereas leaves represent class labels, branches represent conjunctions of features that lead to those class labels. These leaves or branches can be named as children of parent (roof) model. There are edges to children for each of the possible values of that input variable. Each leaf represents a value of the target variable given the values of the input variables represented by the path from the root to leaf. The branches of the tree will develop by adding up more data, and maybe new branches will be developed by this way. As a result, a more precise statistical estimation model will be obtained. In advance studies, by entering more data to our C&RT model structure it will become more significant in terms of statistic and will give more reliable results.

CHAPTER 5

VALIDATION OF THE STATISTICAL MODEL

5.1 Validation Approach for Statistical Modelling

For installation of a reliable support system, the ultimate value for the convergences should have been accurately predicted beforehand. This is a sine qua non for tunnel construction. However, there are some factors directly affecting tunnel convergences. Geological structures, construction methodology, speed of excavation, timing of supports, blasting design, competency of excavation crew and design-excavation consistency can be counted as the main factors affecting the amount of tunnel convergences. No matter how appropriate and accurate the tunnel construction is going on, some amount of convergences cannot be avoided and appreciable part of convergences develop before the measurement step. Besides, there will always be an unsupported section between the last supported section and the excavation face, because of the nature of the excavation process. It is almost impossible to install the supporting material to the zero point of the excavation face just after the excavation. So, there will be a time gap that occurs naturally between supporting and monitoring. That is why, “unsupported stand up time” and "maximum unsupported span length" terms had been suggested by Bieniawski (1989).

Hence, significant amount of convergences cannot be recorded in tunnels, owing to the time gap between convergence measurements and installations of first monitoring device. However, installation of monitoring instruments behind the excavation face and recording of convergences beforehand is crucial for the underground construction.

Nevertheless, these are expensive and accepted as time consuming activities by the contractors, especially for highway tunnels where the construction speed is important for the contractor because of the duration limit defined in the engagement of the project. Besides, medium of the tunnel construction site is generally dark and muddy, moreover due to the big machinery and effects of blasting, the visibility inside the tunnel decreases and monitoring devices may get damaged by this way. For these reasons, contractors install the monitoring devices to the furthest possible distance from the excavation face. According to previous studies (Kim and Chung 2002, Kontogianni and Stiros 2002, Bizjak and Petkovsek 2004, Schubert et al. 2004, Kavvadas 2005), most of the monitoring devices are placed at least 10 m behind of the excavated face.

Yet, this delay in monitoring activity means great amount of deformation data could not be recorded and get lost. Maximum amounts of convergences happen before monitoring. This phenomenon was explained before in Chapter 2 in Figure 2.10 at Hoek (2001) study. So, just after the excavation, up to two diameters distance back from the face, ultimate deformation value should be measured. However, as a result of tardy monitoring activity it has been stated that 30% to 80% of convergences may be vanished and cannot be monitored in most of the tunnel excavations (Kim and Chung 2002, Kontogianni and Stiros 2002, Bizjak and Petkovsek 2004, Kavvadas 2005).

So, when rough and tough conditions in underground excavations were considered, a certain amount of increment for the measured convergences will be reasonable for compensation of missing monitoring amount of convergences. Therefore, measured convergence data in validation step were incremented by certain amount in this study. Besides, by using this approach, ultimate value for tunnel convergences could have been obtained after the excavation and before application of supporting elements. Moreover, just because the raw convergence data were used at the model creation stage, the suggested statistical estimation approach is verified also by using this approach.

5.2. Validation of the Statistical Model for the Tunnel Convergences

In this thesis, to validate the findings of our statistical estimation model, 30-piece data were collected from 5 different tunnel locations. To obtain a reliable estimation model and convergences in the same manner, convergence data collected from field were increased by 30%, 60%, and 80%, respectively. Unless in-situ test methods, such as buried tape extensometers and borehole geophysical methods are not applied in the field, the level of unmeasured convergences is impossible to know at the beginning of statistical modelling. So, the amount of unmeasured convergences were tried to find for further applications of this method by doing an iteration based process.

As geological properties of all tunnels and their locations were given before in Chapter 3 in Section 3.2., these will not be explained again in this section. However, rock mass geotechnical properties and convergence measurement data of the validation tunnels are presented in Table 5.1 with validation results. By using independent variables data given in Table 5.1, appropriate statistical convergence prediction path was followed by using suggested estimation model from Figure 4.4 and 4.5. By this way, estimated convergence value was found out for each independent variable validation data set. After that, estimated convergence values were compared with real convergence monitoring data, which are used for validation. Results are plotted in Figure 5.1.

As can be seen from Figure 5.1, the estimation model findings are almost in the same trends for all three cases. This showed us that our suggested approach is working well. As it was stated before, a significant amount of convergences are not measured and become lost in practice as because of the operational reasons and as it was not given required importance about this subject. However we have to know that how much convergences could not be measured for the convergence prediction data used in Table 3.2. Besides, to obtain a trustworthy approximation, and to find out which of the incremental value (%) should be selected for further applications, incremented data were verified in accordance with the suggested model.

In another words, this is also the way to understand for the determination of how much convergences could not be measured for the tunnels which are used to establish statistical modelling in Table 3.2. Moreover, the obtained R^2 values are the same for the entire 4 situation (raw measured data, 30, 60 and 80% increments). In fact this is an expected case. In statistically, comparison of two variables, multiplying any one of the variable with any constant number will not change the coefficient of determination (R^2). For this aim, a well-known statistical method, Sum of the Squared Error[1] (SSE), was applied for incremented convergence data.

According to SSE method following results was obtained;

- for measured convergences SSE is 0.194348
- for 30% increment of the measured convergences, SSE is 0.104747
- for 60% increment of the measured convergences, SSE is 0.104316
- for 80% increment of the measured convergences, SSE is 0.123463

Amongst these results; the least SSE value was obtained from 60% increment and was suggested for further applications who is intending to use this estimation model suggested in this thesis. It should be taken into account that all SSE results are very close to each other. That is why comparison graph, given in Figure 5.2, almost fits for all three cases. This situation can be explained with the engineer's safety approach. As explained in Section 5.1 there is always a time gap between first convergence measurement and occurred convergences. That is to say, more increment for the measured tunnel convergences will create safer conditions. In another words, tunnel engineer may prefer more conservative approach by choosing 80% increment for the further stages of the tunnel excavation. This approach is also parallel with Hoek et al. (2002) study. In this study, term of “disturbance factor” for the rock masses was stated and it was suggested to decrease the rock mass strength parameters in a certain amount, ranging between 0 and 1, depending on the blasting or excavation quality. Where zero (0) refers to very good quality excavation and one

[1] It is a measure of the discrepancy between the data and an estimation model. A small SSE indicates a tight fit of the model to the data. It is used as an optimality criterion in parameter selection and model selection (Draper and Smith 1998).

(1) refers to very poor excavation and blasting conditions. Therefore, increment for convergences also depends on the excavation or blasting quality. While 80% convergence increment is not enough to describe unmeasured convergences in case of very poor excavation conditions, the 30% convergence increment may be sufficient for good excavation conditions.

When the measured and predicted convergences are compared for validation step, a favorable outcome is obtained. The R^2 value is obtained as 0.8039 for the 60% increment of the measured convergences with lowest SSE. As it was stated before in Chapter 4 Section 4.4, in decision tree structures the branches of the tree will develop by adding up more new data entries and there may be new branches will be developed by this way. Therefore, it is strongly thought that new data entries will develop the statistical prediction model and by this way and the R^2 value will rise. Because, the new data entries either lessen the effect of the extreme values in the model or cause development of new branches which create statistically meaningful paths for the extremities. So, in order to see the effects of extremities to the prediction model two more graphs have been plotted by omitting 6 out of 30 validation data which can be seen in Figure 5.3a. By omitting extremities the R^2 value is obtained as 0.929 for the rest (Figure 5.3b).

Table 5.1. Tunnel data which are used to validate findings of the generated statistical estimation model

Convergence Meas. Section			Field Rock Mass Properties					Measured Mean Convergence Values				Predicted Conv.
Tunnel Name	Km	H_{max} (m)	*RMR*	*Q*	E_{rm} *(MPa)*	C_{rm} *(MPa)*	ϕ_{rm} (°)	Y'	Y' (30%)	Y' (60%)	Y' (80%)	Y' (%)
ECABAT 1 TUNNEL	183+200	34.58	56	0.9	1189.02	0.143	58	0.038	0.049	0.061	0.068	0.083
	183+450	73.50	52	0.5	1154.87	0.271	42	0.021	0.027	0.034	0.038	0.037
	185+480	30.04	53	0.8	1130.31	0.123	57	0.040	0.052	0.064	0.072	0.083
ECABAT 2 TUNNEL	187+970	54.70	49	0.4	1140	0.2	45	0.030	0.038	0.047	0.053	0.037
	188+480	127.30	46	0.5	1150	0.228	30	0.027	0.035	0.044	0.049	0.037
	188+985	30.43	45	0.4	690.09	0.074	37	0.074	0.097	0.119	0.134	0.125
TIREBOLU 2 TUNNEL	3+858	8.82	22	0.14	500	0.03	46	0.328	0.427	0.526	0.591	0.373
	4+466	6.51	16	0.64	800	0.02	48	0.291	0.378	0.465	0.523	0.373
	4+428	18.05	52	0.7	1500	0.3	63	0.103	0.134	0.165	0.186	0.298
	4+407	13.09	52	0.7	1500	0.275	65	0.159	0.207	0.254	0.286	0.298
CAGLAYAN TUNNEL (Right Tube)	48+788	32.41	32	0.05	910	0.141	48	0.021	0.027	0.033	0.037	0.037
	48+951	43.13	31	0.009	650	0.08	31	0.049	0.064	0.078	0.088	0.125
	49+044	58.99	29	0.077	825	0.091	28	0.052	0.068	0.083	0.094	0.125
	49+345	39.69	59	1.2	1230	0.41	56	0.047	0.061	0.075	0.085	0.083
	49+357	32.86	19	0.003	550	0.056	34	0.074	0.097	0.119	0.134	0.125
	50+777	90.40	40	0.8	2440	0.32	46	0.021	0.027	0.034	0.038	0.037
	50+880	72.67	23	0.014	1870	0.085	25	0.021	0.028	0.034	0.039	0.037
	51+148	44.25	31	0.067	1310	0.071	30	0.058	0.075	0.092	0.104	0.125
	51+195	32.93	57	0.82	1310	0.253	56	0.049	0.063	0.078	0.088	0.083
	51+242	32.42	33	0.084	1130	0.116	45	0.020	0.025	0.031	0.035	0.037
TEKIR TUNNEL (Right Tube)	55+333	13.06	28	0.132	850	0.066	52	0.083	0.108	0.133	0.149	0.125
	55+398	29.96	59	0.96	1240	0.382	62	0.043	0.056	0.069	0.077	0.083
	55+403	24.01	45	0.384	1440	0.183	59	0.063	0.082	0.101	0.114	0.149
	55+799	146.07	52	2.25	1214	0.577	46	0.011	0.015	0.018	0.020	0.037
	55+859	121.33	47	2.11	1165	0.459	46	0.016	0.020	0.025	0.028	0.037
	56+353	29.57	56	0.91	966	0.269	58	0.050	0.065	0.080	0.090	0.083
	56+400	21.24	20	0.207	780	0.046	37	0.060	0.078	0.096	0.108	0.125
	56+418	10.99	18	0.102	715	0.024	35	0.114	0.149	0.183	0.206	0.373
	56+447	6.13	18	0.102	685	0.013	37	0.232	0.302	0.372	0.418	0.443
	56+453	5.76	16	0.1	389	0.012	40	0.201	0.262	0.322	0.362	0.443

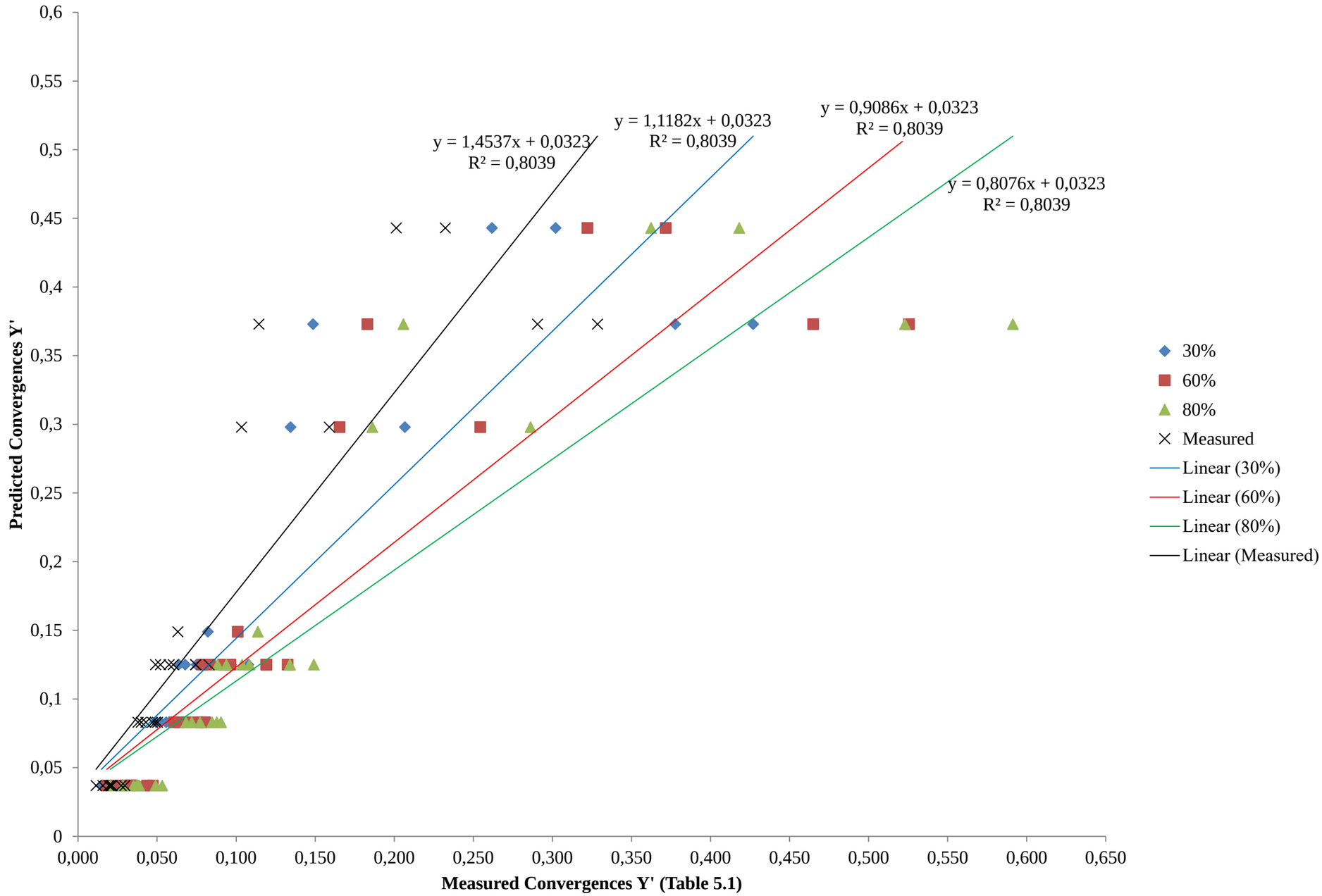

Figure 5.1. Comparison of predicted convergence values (Y'-%) and field convergence measurements and for 30%, 60% and 80% increments

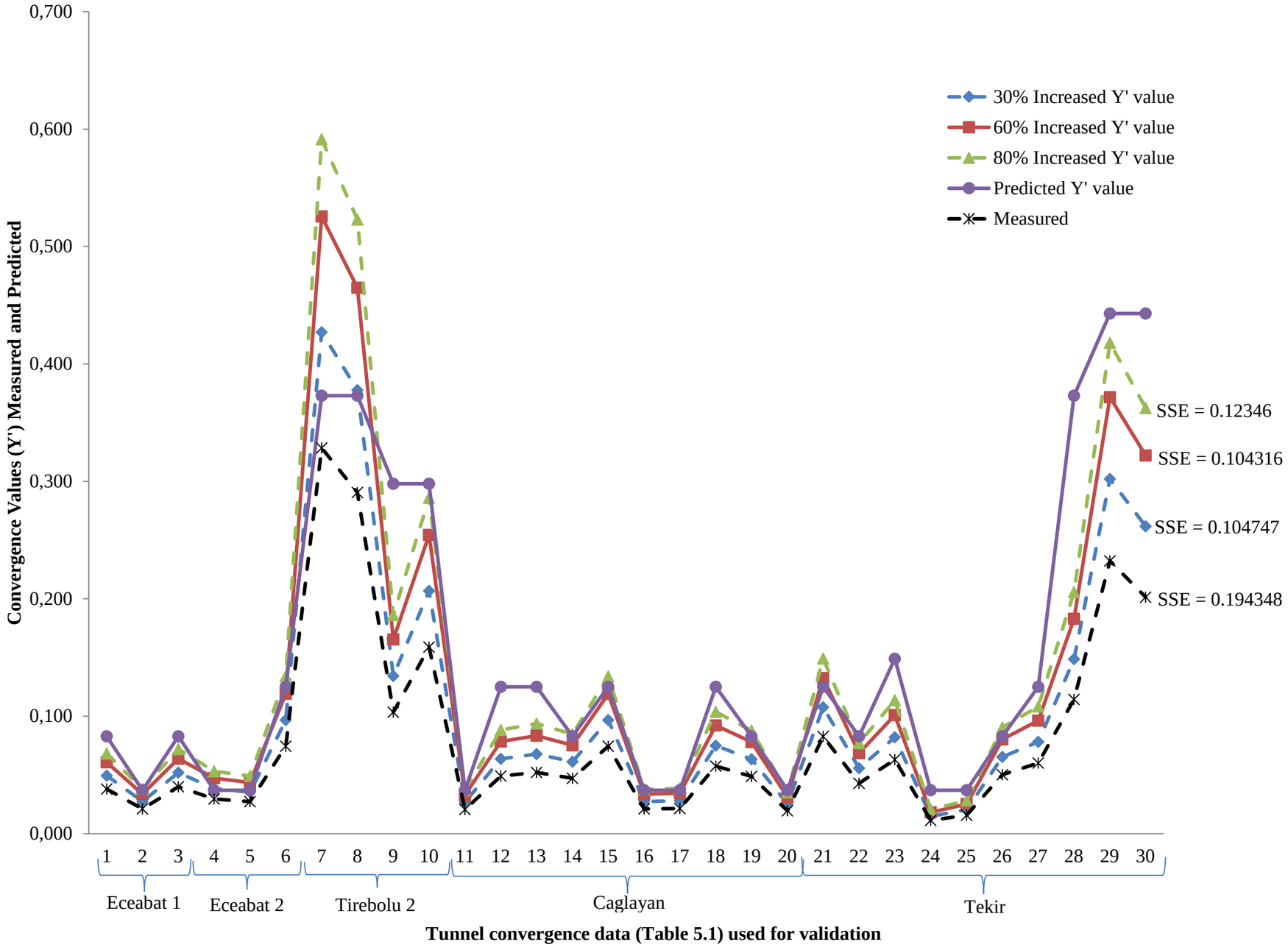

Figure 5.2. Comparison of predicted and measured (increased by x%) normalized convergence data graph in terms of SSE

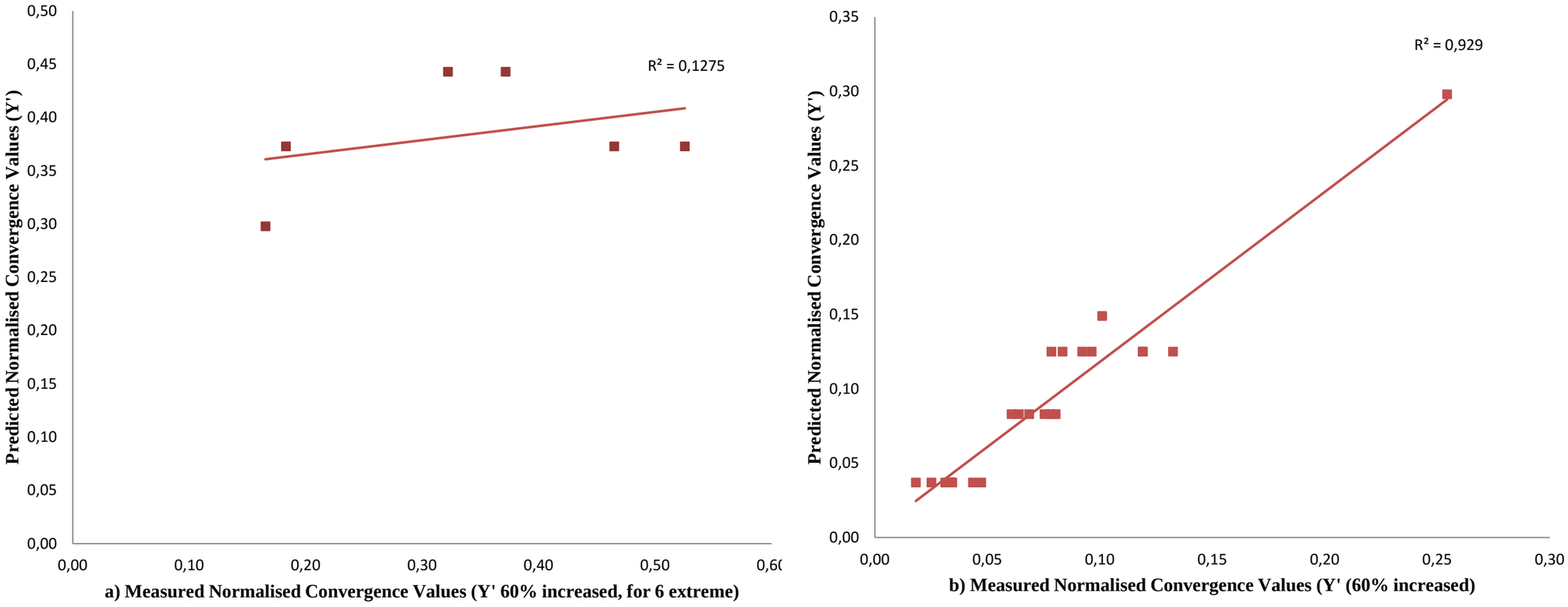

Figure 5.3. Effects of extreme values to the validation

CHAPTER 6

PREDICTION OF DAMAGED ZONE THICKNESS AROUND THE TUNNELS

Another goal of this study is prediction of plastic zone thickness development around the tunnels. As suggested convergence prediction method validated, a prediction model for plastic zone thickness is generated by using validated convergence data. Plastic zone thickness can be determined by using empirical equations, field measurement methods and with back-analysis procedure using numerical software tools. Amongst them, the most effective technique is in-situ measurement but this is expensive and requires time. Besides, this technique cannot be used for the prediction of plastic zone thickness, it can only be used for validation of prediction result and for determination of that zone. As one of the aim of this thesis is to suggest new practical user friendly and cheap approach for prediction of plastic zone thickness, "back-analysis" method was preferred which is the most suitable one for this purpose.

For this aim, tunnel excavation sections, which are used for validation, have been selected and numerical models were created by using finite element modelling method (FEM). A commercial FEM software tool called "*RS*^{2}"[1] was used for this aim.

[1] RS^2 (Phase^2 9.0) is a powerful 2D finite element program for soil and rock applications (RS^2 = Rock and Soil 2-dimensional analysis program). RS^2 can be used for a wide range of engineering projects and includes excavation design, slope stability, groundwater seepage, probabilistic analysis, consolidation, and dynamic analysis capabilities. Complex, multi-stage models can be easily created and quickly analyzed-tunnels in weak or jointed rock, underground powerhouse caverns, open pit mines and slopes, embankments, MSE stabilized earth structures, and much more. Progressive failure, support interaction and a variety of other problems can be addressed (https://www.rocscience.com/rocscience/products/rs2).

Numerical models were generated by using the identical validation tunnel data and cross sections, and then measured and predicted convergences were compared with numerical model findings. By this way, it will be understood whether the findings of numerical and statistical modelling confirm each other. If that is, an estimation method for tunnel plastic zone thickness will be suggested by using numerically measured plastic zone thicknesses. While creating numerical models no supporting element is modelled in this thesis. By this way, both maximum convergences and plastic zone thickness for any underground excavations are obtained, and the worst conditions are modelled moreover the amount of immeasurable convergences can also be obtained.

6.1. Rock Mass Characteristics Used in Numerical Models

In this thesis, RMR ratings of the selected tunnel rocks lie within 30 to 66 (Table 4.1). As there is a well-known relation between RMR and GSI value which is "GSI89 = RMR – 5", (Hoek and Brown 1997), it can be said that the GSI values of the rock masses in this study is about between 25 and 61, which means fair to weak quality. In nature, it is almost hard to find a homogenous rock mass structure, which can be identified easily and separated from others in terms of geological and geotechnical parameters. So, laboratory or empirically obtained rock mass strength parameter values can be change upwardly or downwardly depending upon the measurement location and direction, in nature. Hence, direct usage of the RMR or GSI values are not suggested for geotechnical designs. So, as laboratory or geotechnical drilling data represent one local point of all geological units in excavation sections, numerical models are divided into similar geological and geotechnical property units where unified geotechnical parameters are used, if the modelled section has more than one unit. Because of this, in some of the numerical modelling sections, there are minor differences in terms of the strength parameters. In such sections, two or more geotechnical data are unified to one for numerical modelling.

6.2. General Procedure for Numerical Modelling

For finite element numerical modelling, totally 9 tunnel cross-sections were selected which are already used for validation of the statistical model findings and the same modelling procedures are applied them all. Therefore, general modelling procedure is explained here briefly and output of one of the model is given here. Detailed analysis for all numerical models and data are presented in Appendix B.

All numerical models were created by considering the real cross sections, depths, actual surface topography and overburden thicknesses. Plane strain analysis was selected as analysis type. Plane strain assumes that the excavation is of infinite length normal to the plane section of the analysis. Genuine tunnel cross-sections were used in numerical modelling. As genuine tunnel cross-sections have been used in models, no specific boundary conditions were needed to be identified. Whereas the excavation model boundary was fixed (by using restraints option of the software) from both sides and bottom because of low overburden thickness, top of the model was set free unless its overburden thickness is not more than 3 times of the tunnel diameter.

As any increase in mesh node numbers will greatly increase the size of the matrices used to solve the problem, and will therefore increase solution time and memory requirements, mesh and discretization were generated automatically by the software and meshes are generated by using three-nodded triangles. Before the mesh is generated, boundaries were discretized. This process was done to subdivide the boundary line segments into discretizations which will form the framework of the finite element mesh. However, to obtain a fine result, the mesh density was increased around the tunnel section. All of the model elements were shown in Figure 6.1.

Depending on the project and excavation necessities, single-tubed, double-tubed or inverted excavation sections were applied to numerical models, and in accordance with these, cross-sections models were drawn as 5, 9 or 13 staged.

An ultimate excavation effect zone was defined to all cross sections. The "ground arch" concept of Terzaghi (1946) was used in drawing of this excavation effect zone.

All of the highway tunnels are horseshoe shaped and the dimensions are 11 m in width, 9 m in height and, 12 m in diagonal diameter, respectively. Therefore, diameter of this ultimate effect zone is selected as 40 m, nearly 4 times of the tunnel diameter. In consistent with actual excavation steps (top-heading and bench), this ultimate effect area was divided into 2 parts in excavation sequence; upper around top heading and lower around bench and if necessary invert section effect zone was defined separately. In accordance with the excavation sequence, changes of identified rock mass strength properties were allowed both in the excavation area and the effect zone. Details of this procedure are given below for the most complicated example of this thesis.

Material properties of the model were obtained from whether geotechnical site investigation studies or from laboratory experiments. After that, required rock mass strength parameters were generated by using the software called RocData[2] (Hoek 1997, Hoek et al. 2002, Hoek and Diederichs 2006). One of the appropriate failure criterions, Hoek-Brown (for fair quality rock masses), Generalized Hoek-Brown (for lesser quality weak rock masses) or Mohr-Coulomb (for soils), were used depending on the failure characteristics of the rock mass in the related tunnel section.

[2] A commercial software tool for the analysis of rock and soil strength data, and the determination of strength envelopes and other physical parameters. https://www.rocscience.com

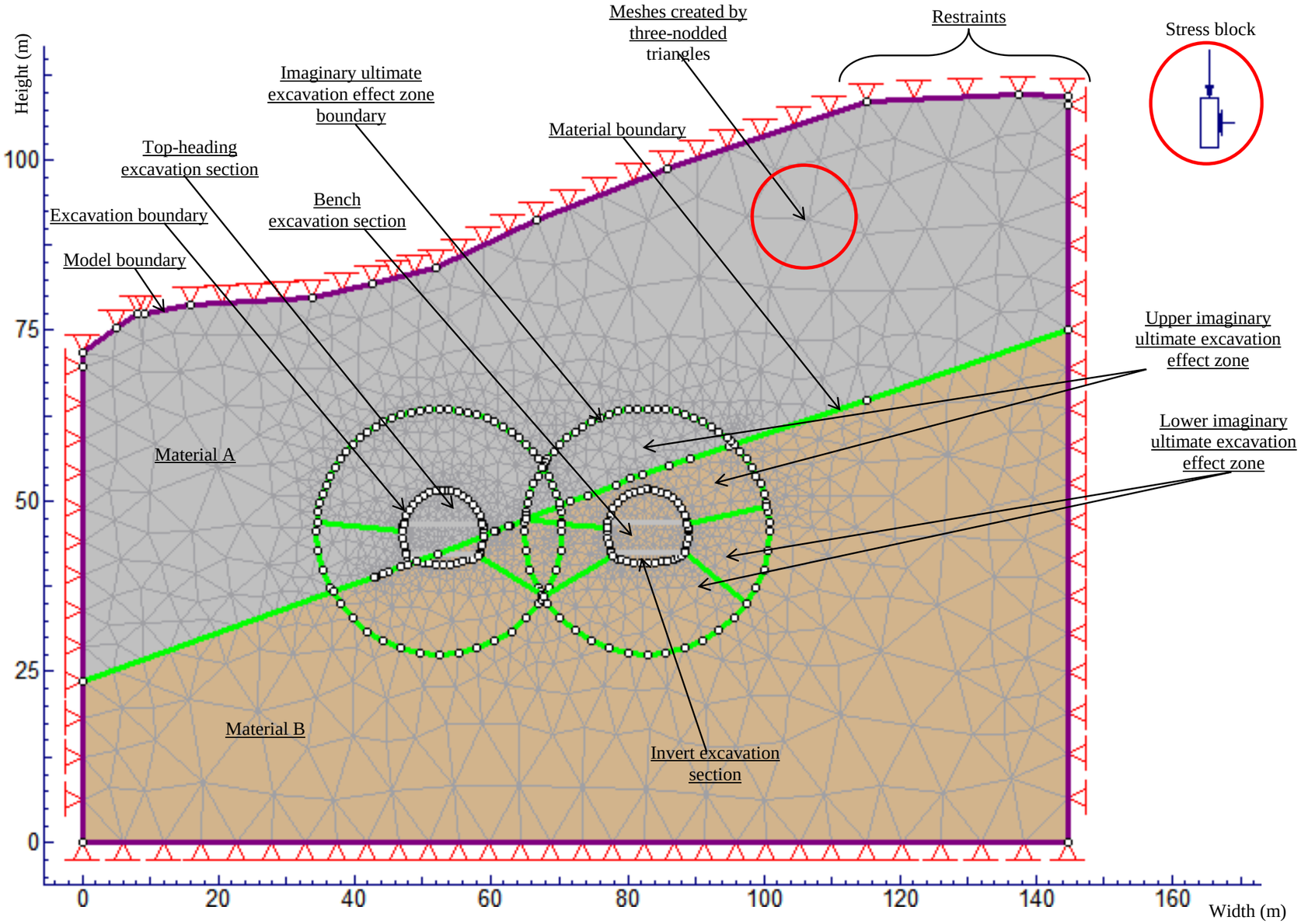

Figure 6.1. Explanation of the numerical modelling elements applied in this study.

In all models the first stage, “stage 1”, was selected as “initial loading stage”, and all material properties were identified as elastic. There is not any excavation activity in this stage. This stage represents just before a new excavation step. As we are concerning with 2D medium, this stage is a must for every new modelling. The second stage represents the first step of top-heading excavation. In this stage, no matter which excavation technique is used, the tunnel face rock mass is disturbed by explosives or excavation machines, and cannot be excavated or hauled at once. Therefore, independent from applied excavation method, there will be a time gap between excavation, hauling and supporting in practice. To demonstrate time gap between excavation and hauling in the numerical model, top-heading excavation was completed in two steps. At first, effects of excavation were reflected to the top-heading rock mass excavation, which is shown as black in the Figure 7.2 at stage 2, by adding up the disturbance factor (Hoek et al. 2002) to relevant material properties in the model. Besides, material properties were also selected as plastic, at this time.

If the material type would have been chosen as elastic, the input rock mass parameters would only have been used for the calculation and plotting of strength factor. In this case, any failure of the tunnel is not observed in the model. Conversely, by selecting the material type as plastic, residual strength parameters can be used in case of failure of the material. Consequently, rock mass around the tunnel excavation loses its stiffness till installation of the first supporting element and within this time gap vast amount of deformations occur depending on magnitude of in-situ stresses, post-failure behavior of rock mass, excavation technique and experience of the excavation crew. Hence, rock mass’ geotechnical parameters were lessened to their residual values by selecting plastic material properties. A realistic numerical modeling application must incorporate with this phenomenon (Satici and Unver, 2015). Therefore, by finalization of the 3rd stage, material types at the upper ultimate effect zone of the top-heading excavation, which is shown as dark-grey in the Figure 6.2 at stage 3, is identified as plastic at the same time. Then, top-heading excavation is completed, which is shown as white in the Figure 6.2 at stage 3.

4th stage is the bench excavation. In this stage, similar to the second stage, there will be a time gap between excavation, hauling and supporting in practice. To demonstrate time gap between excavation and hauling in the numerical model, bench excavation was completed in 2 steps, too. At first, effects of excavation were reflected to the bench rock masses excavation, which are shown as black and reddish-brown, in the Figure 7.2 at stage 4, by adding up the disturbance factor (Hoek et al. 2002) to relevant material properties in the model. Besides, material types were also selected as plastic, again.

In the 5th stage bench excavation is completed which is shown as white in the Figure 6.2 at stage 5. By finalization of the 5th stage, material types at the lower ultimate effect zone of the bench excavation was identified as plastic which are shown as dark-grey and orange in the Figure 6.2 at stage 5.

All of the above procedures are done for the left tube of the tunnel and repeated for the right tube till the end of 9th stage, too. If the modelled tunnel was single-tubed then there will have been only 5 stages, and 9th stage will be the last stage if there was no invert excavation for the modelled section.

In case there is an invert excavation (like as the example in Figure 6.2), the same procedure will be applied into the invert excavation section by adding up four more stages, two for left tube and two for right, to the model.

After that “compute” step was applied. This step carries out the finite element stress analysis for the current model. The last step of the numerical modelling is the “interpret” step which is the post-processing module used for data visualization and interpretation of the RS^2 analysis results. Data Contours can be viewed, such as stress, displacement, strength factor, and results can be displayed on the model or graphed for material queries, bolts, liners, joints etc. Several outputs can be obtained from these calculations.

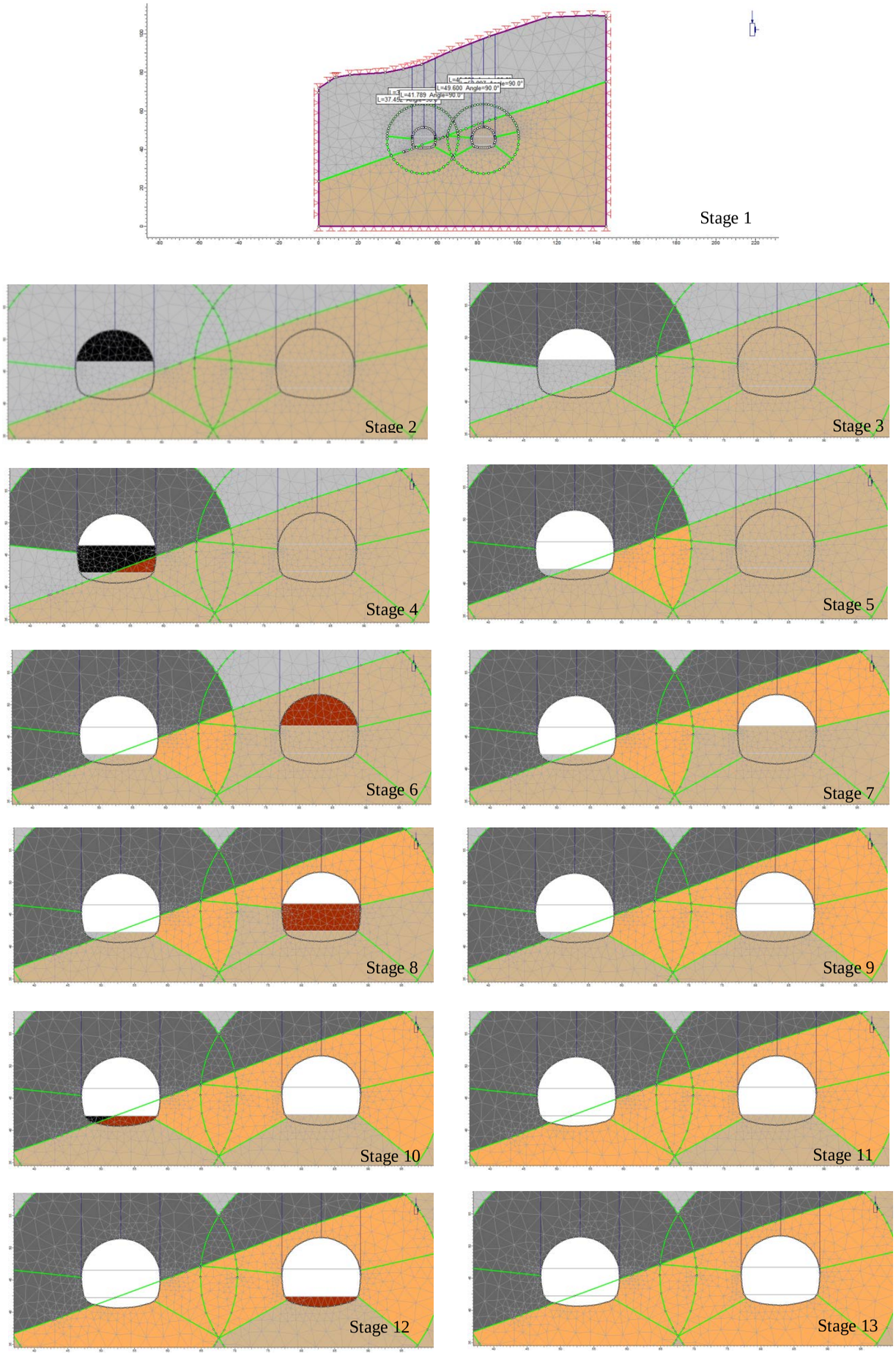

Figure 6.2. Generalized numerical modeling stages applied for the tunnels.

6.3. Determination of Damaged Zone Thickness

To determine the radius of the plastic zone, ultimate position of yielded elements can be used. Extent of the failed zone, which is represented with red crosses and dots in Figure 6.3, also represents the extent of the plastic zone around the tunnel. The radius of the plastic zone can be determined by measuring the distance from the center of the tunnel to the perimeter of the yielded/plastic zone (Figure 6.3).

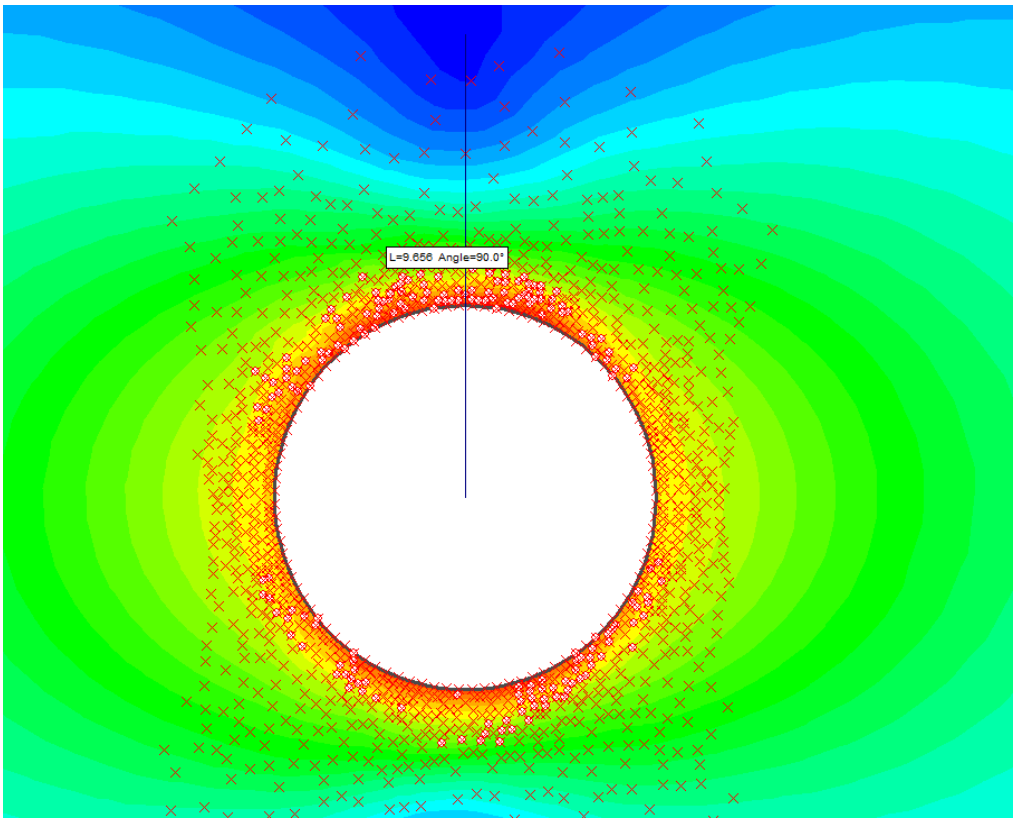

Figure 6.3. Method for determination of plastic zone thickness of a tunnel described in the RS^2.

Undoubtedly, this is the easiest way for determination of plastic zone thickness. However, several sub damaged zones, which are explained in Figures 1.3, 1.4, 1.5 (Chapter 1 at Section 1.4), cannot be measured by this way. Moreover, as can be seen from Figure 6.3, distribution and density of the yielded elements around the excavation is not homogenous. So, this kind of measurement will lead user to

inaccurate results. In Perras and Diederichs (2015) study, it was claimed that the yielded elements, volumetric strain, and principal stress concentrations were found to be the best indicators for determining the depth of different damaged zones. All of these required data can be obtained from the numerical modelling outputs. Besides, by using numerical model outputs, any of the mathematical relation between convergences and damaged zone thicknesses can also be revealed.

For this aim, by using interpret option of the software, convergence values of the numerically modelled tunnel sections were found as a resultant vector for shoulder and roof, at first. After that, these values were converted into normalized convergence data by dividing into related tunnel depth. Then, mean values of the normalized convergences were obtained for each of the modelled tunnel sections. Afterward, yielded elements, volumetric strain, and principal stress concentrations values were measured and plotted against distance from the excavation wall. Thus, one for the total convergences, shown in Figure 6.4, one for the yielded elements, shown in Figure 6.5, and for the volumetric strains, yielded elements and principal stresses, one for each, totally five graphs have been plotted. However, the last three graphs were unified in Figure 6.6 for clearly understanding of the difference between damaged zone thicknesses. All of these graphs, (Figures 6.4, 6.5 and 6.6), are shown here just as a general explanation purpose. In Appendix B, detailed versions of all these graphs are given for every tunnel that is used in this study.

Total convergence values, identified as "displacements" in the software, for any point on the model was obtained from query option. As the tunnel depth is known for any point, normalized convergence values are easily obtained from resultant convergences graph, which is shown here in Figure 6.4. Besides, the software easily generate the yielded elements which also represents ultimate limit of plastic zone or excavation influence zone (Figure 6.5). However, the yielded element thickness represents “excavation influence zone” (EIZ) rather than the “excavation damaged zone” (EDZ) or “highly damaged zone” (HDZ).

Finding the depth of EIZ may be useful in nuclear repository sites in terms of prevention of any harmful leakages. Yet, for highway tunnel excavation this information is not useful. Instead, depths of EDZ and HDZ are more essential for both safer and efficient tunnel excavation.

So, depth of EDZ and HDZ were determined by using the yielded elements, volumetric strain and principal stress graphs. These damaged zone thicknesses are found by using query option of the software. Query of any point for the damaged zone are found by plotting the distance against to selected certain point from the excavation wall. Hence, a point located on the opposite to the deepest yielded element zone thickness on the excavation wall is selected to find out the worst conditions. Then, principal stress, yielded element percentage and volumetric strain graphs were plotted from the selected point through the model boundary. Then the required values are read from the plotted graphs.

The first point where principal stress (σ_3-MPa) value starts to increase is accepted as the end of the highly damaged zone, and starting from the excavation boundary to this point section is HDZ. The point where the yielded element percentage reach the “0” value is the end of the excavation damaged zone and from the end of the HDZ till this point section, is the EDZ. From this point on where the strain value starts to increase through the excavation boundary, is the upper limit of the excavation influence zone, and the distance between the end point of the EDZ and the upper limit of excavation influence zone is the thickness of the EIZ (Perras and Diederichs 2015). All of these are shown in Figure 6.6 and given in Appendix B for all tunnels used in this study. Numerically obtained values of convergences, normalized convergences, EDZ and HDZ values are given below in Tables 6.1 and 6.2, respectively. As can be seen from the Figure 6.7, rock mass post-failure characteristic is coherent with the strain softening behavior, which is explained in section 2 in Figure 2.1, for the modelled tunnel section. The other tunnel sections post-failure characteristics are also coherent with the strain softening behavior and details for all are given in Appendix B.

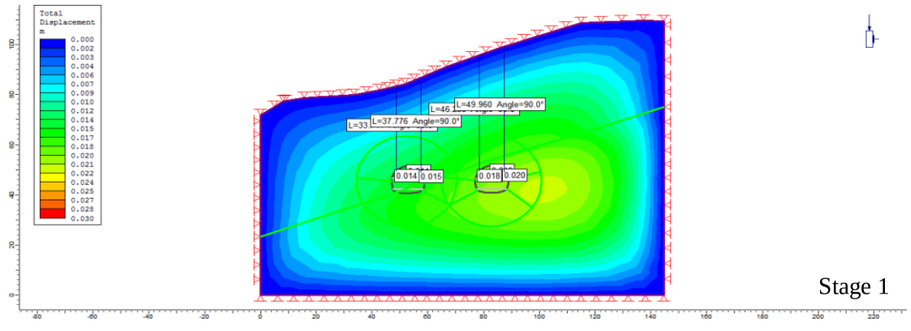

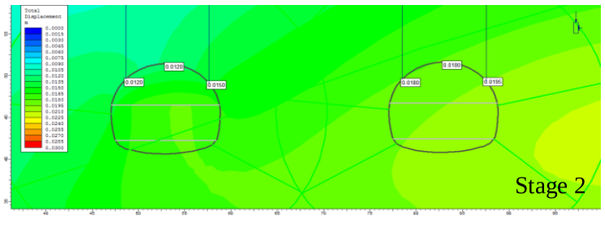

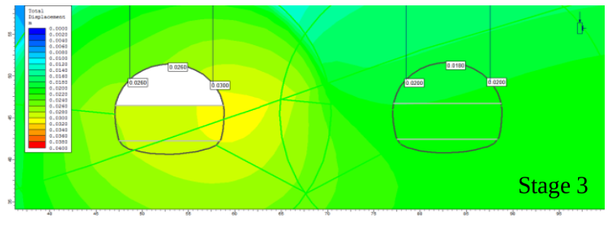

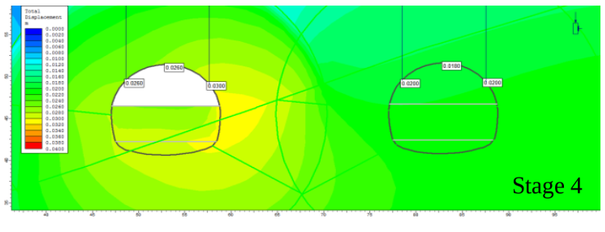

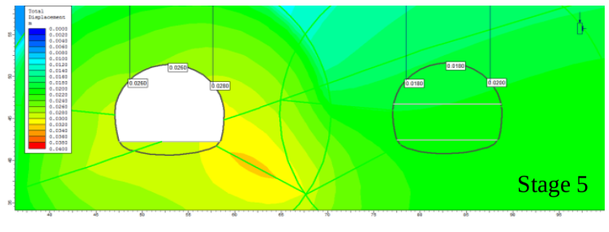

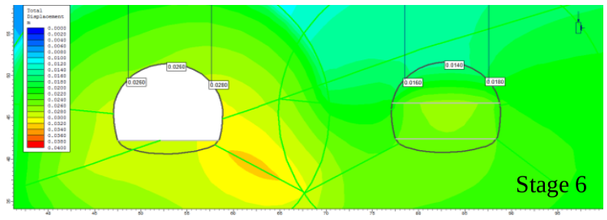

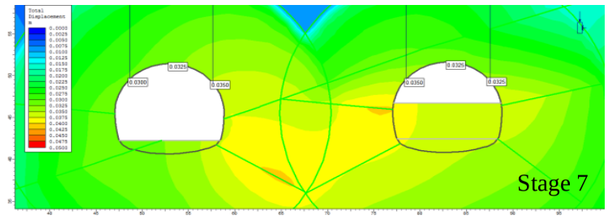

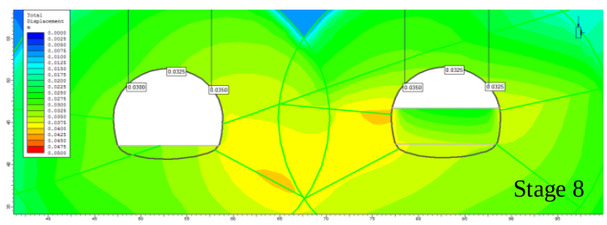

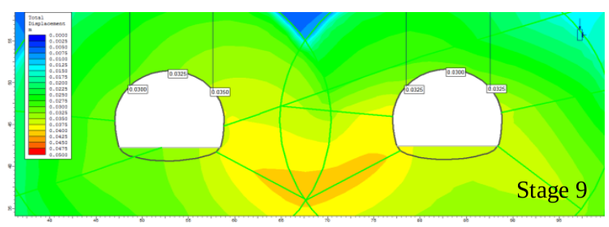

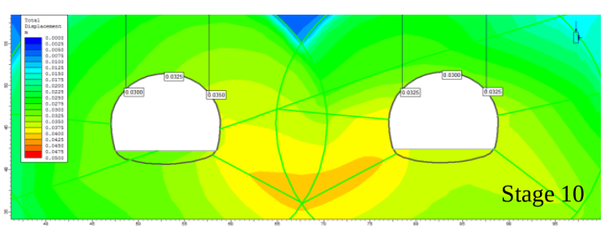

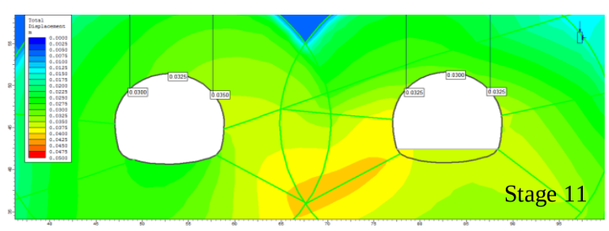

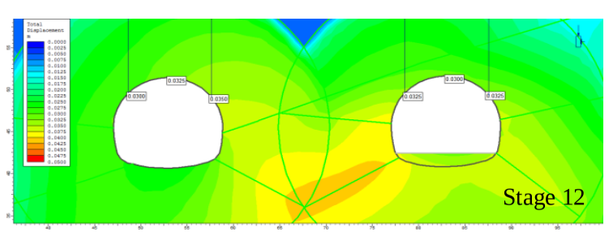

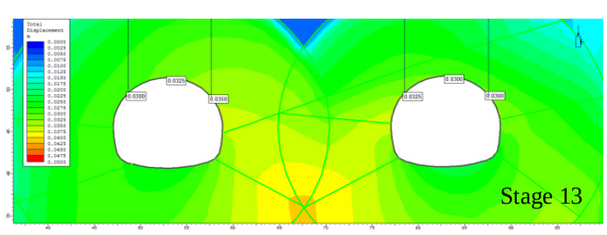

Figure 6.4: Generalized interpretation stages for resultant convergences.

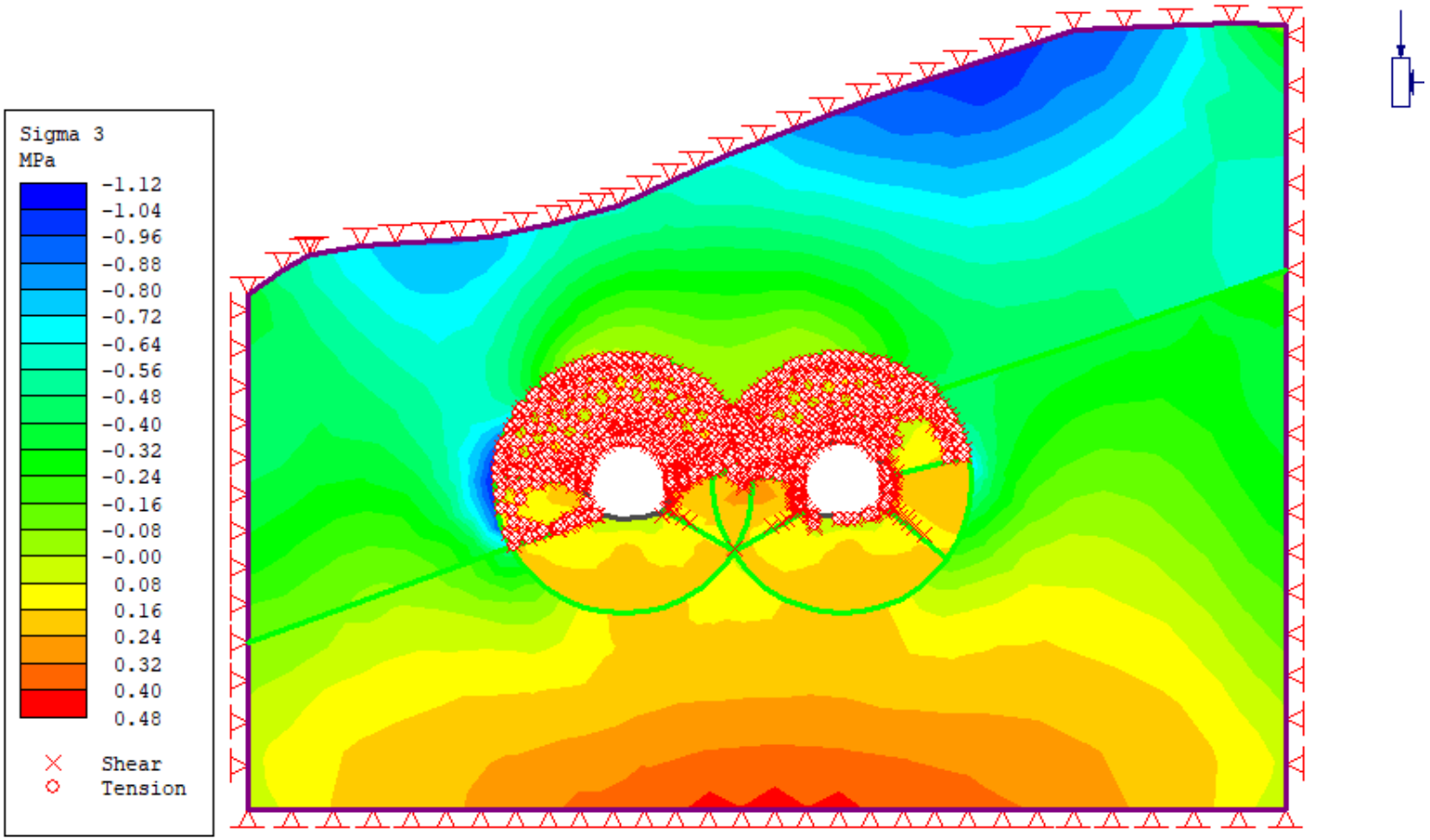

Figure 6.5. Typical tunnel cross-section after an excavation in terms of yielded elements and sigma 3.

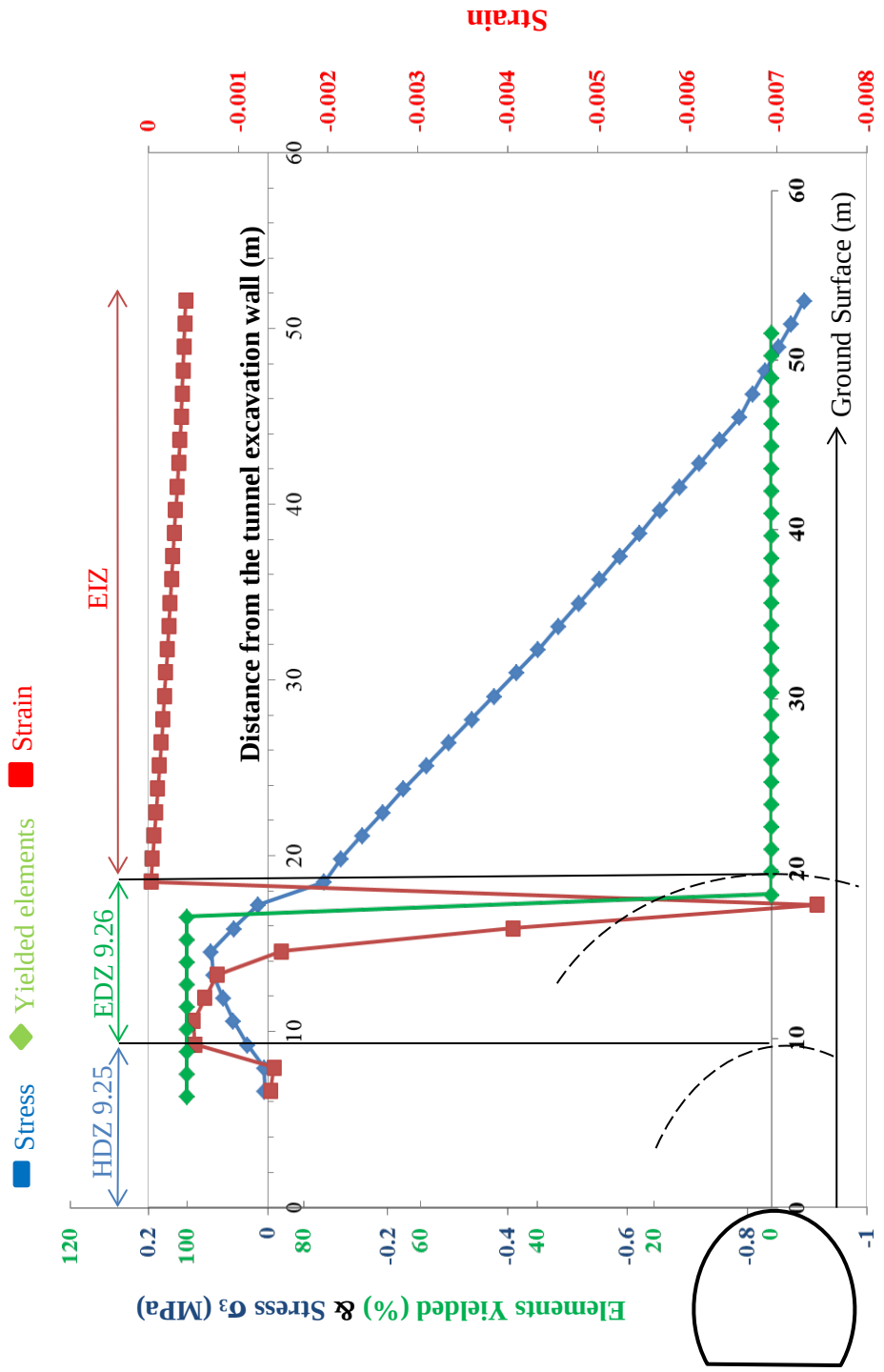

Figure 6.6. Thickness of HDZ and EDZ for an excavated tunnel section

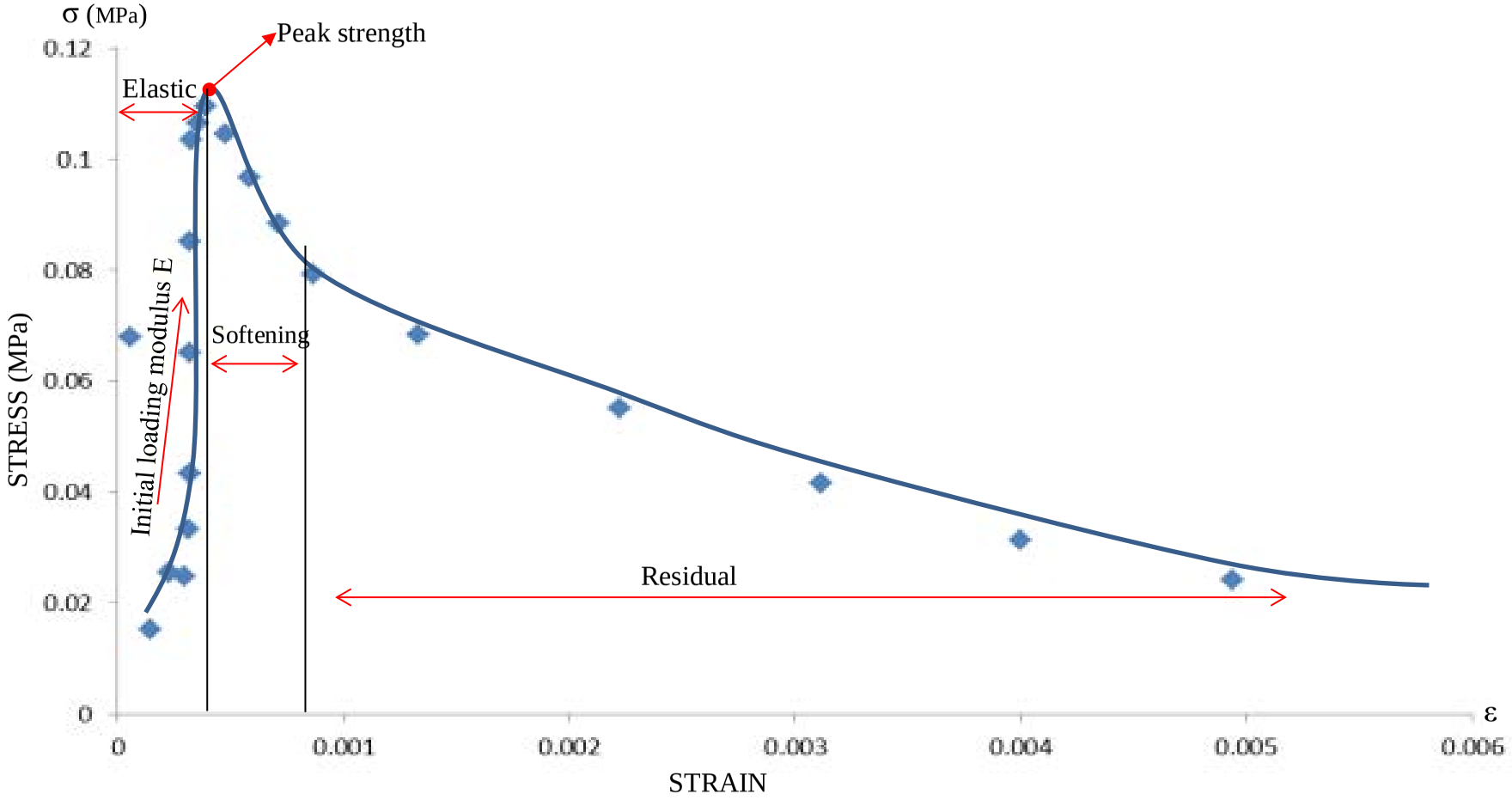

Figure 6.7. Typical stress – strain graph after an excavation completed.

Table 6.1. Numerical model findings in terms of convergences and normalized convergences of the tunnels.

TUNNEL NAME& CROSS SECTION	LEFT TUBE									
	LS-Y (m)	**H (m)**	**LS-Y' (%)**	**R-Y (m)**	**H (m)**	**R-Y' (%)**	**RS-Y (m)**	**H (m)**	**RS-Y' (%)**	**MEAN-Y' (%)**
Eceabat1 185+480	0.0149	21.754	0.068	0.0314	14.638	0.214	0.0116	18.707	0.062	0.115
Eceabat2 188+985	0.0192	22.847	0.084	0.032	17.767	0.180	0.016	22.657	0.070	0.111
Tirebolu 3+858	0.048	15.397	0.311	0.06	9.194	0.652	0.051	14.485	0.352	0.438
Tirebolu 4+407	0.0096	20.641	0.046	0.0176	17.251	0.102	0.0144	25.721	0.056	0.068
Caglayan 49+044	0.0294	37.458	0.078	0.0315	33.227	0.094	0.0357	41.905	0.085	0.086
Caglayan 50+777	0.0406	76.885	0.052	0.0377	73.195	0.051	0.0464	80.941	0.057	0.053
Caglayan 51+148	0.0189	21.934	0.086	0.0231	18.438	0.125	0.021	25.346	0.082	0.098
Tekir 56+353	0.0513	47.406	0.108	0.0513	40.513	0.126	0.057	45.139	0.126	0.120
Tekir 56+400	0.0395	24	0.164	0.0672	18.446	0.364	0.0553	26.151	0.211	0.246
	RIGHT TUBE									
	LS-Y (m)	**H (m)**	**LS-Y' (%)**	**R-Y (m)**	**H (m)**	**R-Y' (%)**	**RS-Y (m)**	**H (m)**	**RS-Y' (%)**	**MEAN-Y' (%)**
Tirebolu 3+858	0.048	13.995	0.342	0.06	7.632	0.786	0.042	12.957	0.324	0.484
Tirebolu 4+407	0.0144	35.506	0.040	0.024	33.087	0.072	0.016	42.312	0.037	0.050
Caglayan 49+044	0.0357	48.559	0.073	0.0294	45.956	0.063	0.0315	53.897	0.058	0.065
Caglayan 50+777	0.0493	86.607	0.056	0.0377	82.53	0.045	0.0435	89.794	0.048	0.050
Caglayan 51+148	0.0231	31.366	0.073	0.0315	26.83	0.117	0.0273	33.999	0.080	0.090
Tekir 56+353	0.0542	43.791	0.123	0.0456	36.422	0.125	0.0485	40.529	0.119	0.123
Tekir 56+400	0.0553	30.406	0.181	0.0711	25.051	0.283	0.0395	30.846	0.128	0.198

Table 6.2. Numerical model findings in terms of normalized convergences and damaged zone thickness of the tunnels.

Tunnel Name	Convergence Measured & Numerically Modeled Tunnel Sections (Km)	Mean Y' (%) Value of Numerical Model	H_{max} (m)	Thickness and Depth of HDZ_{peak} (m)	Thickness of EDZ_{peak} (m)	Depth of EDZ_{peak} (m)	Geological Description
Eceabat	185+480	0.115	30.04	5.98	3	8.98	Clay-claystone-siltstone intercalation and sandstone-sand intercalation
	188+985	0.111	30.43	5.89	1.77	7.66	
Tirebolu	3+858	0.461	8.82	7.14	7.52	14.66	Tuff and dacite
	4+407	0.059	13.08	6.89	0.98	7.87	Tuff, dacite and weathered dacite
Caglayan	49+044	0.075	58.99	9.25	9.26	18.51	Sandstone interbedded conglomerates, claystone
	50+777	0.052	90.39	8.99	11.25	20.24	Limestone and claystone
	51+148	0.094	44.25	6.67	5.01	11.68	Sandstone interbedded conglomerates, weathered claystone and mudstone, residual soil, conglomerates sandstone claystone intercalation
Tekir	56+353	0.121	29.57	6.36	11.66	18.02	Dolomitic limestone
	56+400	0.222	21.24	9.52	8.73	18.25	

CHAPTER 7

VALIDATION OF THE NUMERICAL MODEL

7.1 Validation of Convergences

Whether to understand if there is any meaningful relation between the statistical model findings, convergence monitoring data and the findings of the numerical modelling, all of the results were compared with each other. For this aim, 9 tunnel sections from 5 different ongoing tunnels used in validation of the statistical model, and in numerical modelling chapters (Chapters 5 and 6), were compared and interpreted. To obtain reliable numerical model validation, the tunnel sections which have geotechnical drilling on it, were selected. By this way, real rock mass geotechnical parameters were used instead of using derived ones. For this reason, 9 out of 30 tunnel sections have been used, for the numerical model validation step.

Comparison results were given in Table 7.1. By using these data, numerical model findings versus convergence monitoring data graph (Figure 7.1), was plotted. As can be seen from Figure 7.1, the R^2 value for numerical model findings and measured convergence data is obtained as 0.67. This is considered to be a reasonable coefficient of determination value.

Table 7.1. Comparison of mean normalized tunnel convergence data, which are selected for validation of the findings of statistical modeling, with the numerical modelling mean normalized convergence results[1].

Tunnel Name	Conv. Meas. Tun. Sect. (Km)	Num. Mod. Tun. Sect. (Km)	Meas. Mean Y' Value (%60)	Mean Y' (%) Value of Numerical Model[2]	Y' (%) Value of Phase Model[3] (Left or Single Tube)	Y' (%) Value of Phase Model[4] (Right Tube)
ECABAT1	185+480	185+480	0.0639	0.115	0.115	
ECABAT2	188+985	188+985	0.119	0.111	0.111	
TIREBOLU 2	3+858	3+858	0.525	0.461	0.439	0.484
	4+407	4+407	0.254	0.059	0.068	0.050
CAGLAYAN	49+044	49+044	0.083	0.075	0.086	0.065
	50+777	50+777	0.033	0.052	0.053	0.050
	51+148	51+148	0.092	0.094	0.098	0.090
TEKIR	56+353	56+353	0.080	0.121	0.120	0.122
	56+400	56+400	0.096	0.222	0.246	0.197

1 *Validation convergence data and cross sections were taken from Table 6.1. The same tunnel sections have been preferred for validation and numerical modelling to ensure the consistency between two data sets.*

2 *As they are coherent with each other and for the sake of clarity mean convergence values of left and right tubes have been taken into account together*

3 *As they are coherent with each other and for the sake of clarity; average convergence values of left shoulder, roof and right shoulder have been taken into account together for the left tube or single tubed tunnel sections.*

4 *As they are coherent with each other and for the sake of clarity; average convergence values of left shoulder, roof and right shoulder have been taken into account together for the right tube in the modeled tunnel section.*

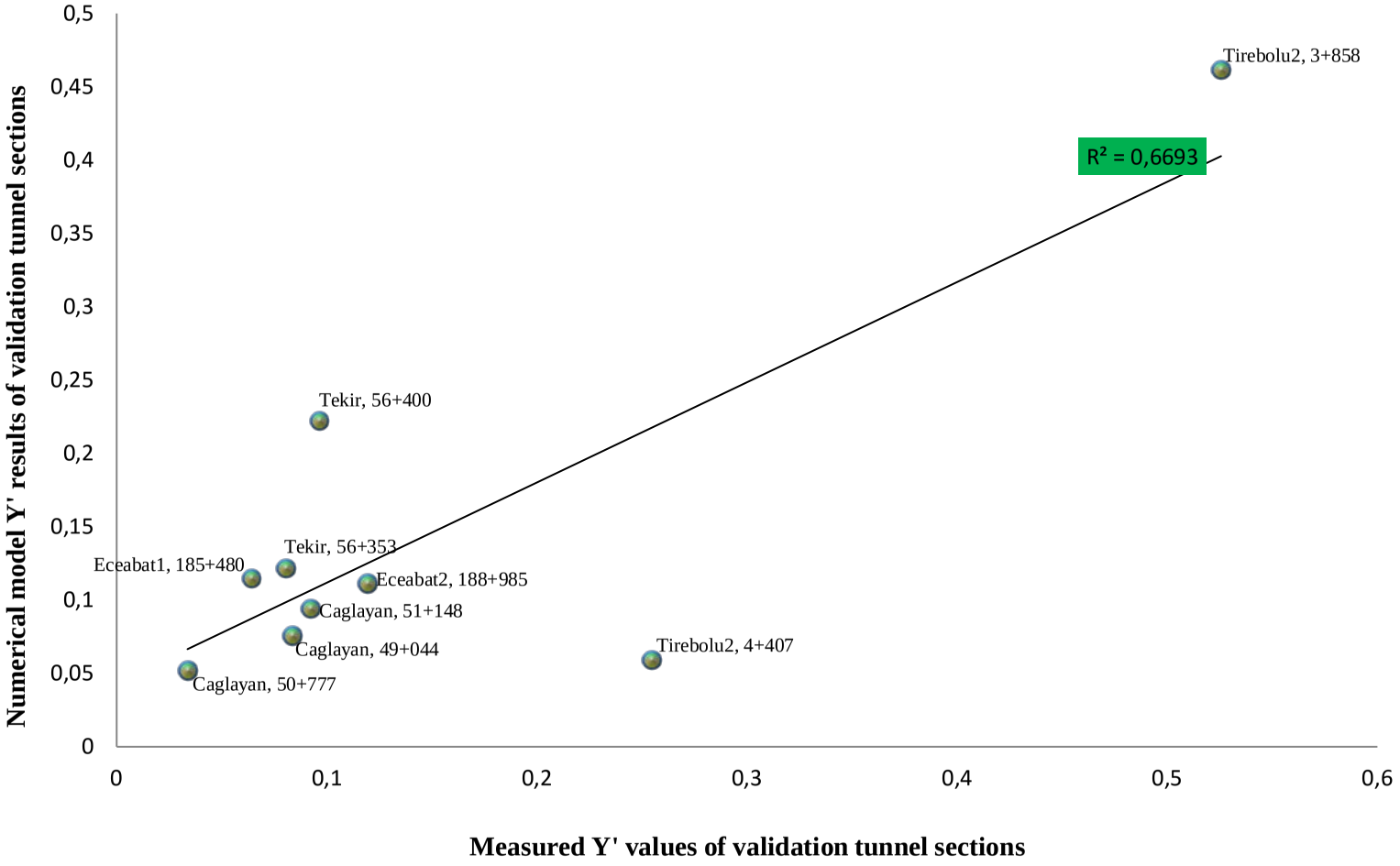

Figure 7.1. Comparison of numerical model convergences (Y') results with measured convergences (Y') values of the tunnels.

This value is not very high, but it should be kept in mind that, there are some assumptions in numerical modellings which affect the results. For example; in numerical modellings, the medium is accepted as homogenous for all of the identified rock masses, besides in-situ stresses could not be measured directly and instead horizontal to vertical stress ratio value was used, and this value was derivated from the Poisson's ratio. Groundwater conditions could not have been determined either. So, all of these assumptions hinder the determination of accurate convergence in numerical model tunnel excavation. Moreover, statistical modelling convergence data were obtained from in-situ convergence monitoring activity and these monitoring activities were furnished at least ten meters behind the excavation face. So, important amount of convergences losses have occurred. Due to all these unfavorable conditions, the obtained R^2 value for measured and modelled convergences are considered to be quite reasonable when compared to previous researches studies (Kim and Chung 2002, and Kontogianni and Stiros 2002).

Amongst these, unmeasured tunnel convergences were tried to be predicted by using measured tunnel convergences and numerical models by Kim and Chung (2002). For this aim, initial and final convergence values from 4 different tunnels at 50 sections were measured and compared at 1D distance from the tunnel face. Although the measured and predicted sections are the identical, R^2 values were obtained as 0.34, 0.63, 0.84 and 0.91 respectively in this study. In Kontogianni and Stiros (2002) study, tunnel convergences were predicted by empirical and numerical methods in 15 sections from 5 tunnels, and as about 30% difference between measured and predicted was observed. In this study R^2 value was not mentioned. The other studies about back analysis techniques, which are explained in the literature section (Chapter 2), try to determine whether rock mass parameters and stress distributions around the excavation or only used to compare the numerical analysis convergence results with the field measurements.

Therefore, when compared to findings of previous studies (Kim and Chung 2002, Kontogianni and Stiros 2002), the R^2 value obtained in this study as 0.67, which is close enough to 1, and is reasonable. Moreover, diversity of the tunnels and convergence data used in this study are much more than the previous studies, too (Dalgic 2002, Golshania et al. 2007, Hao and Azzam 2005, Kim and Chung 2002, Kontogianni and Stiros 2002, Kontogianni and Stathis 2003, Kavvadas 2005, Kontogianni and Stiros 2005, Bizjak and Petkovsek 2004, Schubert et al. 2004, Wu et al. 2004, Sharan 2005, Li et al. 2006, Hsiao et al. 2009, Pellet et al. 2009, Mahdevari and Torabi 2012, Sharifzadeh et al. 2012, Adoko et al. 2013, Mahdevari et al. 2013, Xia et al. 2013).

7.2 Validation of Damaged Zone Thickness

Another target of this study is to find out the thickness of the damaged zones. So, damaged zone thicknesses were compared both with convergence monitoring data, and statistical prediction model findings (Table 7.2). In this table; HDZ and EDZ thicknesses were compared with measured and statistically predicted normalized convergence data. However, damaged zone thicknesses were not compared with the convergence findings of the numerical model as because it was derived from the numerical model itself. There are some differences between the results in terms of normalized convergences. In Ttable 7.2, the discrete convergence results were highlighted with red and consistent ones are highlighted with green. For these distinctions two possibilities can be considered. The first, it may be because of the assumptions in the numerical modelling and the second it may be because of the more reliable data requirements for statistical modellings. However, it can be easily seen that distinctions are become significant especially for the numerical modelling results. This was also observed in Figure 7.1. So, it can be said that these dissimilarities stem from probably because of the some assumptions used in numerical models.

While drawing the border of the damaged zones it was observed that these zones are not regular in shape. This situation had also taken notice of the previous researchers. This condition should also happen to similar in nature, because of the heterogeneous stress and rock mass conditions. So, there is no smooth transition expected within the HDZ, EDZ and EIZ. As the damaged zone thicknesses are variable around the excavation, one by one determination of these thicknesses for every point around the excavation are not practical, so the peak values of HDZ and EDZ were used for generation of empirical relations. Therefore, in the Figures 7.2 and 7.3, normalized peak HDZ (HDZ') and EDZ (EDZ') values were compared with both measured and predicted Y' values. As the normalized convergence data is used for prediction, both of the damaged zone thicknesses were normalized also with tunnel depth to be consistent with the convergence data. Comparison results show that there is significant relation within damaged zone thicknesses and convergences, both for measured and also predicted data (Figure 7.2 and 7.3).

In the highly damaged zone, R^2 values are obtained as 0.8453 when compared with the measured convergences, and 0.834 when compared with the predicted convergences (Figure 7.2). For the excavation damaged zone, R^2 values are obtained as 0.7723 when compared with the measured convergences and 0.6081 when compared with the predicted convergences (Figure 7.3).

Table 7.2. Comparison of numerically determined peak damaged zone thicknesses with measured and predicted convergences

Tunnel Name	Convergence Measured & Numerically Modeled Tunnel Sections (Km)	Meas. Y' Mean Value (%60)	Statistically Pred. Y' Mean Value (%)	Mean Y' (%) Value of Numerical Model	H_{max} (m)	Thickness and Depth of HDZ_{peak} (m)	Thickness of EDZ_{peak} (m)	Depth of EDZ_{peak} (m)	HDZ'_{peak} (%)	EDZ'_{peak} (%)
ECEABAT	185+480	0.064	0.083	0.115	30.038	5.98	3	8.98	19.90	29.89
	188+985	0.119	0.125	0.111	30.429	5.89	1.77	7.66	19.35	25.17
TIREBOLU	3+858	0.525	0.373	0.461	8.821	7.14	7.52	14.66	80.94	166.19
	4+407	0.254	0.298	0.059	13.087	6.89	0.98	7.87	52.64	60.13
CAGLAYAN	49+044	0.083	0.125	0.075	58.993	9.25	9.26	18.51	15.67	31.37
	50+777	0.033	0.037	0.052	90.399	8.99	11.25	20.24	9.94	22.38
	51+148	0.092	0.125	0.094	44.254	6.67	5.01	11.68	15.07	26.39
TEKIR	56+353	0.080	0.083	0.121	29.57	6.36	11.66	18.02	21.50	60.94
	56+400	0.096	0.125	0.222	21.24	9.52	8.73	18.25	44.82	85.92

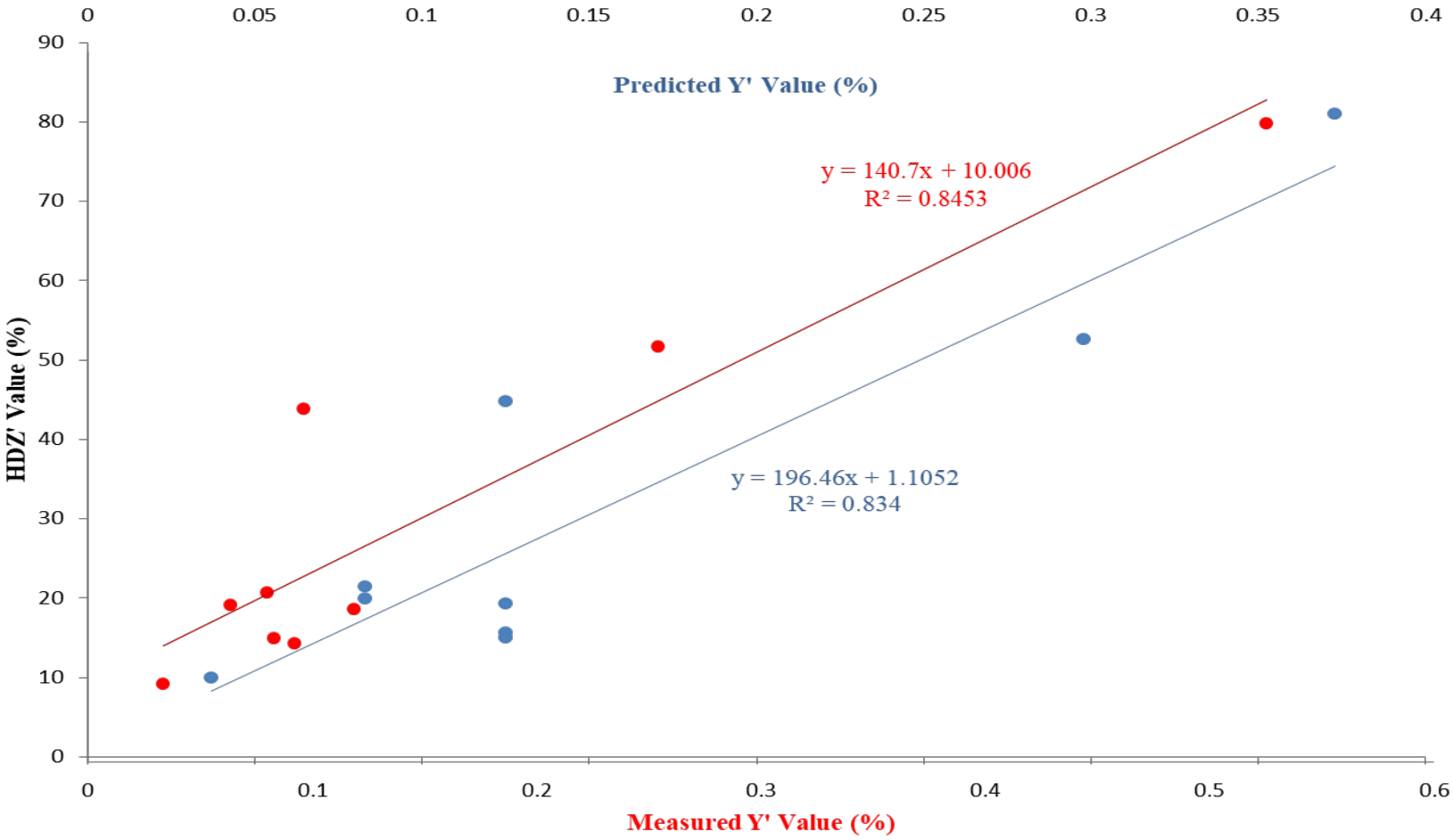

Figure 7.2. Comparison of numerically-obtained normalized peak HDZ values (HDZ' in Table 7.2 orange color column) with measured and predicted normalized convergence (Y') values. Blue dots represents predicted normalized convergence values obtained from statistical modelling in Table 7.2, and red dots represents measured normalized convergence values obtained from field in Table 7.2.

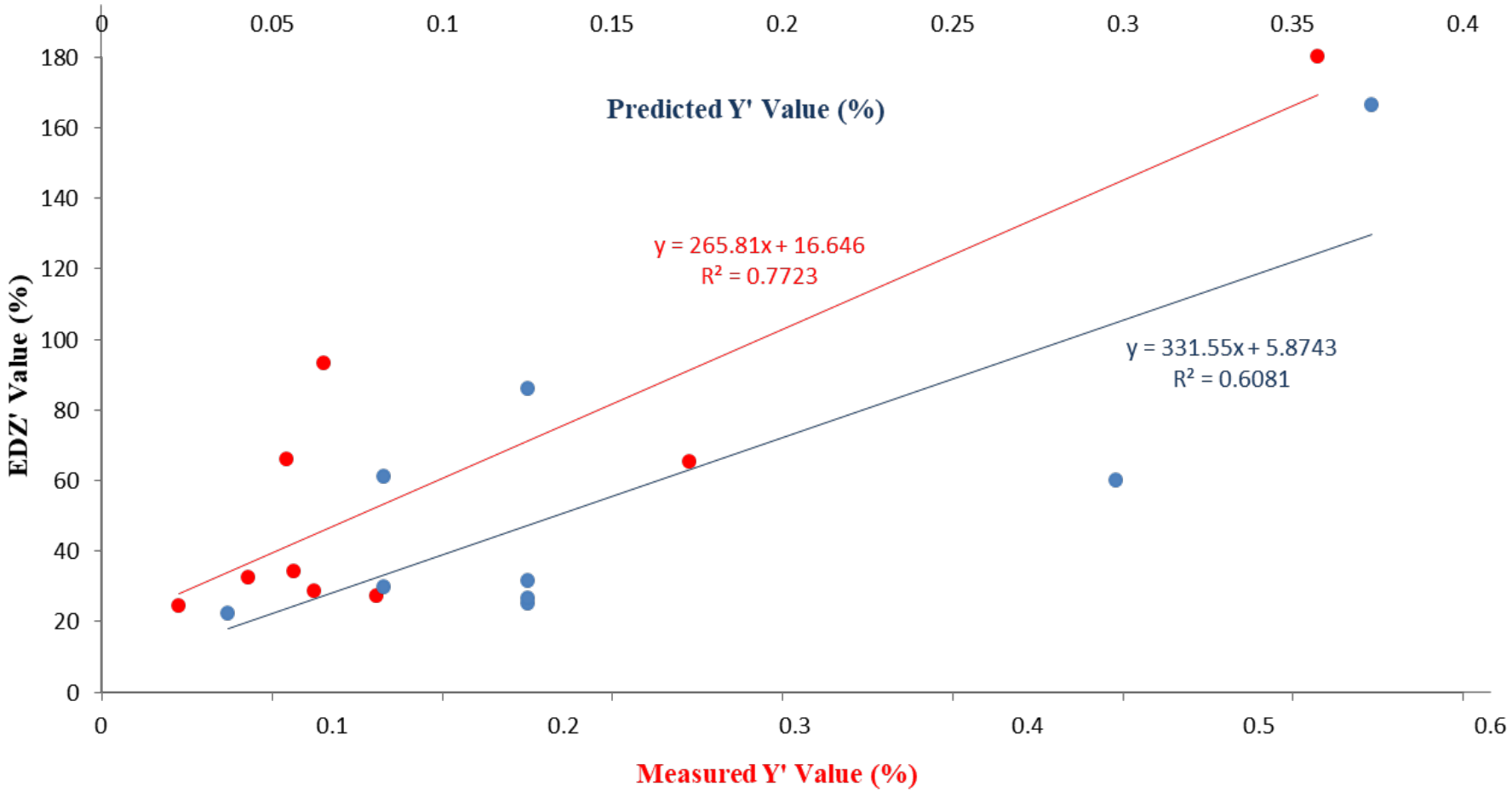

Figure 7.3. Comparison of numerically-obtained normalized peak EDZ values (EDZ' in Table 7.2 aqua green color column) with measured and predicted normalized convergence (Y') values. Blue dots represents predicted normalized convergence values, obtained from statistical modelling in Table 7.2, and red dots represents measured normalized convergence values, obtained from field in Table 7.2.

As it can be understood from the R^2 values, the relation between damaged zone thicknesses and convergence values can be used for advance prediction of tunnel convergences and damaged zone thicknesses. The obtained equations based on the studied tunnels are given below;

$$y_{HDZ} = (140.7x_{m'} + 10.006)\text{x}\left({}^{H}/_{100}\right) \quad \text{for measured Y'\& HDZ}_p \qquad [22]$$

$$y_{HDZ} = \left(196.46x_{p'} + 1.1052\right)\text{x}\left({}^{H}/_{100}\right) \quad \text{for predicted Y'\& HDZ}_p \qquad [23]$$

$$y_{EDZ} = (265.81x_{m'} + 16.646)\text{x}\left({}^{H}/_{100}\right) \quad \text{for measured Y'\& EDZ}_p \qquad [24]$$

$$y_{EDZ} = \left(331.55x_{p'} + 5.8743\right)\text{x}\left({}^{H}/_{100}\right) \quad \text{for predicted Y'\& EDZ}_p \qquad [25]$$

In these equations; " $x_{m'}$, $x_{p'}$ " stands for measured or predicted value of normalized convergences " y' " depending on its use. "y" stands for the thickness of the peak HDZ or EDZ and H stands for the overburden thickness.

In this study, while querying convergence data in the generated numerical models, it was observed that all normalized convergences, converge through to one constant value in case the convergence values of each point is adding up and then their mean values were taking. For instance, let us assume that there are seven convergence measurement points exist on a tunnel; three on the left side, three on the right and one is located on the roof. Besides, evenly distribution of these points around the excavation is not necessary either. After measurement of the resultant convergences of these points, each point is divided into its overburden thickness. When these values are added up to each other and divided up into total number of convergence measurement points, it was observed that the same constant value "C_c" is obtained always for any points around the excavation.

So, the following equation is proposed to formulize this constant value;

$$C_c = \frac{\left(\frac{CV_{x_1y_1}}{h_{x_1y_1}} + \frac{CV_{x_2y_2}}{h_{x_2y_2}} + \frac{CV_{x_3y_3}}{h_{x_3y_3}} + \cdots\ldots \frac{CV_{x_ny_n}}{h_{x_ny_n}}\right)}{n} \qquad [26]$$

In this equation;

- CV stands for “resultant total convergence value of the excavation wall at point x,y”,
- n stands for number of the convergence monitoring points,
- C_c stands for the “Convergence Constant” for the tunnel selected section which has similar topographic and geologic conditions

By using this method, some random points are selected on tunnel wall for convergence reading and the equation 26 is applied to recorded convergence values. So, once the convergence constant was found for the tunnel, convergence value of any unknown point on the tunnel wall can easily be predicted by using inverse function of this equation. There is only one limitation of this approach that is this equation should be used for the specified geological sections having similar topography along the tunnel axis. In any ongoing tunnel excavation, once the tunnel C_c value is obtained by using numerical models and verified with convergence monitoring data, this constant can be used for determination of any unknown convergences which are at the same section but in different position of the tunnel, or it can also be used for prediction of convergences at next excavation section which may have similar geological, geotechnical and topographic properties.

CHAPTER 8

DISCUSSION

Horseshoe-shaped highway tunnel convergences and damaged zone thicknesses, which are excavated with drilling and blasting or conventional techniques, were tried to be identified in this study, by using previously measured tunnel convergence data and geological - geotechnical ground parameters. Tunnel convergence data were collected from various tunnel construction sites around Turkey. However, most of the collected convergence data were not measured accurately by the crew or there were not any logical relations within the convergences and related rock mass. For instance, it was seen that some of the collected tunnel convergence data was measured as 1 or 2 mm and there was not any variation observed for this value during the excavation. So, this kind of data could not be used. In the other case, the measured convergence data were not reliable. Namely, while there was strong rock mass structure, very high convergences have been obtained or the rock mass was weak and very low convergence values were measured. This situation implies the convergence measurements or the rock mass parameters are not determined correctly. So, lots of time was consumed to obtain a reliable convergence measurement data. Nevertheless, it was thought that there is an error tolerance in convergence data used in this study. There are several reasons of this; one of them is the measurement uncertainty itself, the other is contractor's view of aspect to convergence measurement activity, the other is the delay in installation of convergence monitoring points, and the other is accident, excavation machine's hit to convergence monitoring sections. In all these cases, reliable convergence monitoring data cannot be obtained or the results become inaccurate. So, it was tried to use the most reliable data under the authors control in the field and findings of suggested statistical model also prove the reliability of used data.

Besides, another difficulty of this study was obtaining of the required geotechnical data. As its very nature of tunnel constructions, it is located in mountainous topography. Owing to the tunnel route's steep and abrupt morphology, geotechnical drilling and site investigation studies were harder when compared to other site studies. Moreover, completion of these drillings took longer than as usual and was more expensive. As a result of this, limited number of geotechnical drilling could be done along the tunnel route. This is another limitation of the study. As it was impossible to obtain a real rock mass data before the excavation reached the related section, input data were obtained from the geotechnical drilling points for statistical and numerical modelling. 112 input data were used for statistical modelling, and 30 data for validation and numerical modelling. Numerical modelling results showed consistency with field measurement.

Field stress value is necessary for finite element, finite difference or discrete element model user (Sheorey 1994). This value is obtained from empirical equation based on Poisson's ratio of the geological material. In-situ measurement of this value for every tunnel and every modelled section are very expensive. However, this is the best and the most reliable way to obtain the principal stresses (Sheorey 1994). So, empirically obtaining of field stress value can be accepted as another shortcoming of this study. Getting field stress values from the in-situ measurements will increase the prediction capacity of the suggested methods. Besides, tectonic stresses have also significant effect on tunnel behavior after an excavation completed, so if it is possible to measure the tectonic stresses it will give additional information when the seismic loading option is used in the finite element models. Researchers, who want to use methods and formulations suggested in this study, should add a lot of reliable tunnel convergence and geotechnical data to the suggested statistical prediction method. Besides, an experimental tunnel excavation study can be furnished for further verification of the prediction methods suggested in this thesis or any section of a new highway tunnel excavation can be used for this purpose during the normal construction period. Furthermore, if any tunnel section will be used for this purpose, it is strongly suggested to use rod extensometers buried ahead of the excavation area or usage of some geophysical techniques.

This is the best and most reliable way to measure convergences, and damaged zone propagation. In this way, the suggested statistical prediction method and damaged zone thicknesses estimations can be checked accurately.

Although there exists some difficulties described above, our findings are thought to be very practical in terms of use in the field when compared with the previous studies about this subject. Previous convergence and damaged zone estimation methods depend on empirical and statistical methods or back analysis application of numerical methods. As far as now, damaged zone thickness was generally estimated for nuclear depository sites. In this thesis, the suggested convergence estimation method is a kind of decision tree structure designed for the regression of real numbers with C&RT, which is very practical in use when compared to ANN structure. The findings of this estimation structure can easily be understood and interpreted by any user who has a little knowledge about decision tree structures, whereas this is very difficult in ANN structure.

According to findings of the statistical prediction model (Figure 4.4 and 4.5), the lowest normalized convergence value was obtained as 0.037 in case the C_{rm} value is higher than 0.074 MPa and the ϕ_{rm} value is lower than 55°. The highest normalized convergence value is obtained as 0.443 in case the C_{rm} is lower than or equal to 0.013. These are unitless numbers and can be applied to any tunnel, by multiplying it with related tunnel depth and dividing into 100, to find out the convergence values. Each conditional paths given in Figures 4.4 and 4.5 have their own normalized convergence values. For example, for 50 and 100 meters of overburden thicknesses and for the highest and lowest normalized convergences, the highest convergence values are obtained as 2.2 cm and 4.43 cm and the lowest values are obtained as 1.85 cm and 3.7 cm, respectively. According to findings of numerical modelling, highly damaged zone and excavation damage zone thicknesses are obtained as between the lowest 5.89 and the highest 9.52 m, and the lowest 7.66 and highest 20.24 m, respectively. According to findings of this study it can be said that both convergence prediction methods and plastic zone determination techniques suggested in this study give satisfactory results.

Moreover, findings of this study are compared with previous ANN estimation structure and numerical modelling results. In both comparisons, results of this study are very close to previous ANN findings and numerical modelling results, and are proved the reliability of itself. However, the convergence prediction capacity of the independent variables is more powerful especially for the C_{rm} and ϕ_{rm} values, if these are more than 0.040 MPa and 55° respectively. This is from the quantitative lackness of data for tunnel convergence and rock mass geotechnical data. Increasing convergence and geotechnical data will increase the prediction sensitivity of the C&RT model, and this will also broaden the prediction range in terms of independent variables.

For prediction of damaged zone thicknesses, the suggested empirical equations are quite practical and useful tools. However, as similar with the statistical estimation, increasing number of data will definitely increase the prediction capacity of these equations. Nevertheless, it should be kept in mind that damaged zone thickness prediction equations were derived from numerical analysis and then have some assumptions (such as homogeneous medium, in-situ stresses and groundwater conditions) which affect the results. Yet, computer aided modelling operations, such as finite element numerical modelling, are a piece of work of the arts for the engineers who creates the design. So, the prediction capability of the numerical models strongly depends on the engineers' knowledge level and how well projected the geological structure to the numerical models.

Every underground excavation is unique and should be evaluated to its very own properties while construction is going on. For this aim, rock mass classifications, site investigation findings, engineering geological maps, geological and geotechnical properties should have been considered at first. These data will be a good starting point for the tunnel engineer. After that, by using these data, tunnel construction should be monitored at every excavation step, in terms of convergences and rock mass conditions. If necessary, numerical models should be regenerated especially for the critical sections.

It should always be kept in mind that all of the approaches about evaluation of tunnel convergences and rock mass structure should be used for pre-judgement. In fact, instrumental measurement techniques especially buried ones (such as road extensometers) are the best way to measure the convergences before the excavation. Other instrumental monitoring techniques may cause loss of convergence data. However, buried devices are expensive and require deliberate attention and consume crew's time. In such cases, our suggested methods can be used for the estimation of convergences and damaged zone thickness.

CHAPTER 9

CONCLUSIONS AND RECOMMENDATIONS

There were two main goals of this thesis, prediction of tunnel convergences, and prediction of plastic zone thicknesses around the horseshoe-shaped highway tunnel excavation. Based on the findings of this study, the followings are obtained and proposed;

a) Totally 142 tunnel cross sections (112 for prediction model and 30 for validation) were evaluated on the basis of this study. Geological structures of the studied tunnel rock masses are igneous and sedimentary.
b) RMR values of the studied tunnels lie within 30 - 67 and Q values are 0.005-5.75, respectively. These values refer to weak to fair quality rock masses.
c) H, C_{rm}, Φ_{rm} and E_{rm} values are 4 - 388 m, 0.012 - 0.684 MPa, 14 - 62°, 4-14000 MPa, respectively.
d) ANN, C&RT and CHAID methods gave satisfactory results on prediction of convergences.
e) C&RT and ANN have almost the same explanation ratios for prediction on convergences. However, C&RT method was preferred because it is easier to use.
f) As result of convergence prediction model, 11 conditional paths were obtained. So, any user who wants to estimate tunnel convergences can follow the suitable paths.
g) Tunnel overburden thickness (H) was determined as the most effective parameter on tunnel convergences and C_{rm} is found to be as the second most effective. Φ_{rm}, E_{rm}, RMR and Q parameters are found to be the other effective parameters on tunnel convergences.

h) Findings of the statistical models were validated by 30 different tunnel cross-sections and obtained results show that our suggested decision tree method "C&RT", for prediction of convergences can be used in the field.

i) According to findings of the statistical prediction model (Figure 4.4 and 4.5), the lowest normalized convergence value was obtained as 0.037 in case the C_{rm} value is higher than 0.074 MPa and the ϕ_{rm} value is lower than 55°. The highest normalized convergence value is obtained as 0.443 in case the C_{rm} is lower than or equal to 0.013. These are unitless numbers and can be applied to any tunnel, by multiplying it with related tunnel depth and dividing into 100, to find out the convergence values.

j) Based on the modeling and measured convergences, damaged zones around the tunnel excavation are not regular and there are transitions between them.

k) According to our findings which depend on numerical modelling, highly damaged zone thickness is obtained as between 5.89 and 9.52 m, while excavation damaged zone thickness is in between 7.66 and 20.24 m. These are the peak values and observed in a local point of the excavation surface in the numerical modelling. Unless the rock bolts are not used solely and used in a pre-specified pattern with steel set and shotcrete, it can be said that 6 to 10 m length rock bolts may be sufficient for the stabilization of weak to fair rock masses in tunnel excavations.

l) At the end of the comparison of convergences and plastic zone thicknesses between measured and predicted tunnel converge values the following equations were obtained;

- $y_{HDZ} = (140.7x_{m'} + 10.006)\text{x}(H/100)$, for measured Y'& HDZ_p
- $y_{HDZ} = (196.46x_{p'} + 1.1052)\text{x}(H/100)$, for predicted Y'& HDZ_p
- $y_{EDZ} = (265.81x_{m'} + 16.646)\text{x}(H/100)$, for measured Y'& EDZ_p
- $y_{EDZ} = (331.55x_{p'} + 5.8743)\text{x}(H/100)$, for predicted Y'& EDZ_p

In these equations; " $x_{m'}$, $x_{p'}$ " stands for measured or predicted value of normalized convergences " y' " depending on its use. "y" stands for thickness of the peak HDZ or EDZ and H stands for the overburden thickness.

m) In this study, it was observed that all normalized convergences, converge to one constant value in case the convergence values of each point is adding up and then their mean values were taking. It was observed that the same constant value "C_c" is obtained always for any points around the excavation. So, the following equation is proposed to formulate this constant value;

$$C_c = \frac{\left(\frac{CV_{x_1y_1}}{h_{x_1y_1}} + \frac{CV_{x_2y_2}}{h_{x_2y_2}} + \frac{CV_{x_3y_3}}{h_{x_3y_3}} + \cdots \ldots \frac{CV_{x_ny_n}}{h_{x_ny_n}}\right)}{n}$$

In this equation; CV stands for "resultant total convergence value of the excavation wall at point x,y", n stands for number of the convergence monitoring points, C_c stands for the "Convergence Constant" for the tunnel. There is only one limitation of this approach that is this equation should be used for the specified geological sections having similar topography along the tunnel axis.

n) Engineering geology, geotechnical site investigations and rock mass classification systems (RMR, Q and NATM etc.) are good starting points for a reliable tunnel design and construction. However, these systems should not be used by itself as unique methods for the tunnel design and should be supported by some advanced studies such as suggested methods in this thesis.

o) Using buried type tape extensometers and borehole geophysic methods are strongly suggested for the accurate determination of yield zone thicknesses and convergences before the advance of an excavation.

REFERENCES

Adoko, A.C., Jiao, Y.Y., Wub, L., Wang, Z.H., 2013, *Predicting Tunnel Convergence Using Multivariate Adaptive Regression Spline And Artificial Neural Network,* Tunneling and Underground Space Technology, v38, p; 368-376

Alejano, L.R., Dono, R.A., Alonso, E., Manín, F.G., 2009, Ground Reaction Curves For Tunnels Excavated In Different Quality Rock Masses Showing Several Types Of Post-Failure Behavior, Tunneling and Underground Space Technology, v24, p;689-705

Alejano, L. R., Dono, A. R, Veiga M., 2012, Plastic Radii And Longitudinal Deformation Profiles Of Tunnel Excavated In Strain-Softening Rock Masses, Tunneling and Underground Space Technology, v30, p; 169-182

Barton, N., 2002, Some New Q-Value Correlations To Assist In Site Characterization And Tunnel Design, International Journal of Rock Mechanics & Mining Sciences, v39, p; 185–216

Basarir, H., Genis, M., Ozarslan, A., 2010, The Analysis of Radial Displacements Occurring Earth, Face of a Circular Opening in Weak Rock Mass, International Journal of Rock Mechanics & Mining Sciences, v47, p.771–783

Bieniawski, Z.T., 1989, Engineering Rock Mass Classification, John Wiley and Sons

Bieniawski Z.T., 1990, Tunnel Design By Rock Mass Classifications, US Army engineers waterways experiment station technical report GL-79-19

Bizjak, K. F., Petkovsek, B., 2004, Displacement Analysis Of Tunnel Support In Soft Rock Around A Shallow Highway Tunnel At Golovec, Engineering Geology, v75, p; 89–106

Blumling, P., Bernier, B., Lebon, P., Martin, D.C., 2007, The Excavation Damaged Zone In Clay Formations Time-Dependent Behavior And Influence On Performance Assessment, Physics and Chemistry of the Earth, v32, p; 588–599

Breiman, L., Friedman, J.H., Olshen, R.A., Stone, C.J., 1984, Classification and Regression Trees, Monterey, CA: Wadsworth & Brooks/Cole Advanced Books & Software.

Brodley, C.E., Utgoff, P.E., 1995, Multivariate Decision Trees, Machine Learning, v.19, p;45-77

Cai, M., Kaiser, P.K., Tasaka, Y., Minami, M., 2007, Determination Of Residual Strength Parameters Of Jointed Rock Masses Using The GSI System, International Journal of Rock Mechanics & Mining Sciences, v44, p; 247–265

Cybenko, G., 1989, Approximation by Superpositions of a Sigmoidal Function, Mathematics of Control, Signals, and Systems, v2(4), p;303–314

Dalgic, S., 2002, A Comparison Of Predicted And Actual Tunnel Behavior In The Istanbul Metro, Turkey, Engineering Geology, v63, p.69-82

Deere, D.U., Miller, R.P., 1966, Enginnering Classification and Index Properties for Intact Rock, Tech. Rept. No AFWL-65-116

Draper, N.R., Smith, H., 1998, Applied Regression Analysis, Wiley-Interscience, 3rd edition

Devore, J.L., 2011, Probability and Statistics for Engineering and the Sciences 8th Ed., Boston, MA, Cengage Learning, p;508–510

Fakhimi, A., Salehic, D., Mojtabaid, N., 2004, Numerical Back Analysis For Estimation Of Soil Parameters in The Resalat Tunnel Project, Tunnelling and Underground Space Technology, v.19 p.57–67

Fattahi, H., Farsangi, E.A.M., Shojaee, S., Mansouri, H., 2014, Selection of a Suitable Method for the Assessment of Excavation Damage Zone Using Fuzzy

AHP in Aba Saleh Almahdi Tunnel, Iran, Arabian Journal of Geosciences, v8, pp 2863-2877
Fenner, R., 1938, Untersuchungen Zur Erkenntnis Des Gebirgs Druckes, p; 638

Friedman J. H., 1991, Multivariate Adaptive Regression Splines, The Annals of Statistics, v19, p;1-141

Gandomi, A., Fridline, M.M., Roke, D.A., 2013, Decision Tree Approach for Soil Liquefaction Assessment, The Scientific World Journal, v2013, p.8

Glantz, S.A., Slinker, B.K., 1990 Primer of Applied Regression and Analysis of Variance, McGraw-Hill

Golshania, A., Odaa, M., Okuia, Y., Takemurab, T. Munkhtogooa, E., 2007, Numerical Simulation of The Excavation Damaged Zone Around an Opening in Brittle Rock, International Journal of Rock Mechanics & Mining Sciences, v44, p.835–845

Hao, Y.H., Azzam, R., 2005, The Plastic Zones and Displacements Around Underground Openings in Rock Masses Containing A Fault, Tunnelling and Underground Space Technology, v20 p.49–61

Hammah, R.E., Yacoub, T., Corkum B., Curran, J.H., 2008, The Practical Modeling of Discontinuous Rock Masses with Finite Element Analysis, American Rock Mechanics Association, 08-180

Hastie, T., Tibshirani, R., Friedman, J.H., 2001, The Elements Of Statistical Learning : Data Mining, Inference, and Prediction, New York: Springer Verlag

Hisatake, M., Hieda, Y., 2008, Three-Dimensional Back-Analysis Method for The Mechanical Parameters of The New Ground Ahead of a Tunnel Face, Tunnelling and Underground Space Technology, v23 p.373–380

Hoek, E., Brown, E.T., 1997, Practical Estimates of Rock Mass Strength, International Journal of Rock Mechanics and Mining Sciences, v34, p; 1165-1186

Hoek, E., 2001, Big Tunnels In Bad Rock 2000 Terzaghi Lecture, ASCE Journal of Geotechnical and Geoenvironmental Engineering, v127, p; 726-740

Hoek, E., Torres, C.C., Corkum, B., 2002, Hoek-Brown Failure Criterion-2002 Edition, In Proceedings of the 5th North American rock mechanics symposium, Toronto, Canada, v.1, p;267–73

Hoek, E., Diederichs, M.S., 2006, Empirical Estimation of Rock Mass Modulus, International Journal of Rock Mechanics & Mining Sciences, v43, p; 203–215

Hsiao, F.Y., Wang, C.L., Chern, J.C., 2009, Numerical Simulation of Rock Deformation for Support Design in Tunnel Intersection Area, Tunnelling and Underground Space Technology, v24, p.14–21

Hyndman, R.J., Koehler, A.B., 2006, "Another look at measures of forecast accuracy", International Journal of Forecasting, v22(4), p:679–688

Jinga, L., Hudson, J.A., 2002, Numerical Methods In Rock Mechanics, International Journal of Rock Mechanics & Mining Sciences, v.39 p.409–427

Kavvadas, M.J., 2005, Monitoring Ground Deformation In Tunneling: Current Practice In Transportation Tunnels, Engineering Geology, v79, p; 93– 113

Kayri, M and Kayri, I., 2015, The Comparison of Gini and Twoing Algorithms in Terms of Predictive Ability and Misclassification Cost in Data Mining: An Empirical Study, Inter. Journal of Computer Trends and Technology, v. 27(1)

Kim, B. N. Y., Chung H. S., 2002, A Study on Prediction of Final Displacement of Road Tunnel Section During Excavation in Highly Weathered Rock by NATM, KSCE Journal of Civil Engineering, v6, p; 399-405

Kim, H.M., Rutqvist, J., Jeong, J.H., Choi, B.H., Ryu, D.W., Song, W.K., 2012, Characterizing Excavation Damaged Zone and Stability of Pressurized Lined Rock Caverns for Underground Compressed Air Energy Storage, Rock Mechanic Rock Engineering

Kontogianni, V., Stiros, S.C., 2002, Predictions And Observations Of Convergence In Shallow Tunnels: Case Histories In Greece, Engineering Geology, v63, p; 333– 345

Kontogianni, V., Stathis, S., 2003, Tunnel Monitoring During The Excavation Phase: 3-D Kinematic Analysis Based On Geodetic Data, Proceedings of 11th FIG Symposium on Deformation Measurements, Santorini, Greece,

Kontogianni, V. A., Stiros, S.C., 2005, Induced Deformation During Tunnel Excavation: Evidence From Geodetic Monitoring, Engineering Geology, v79, p; 115–126

Kontogianni, V., Psimoulis, P., Stiros, S., 2006, What Is The Contribution Of Time-Dependent Deformation In Tunnel Convergence?, Engineering Geology, v82, p; 264– 267

Kwon, S., Lee, C.S., Cho, S.J., Jeon, S.W., Cho, W.J., 2009, An Investigation Of The Excavation Damaged Zone At The Kaeri Underground Research Tunnel, Tunnelling and Underground Space Technology, v24, p; 1–13

Lee, Y.K., Pietruszczak, S., 2008, A New Numerical Procedure For Elasto-Plastic Analysis of a Circular Opening Excavated in a Strain-Softening Rock Mass, Tunnelling and Underground Space Technology, v.23, p.588–599

Lee, S., Park, I, 2013, Application of Decision Tree Model for the Ground Subsidence Hazard Mapping Near Abandoned Underground Coal Mines, Journal of Environmental Management, v127, p166-76

Lei, Q., Latham, J.P., Xiang, J., Tsang, C.F., 2017, Role of Natural Fractures in Damage Evolution Around Tunnel Excavation in Fractured Rocks, Engineering Geology, v231, p.100–113

Li, S., Yang, J., Hao, W, Shanga, Y., 2006, Intelligent Back-Analysis of Displacements Monitored in Tunnelling, International Journal of Rock Mechanics & Mining Sciences, v43 p.1118–1127

Lia, S., Yua, H., Liua, Y., Wub, F., 2008, Results From in Situ Monitoring of Displacement, Bolt Load, and Disturbed Zone of a Power House Cavern During Excavation Process, International Journal of Rock Mechanics & Mining Sciences, v45, p.1519–1525

Lin, C., Zhou, L., Li, S., Xu, Z., Li, L., Wu, J., Zhang, Y., 2015, Tunnel Monitoring and Measurement Case Study in Qiyueshan Tunnel, 3rd International Conference on Material, Mechanical and Manufacturing Engineering (IC3ME 2015)

Lunardi, P., 2000, The Design And Construction Of Tunnels Using The Approach Based On The Analysis Of Controlled Deformation In Rocks And Soils, T&T International ADECO-RS Approach

Mahdevari, S., Torabi, S. R., 2012, Prediction Of Tunnel Convergence Using Artificial Neural Networks, Tunnelling and Underground Space Technology, v28, p; 218–228

Mahdevari, S., Haghighat, H. S., Torabi, S. R., 2013, A Dynamical Approach Based On SVM Algorithm For Prediction Of Tunnel Convergence During Excavation, Tunneling and Underground Space Technology, v38, p; 59–68

Martino, J.B., Chandler, N.A., 2004, Excavation-Induced Damage Studies At The Underground Research Laboratory, International Journal of Rock Mechanics & Mining Sciences, v41, p; 1413–1426

Murthy, S.K., 1998, Automatic Construction of Decision Trees from Data: A Multi-Disciplinary Survey, Data Mining and Knowledge Discovery, v.2(4), p;345-389

Nisbet, R., Elder, J., Miner, G., 2009, Handbook of Statistical Analysis and Data Mining Applications, Elseiver, Canada

Pham, B.T., Bui,D.T., Dholakia,M.B., Prakash, I., Pham, H.V., 2016, A Comparative Study of Least Square Support Vector Machines and Multiclass Alternating Decision Trees for Spatial Prediction of Rainfall-Induced Landslides in a Tropical Cyclones Area, Geotechnical and Geological Engineering, v34, p.1807–1824

Palmstrom, A., Einar, B., 2006, Use And Misuse Of Rock Mass Classification Systems With Particular Reference To The Q-System, Tunneling and Underground Space Technology, v21, p; 575–593

Pellet, F., Roosefid, M., Deleruyelle, F., 2009, On The 3D Numerical Modelling Of The Time-Dependent Development of The Damage Zone Around Underground Galleries During And After Excavation, Tunnelling and Underground Space Technology, v.24 p.665–674

Perras, M. A., Diederichs, M. S., 2015, Predicting excavation damage zone depths in brittle rocks, Journal of Rock Mechanics and Geotechnical Engineering, v8, p; 60-74

Pierpaolo, O., 2005, Back-Analysis Techniques For The Improvement Of The Understanding Of Rock In Underground Constructions, Tunneling and Underground Space Technology, v20, p; 7–21

Quinlan, J.R., 1986, Induction of Decision Trees, Machine Learning 1: p.81-106, Kluwer Academic Publishers

Rabcewicz,L.,1964.http://www.eos.ubc.ca/courses/eosc547/lecturematerial/Rabcewicz NATM.pdf

Rahimi, B., Kourosh, S., Sharifzadeh, M., 2014, Evaluation of Rock Mass Engineering Geological Properties Using Statistical Analysis and Selecting Proper Tunnel Design Approach in Qazvin–Rasht Railway Tunnel, Tunnelling and Underground Space Technology, v41, p.206-222

Ramamurthy, T., 2004, A Geo-Engineering Classification For Rocks And Rock Masses, International Journal of Rock Mechanics & Mining Sciences, v41, p; 89–101

Ramulu, M. Chakraborty, A.K., Sitharam, T.G., 2009, *Damage Assessment of Basaltic Rock Mass Due to Repeated Blasting in a Railway Tunnelling Project – A Case Study,* Tunnelling and Underground Space Technology, v24, p.208–221

Rokach, L., Maimon, O., 2005, Top-Down Induction of Decision Trees Classifiers-A Survey, IEEE Transactions on Systems, Man, and Cybernetics, Part C. 35(4), p.476–487

Rokach, L., Maimon, O., 2008, Data Mining With Decision Trees: Theory and Applications, World Scientific Pub Co Inc.

Rokach, L., Maimon, O., 2010, Data Mining And Knowledge Discovery Handbook, Springer, 2nd edition, NewYork, p164

Rosenblatt, F., 1961, Principles of Neurodynamics: Perceptrons and the Theory of Brain Mechanisms, Spartan Books, Washington DC

Sakurai, S., Takeuchi, K., 1983, Back Analysis of Measured Displacements Of Tunnels, Rock Mechanics and Rock Engineering, v16, p; 173-180

Sakurai, S., Akutagawa, S., Takeuchi, K., Shinji, M., Shimizu, N., 2003, Back Analysis for Tunnel Engineering as a Modern Observational Method, Tunneling and Underground Space Technology, v18, p; 185–196

Satici, O., Unver, B., 2015, Assessment of tunnel portal stability at jointed rock mass: A comparative case study, Computers and Geotechnics, v64, p.72-82

Sato, T., Kikuchi, T., Sugihara, K., 2000, In-Situ Experiments On An Excavation Disturbed Zone Induced By Mechanical Excavation In Neogene Sedimentary Rock At Tono Mine, Central Japan, Engineering Geology, v56, p; 97–108

Schubert, W., Grossauer, K. Button, E.A., 2004, Interpretation of Displacement Monitoring Data For Tunnels in Heterogeneous Rock Masses, International Journal of Rock Mechanics & Mining Sciences, v41 p.538–539

Sharan, S.K., 2005, Exact and Approximate Solutions For Displacements Around Circular Openings In Elastic–Brittle–Plastic Hoek–Brown Rock, International Journal of Rock Mechanics & Mining Sciences, v42, p.542–549

Sharifzadeh, M., Daraei, R., Broojerdi, M. S., 2012, Design Of Sequential Excavation Tunneling In Weak Rocks Through Findings Obtained From Displacements Based Back Analysis, Tunneling and Underground Space Technology, v28, p; 10–17

Sheorey, P.R., 1994, A Theory For In Situ Stresses In Isotropic And Transversely Isotropic Rock, International Journal of Rock Mechanics & Mining Sciences, v31, p.23-34

Siren, T., Kantia, P., Rinne, M., 2015, Considerations and Observations of Stress-Induced and Construction-Induced Excavation Damage Zone in Crystalline Rock, International Journal of Rock Mechanics & Mining Sciences, v73, p; 165–174

Sterpi, D., 1999, An Analysis Of Geotechnical Problems Involving Strain Softening Effects, International Journal For Numerical And Analytical Methods In Geomechanics, v23, p; 1427- 1454

Sterpi, D., Gioda, G., 2009, Visco-Plastic Behaviour Around Advancing Tunnels In Squeezing Rock, Rock Mechanics and Rock Engineering, v42, p; 319–339

Strobl, C., Malley, J., Tutz, G., 2009, An Introduction to Recursive Partitioning: Rationale, Application and Characteristics of Classification and Regression Trees, Bagging and Random Forests, Psychological Methods, v.14(4), p.323–348

Terzaghi, K., 1946, Rock Defects and Loads on Tunnel Supports, Youngstown, Ohio.

Torres, C.C., Fairhurst, C., 1999, The Elasto-Plastic Response of Underground Excavations in Rock Masses That Satisfy The Hoek & Brown Failure Criterion, International Journal of Rock Mechanics and Mining Sciences, v36, p.777-809

Torres, C.C., Fairhurst, C., 2000, Application Of The Convergence-Confinement Method Of Tunnel Design To Rock Masses That Satisfy The Hoek-Brown Failure Criterion, Tunneling and Underground Space Technology, v15, p;187-213

Verma, H.K., Samadhiya, N.K., Singh, M., Goela, R.K., Singh, P.K., 2018, Blast Induced Rock Mass Damage Around Tunnels, Tunnelling and Underground Space Technology, v71, p.149-158

Wanga, S., Ni, P., Guo, M., 2013, Spatial Characterization of Joint Planes And Stability Analysis of Tunnel Blocks, Tunnelling and Underground Space Technology v.38, p.357–367

Wu, J.H., Ohnishi, Y., Nishiyama, S., 2004, Simulation of the Mechanical Behavior of Inclined Jointed Rock Masses During Tunnel Construction Using Discontinuous Deformation Analysis (DDA), International Journal of Rock Mechanics & Mining Sciences, v41, p.731–743

Wu, F., Liu, J., Liu, T., Zhuang, H., Yan, C., 2009, A Method For Assessment of Excavation Damaged Zone (EDZ) of a Rock Mass And Its Application To a Dam Foundation Case, Engineering Geology, v.104 p.254–262

Xia, X., Li, H.B., Li, J.C., Liu, B., Yu, C., 2013, A Case Study On Rock Damage Prediction and Control Method For Underground Tunnels Subjected to Adjacent Excavation Blasting, Tunnelling and Underground Space Technology, v35 p.1–7

Yanga, J.H., Yaoa, C., Jianga, Q.H. Lub, W.B., Jianga, S.H., 2017, 2d Numerical Analysis of Rock Damage Induced by Dynamic In-Situ Stress Redistribution and Blast Loading in Underground Blasting Excavation, Tunnelling and Underground Space Technology, v70, p.221-232

Yassaghi, A., Salari-Rad, H., 2005, Squeezing Rock Conditions At An Igneous Contact Zone In The Taloun Tunnels, Tehran-Shomal Freeway, Iran: A Case Study, International Journal of Rock Mechanics & Mining Sciences, v42, p; 95–108

Yi, X., Feng, G., Xingguang, L., Xin, L., 2017, Permeability and Pressure Distribution Characteristics of The Roadway Surrounding Rock in the Damaged Zone of an Excavation, International Journal of Mining Science and Technology, v27, p.211-219

Zhang, L.Q., Yue, Z.Q., Yang, Z.F., Qi, J.X., Liu, F.C., 2006, A Displacement-Based Back-Analysis Method for Rock Mass Modulus and Horizontal in Situ Stress in Tunneling, Tunneling and Underground Space Technology, v21, p; 636–649

Zhang, Q., Jiang, B.S., Wang, S., Ge, X., Zhang, H., 2012, Elasto-Plastic Analysis of a Circular Opening in Strain-Softening Rock Mass, International Journal of Rock Mechanics & Mining Sciences, v50, p.38-46

Zhang, W.G., Goh, A.T.C., 2013, Multivariate Adaptive Regression Splines For Analysis Of Geotechnical Engineering Systems, Computers and Geotechnics, v48, p; 82-95

https://www.rocscience.com/rocscience/products/rs2

APPENDIX A

DETAILED METHODOLOGY FLOWCHART

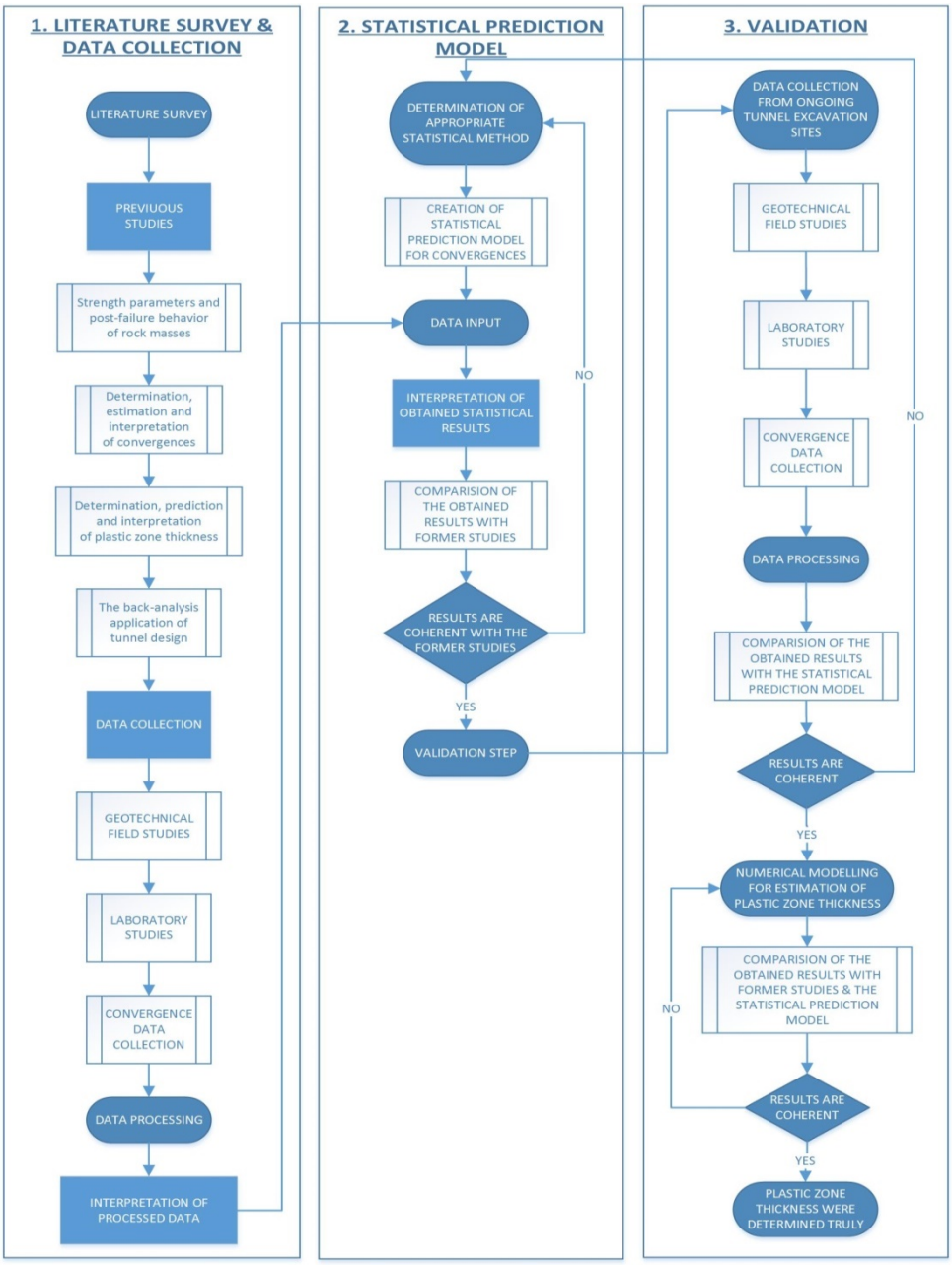

Figure A.1. Detailed flowchart of the proposed study methodology

APPENDIX B

NUMERICAL MODELLINGS

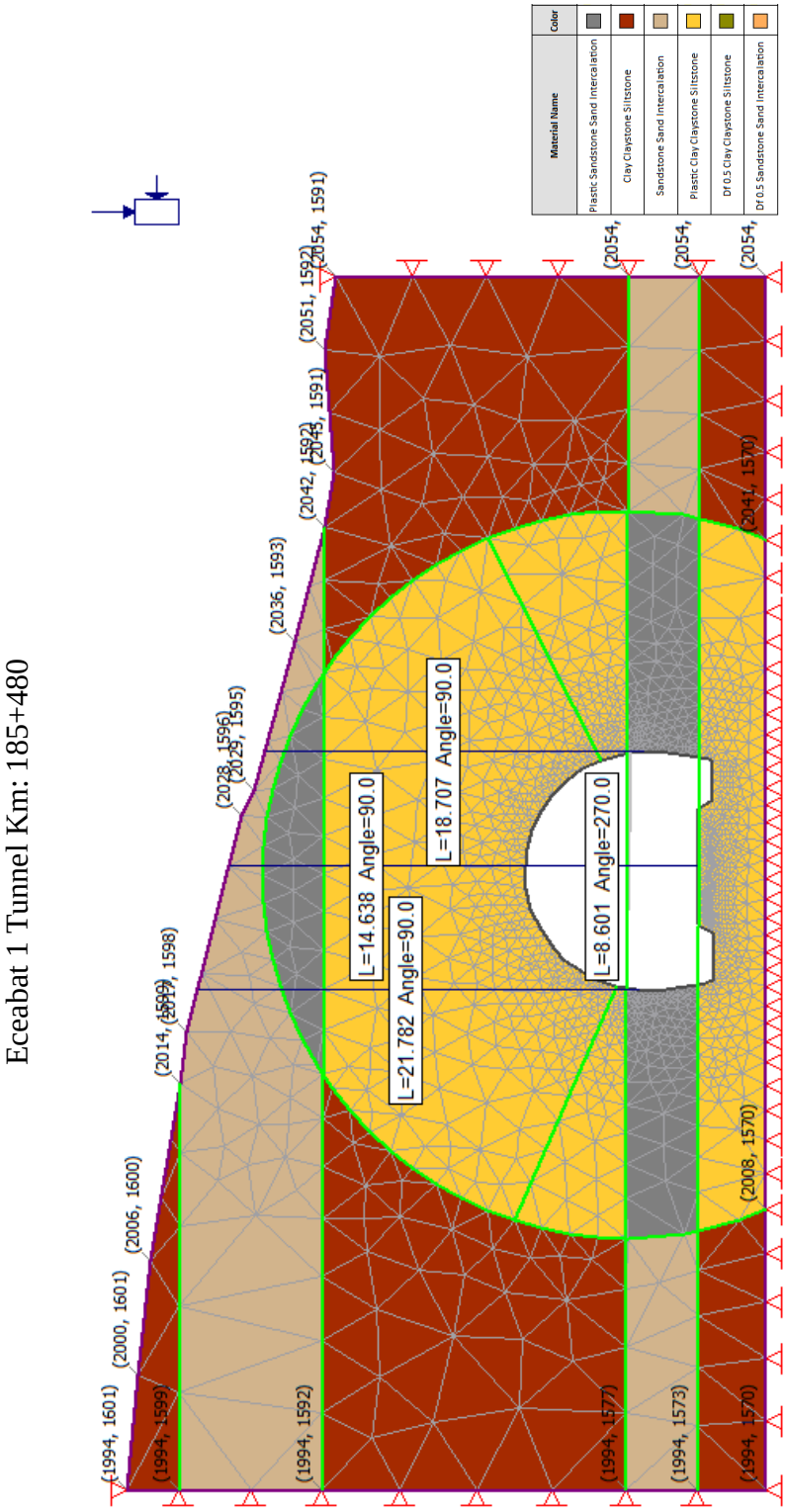

Eceabat 1 Tunnel Km: 185+480

Figure B.1. Numerical model geometry, dimensions, meshes and geological cross section of the Eceabat 1 Tunnel excavation at Km: 185+480

Material Name	Color	Initial Element Loading	Unit Weight (MN/m3)	Elastic Type	Young's Modulus (MPa)	Poisson's Ratio	Failure Criterion	Material Type	Intact Compressive Strength (MPa)	mb (peak)	mb (residual)	s (peak)	s (residual)	a (peak)	a (residual)	Dilation Parameter	Piezo Line	Ru
Plastic Sandstone Sand Intercalation		Field Stress and Body Force	0.021	Isotropic	374.1	0.42	Generalized Hoek-Brown	Plastic	25	0.892595	0.892595	0.00024	0.00024	0.531267	0.531267	0	None	0
Clay Claystone Siltstone		Body Force Only	0.02	Isotropic	182.7	0.43	Generalized Hoek-Brown	Elastic	20	0.287163		0.000138		0.543721			None	0
Sandstone Sand Intercalation		Body Force Only	0.021	Isotropic	374.1	0.42	Generalized Hoek-Brown	Elastic	25	0.892595		0.00024		0.531267			None	0
Plastic Clay Claystone Siltstone		Field Stress and Body Force	0.02	Isotropic	182.7	0.3	Generalized Hoek-Brown	Plastic	20	0.287163	0.287163	0.000138	0.000138	0.543721	0.543721	0	None	0
Df 0.5 Clay Claystone Siltstone		Field Stress and Body Force	0.02	Isotropic	119.4	0.43	Generalized Hoek-Brown	Plastic	20	0.110794	0.110794	2.33091e-005	2.33091e-005	0.543721	0.543721	0	None	0
Df 0.5 Sandstone Sand Intercalation		Field Stress and Body Force	0.021	Isotropic	221.4	0.3	Generalized Hoek-Brown	Plastic	25	0.365504	0.365504	4.53999e-005	4.53999e-005	0.531267	0.531267	0	None	0

Figure B.1.1. Material properties which are used in numerical modelling of Eceabat 1 Tunnel excavation at Km: 185+480

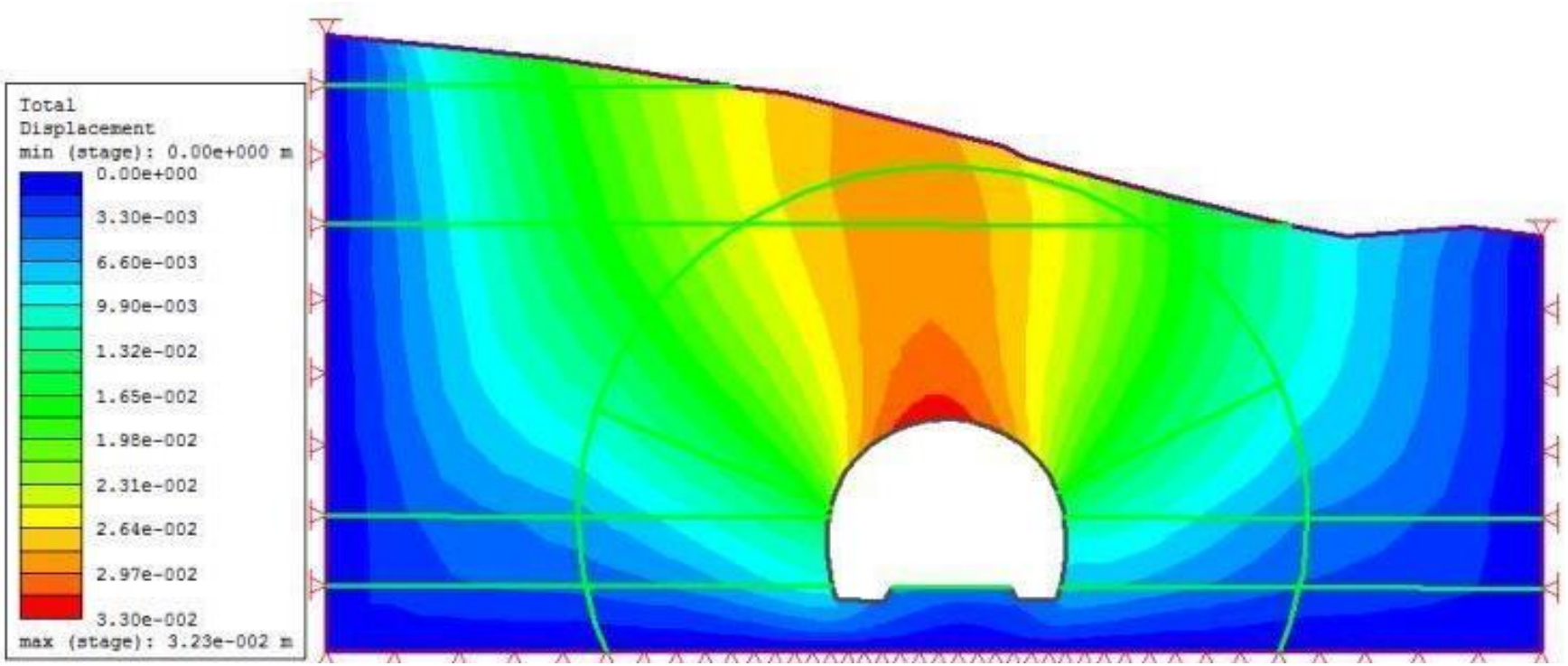

Figure B.1.2. Numerical modelling results in terms of total displacements of Eceabat 1 Tunnel excavation at Km: 185+480

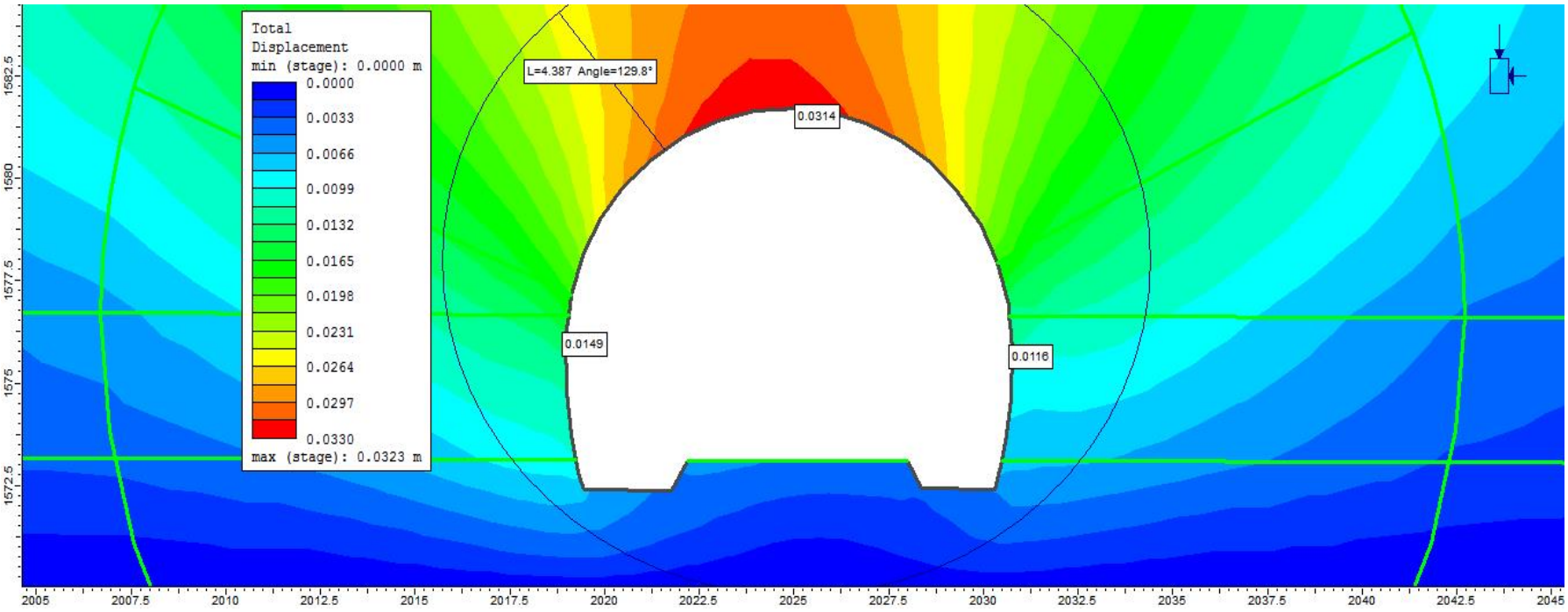

Figure B.1.3. Closer view of total displacement results on left shoulder, roof and right shoulder of Eceabat 1 Tunnel excavation at Km: 185+480

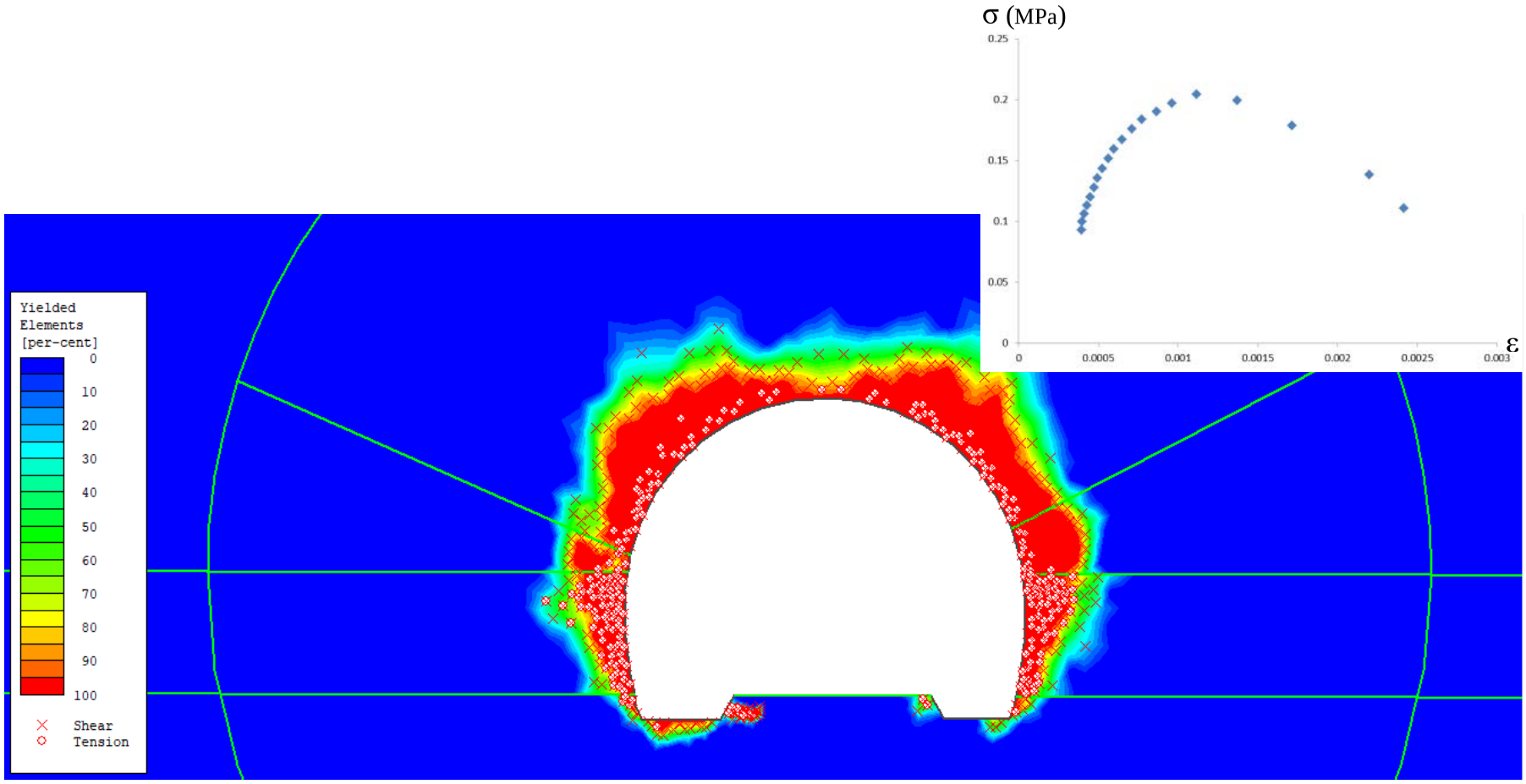

Figure B.1.4. Closer view of yielded elements and stress – strain graph of Eceabat 1 Tunnel excavation at Km: 185+480

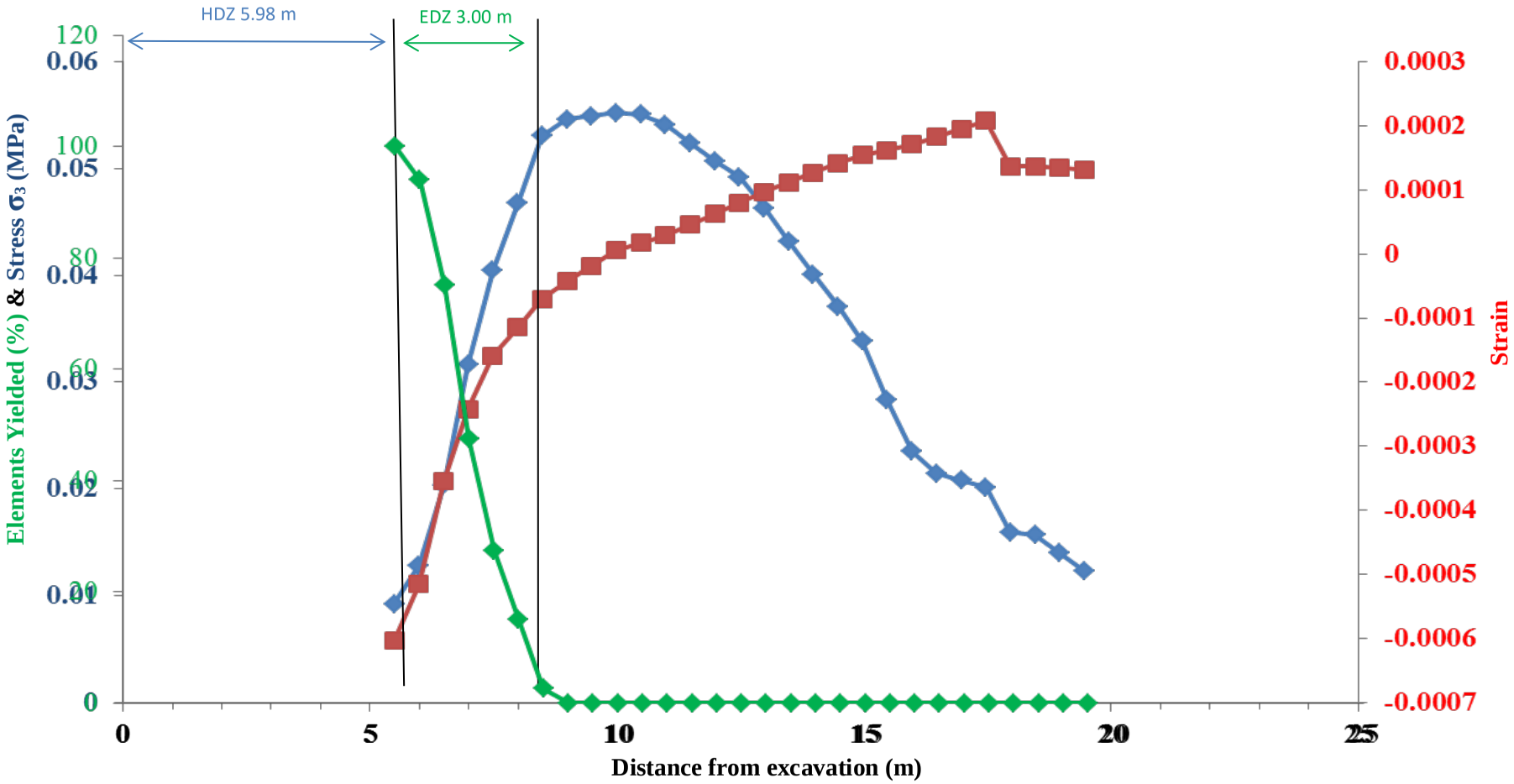

Figure B.1.5. Thickness of HDZ, EDZ and EIZ of Eceabat T1 Tunnel at km 185+480

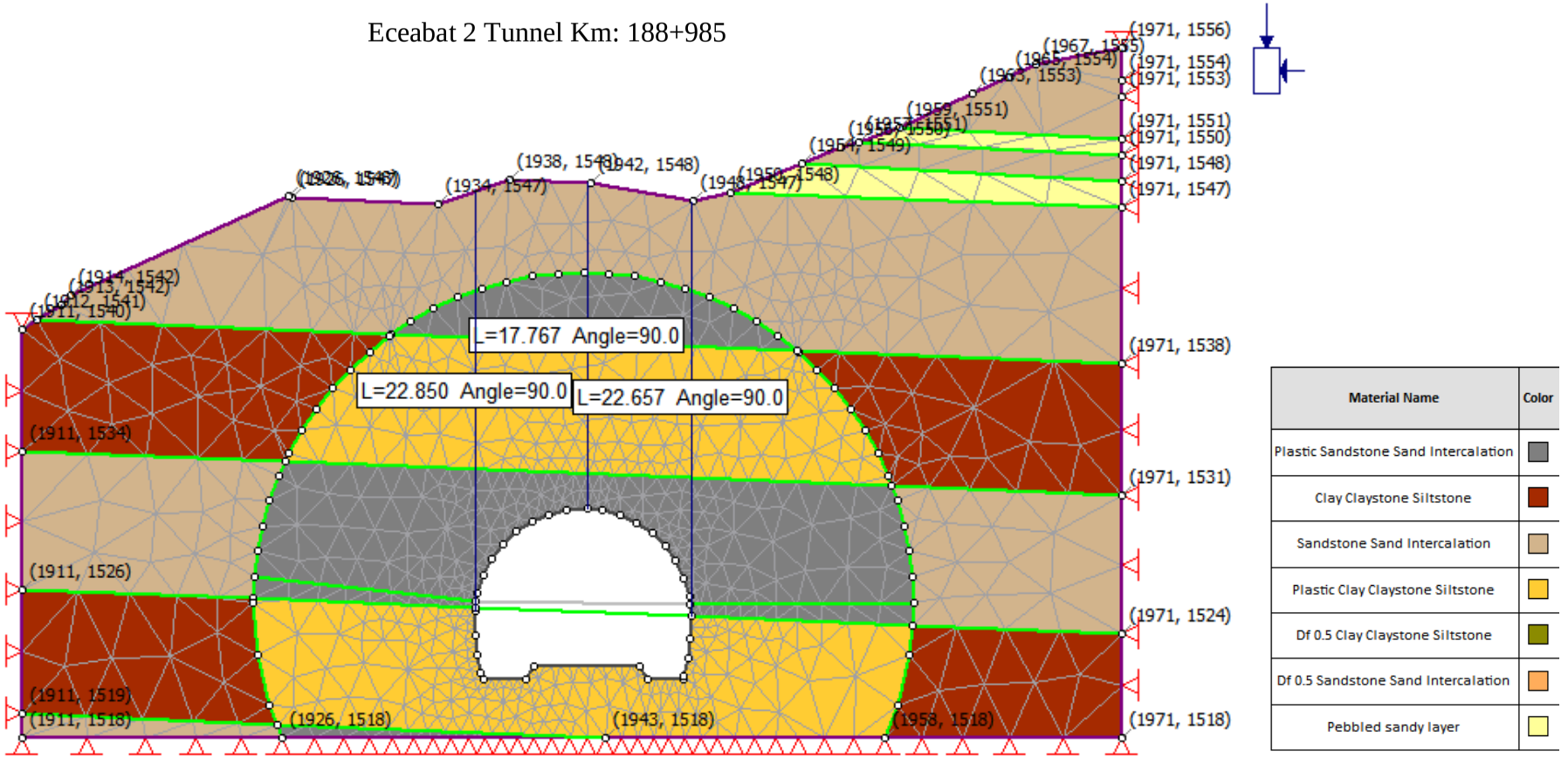

Figure B.2. Numerical model geometry, dimensions, mesh and geological cross section of Eceabat 2 Tunnel excavation at Km: 188+985

Material Name	Color	Initial Element Loading	Unit Weight (MN/m3)	Elastic Type	Young's Modulus (MPa)	Poisson's Ratio	Failure Criterion	Material Type	Intact Compressive Strength (MPa)	mb (peak)	mb (residual)	s (peak)	s (residual)	a (peak)	a (residual)	Material Name	Dilation Parameter	Material Name	Piezo Line	Ru
Plastic Sandstone Sand Intercalation		Field Stress and Body Force	0.021	Isotropic	374.1	0.42	Generalized Hoek-Brown	Plastic	25	0.892595	0.892595	0.00024	0.00024	0.531267	0.531267	andstone Sand	0	Sandstone Sand	None	0
Clay Claystone Siltstone		Body Force Only	0.02	Isotropic	182.7	0.43	Generalized Hoek-Brown	Elastic	20	0.287163		0.000138		0.543721		Clay laystone iltstone		Clay Claystone Siltstone	None	0
Sandstone Sand Intercalation		Body Force Only	0.021	Isotropic	374.1	0.42	Generalized Hoek-Brown	Elastic	25	0.892595		0.00024		0.531267		andstone Sand ercalatio		Sandstone Sand tercalatio	None	0
Plastic Clay Claystone Siltstone		Field Stress and Body Force	0.02	Isotropic	182.7	0.3	Generalized Hoek-Brown	Plastic	20	0.287163	0.287163	0.000138	0.000138	0.543721	0.543721	Clay laystone	0	Clay Claystone	None	0
Df 0.5 Clay Claystone Siltstone		Field Stress and Body Force	0.02	Isotropic	119.4	0.43	Generalized Hoek-Brown	Plastic	20	0.110794	0.110794	2.33091e-005	2.33091e-005	0.543721	0.543721	Clay laystone	0	Df 0.5 Clay Claystone	None	0
Df 0.5 Sandstone Sand Intercalation		Field Stress and Body Force	0.021	Isotropic	221.4	0.3	Generalized Hoek-Brown	Plastic	25	0.365504	0.365504	4.53999e-005	4.53999e-005	0.531267	0.531267	andstone Sand	0	Sandstone Sand	None	0
Pebbled sandy layer		Body Force Only	0.021	Isotropic	353.986	0.3	Generalized Hoek-Brown	Elastic	15	1.17992		0.000300185		0.527338		Pebbled sandy layer		Pebbled sandy layer	None	0

Figure B.2.1. Material properties which are used in numerical modelling of Eceabat 2 Tunnel excavation at Km: 188+985

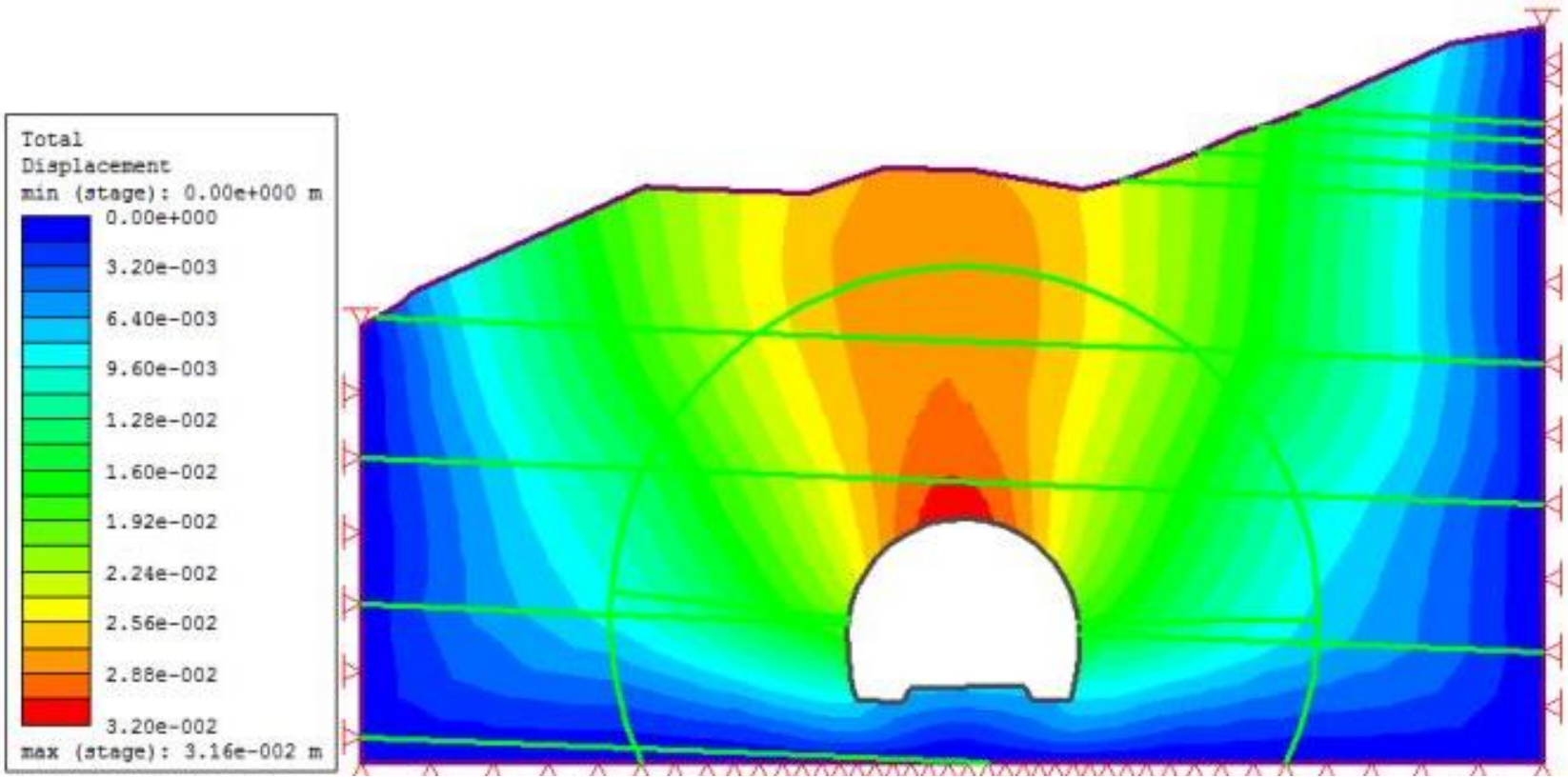

Figure B.2.2. Numerical modelling results in terms of total displacements of Eceabat2 Tunnel excavation at Km: 188+985

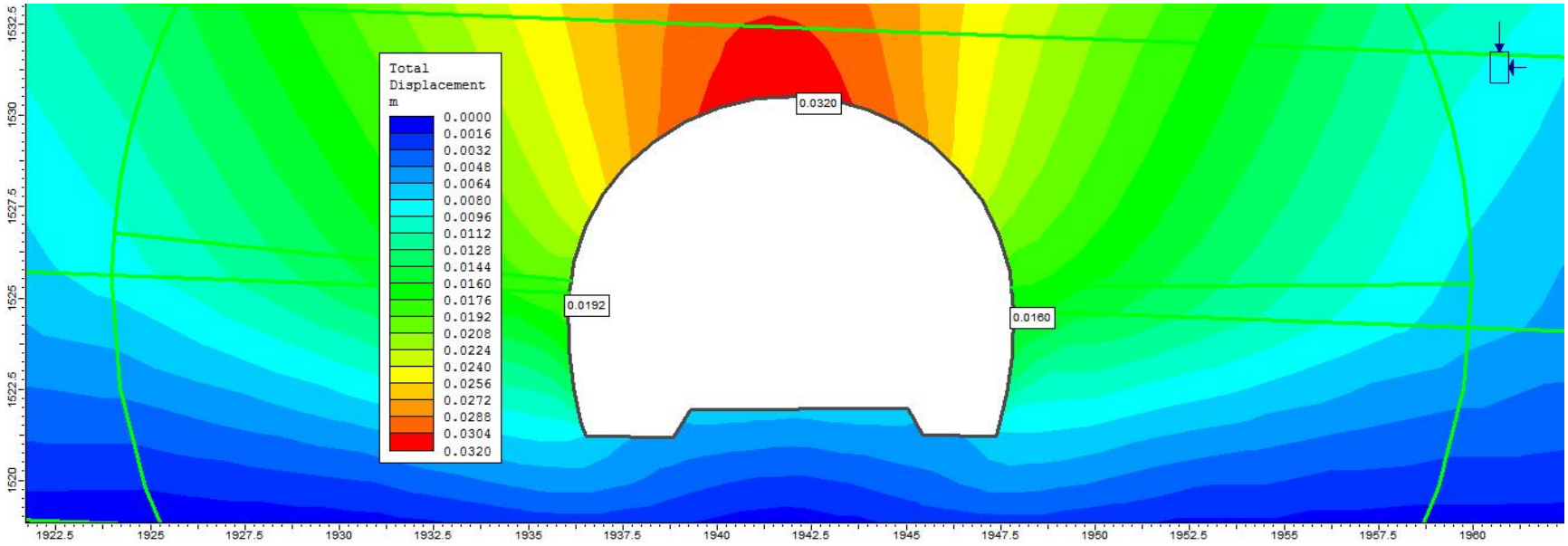

Figure B.2.3. Closer view of total displacement results on left shoulder, roof and right shoulder of Eceabat 2 Tunnel excavation at Km: 188+985

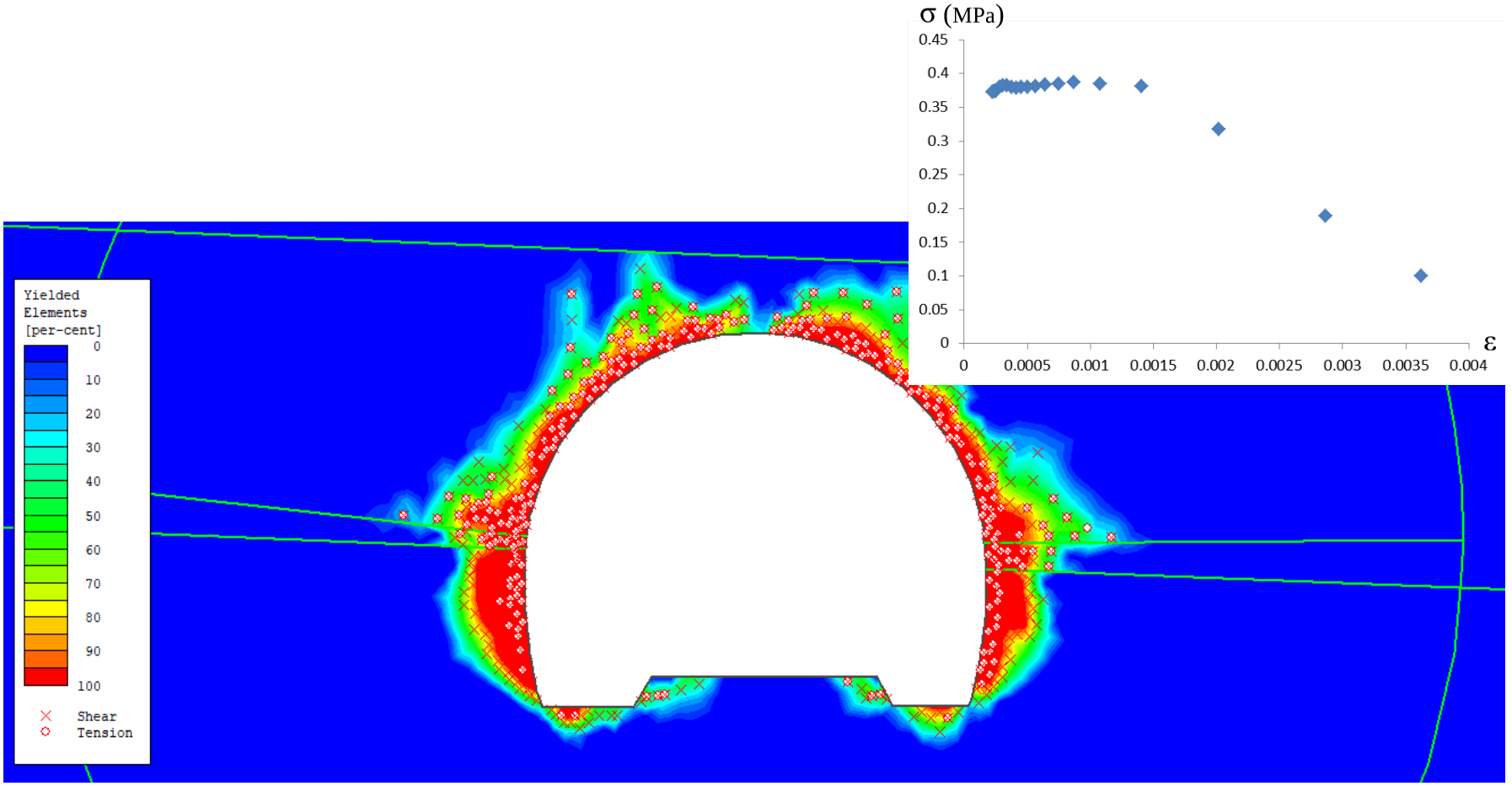

Figure B.2.4. Closer view of yielded elements and stress – strain graph of Eceabat 2 Tunnel excavation at Km: 188+985

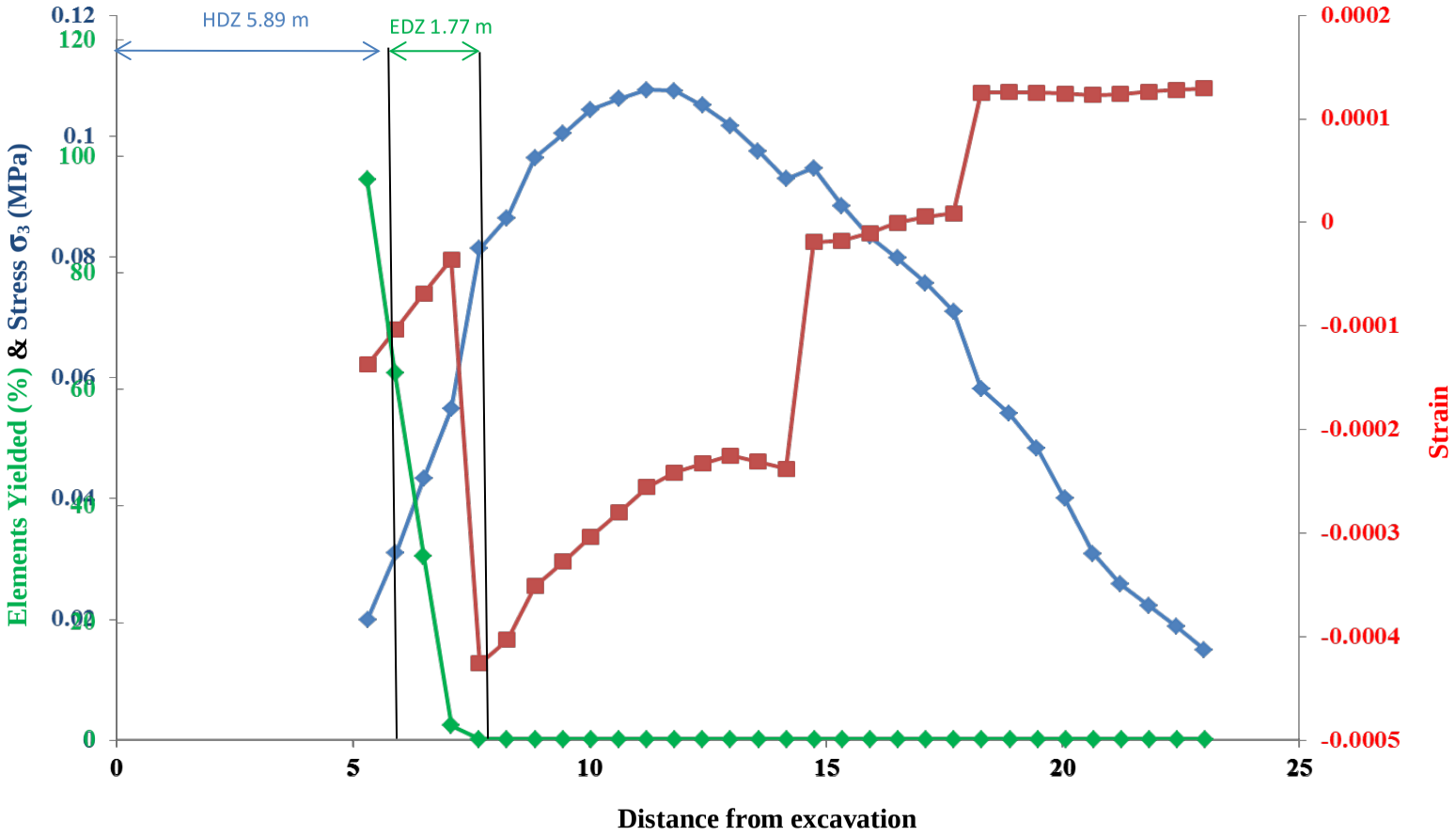

Figure B.2.5. Thickness of HDZ, EDZ and EIZ of Eceabat T2 Tunnel at km 188+985

Tirebolu 2 Tunel Km: 3+858

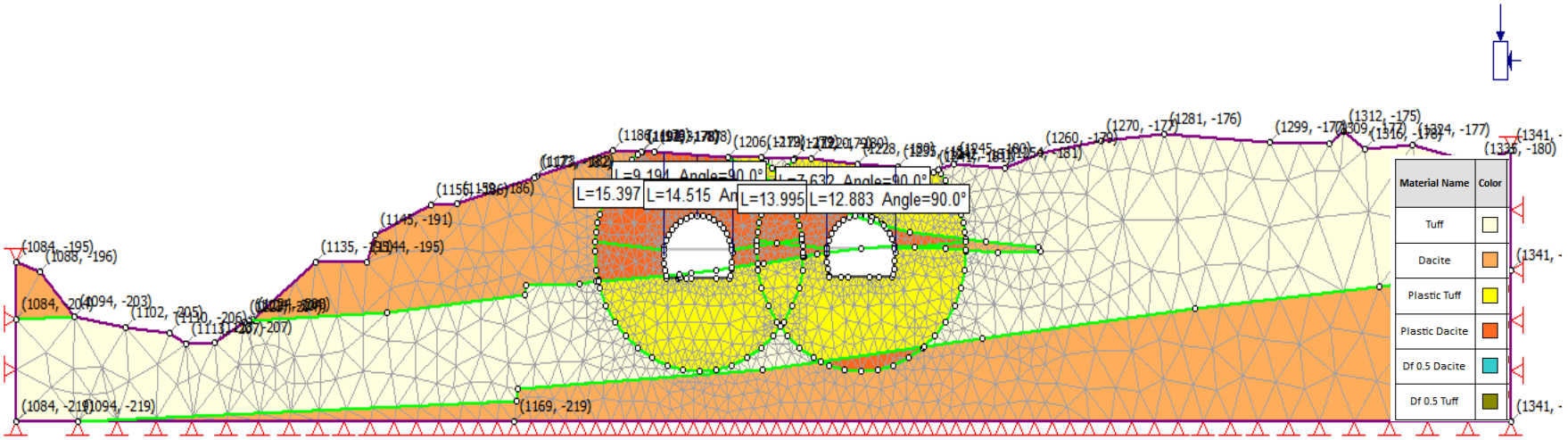

Figure B.3. Numerical model geometry, dimensions, mesh and geological cross section of Tirebolu 2 Tunnel excavation at Km: 3+858

Material Name	Color	Initial Element Loading	Unit Weight (MN/m3)	Elastic Type	Young's Modulus (MPa)	Poisson's Ratio	Failure Criterion	Material Type	Intact Compressive Strength (MPa)	mb (peak)	mb (residual)	s (peak)	s (residual)	a (peak)	a (residual)	Dilation Parameter	Piezo Line	Ru
Tuff		Body Force Only	0.022	Isotropic	202.534	0.3	Generalized Hoek-Brown	Elastic	20	0.49348		0.000172232		0.538237			None	0
Dacite		Body Force Only	0.024	Isotropic	506.336	0.3	Generalized Hoek-Brown	Elastic	25	0.74022		0.000172232		0.538237			None	0
Plastic Tuff		Field Stress and Body Force	0.022	Isotropic	202.534	0.3	Generalized Hoek-Brown	Plastic	20	0.49348	0.49348	0.000172232	0.000172232	0.538237	0.538237	0	None	0
Plastic Dacite		Field Stress and Body Force	0.024	Isotropic	506.336	0.3	Generalized Hoek-Brown	Plastic	25	0.74022	0.74022	0.000172232	0.000172232	0.538237	0.538237	0	None	0
Df 0.5 Dacite		Field Stress and Body Force	0.024	Isotropic	317.971	0.3	Generalized Hoek-Brown	Plastic	25	0.292474	0.292474	3.04325e-005	3.04325e-005	0.538237	0.538237	0	None	0
Df 0.5 Tuff		Field Stress and Body Force	0.022	Isotropic	127.188	0.3	Generalized Hoek-Brown	Plastic	20	0.194983	0.194983	3.04325e-005	3.04325e-005	0.538237	0.538237	0	None	0

Figure B.3.2. Material properties which are used in numerical modelling of Tirebolu 2 Tunnel excavation at Km: 3+858

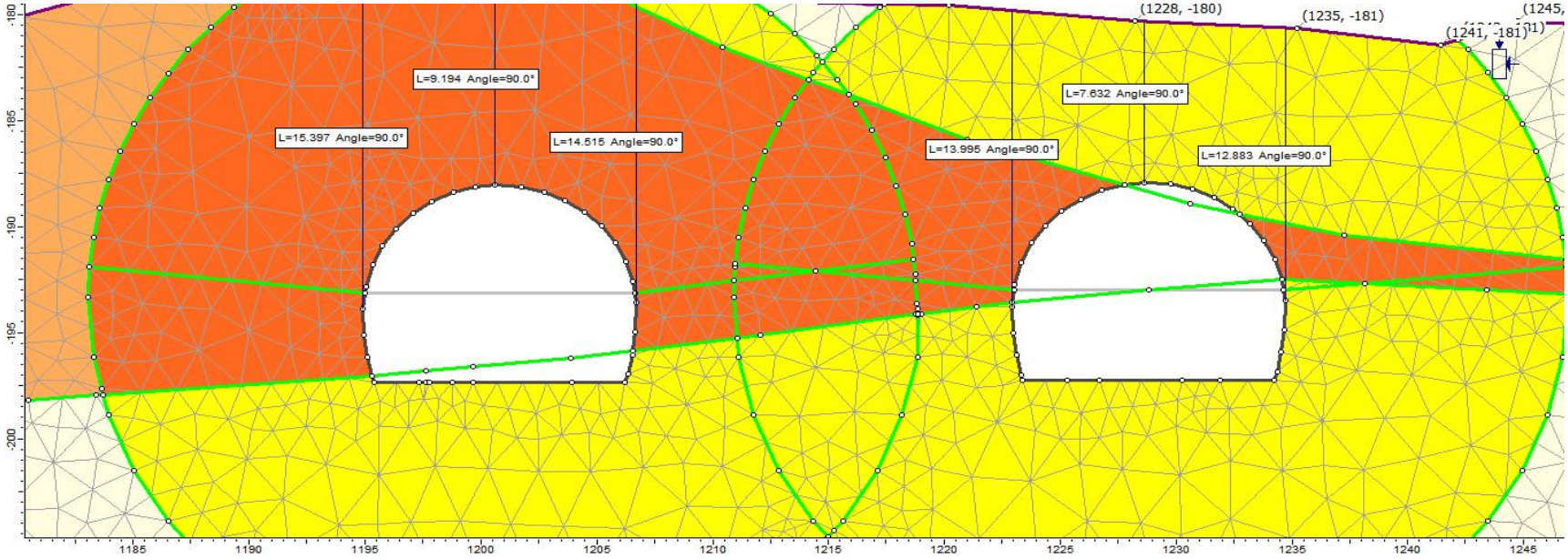

Figure B.3.1. Closer view of numerical model geometry, dimensions, mesh and geological cross section of Tirebolu 2 Tunnel excavation at Km: 3+858

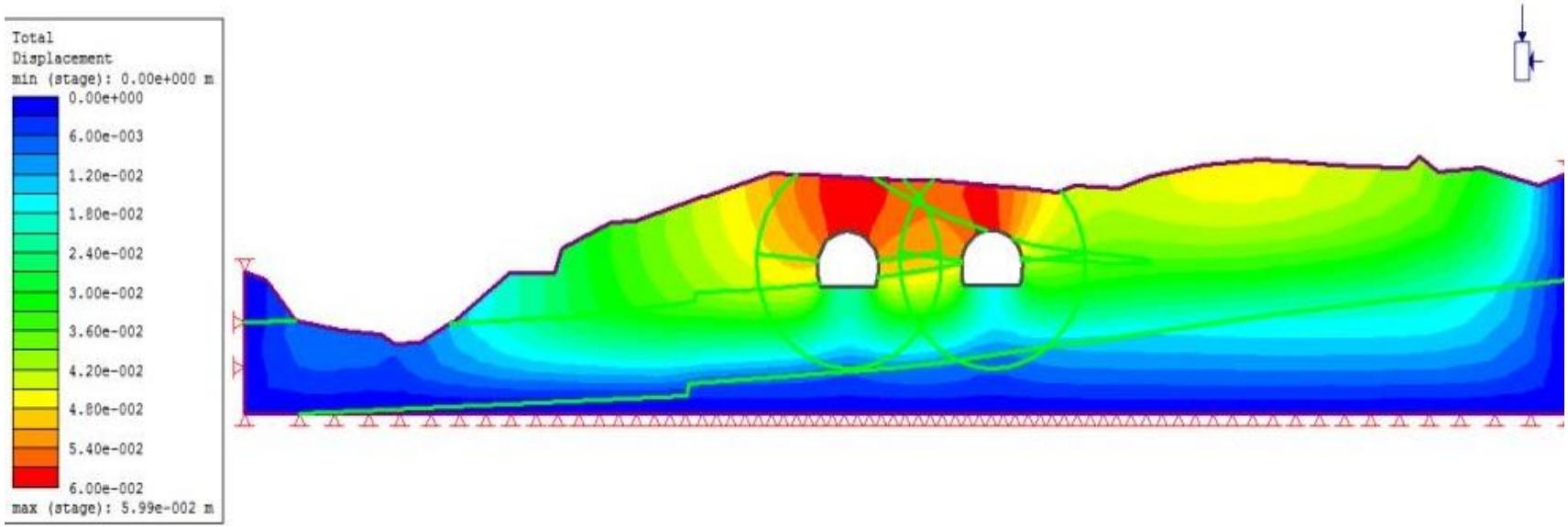

Figure B.3.3. Numerical modelling results in terms of total displacements of Tirebolu 2 Tunnel excavation at Km: 3+858

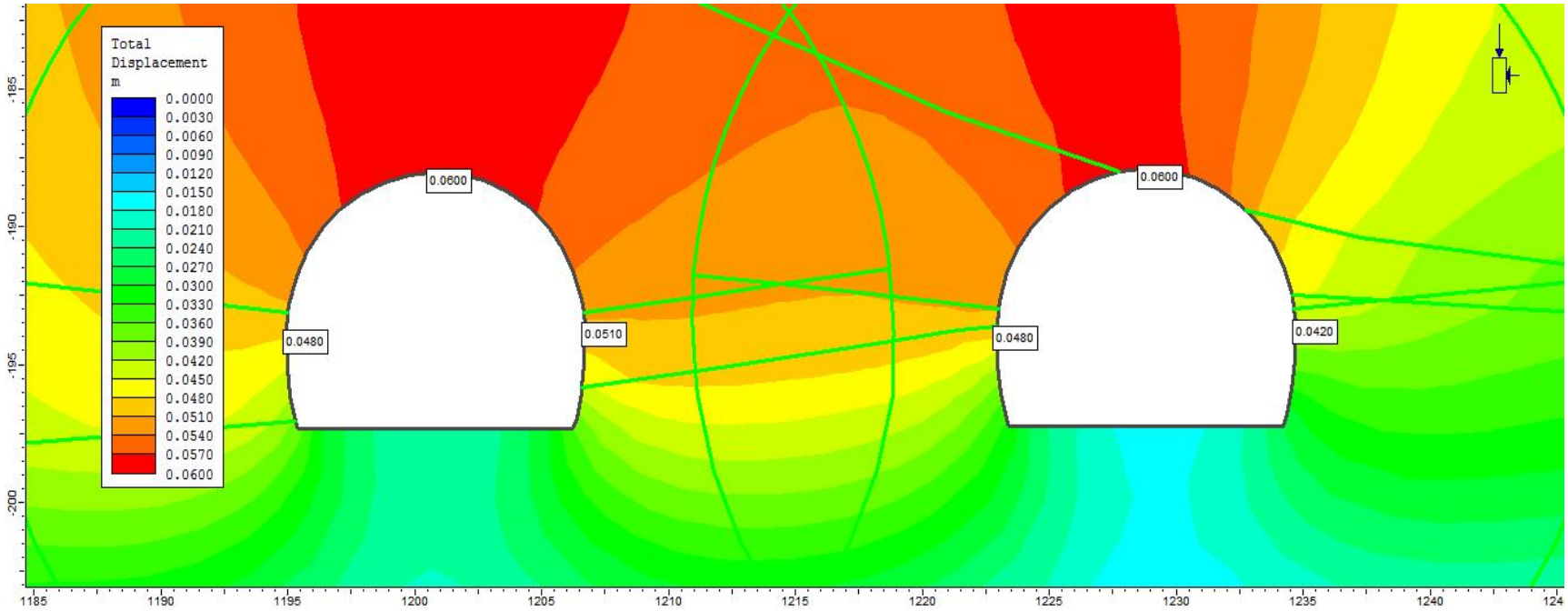

Figure B.3.4. Closer view of total displacement results on left shoulder, roof and right shoulder of Tirebolu 2 Tunnel excavation at Km: 3+858

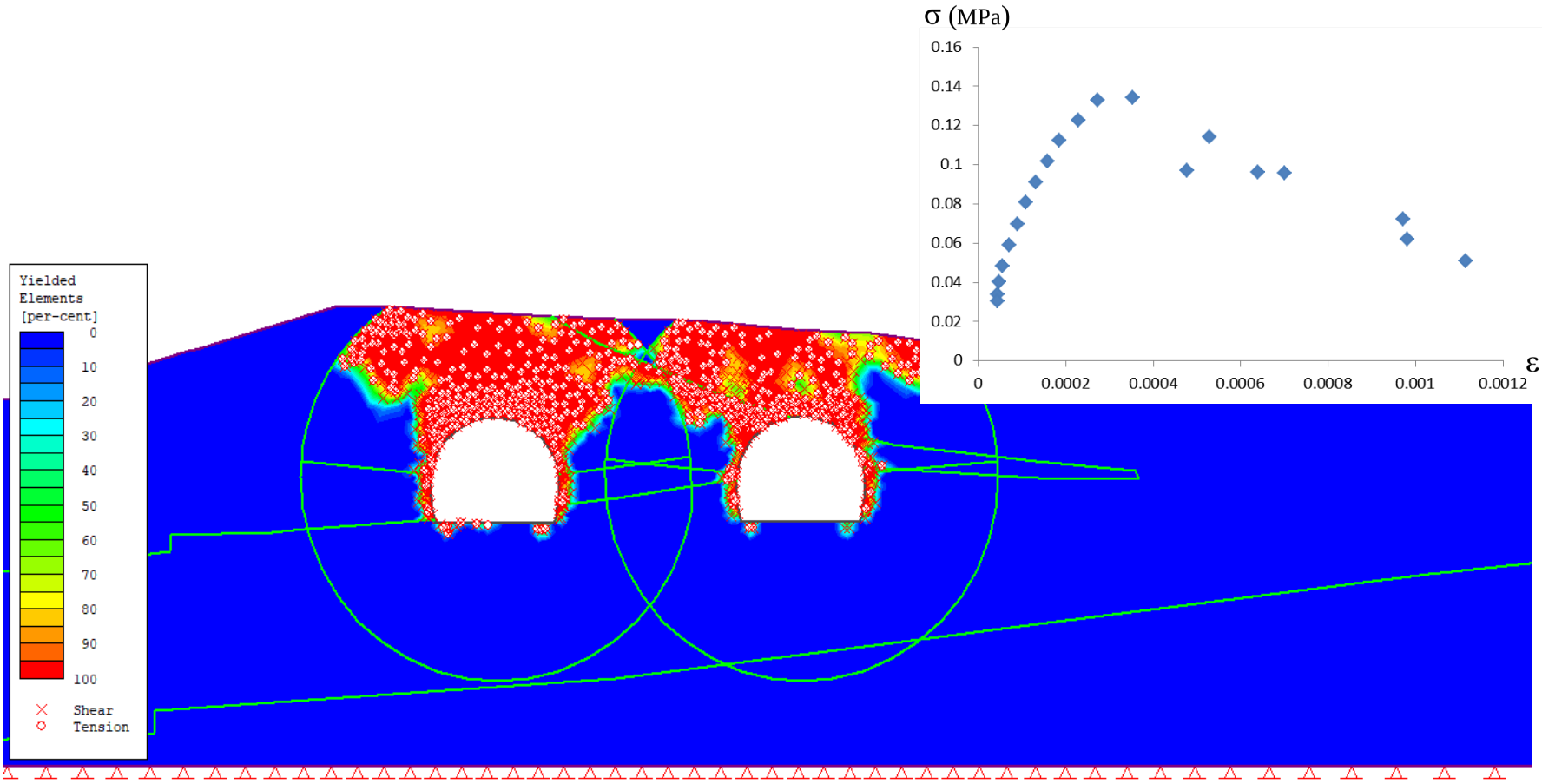

Figure B.3.5. Closer view of yielded elements and strain – stress graph of Tirebolu 2 Tunnel excavation at Km: 3+858

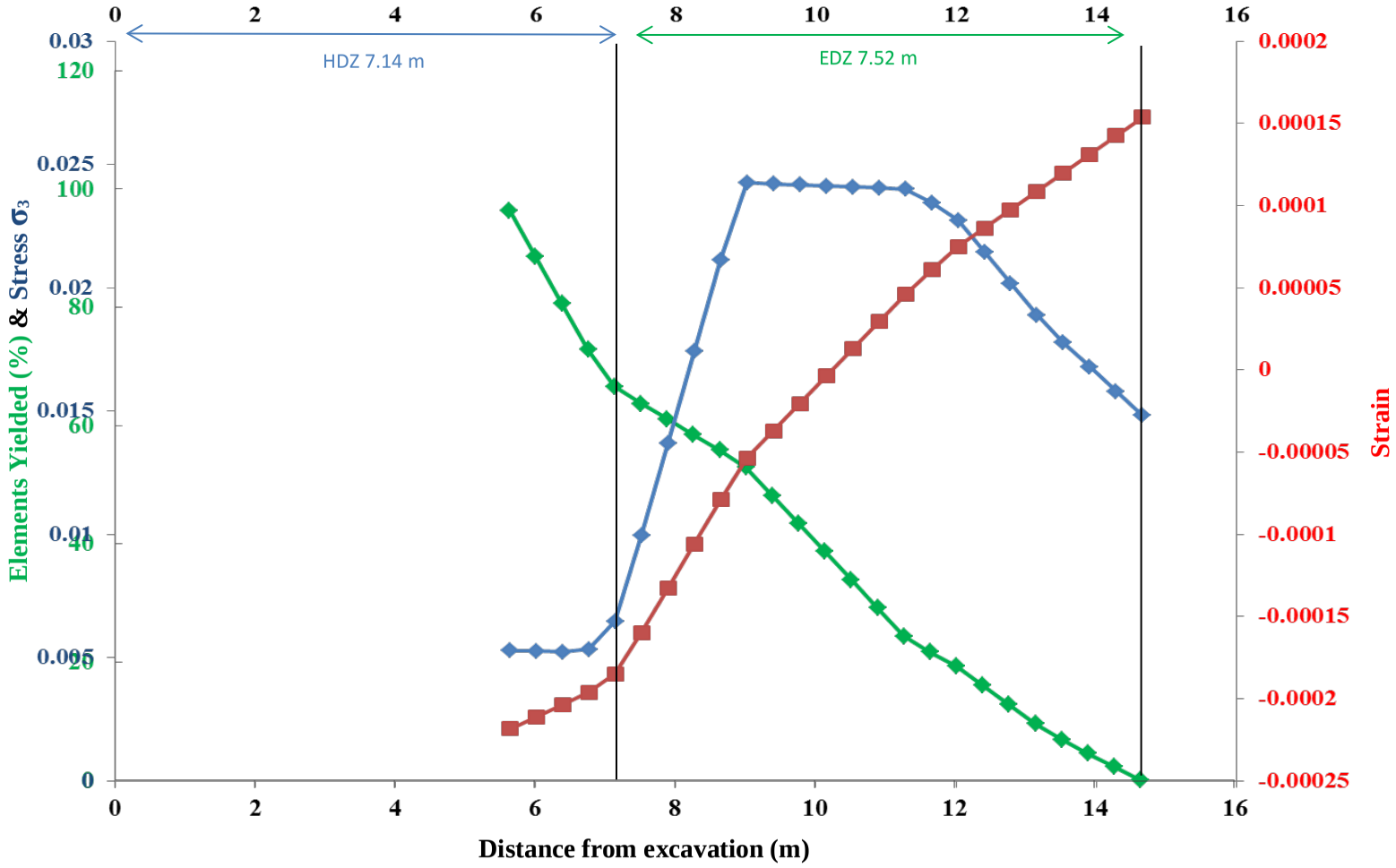

Figure B.3.6 Thickness of HDZ, EDZ and EIZ of Tirebolu 2 Tunnel excavation at km 3+858

Tirebolu 2 Tunnel Km: 4+407

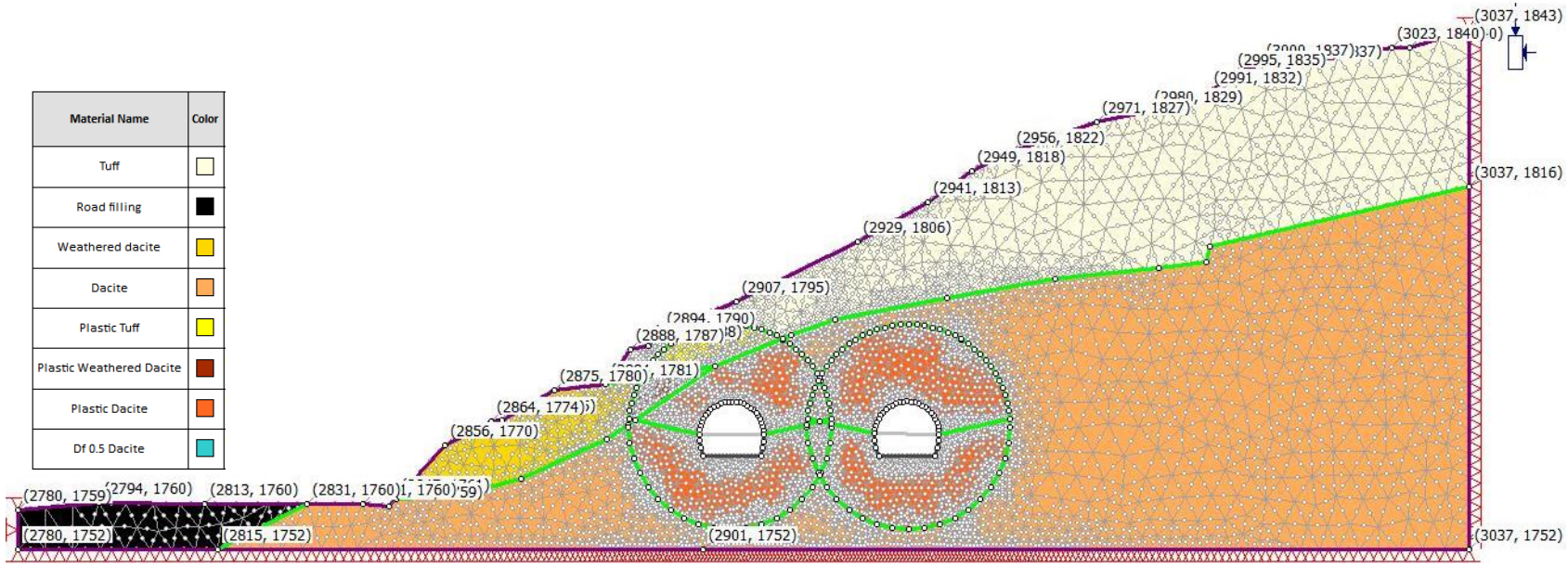

Figure B.4. Numerical model geometry, dimesions, mesh and geological cross section of Tirebolu 2 Tunnel excavation at Km: 4+407

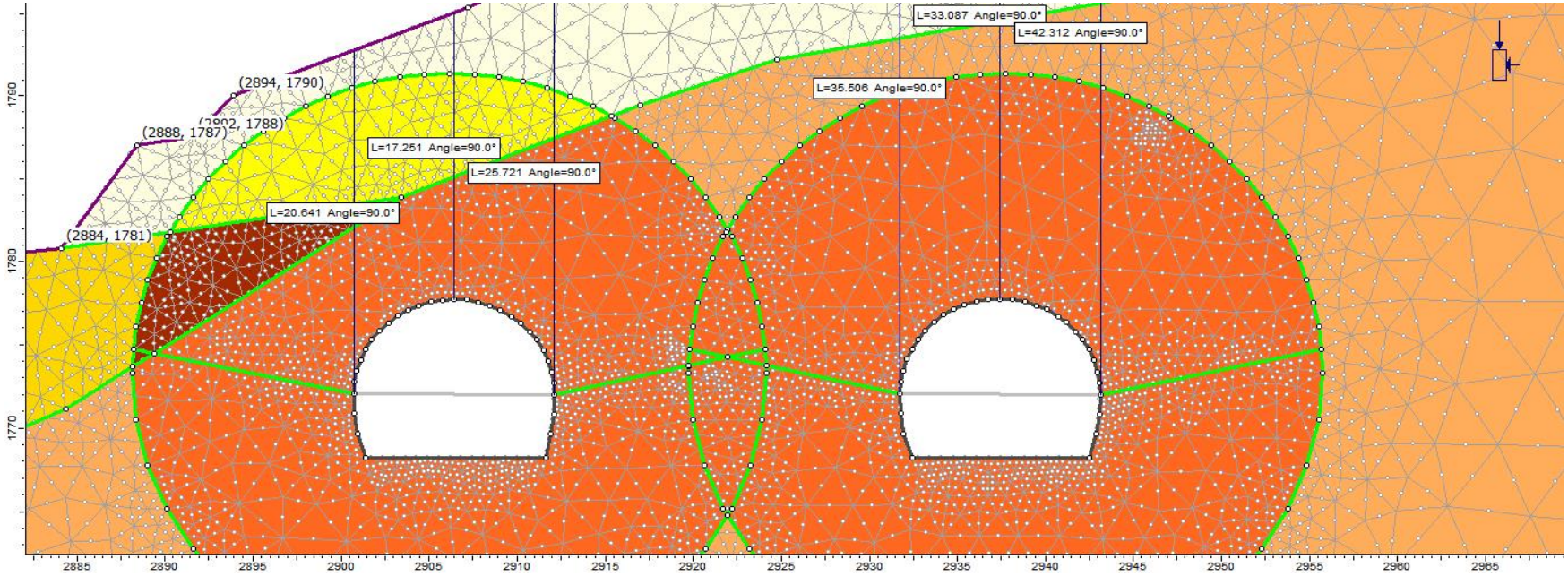

Figure B.4.1: Closer view of numerical model geometry, dimensions, mesh and geological cross section of Tirebolu 2 Tunnel excavation at Km: 4+407

Material Name	Color	Initial Element Loading	Unit Weight (MN/m3)	Elastic Type	Young's Modulus (MPa)	Poisson's Ratio	Failure Criterion	Material Type	Tensile Strength (MPa)	Friction Angle (peak) (deg)	Cohesion (peak) (MPa)	Intact Compressive Strength (MPa)	mb (peak)	mb (residual)	s (peak)	s (residual)	a (peak)	a (residual)	Dilation Parameter	Piezo Line	Ru
Tuff		Body Force Only	0.022	Isotropic	2153.8	0.3	Generalized Hoek-Brown	Elastic				42	1.5806		0.00142219		0.510622			None	0
Road filling		Body Force Only	0.019	Isotropic	200	0.3	Mohr Coulomb	Elastic	0	35	10.5									None	0
Weathered dacite		Body Force Only	0.023	Isotropic	397.138	0.3	Generalized Hoek-Brown	Elastic				31	1.4749		0.000300185		0.527338			None	0
Dacite		Body Force Only	0.024	Isotropic	1500.33	0.3	Generalized Hoek-Brown	Elastic				31	3.76602		0.00277005		0.50705			None	0
Plastic Tuff		Field Stress and Body Force	0.022	Isotropic	2153.8	0.3	Generalized Hoek-Brown	Plastic				42	1.5806	1.5806	0.00142219	0.00142219	0.510622	0.510622	0	None	0
Plastic Weathered Dacite		Field Stress and Body Force	0.023	Isotropic	318.432	0.3	Generalized Hoek-Brown	Plastic				28	1.2359	1.2359	0.000240369	0.000240369	0.531267	0.531267	0	None	0
Plastic Dacite		Field Stress and Body Force	0.024	Isotropic	1500.33	0.3	Generalized Hoek-Brown	Plastic				31	3.76602	3.76602	0.00277005	0.00277005	0.50705	0.50705	0	None	0
Df 0.5 Dacite		Field Stress and Body Force	0.024	Isotropic	208.624	0.3	Generalized Hoek-Brown	Plastic				31	0.562313	0.562313	4.53999e-005	4.53999e-005	0.531267	0.531267	0	None	0

Figure B.4.2. Material properties which are used in numerical modelling of Tirebolu 2 Tunnel excavation at Km: 4+407

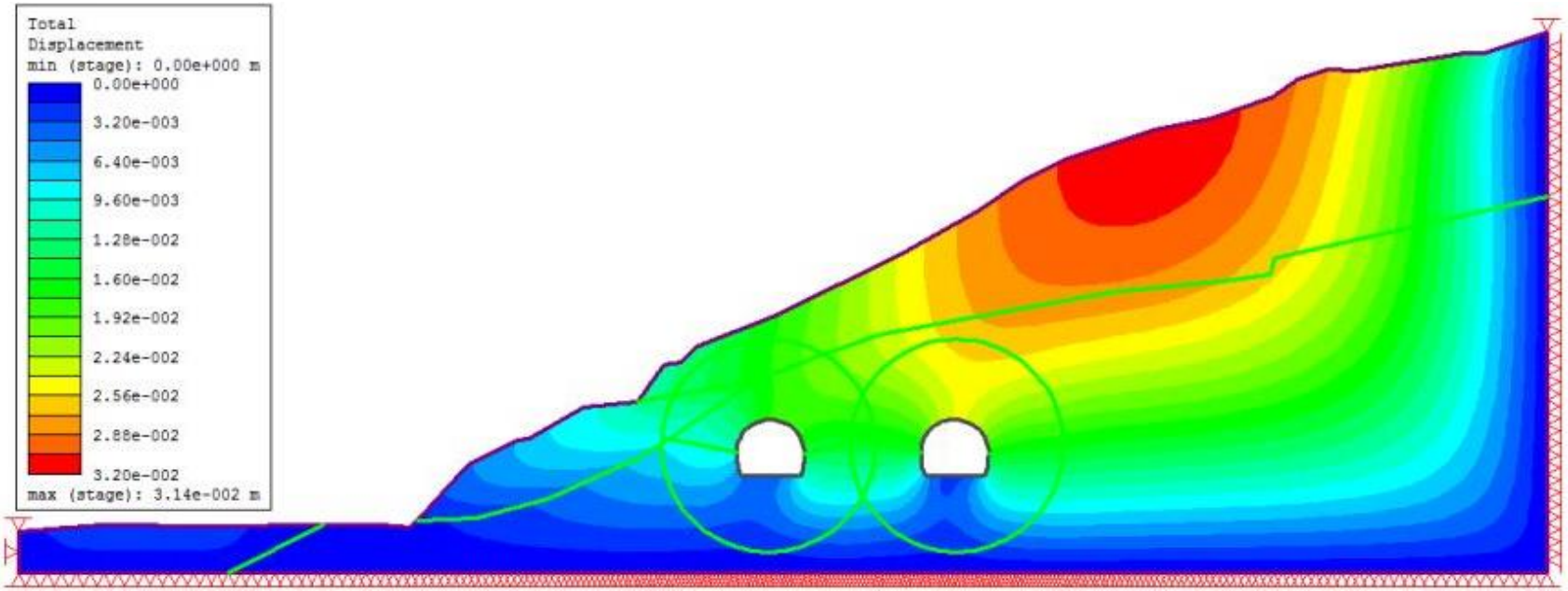

Figure B.4.3. Numerical modelling results in terms of total displacements of Tirebolu 2 Tunnel excavation at Km: 4+407

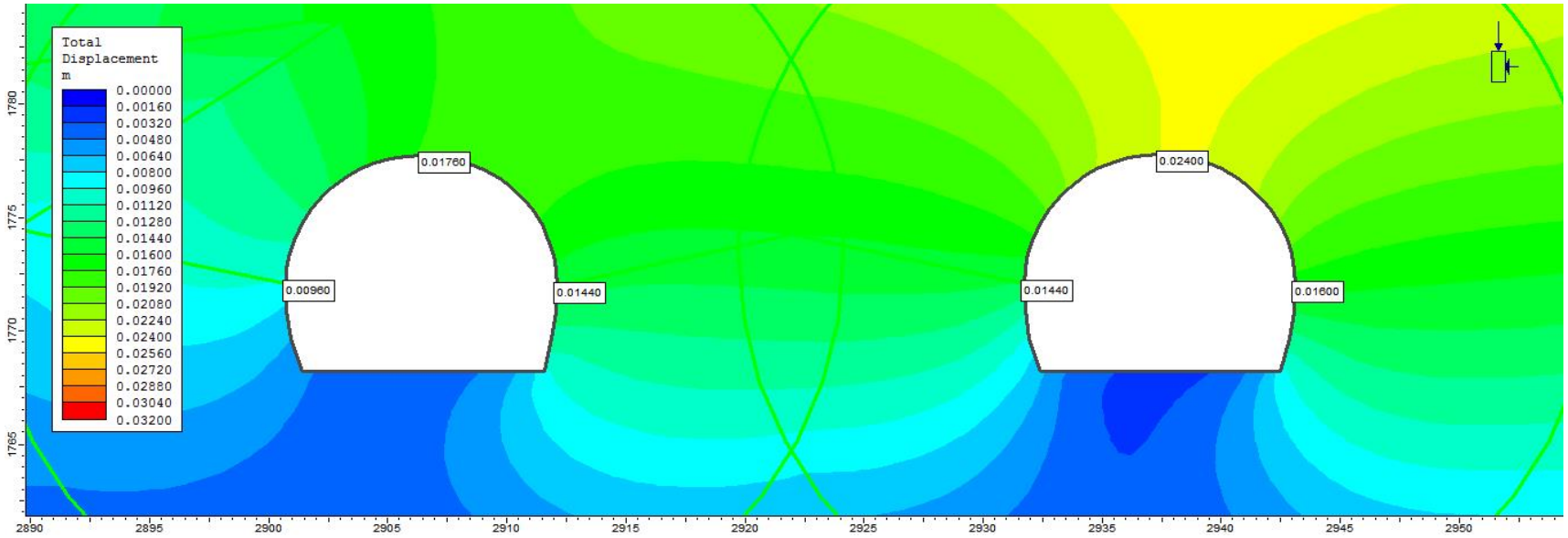

Figure B.4.4 Closer view of total displacement results on left shoulder, roof and right shoulder of Tirebolu 2 Tunnel excavation at Km: 4+407

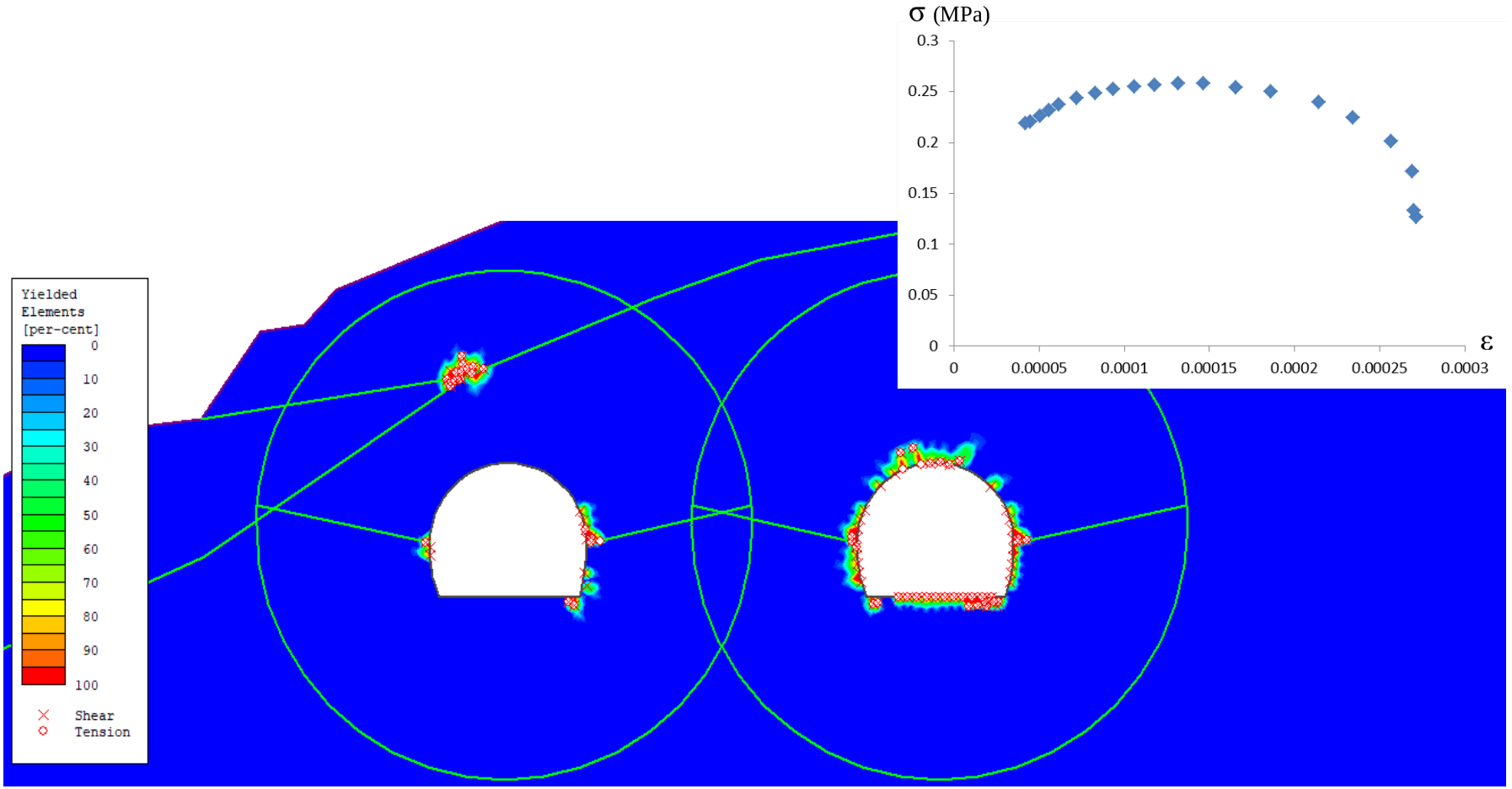

Figure B.4.5. Closer view of yielded elements and stress – strain graph of Tirebolu 2 Tunnel excavation at Km: 4+407

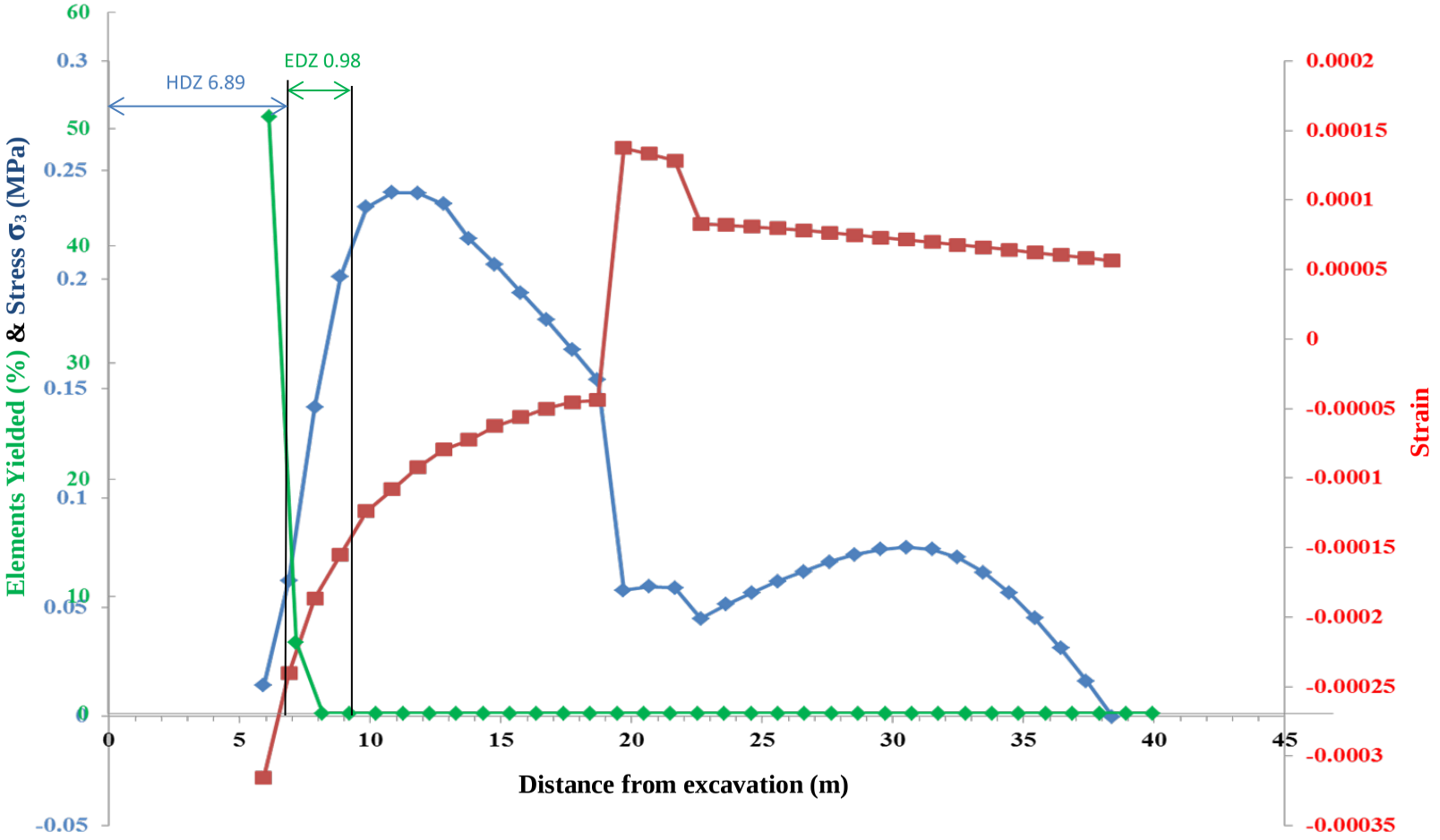

Figure B.4.6. Thickness of HDZ, EDZ and EIZ of Tirebolu 2 Tunnel excavation at km 4+407

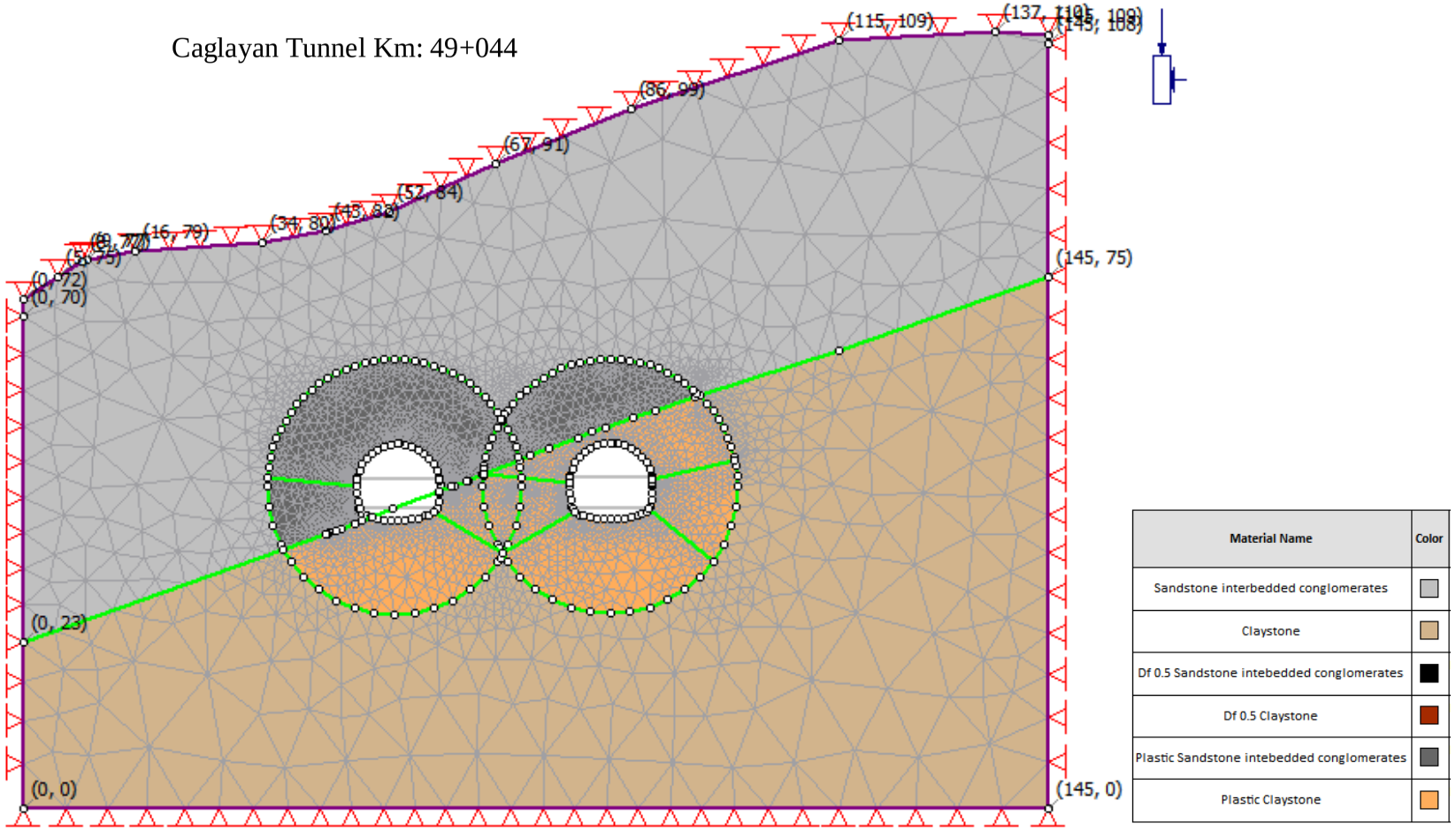

Figure B.5. Numerical model geometry, dimensions, mesh and geological cross section of Caglayan Tunnel excavation at Km: 49+044

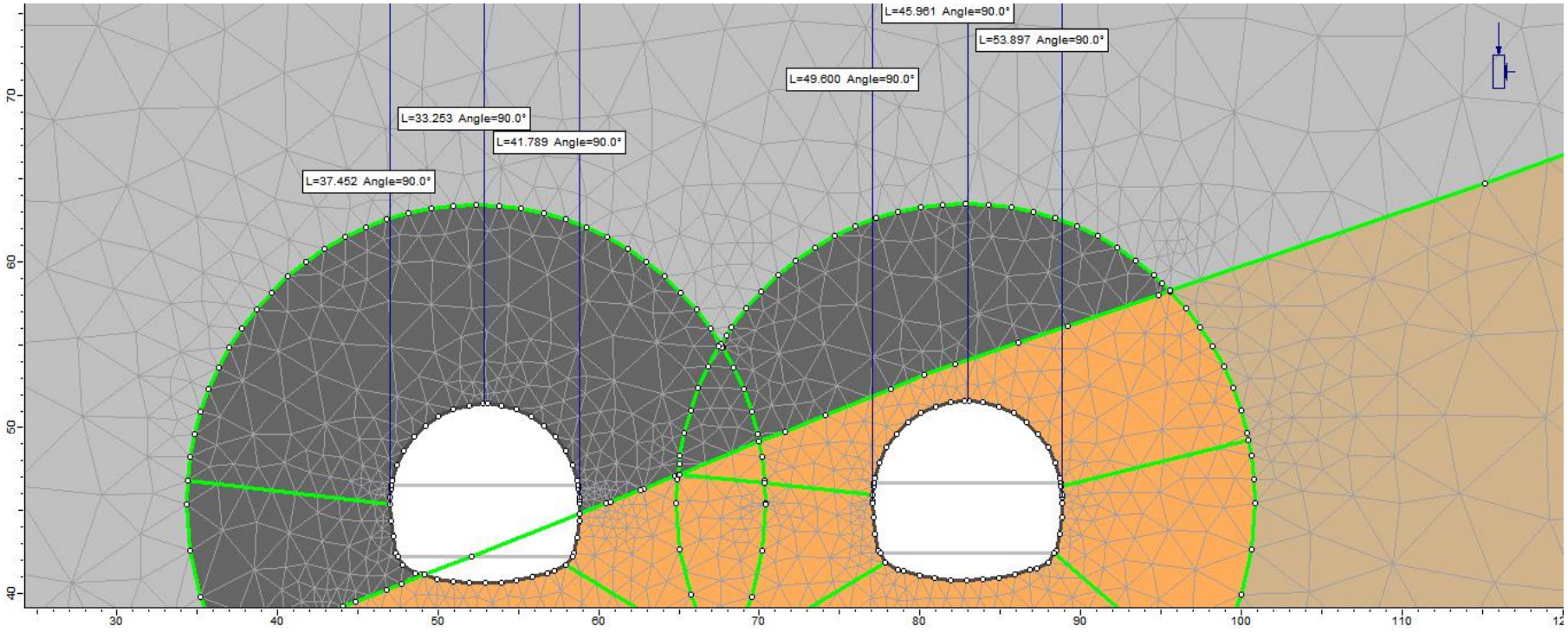

Figure B.5.1 Closer view of numerical model geometry, dimensions, mesh and geological cross section of Caglayan Tunnel excavation at Km: 49+044

Material Name	Color	Initial Element Loading	Unit Weight (MN/m3)	Elastic Type	Young's Modulus (MPa)	Poisson's Ratio	Failure Criterion	Material Type	Intact Compressive Strength (MPa)	mb (peak)	mb (residual)	s (peak)	s (residual)	a (peak)	a (residual)	Dilation Parameter	Piezo Line	Ru
Sandstone interbedded conglomerates		Body Force Only	0.024	Isotropic	1715.35	0.2525	Generalized Hoek-Brown	Elastic	19.11	2.31011		0.00142219		0.510622			None	0
Claystone		Body Force Only	0.021	Isotropic	627.593	0.278	Generalized Hoek-Brown	Elastic	15.67	0.475231		0.000374886		0.523899			None	0
Df 0.5 Sandstone intebedded conglomerates		Field Stress and Body Force	0.024	Isotropic	821.481	0.2525	Generalized Hoek-Brown	Plastic	19.11	1.14444	1.14444	0.00038331	0.00038331	0.510622	0.510622	0	None	0
Df 0.5 Claystone		Field Stress and Body Force	0.021	Isotropic	345.11	0.278	Generalized Hoek-Brown	Plastic	15.67	0.20409	0.20409	7.73889e-005	7.73889e-005	0.523899	0.523899	0	None	0
Plastic Sandstone intebedded conglomerates		Field Stress and Body Force	0.024	Isotropic	1715.35	0.2525	Generalized Hoek-Brown	Plastic	19.11	2.31011	2.31011	0.00142219	0.00142219	0.510622	0.510622	0	None	0
Plastic Claystone		Field Stress and Body Force	0.021	Isotropic	627.593	0.278	Generalized Hoek-Brown	Plastic	15.67	0.475231	0.475231	0.000374886	0.000374886	0.523899	0.523899	0	None	0

Figure B.5.2. Material properties which are used in numerical modelling of Caglayan Tunnel excavation at Km: 49+044

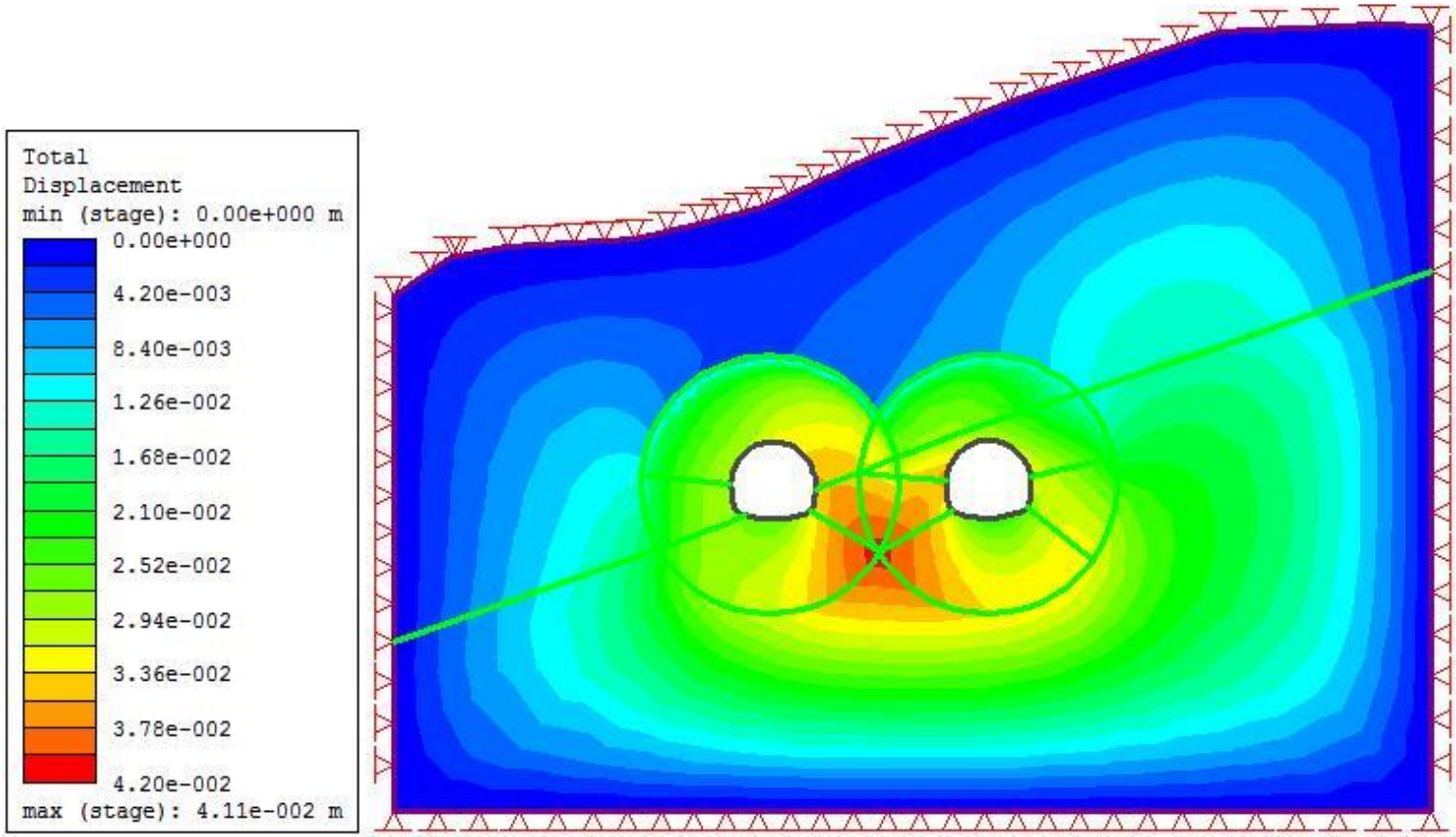

Figure B.5.3. Numerical modelling results in terms of total displacements of Caglayan Tunnel excavation at Km: 49+044

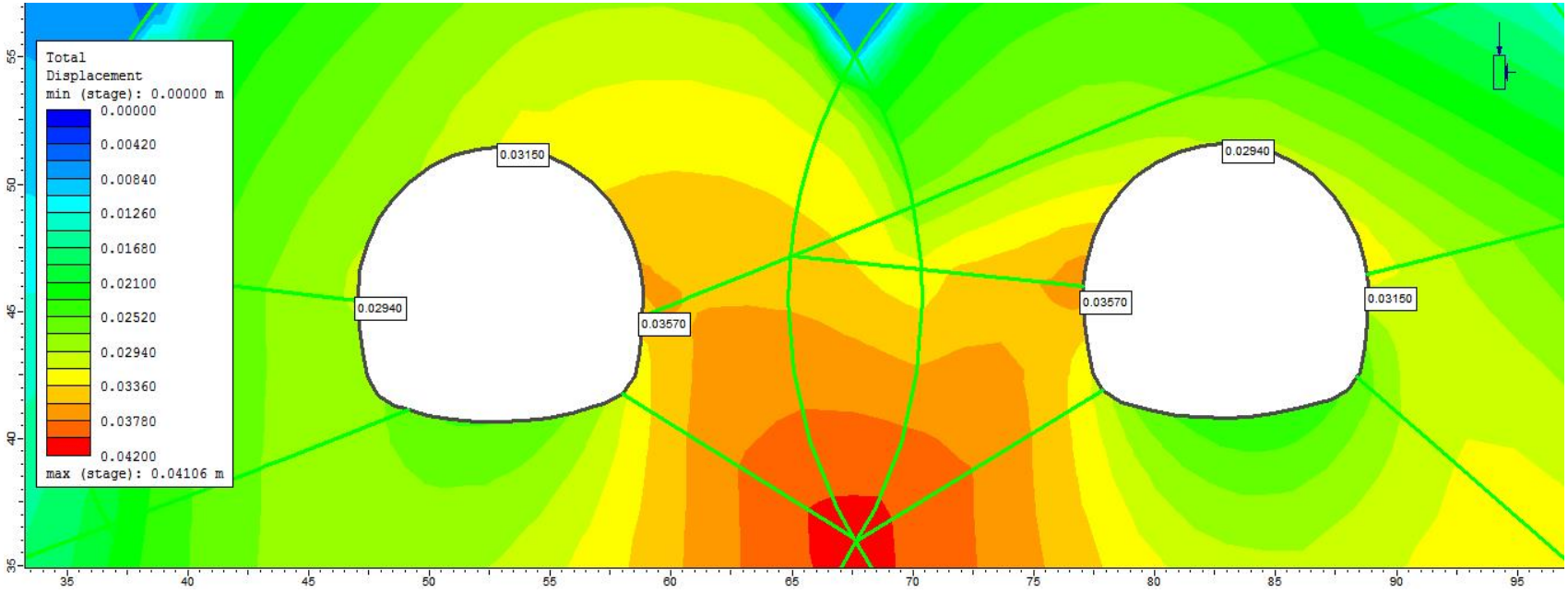

Figure B.5.4. Closer view of total displacement results on left shoulder, roof and right shoulder of Caglayan Tunnel excavation at Km: 49+044

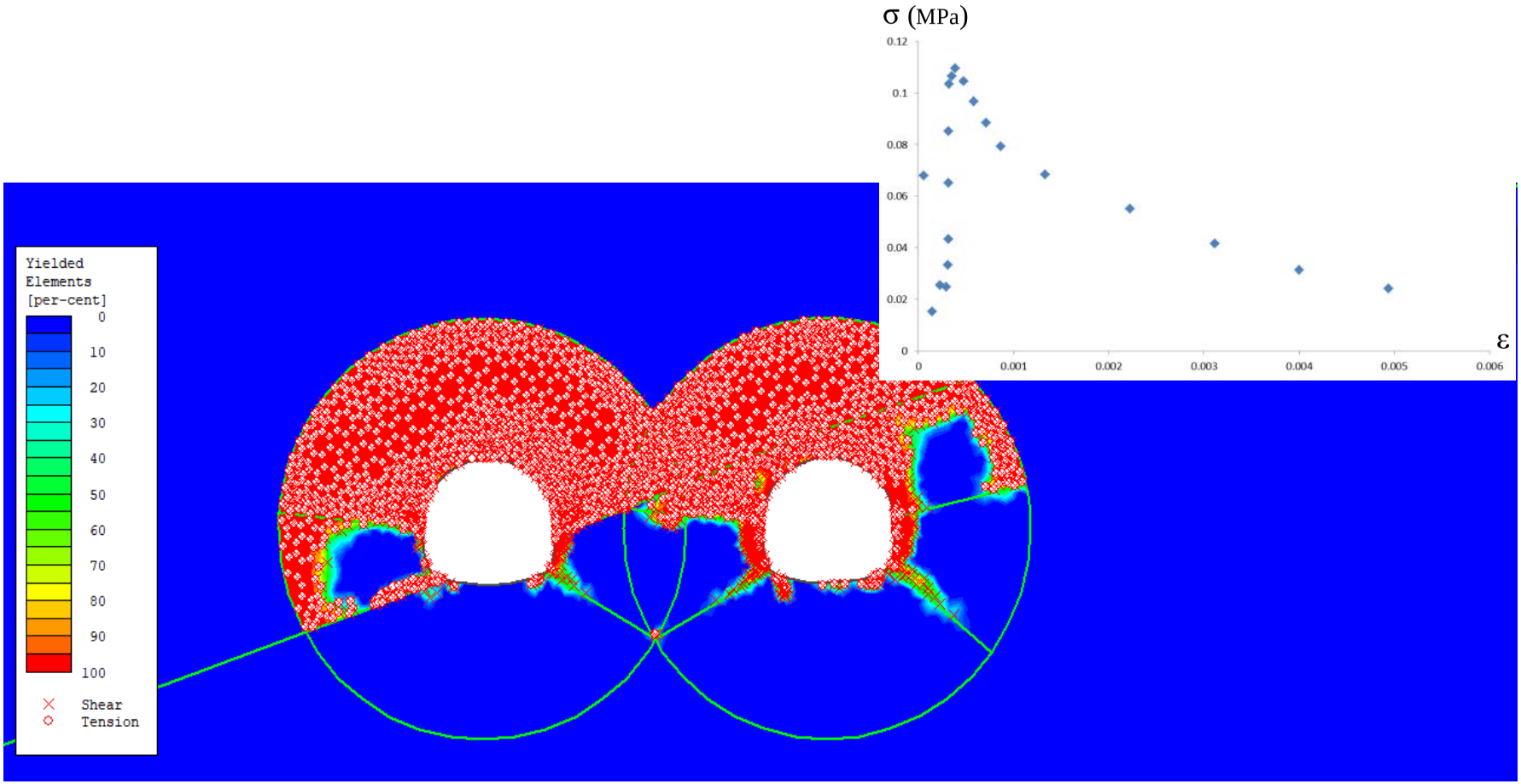

Figure B.5.5. Closer view of yielded elements and stress – strain graph of Caglayan Tunnel excavation at Km: 49+044

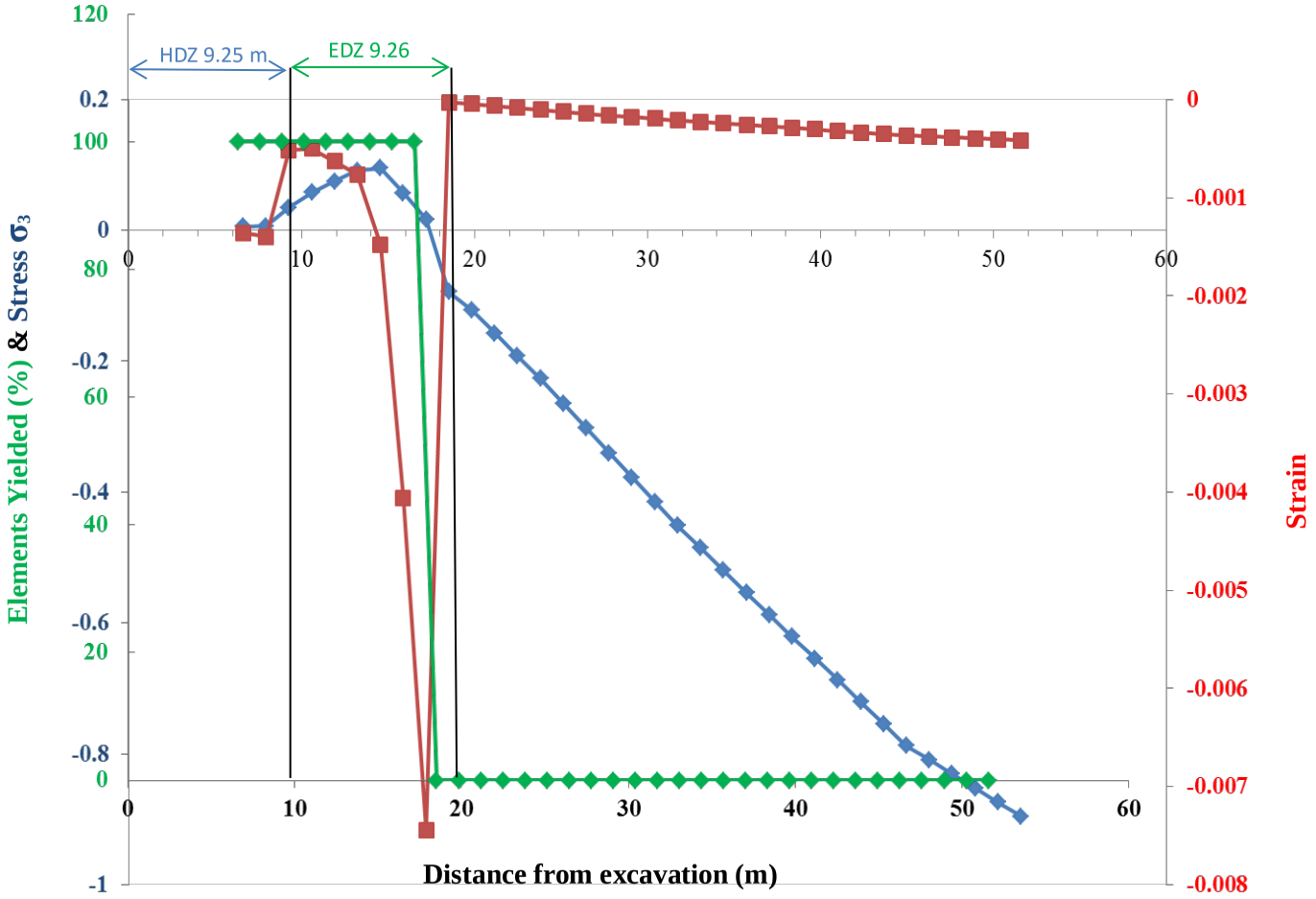

Figure B.5.6. Thickness of HDZ, EDZ and EIZ of Caglayan Tunnel excavation at Km: 49+044

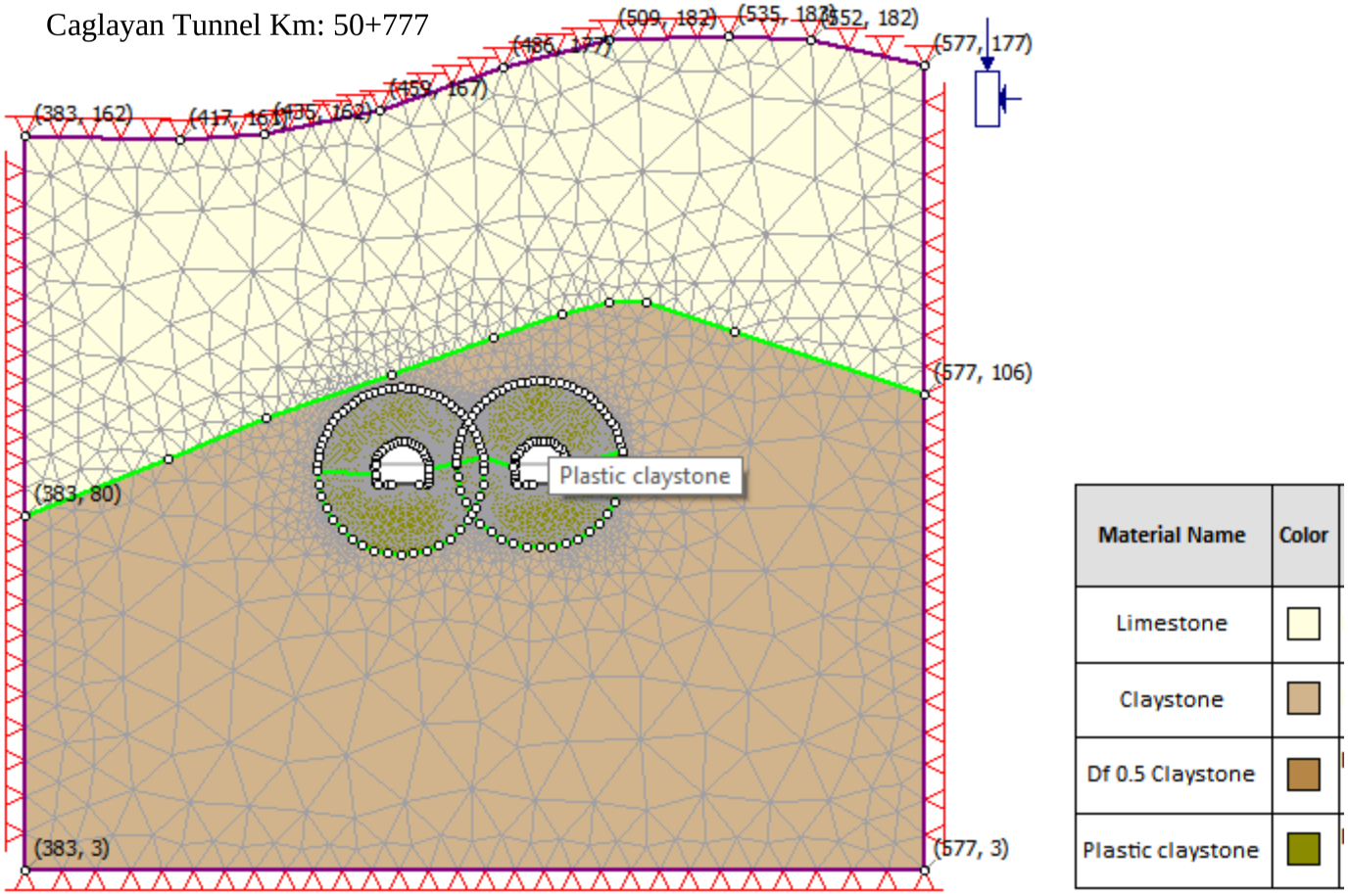

Figure B.6. Numerical model geometry, dimesions, mesh and geological cross section of Caglayan Tunnel excavation at Km:50+777

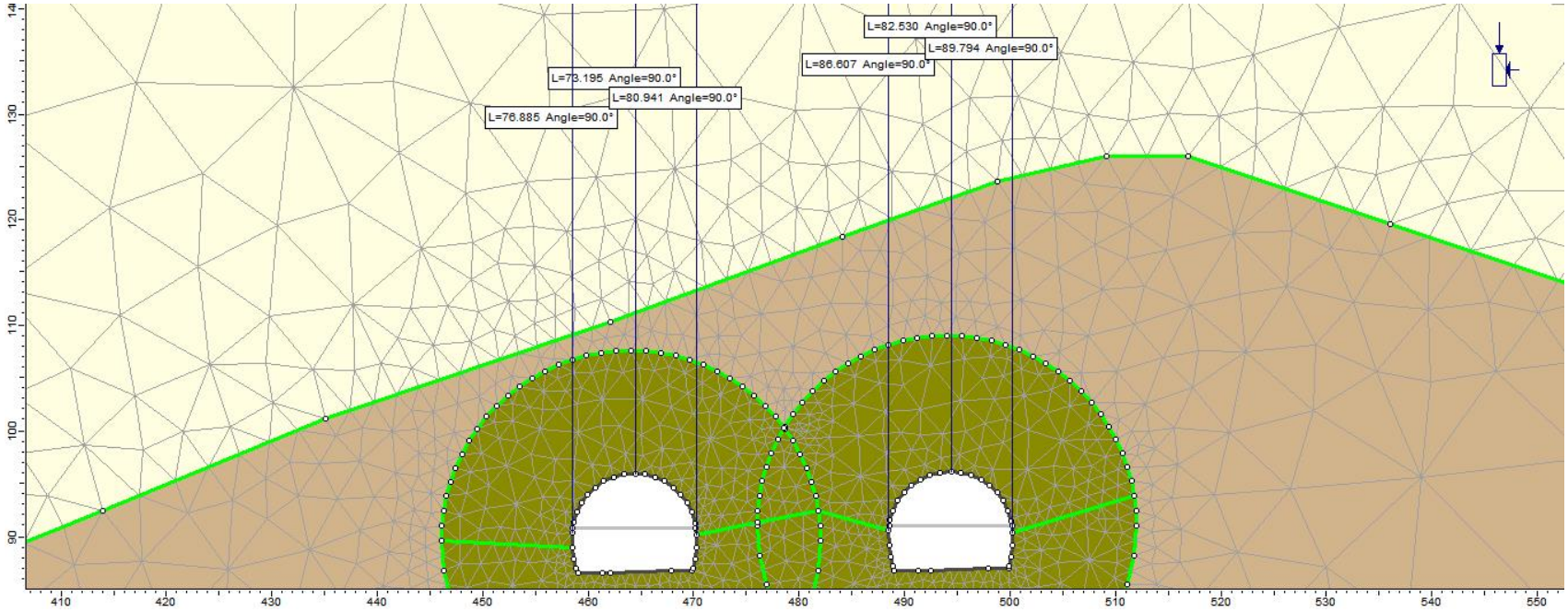

Figure B.6.1. Closer view of numerical model geometry, dimensions, mesh and geological cross section of Caglayan Tunnel excavation at Km: 50+777

Material Name	Color	Initial Element Loading	Unit Weight (MN/m3)	Elastic Type	Young's Modulus (MPa)	Poisson's Ratio	Failure Criterion	Material Type	Intact Compressive Strength (MPa)	mb (peak)	mb (residual)	s (peak)	s (residual)	a (peak)	a (residual)	Dilation Parameter	Piezo Line	Ru
Limestone		Body Force Only	0.02455	Isotropic	6691.44	0.234	Generalized Hoek-Brown	Elastic	54.105	1.87342		0.00309559		0.506582			None	0
Claystone		Body Force Only	0.021	Isotropic	920.2	0.38	Generalized Hoek-Brown	Elastic	15.67	0.783523		0.001776		0.509269			None	0
Df 0.5 Claystone		Field Stress and Body Force	0.021	Isotropic	345.11	0.38	Generalized Hoek-Brown	Plastic	15.67	0.20409	0.20409	7.73889e-005	7.73889e-005	0.523899	0.523899	0	None	0
Plastic claystone		Field Stress and Body Force	0.021	Isotropic	920.2	0.38	Generalized Hoek-Brown	Plastic	15.67	0.783523	0.783523	0.001776	0.001776	0.509269	0.509269	0	None	0

Figure B.6.2. Material properties which are used in numerical modelling of Caglayan Tunnel excavation at Km: 50+777

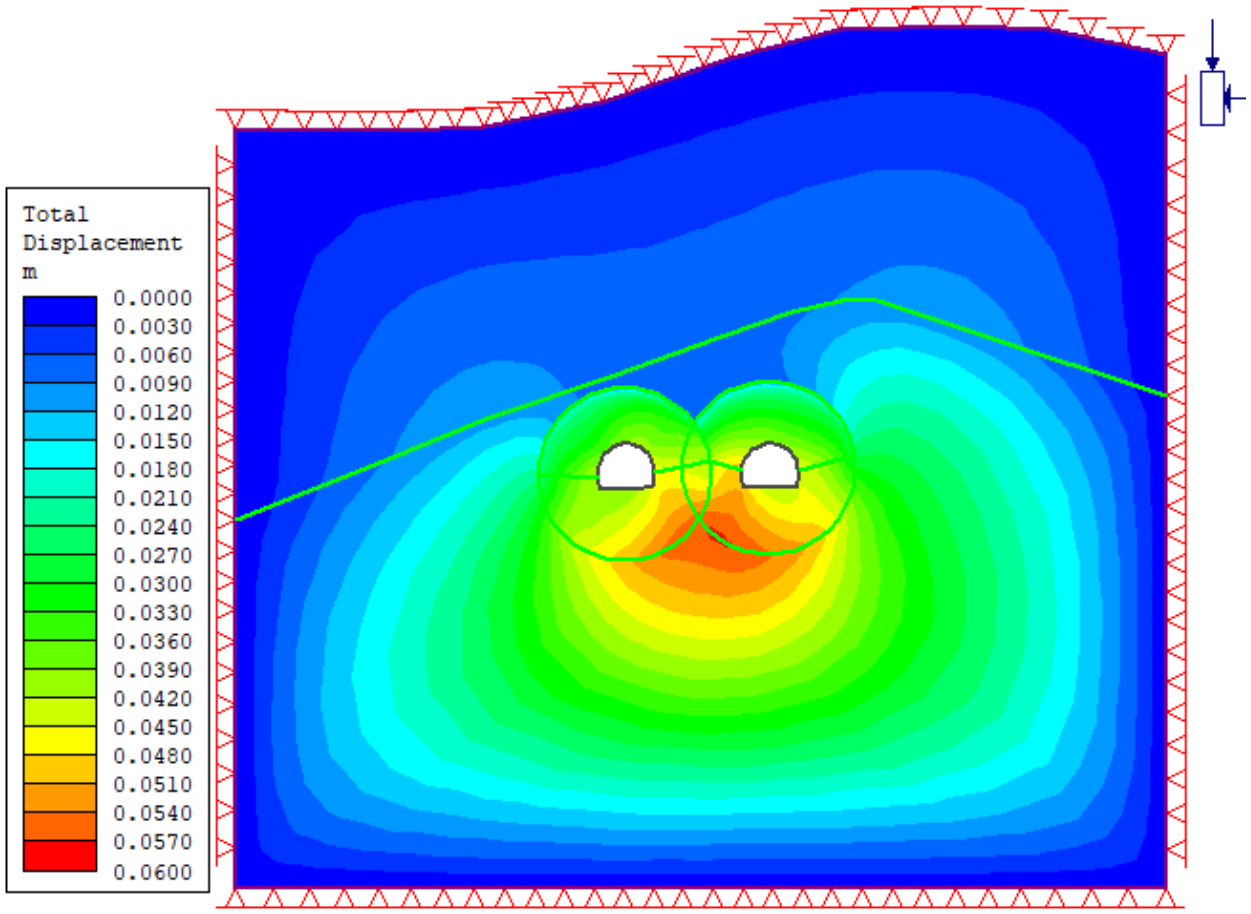

Figure B.6.3. Numerical modelling results in terms of total displacements of Caglayan Tunnel excavation at Km: 50+777

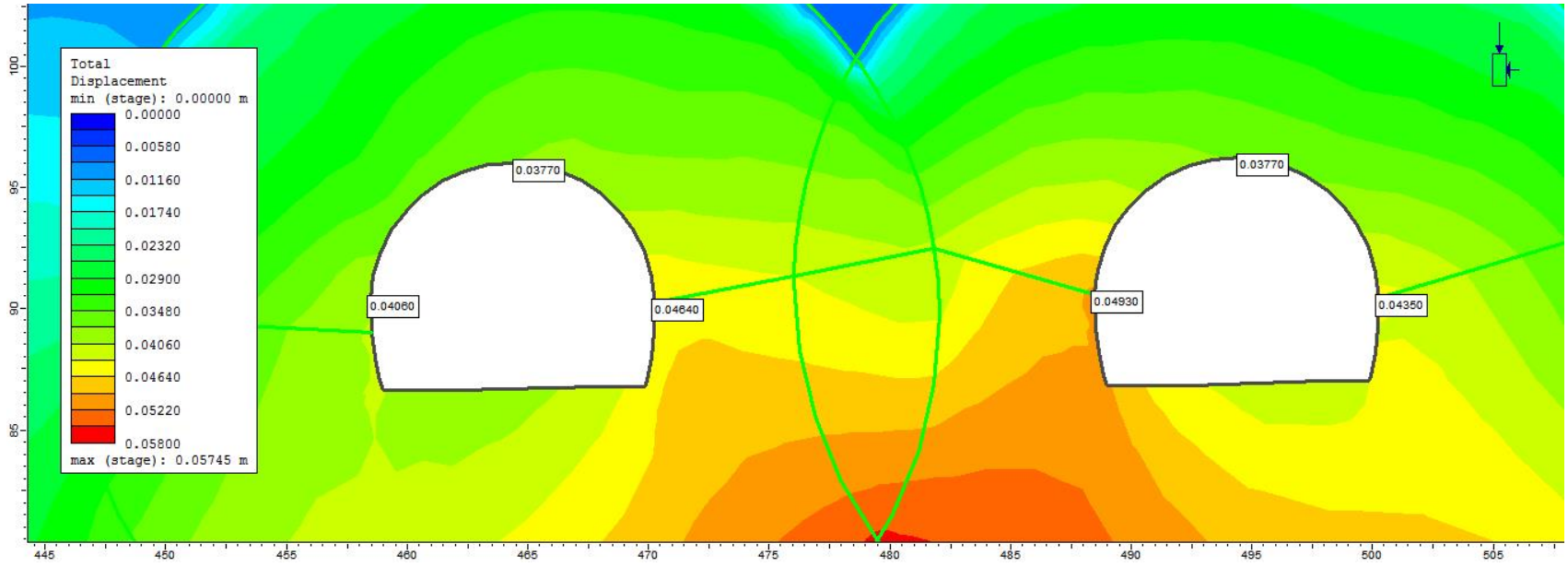

Figure B.6.4 Closer view of total displacement results on left shoulder, roof and right shoulder of Caglayan Tunnel excavation at Km: 50+777

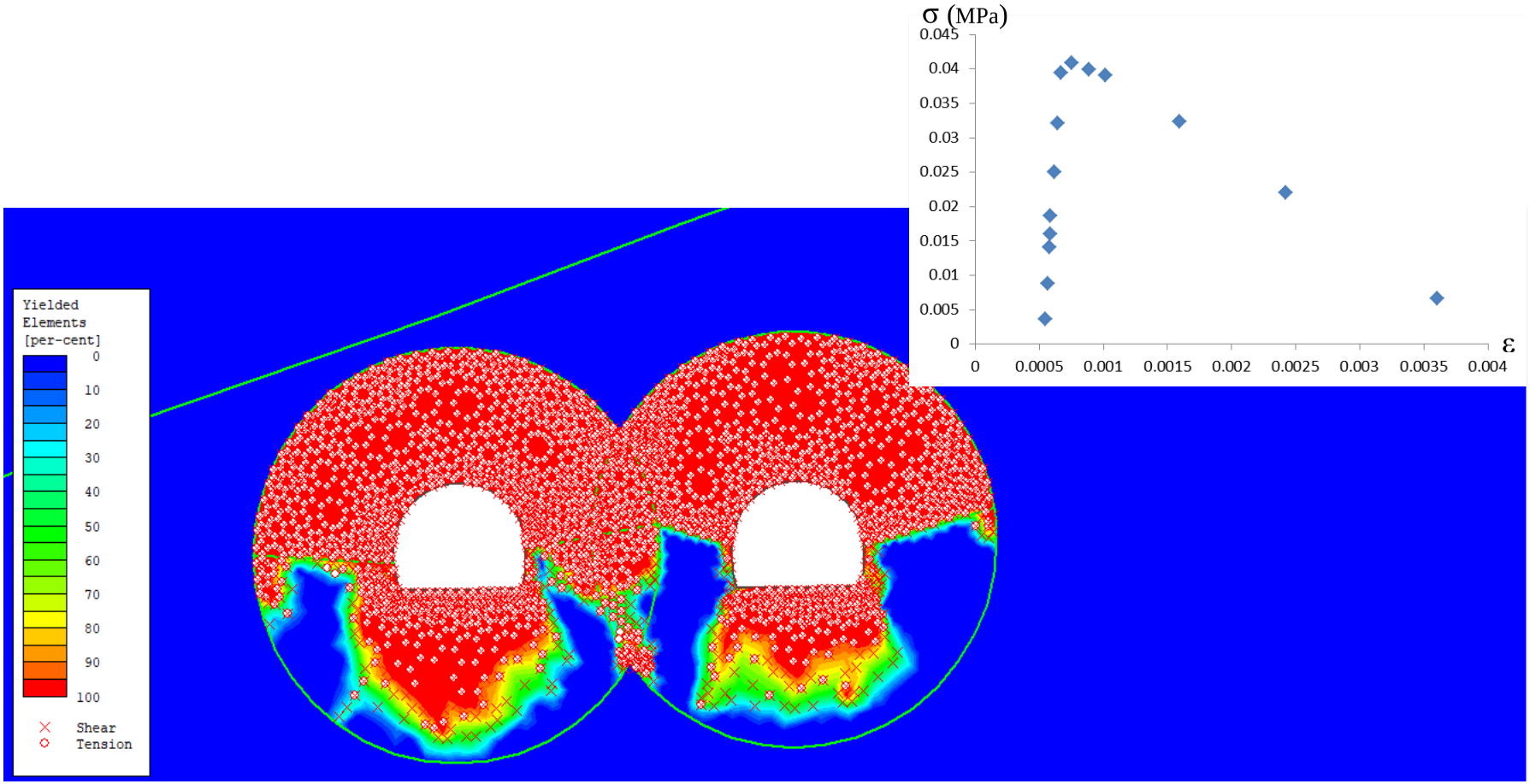

Figure B.6.5. Closer view of yielded elements of Caglayan Tunnel excavation at Km: 50+777

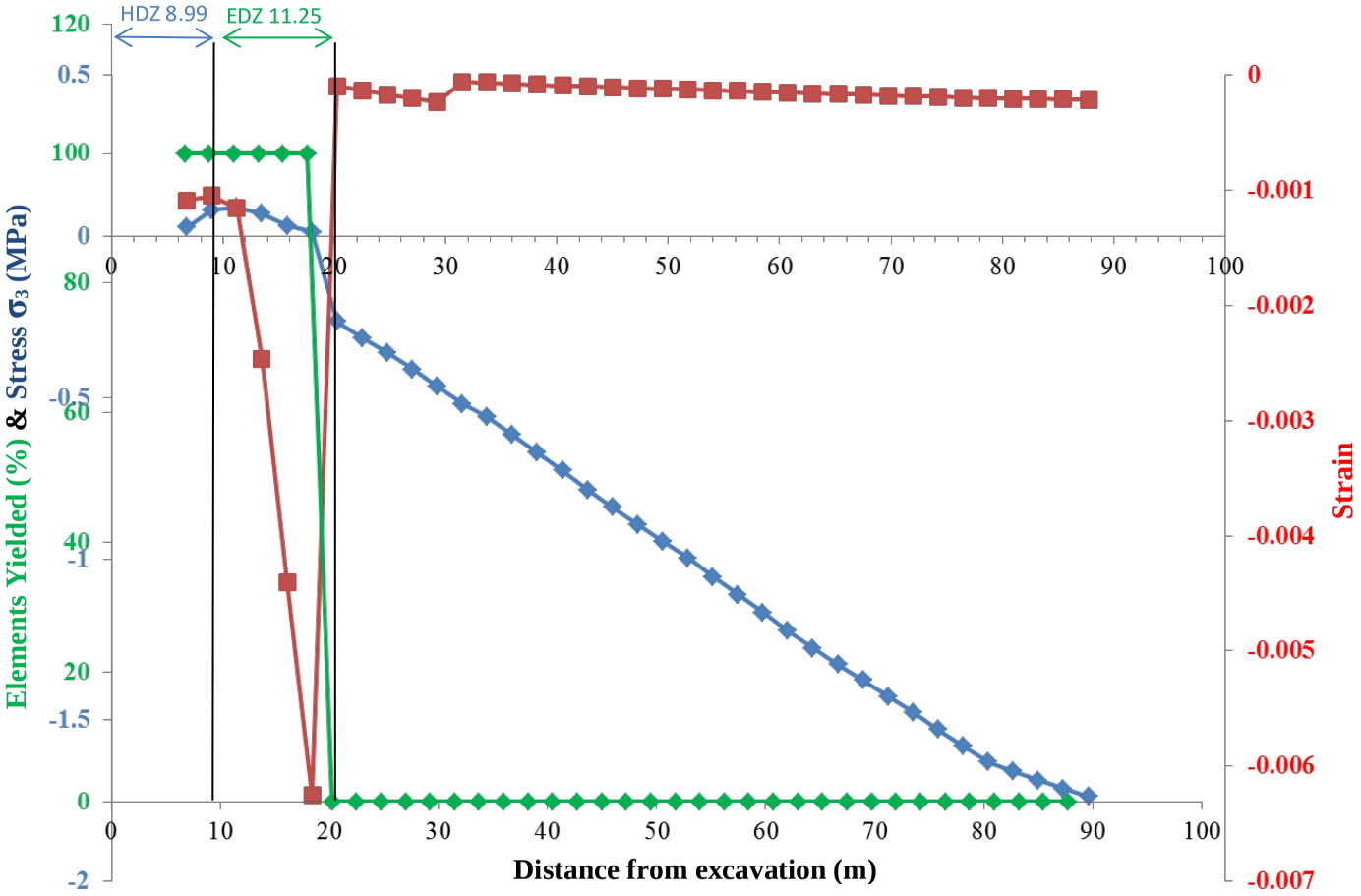

Figure B.6.6. Thickness of HDZ, EDZ and EIZ of Caglayan Tunnel excavation at Km: 50+777

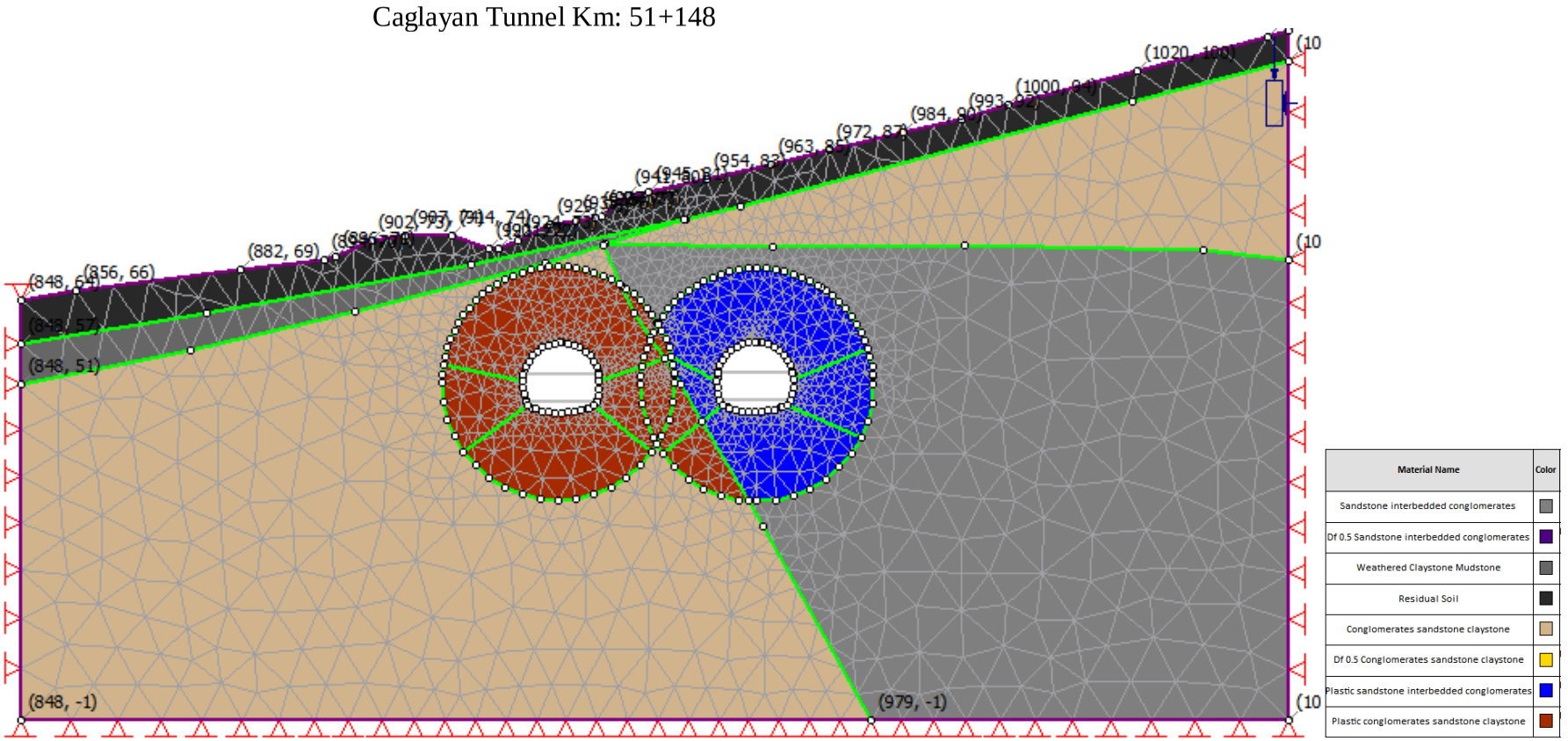

Figure B.7. Numerical model geometry, dimensions, mesh and geological cross section of Caglayan Tunnel excavation at Km:51+148

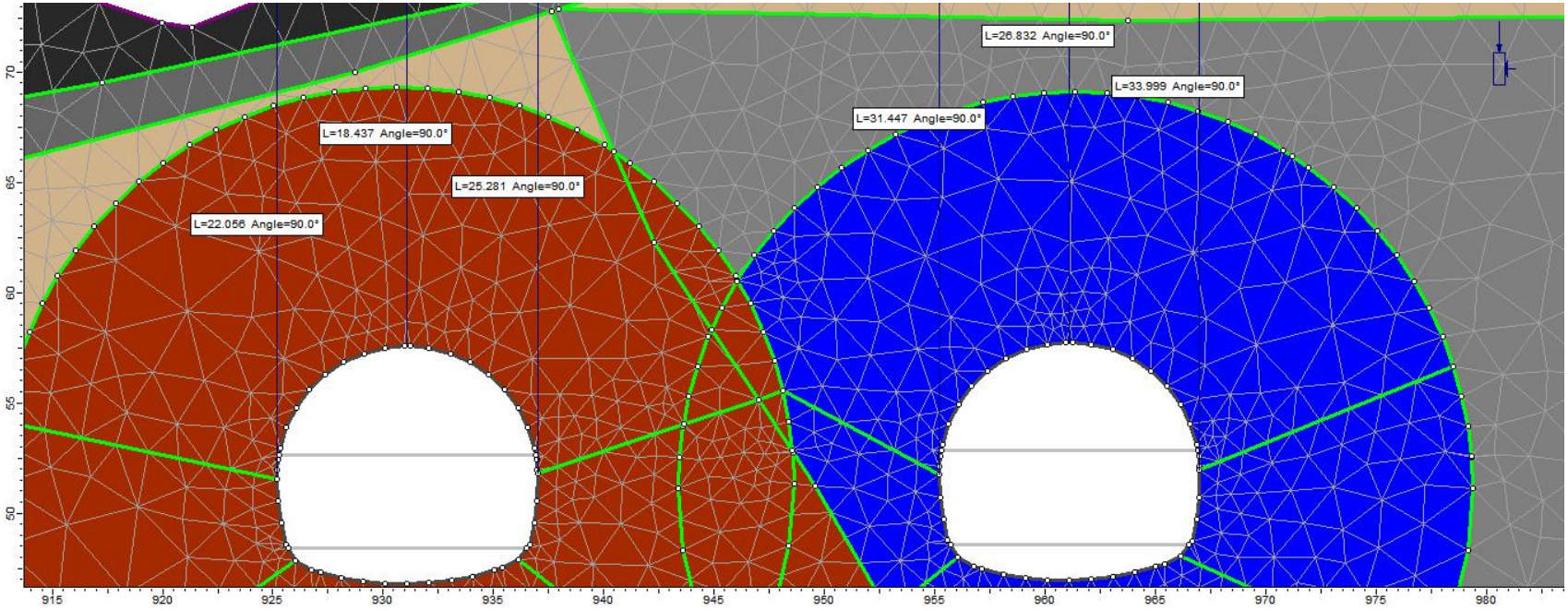

Figure B.7.1. Closer view of numerical model geometry, dimensions, mesh and geological cross section of Caglayan Tunnel excavation at Km: 51+148

Material Name	Color	Initial Element Loading	Unit Weight (MN/m3)	Elastic Type	Young's Modulus (MPa)	Poisson's Ratio	Failure Criterion	Material Type	Tensile Strength (MPa)	Friction Angle (peak) (deg)	Cohesion (peak) (MPa)	Intact Compressive Strength (MPa)	mb (peak)	mb (residual)	s (peak)	s (residual)	a (peak)	a (residual)	Dilation Parameter	Piezo Line	Ru
Sandstone interbedded conglomerates		Body Force Only	0.024	Isotropic	1715.35	0.3	Generalized Hoek-Brown	Elastic				19.11	2.31011		0.00142219		0.510622			None	0
Df 0.5 Sandstone interbedded conglomerates		Field Stress and Body Force	0.024	Isotropic	821.481	0.2525	Generalized Hoek-Brown	Plastic				19.11	1.14444	1.14444	0.00038331	0.00038331	0.510622	0.510622	0	None	0
Weathered Claystone Mudstone		Body Force Only	0.013	Isotropic	21.9	0.3	Mohr Coulomb	Elastic	0	15	0.05									None	0
Residual Soil		Body Force Only	0.011	Isotropic	15.8	0.3	Mohr Coulomb	Elastic	0	10	0.01									None	0
Conglomerates sandstone claystone		Body Force Only	0.024	Isotropic	2568.19	0.28	Generalized Hoek-Brown	Elastic				44.93	1.32567		0.000653392		0.517064			None	0
Df 0.5 Conglomerates sandstone claystone		Field Stress and Body Force	0.024	Isotropic	1309.94	0.22	Generalized Hoek-Brown	Plastic				44.93	0.60423	0.60423	0.000150733	0.000150733	0.517064	0.517064	0	None	0
Plastic sandstone interbedded conglomerates		Field Stress and Body Force	0.024	Isotropic	1715.35	0.2525	Generalized Hoek-Brown	Plastic				19.11	2.31011	2.31011	0.00142219	0.00142219	0.510622	0.510622	0	None	0
Plastic conglomerates sandstone claystone		Field Stress and Body Force	0.024	Isotropic	2568.19	0.22	Generalized Hoek-Brown	Plastic				44.93	1.32567	1.32567	0.000653392	0.000653392	0.517064	0.517064	0	None	0

Figure B.7.2. Material properties which are used in numerical modelling of Caglayan Tunnel excavation at Km: 51+148

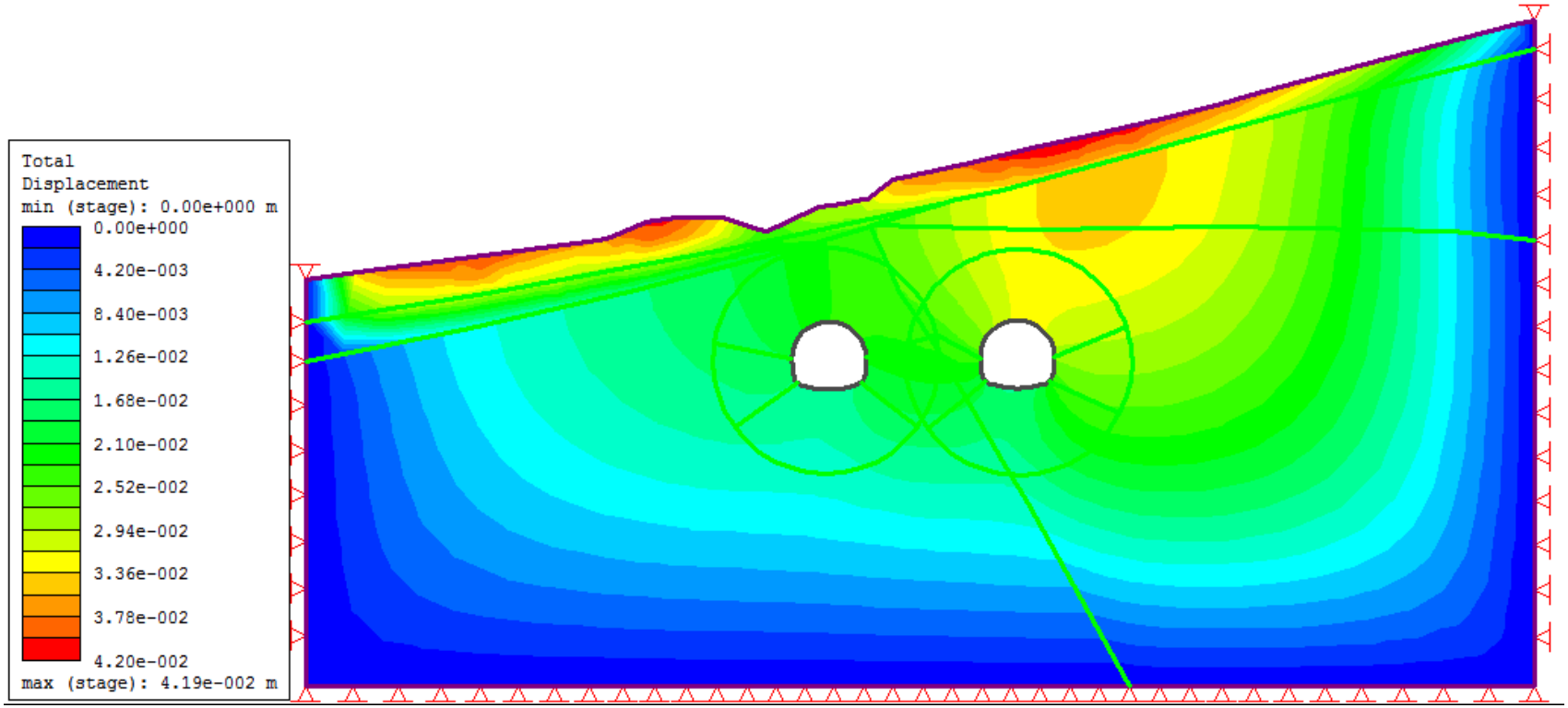

Figure B.7.3. Numerical modelling results in terms of total displacements of Caglayan Tunnel excavation at Km: 51+148

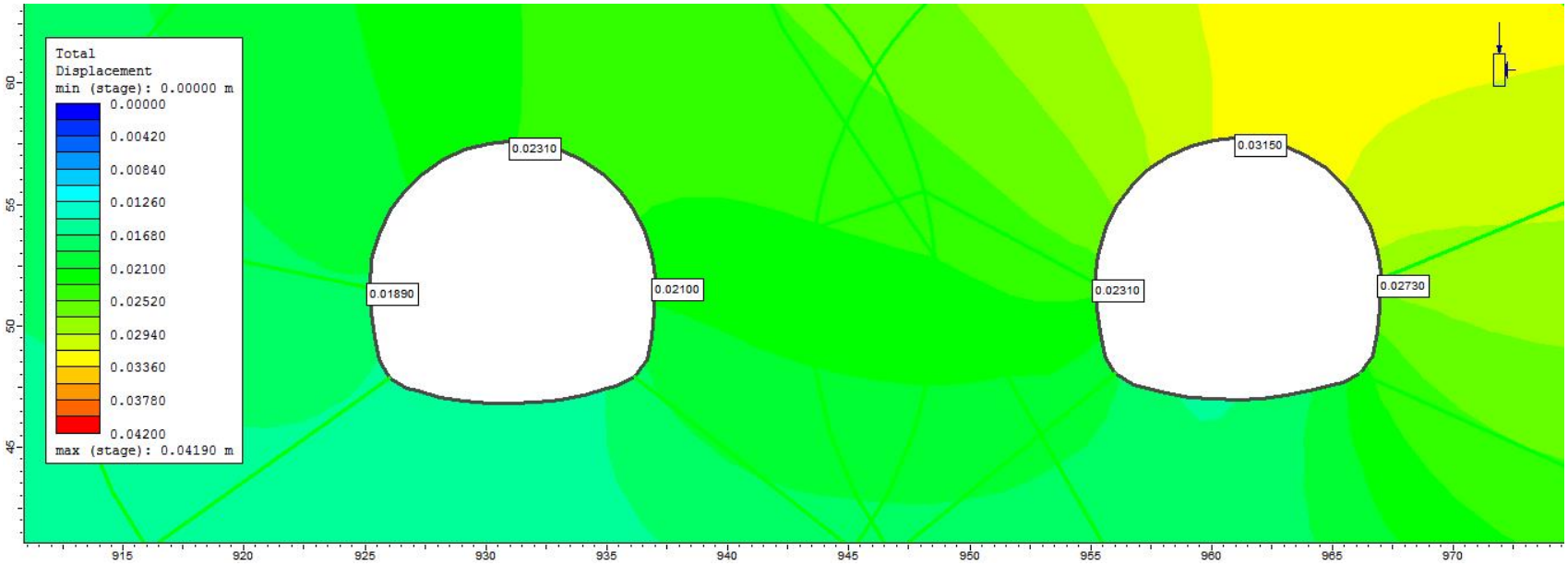

Figure B.7.4. Closer view of total displacement results on left shoulder, roof and right shoulder of Caglayan Tunnel excavation at Km: 51+148

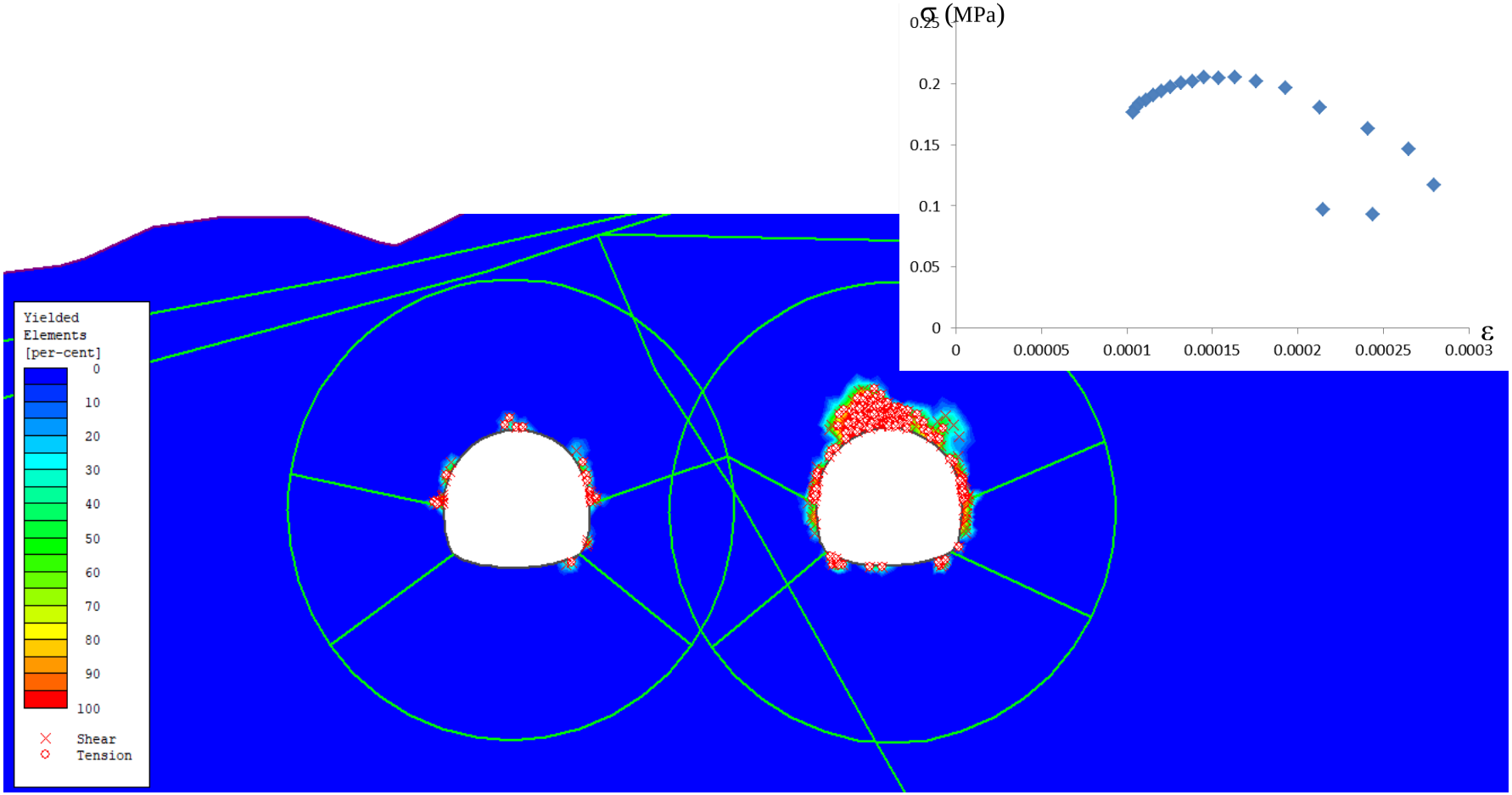

Figure B.7.5. Closer view of yielded elements and stress – strain graph of Caglayan Tunnel excavation at Km: 51+148

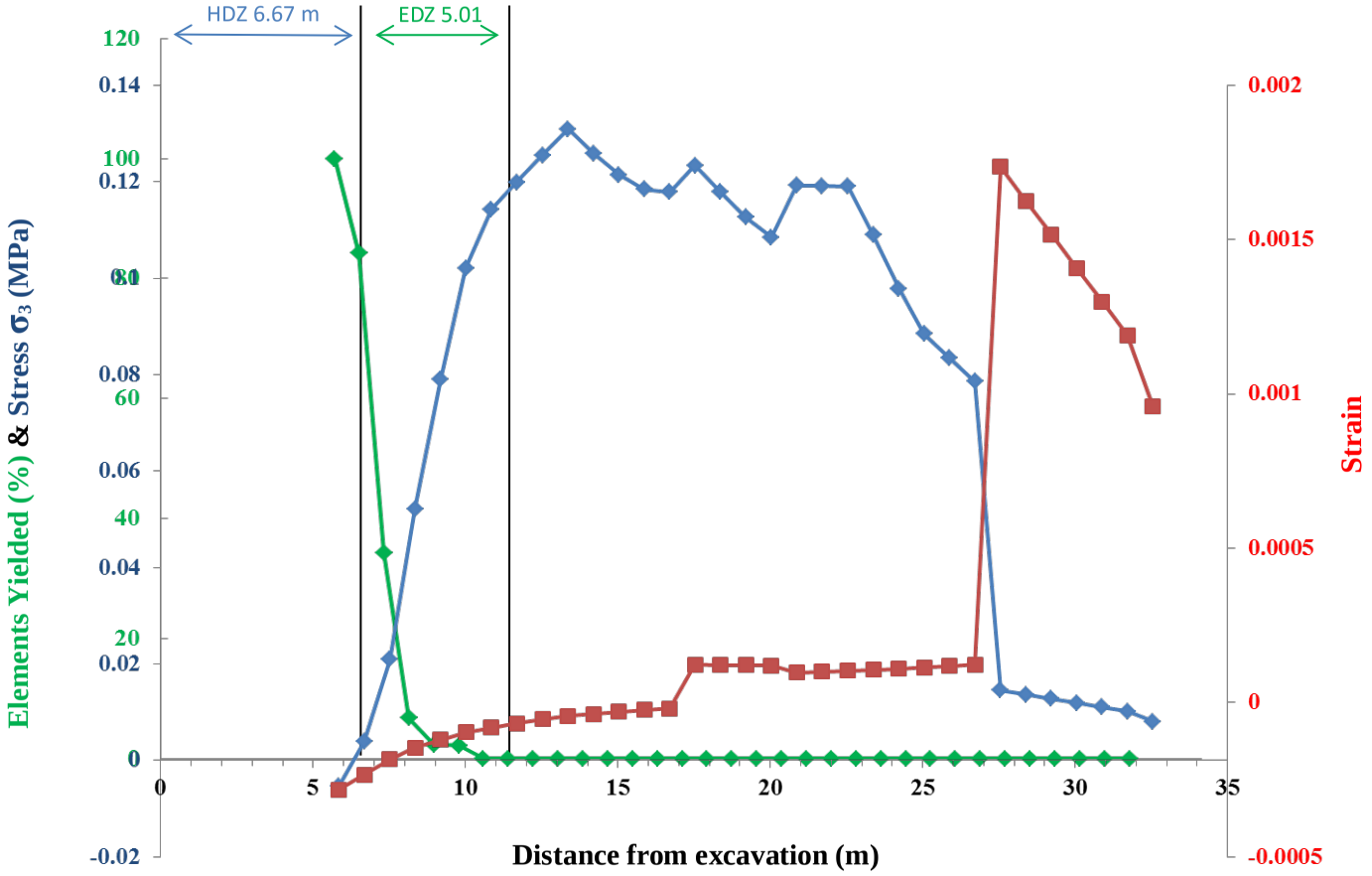

Figure B.7.6. Thickness of HDZ, EDZ and EIZ of Caglayan Tunnel excavation at Km: 51+148

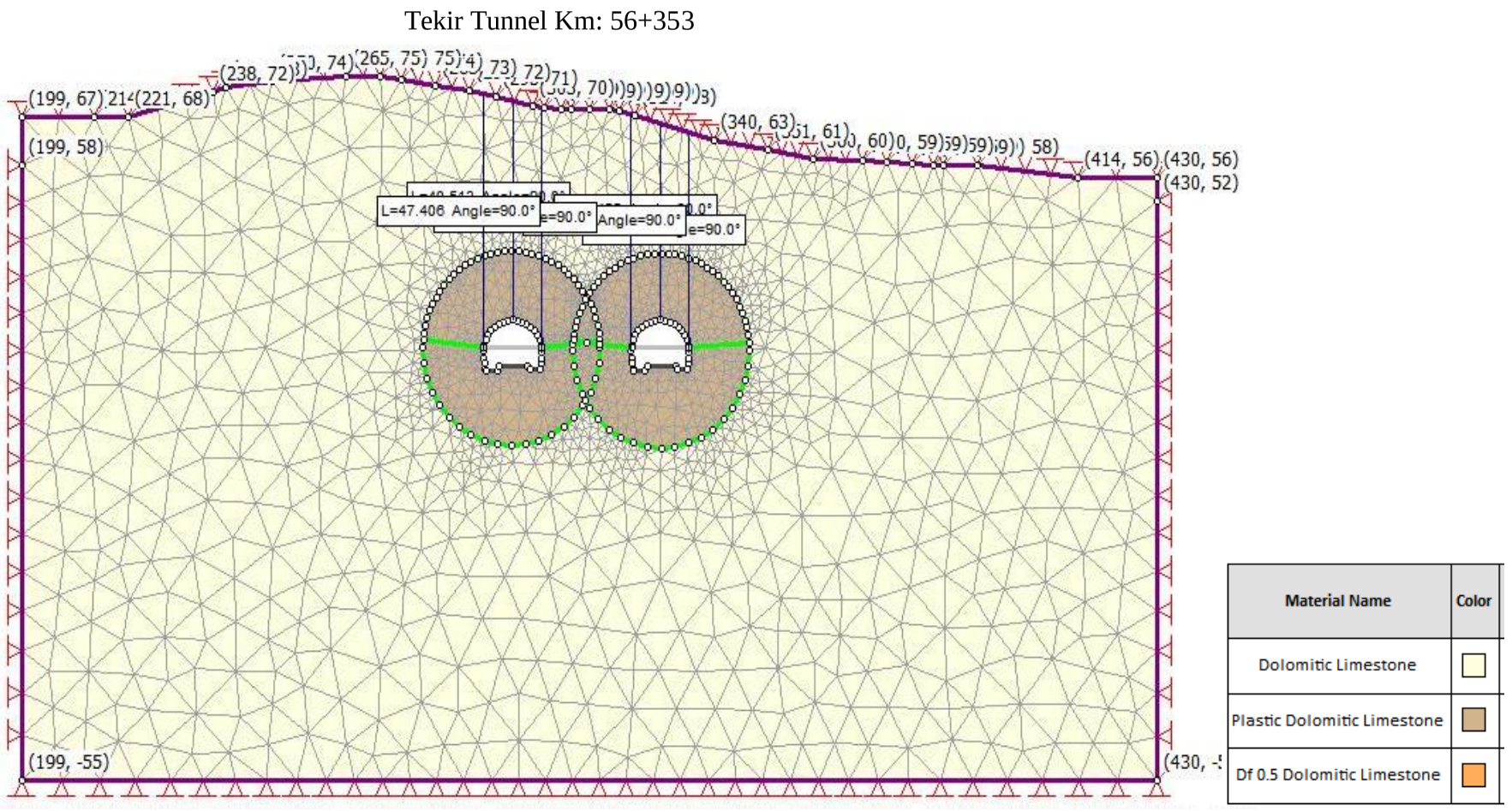

Figure B.8. Numerical model geometry, dimensions, mesh and geological cross section of Tekir Tunnel excavation at Km:56+353

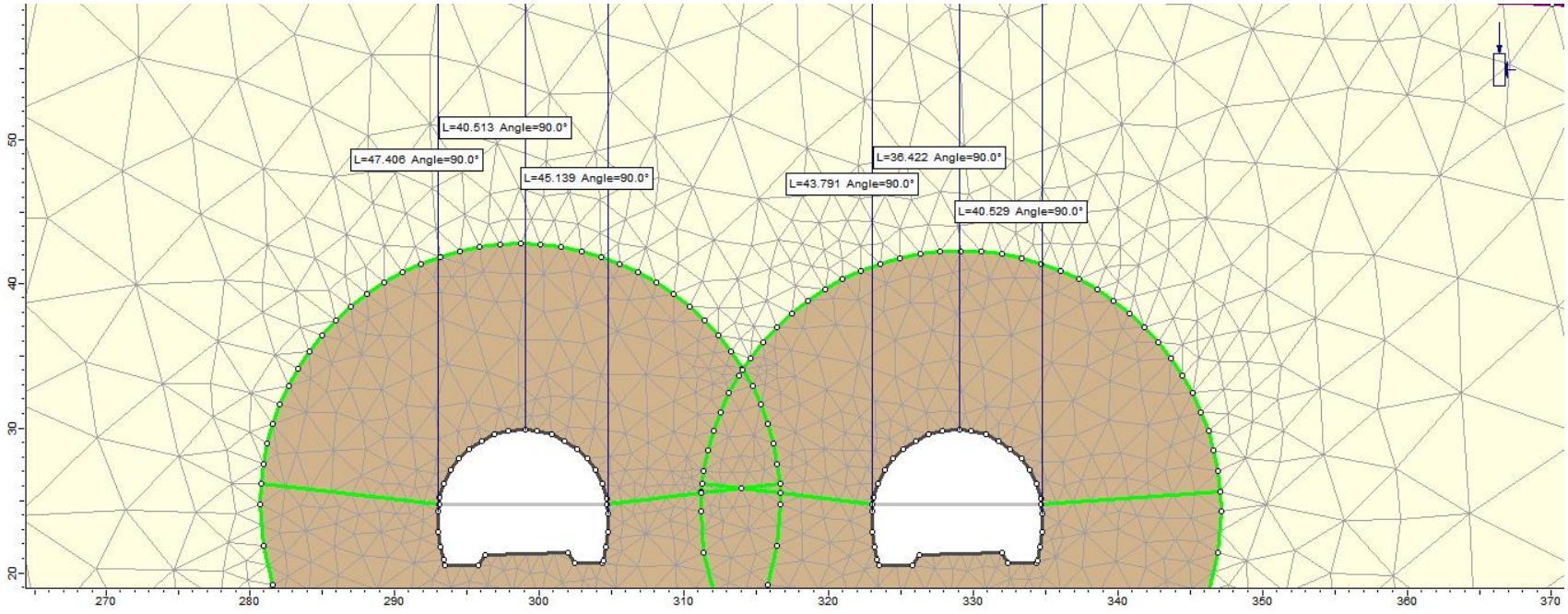

Figure B.8.1. Closer view of numerical model geometry, dimensions, mesh and geological cross section of Tekir Tunnel excavation at Km: 56+353

Material Name	Color	Initial Element Loading	Unit Weight (MN/m3)	Elastic Type	Young's Modulus (MPa)	Poisson's Ratio	Failure Criterion	Material Type	Intact Compressive Strength (MPa)	mb (peak)	mb (residual)	s (peak)	s (residual)	a (peak)	a (residual)	Dilation Parameter	Piezo Line	Ru
Dolomitic Limestone		Body Force Only	0.024	Isotropic	1331.5	0.29	Generalized Hoek-Brown	Elastic	20.02	1.17319		0.00127263		0.511368			None	0
Plastic Dolomitic Limestone		Body Force Only	0.024	Isotropic	1331.5	0.29	Generalized Hoek-Brown	Plastic	20.02	1.17319	1.17319	0.00127263	0.00127263	0.511368	0.511368	0	None	0
Df 0.5 Dolomitic Limestone		Body Force Only	0.024	Isotropic	641.293	0.29	Generalized Hoek-Brown	Plastic	20.02	0.574326	0.574326	0.000335463	0.000335463	0.511368	0.511368	0	None	0

Figure B.8.2. Material properties which are used in numerical modelling of Tekir Tunnel excavation at Km: 56+353

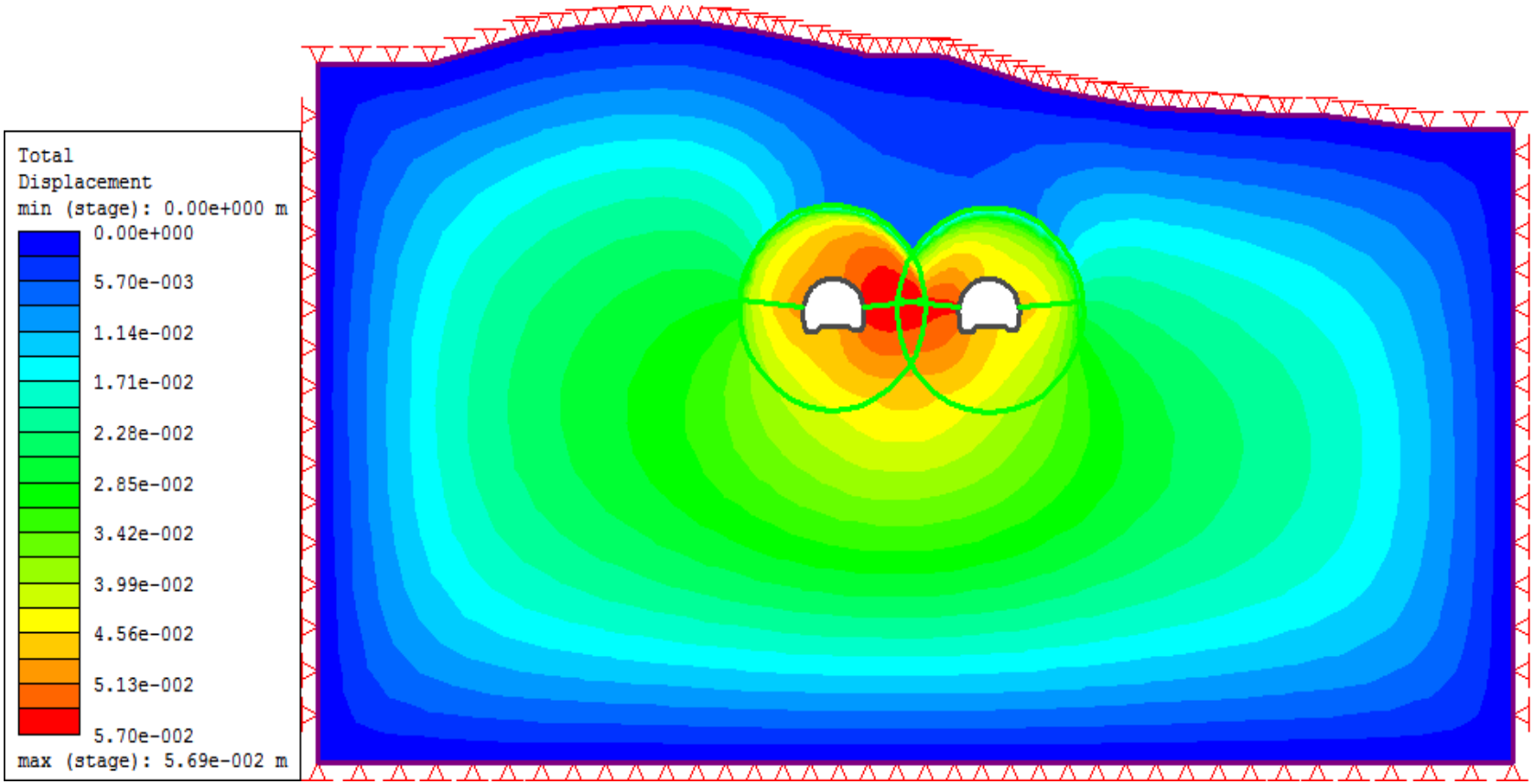

Figure B.8.3. Numerical modelling results in terms of total displacements of Tekir Tunnel excavation at Km: 56+353

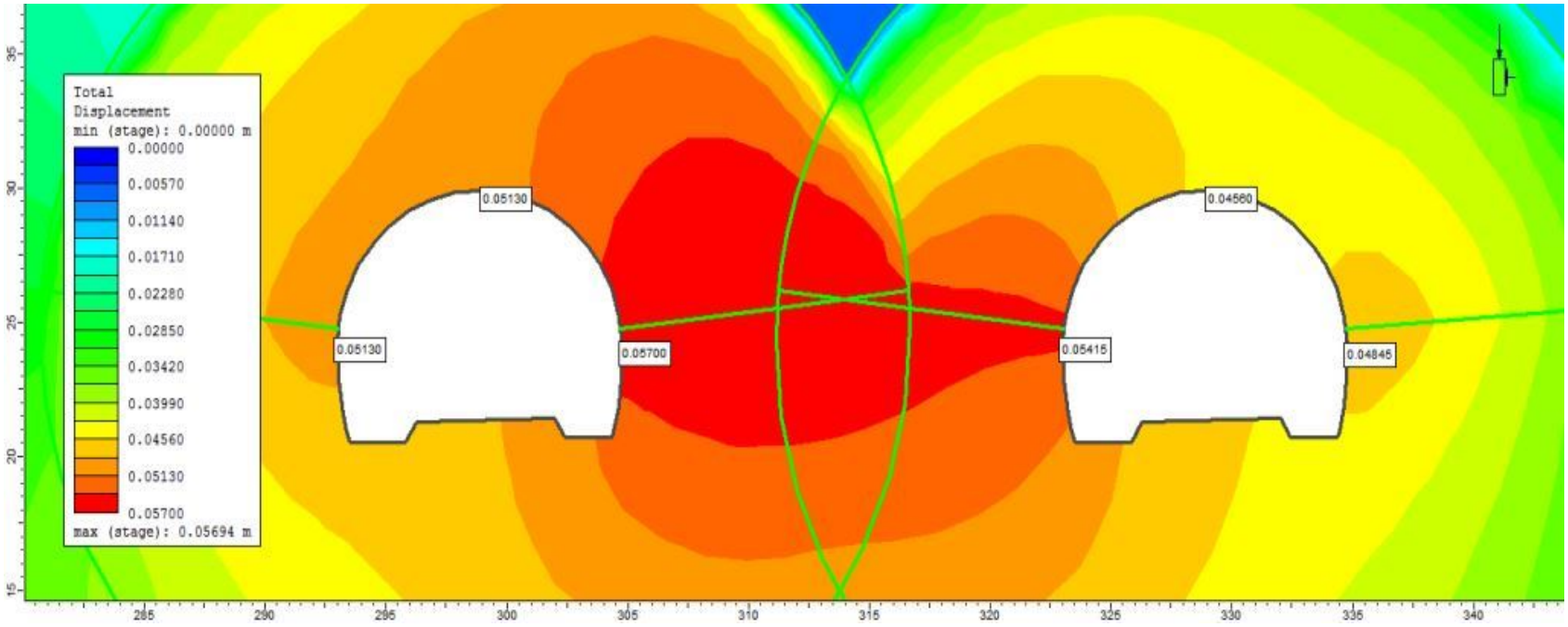

Figure B.8.4. Closer view of total displacement results on left shoulder, roof and right shoulder of Tekir Tunnel excavation at Km: 56+353

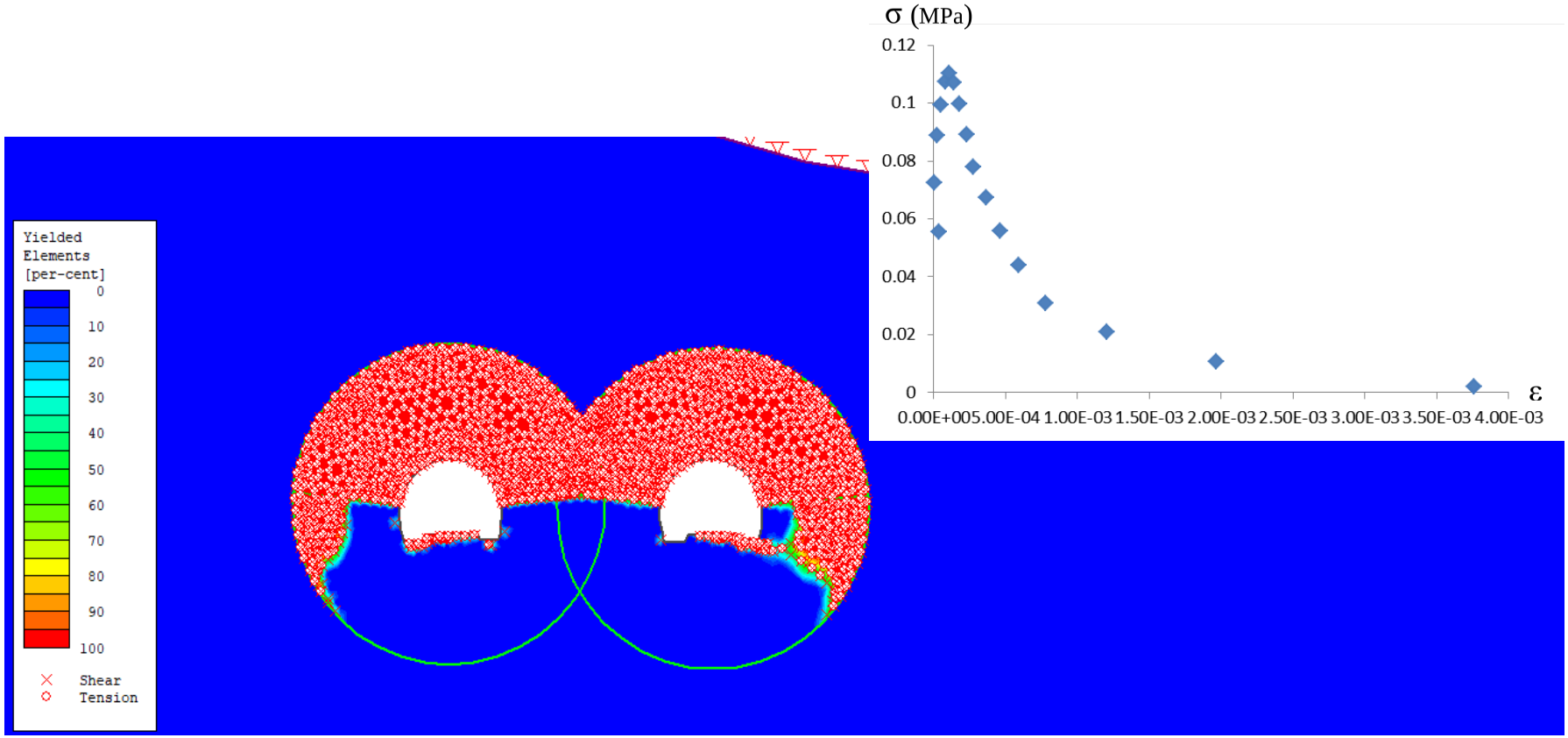

Figure B.8.5. Closer view of yielded elements and stress – strain graph of Tekir Tunnel excavation at Km: 56+353

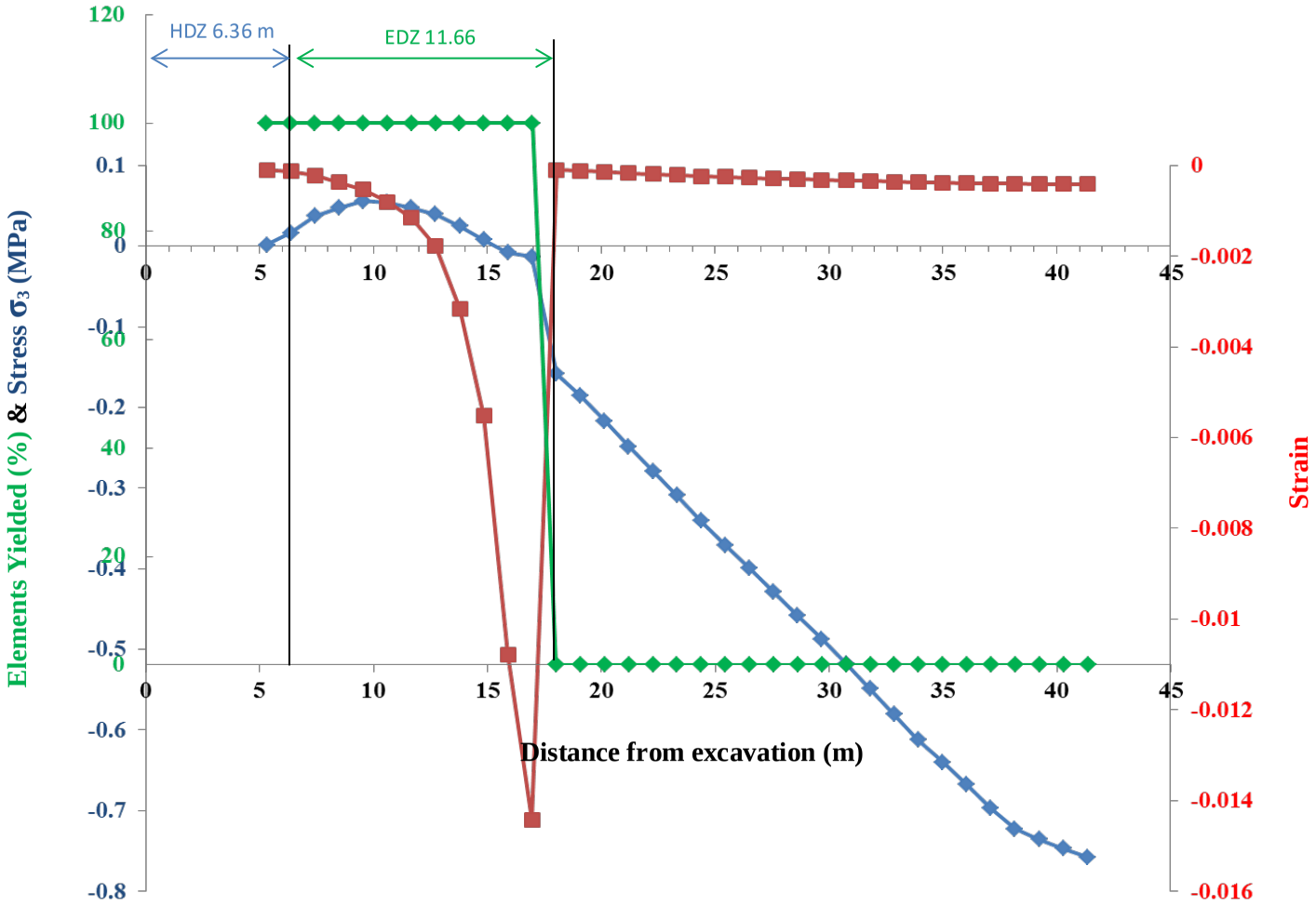

Figure B.8.6. Thickness of HDZ, EDZ and EIZ of Tekir Tunnel excavation at Km: 56+353

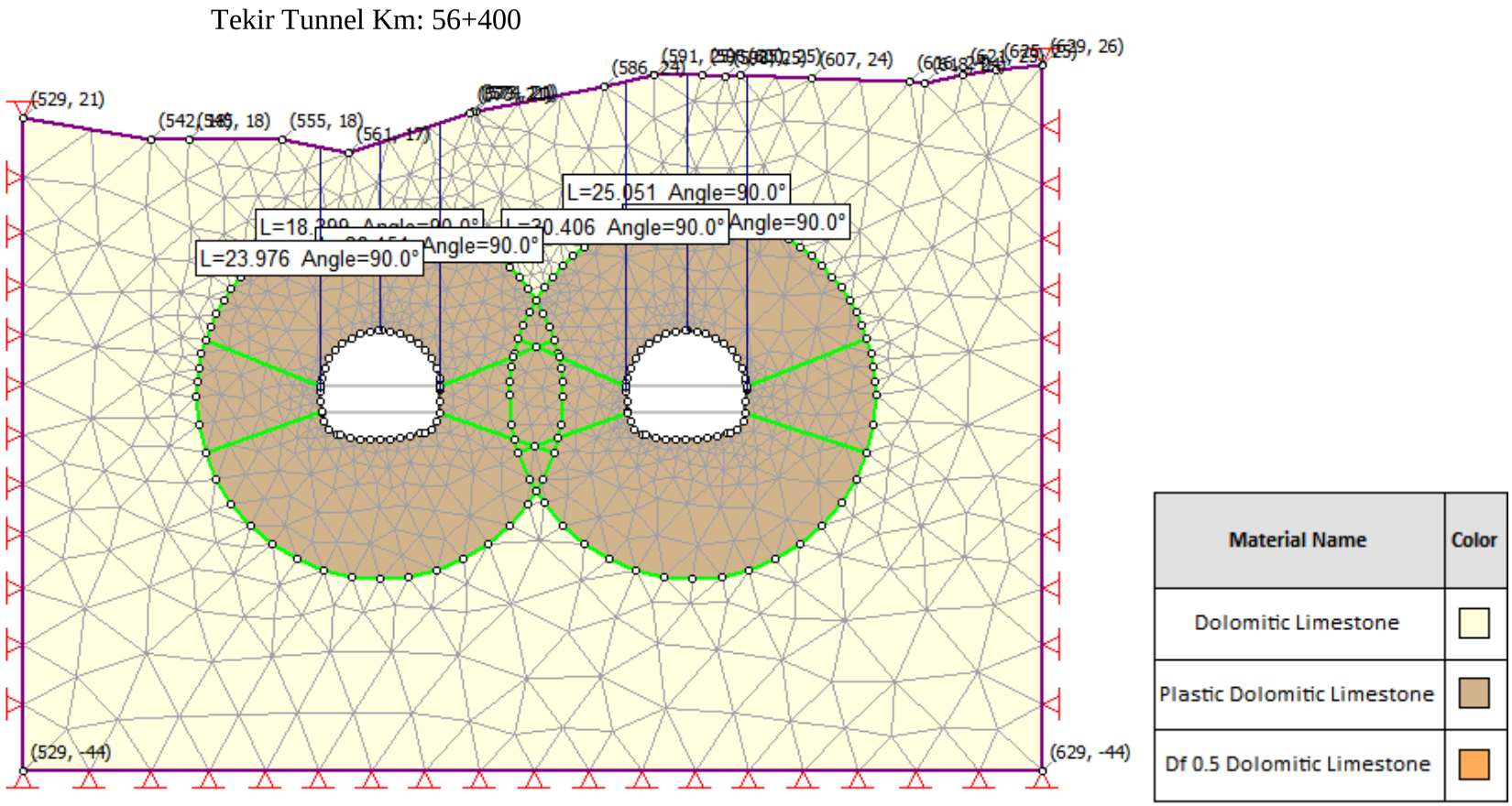

Figure B.9. Numerical model geometry, dimesions, mesh and geological cross section of Tekir Tunnel excavation at Km:56+400

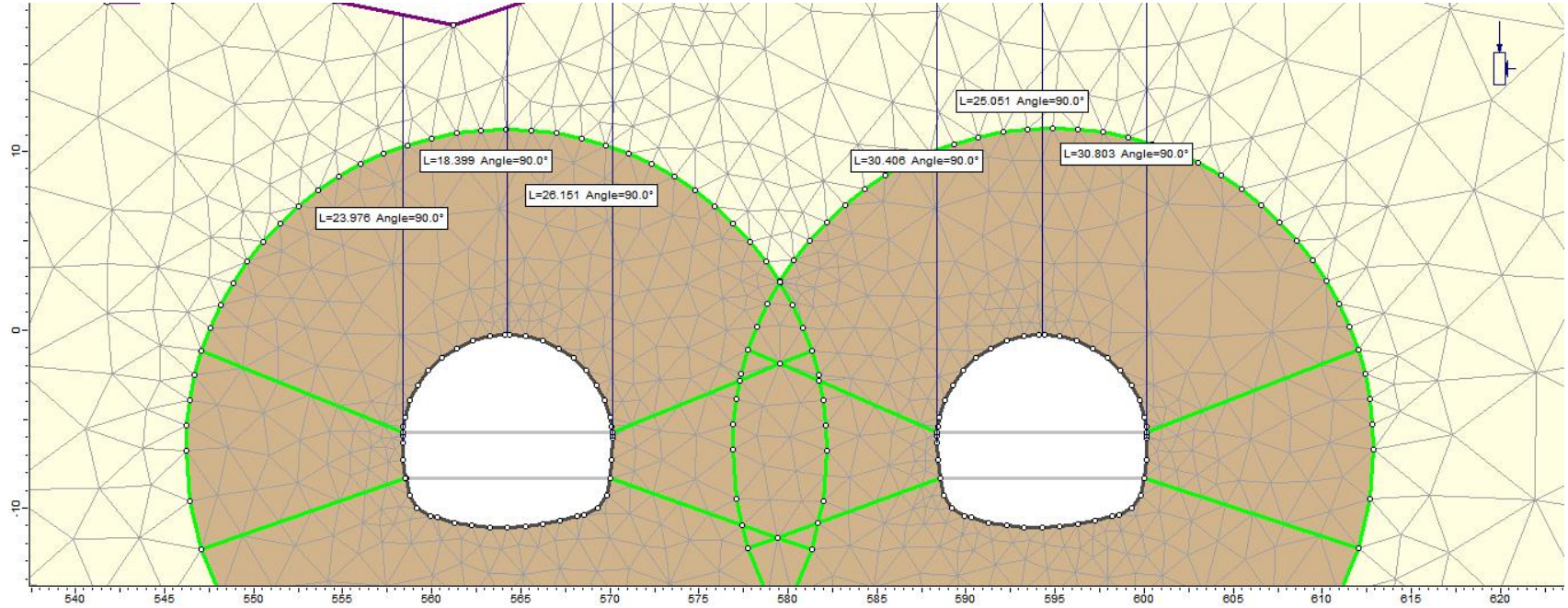

Figure B.9.1. Closer view of numerical model geometry, dimensions, mesh and geological cross section of Tekir Tunnel excavation at Km: 56+400

Material Name	Color	Initial Element Loading	Unit Weight (MN/m3)	Elastic Type	Young's Modulus (MPa)	Poisson's Ratio	Failure Criterion	Material Type	Intact Compressive Strength (MPa)	mb (peak)	mb (residual)	s (peak)	s (residual)	a (peak)	a (residual)	Dilation Parameter	Piezo Line	Ru
Dolomitic Limestone		Body Force Only	0.023	Isotropic	701.522	0.29	Generalized Hoek-Brown	Elastic	18.72	0.82085		0.000418942		0.522344			None	0
Plastic Dolomitic Limestone		Body Force Only	0.023	Isotropic	701.522	0.29	Generalized Hoek-Brown	Plastic	18.72	0.82085	0.82085	0.000418942	0.000418942	0.522344	0.522344	0	None	0
Df 0.5 Dolomitic Limestone		Body Force Only	0.023	Isotropic	379.361	0.29	Generalized Hoek-Brown	Plastic	18.72	0.35674	0.35674	8.8427e-005	8.8427e-005	0.522344	0.522344	0	None	0

Figure B.9.2. Material properties which are used in numerical modelling of Tekir Tunnel excavation at Km:56+400

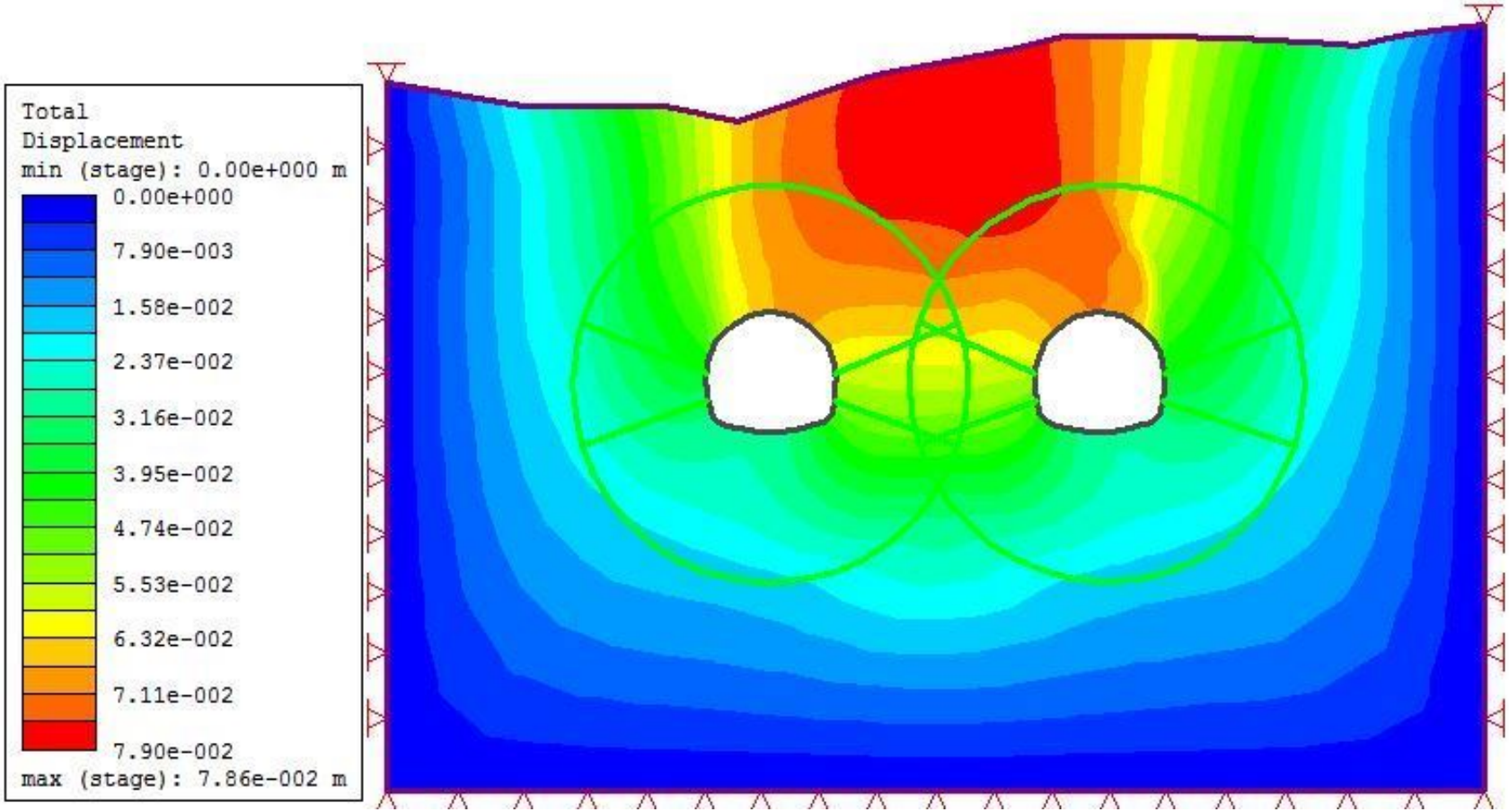

Figure B.9.3. Numerical modelling results in terms of total displacements of Tekir Tunnel excavation at Km:56+400

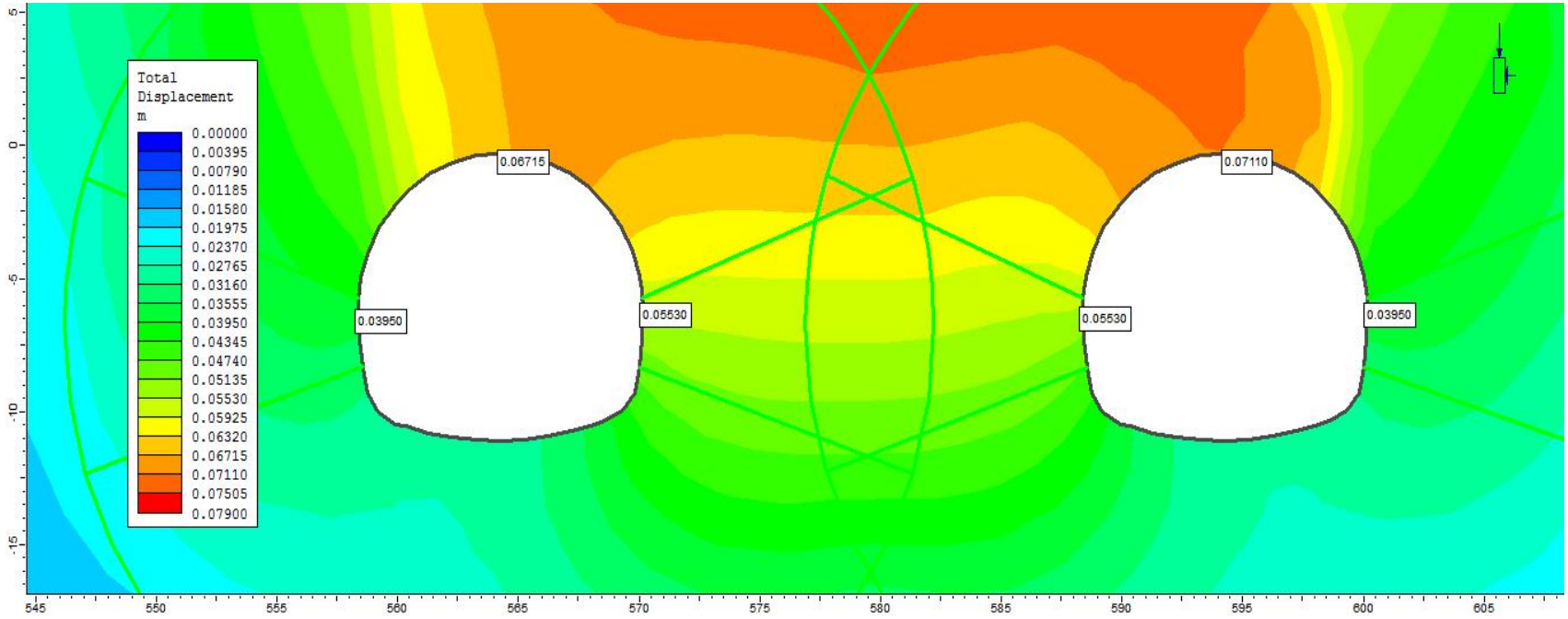

Figure B.9.4. Closer view of total displacement results on left shoulder, roof and right shoulder of Tekir Tunnel excavation at Km:56+400

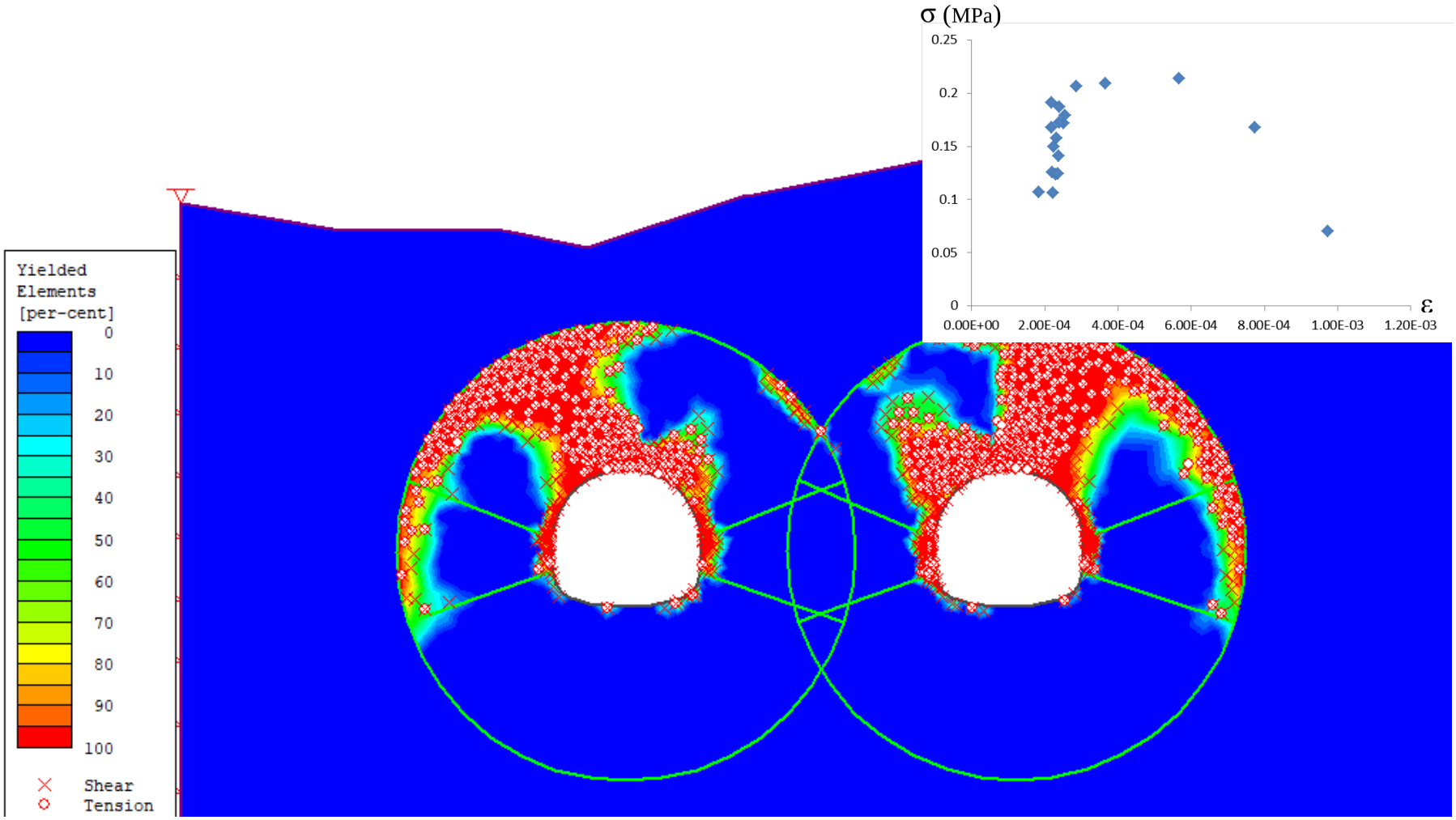

Figure B.9.5. Closer view of yielded elements of Tekir Tunnel excavation at Km: 56+400

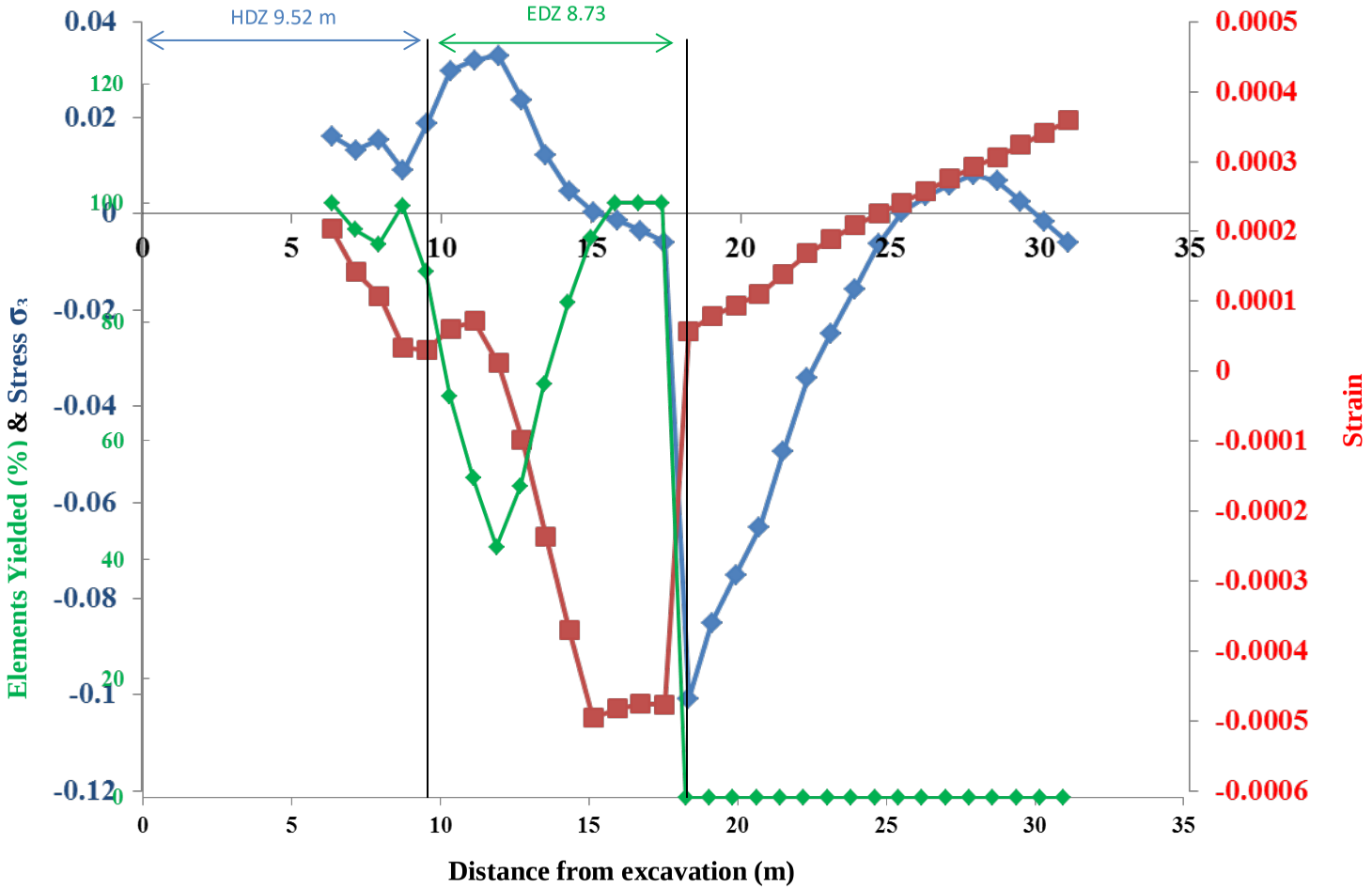

Figure B.9.6. Thickness of HDZ, EDZ and EIZ of Tekir Tunnel excavation at Km:56+400

APPENDIX C

DETAILS OF ALL INDEPENDENT VARIABLE INPUT PARAMETERS

Table C.1. Details of all independent variable input parameters

TUNNELS					Hoek's Approach			Input Parameter's of RMR System		Input Parameter's of Q System				
	Km	H (m)	RQD	RMR	Q	C_{rm} (MPa)	ϕ_{rm} (°)	E_{rm} (MPa)	UCS SCORE	RQD SCORE	J_N	J_R	J_A	J_W	SRF
Konak Tunnel	0+605	7.55	28.84	34.65	0.12	0.018	32.56	4.65	1.55	6.60	12	1.5	4	0.66	5
	0+606	5.18	28.84	34.65	0.12	0.015	35.28	4.65	1.55	6.60	12	1.5	4	0.66	5
	0+609	4.90	28.84	34.65	0.12	0.014	35.68	4.65	1.55	6.60	12	1.5	4	0.66	5
	0+613	7.97	10.77	32.02	0.04	0.015	28.55	49.41	1.40	4.12	12	1.5	4	0.66	5
	0+614	5.96	10.77	32.02	0.04	0.012	30.61	49.41	1.40	4.12	12	1.5	4	0.66	5
	0+620	7.41	17.86	32.75	0.07	0.012	26.59	38.10	1.23	5.02	12	1.5	4	0.66	5
	0+622	9.40	17.86	32.75	0.07	0.014	24.96	38.10	1.23	5.02	12	1.5	4	0.66	5
	0+643	15.50	16.73	32.54	0.07	0.017	20.20	7.02	1.17	4.87	12	1.5	4	0.66	5
	0+650	15.38	16.73	32.54	0.07	0.017	20.25	7.02	1.17	4.87	12	1.5	4	0.66	5
	0+652	17.60	10.98	32.70	0.04	0.035	28.68	86.32	2.05	4.15	12	1.5	4	0.66	5
	0+655	16.69	16.73	32.54	0.07	0.017	19.75	7.02	1.17	4.86	12	1.5	4	0.66	5
	0+660	16.36	10.98	32.70	0.04	0.034	29.20	86.32	2.05	4.15	12	1.5	4	0.66	5
	0+667	19.22	10.98	32.70	0.04	0.037	28.06	86.32	2.05	4.15	12	1.5	4	0.66	5
	0+754	34.02	16.02	33.27	0.17	0.083	36.31	64.90	1.99	4.77	6	2	4	0.66	5
	0+942	58.89	16.02	33.27	0.09	0.070	20.57	64.90	1.99	4.77	6	0.5	4	0.66	2.5
	0+960	58.87	17.68	32.74	0.09	0.041	14.24	38.08	1.25	4.99	6	0.5	4	0.66	2.5
	0+993	59.11	17.68	32.74	0.09	0.041	14.22	28.20	1.25	4.99	6	0.5	4	0.66	2.5
	1+152	82.23	44.68	38.76	0.24	0.153	30.22	37.94	3.01	9.24	6	0.5	4	0.66	2.5

Table C.1. Continued

1+238	86.63	44.68	38.76	0.24	0.154	30.19	213.47	3.01	9.24	6	0.5	4	0.66	2.5
1+535	98.32	30.23	38.17	0.16	0.311	39.91	310.22	4.85	6.81	6	0.5	4	0.66	2.5
1+536	98.32	30.23	38.17	0.16	0.292	38.22	310.22	4.85	6.81	6	0.5	4	0.66	2.5
1+730	91.69	26.18	49.57	4.36	0.386	46.52	420.06	3.87	6.19	9	3	2	1	1
1+739	91.09	26.18	49.57	4.36	0.384	46.57	420.06	3.87	6.19	9	3	2	1	1
1+958	62.97	38.91	47.19	2.60	0.383	53.24	812.23	6.95	8.24	9	3	2	1	2.5
1+979	59.82	38.91	47.19	2.59	0.371	53.59	812.23	6.95	8.24	9	3	2	1	2.5
2+148	38.73	9.20	35.47	0.07	0.164	47.13	270.59	5.03	3.94	6	1.5	4	0.66	5
2+153	38.45	9.20	35.47	0.07	0.164	47.18	270.59	5.03	3.94	6	1.5	4	0.66	5
2+155	38.36	9.20	35.47	0.07	0.163	47.20	270.59	5.03	3.94	6	1.5	4	0.66	5
2+164	37.69	33.04	38.39	0.27	0.169	47.94	307.54	4.63	7.26	6	1.5	4	0.66	5
2+175	36.56	33.04	38.79	0.18	0.174	49.09	321.21	5.03	7.26	12	2	4	0.66	5
2+176	36.49	6.65	34.78	0.03	0.149	46.54	256.07	4.63	3.65	12	2	4	0.66	5
2+186	34.71	6.65	34.78	0.03	0.144	46.91	256.07	4.63	3.65	12	2	4	0.66	5
2+186	34.39	6.65	34.78	0.03	0.143	46.98	256.07	4.63	3.65	12	2	4	0.66	5
2+196	30.23	14.96	32.72	0.08	0.064	34.66	4.36	1.58	4.63	12	2	4	0.66	5
2+196	29.17	14.96	32.72	0.08	0.062	35.18	4.36	1.58	4.63	12	2	4	0.66	5
Tekir Tunnel	55+328	11.77	58.69	38.18	0.16	0.056	48.82	545.62	2.33	11.85	24	1.5	3	0.66	5
	55+333	13.06	48.23	36.40	0.13	0.060	48.02	576.65	2.51	9.88	24	1.5	3	0.66	5
	55+398	29.96	58.69	38.18	0.32	0.102	41.83	545.62	2.33	11.85	12	1.5	3	0.66	5
	55+403	24.01	48.23	36.40	0.26	0.089	43.49	576.65	2.52	9.88	12	1.5	3	0.66	5
	55+724	145.42	41.21	46.70	2.06	0.464	39.17	913.90	4.06	8.63	12	3	2	1	2.5
	55+729	146.43	41.21	46.70	2.06	0.466	39.11	913.90	4.06	8.63	12	3	2	1	2.5
	55+794	137.45	41.21	46.70	2.06	0.447	39.61	913.90	4.06	8.63	12	3	2	1	2.5
	55+799	146.07	41.21	46.70	2.06	0.465	39.13	913.90	4.06	8.63	12	3	2	1	2.5
	55+859	121.33	41.21	46.70	2.06	0.413	40.59	913.90	4.06	8.63	12	3	2	1	2.5
	55+864	111.25	41.21	46.70	2.06	0.391	41.27	913.90	4.06	8.63	12	3	2	1	2.5

Table C.1. Continued

56+278	36.73	58.22	45.80	0.96	0.163	46.54	674.18	3.04	11.76	12	3	2	0.66	5
56+283	31.70	58.22	45.80	0.96	0.149	47.64	674.18	3.04	11.76	12	3	2	0.66	5
56+348	30.14	58.22	45.80	0.96	0.144	48.01	674.18	3.04	11.76	12	3	2	0.66	5
56+353	29.57	58.22	45.80	0.96	0.143	48.16	674.18	3.04	11.76	12	3	2	0.66	5
56+400	21.24	39.09	35.17	0.32	0.083	45.76	567.95	2.90	8.27	24	3	2	0.66	5
56+418	10.99	29.00	33.05	0.23	0.047	47.39	346.65	2.42	6.62	24	3	2	0.66	5
56+447	6.13	39.09	35.17	0.32	0.038	54.46	567.95	2.90	8.27	24	3	2	0.66	5
56+453	5.76	29.00	33.05	0.23	0.031	51.92	346.65	2.42	6.62	24	3	2	0.66	5
Zon. Erg. Road Left Tunnel 1														
2+234	23.40	85.00	66.27	2.12	0.537	60.32	3963.79	7.15	17.12	24	3	2	1	2.5
2+243	26.10	85.00	66.27	4.25	0.548	59.82	3963.79	7.15	17.12	12	3	2	1	2.5
2+260	58.90	85.00	66.27	4.25	0.684	55.54	3963.79	7.15	17.12	12	3	2	1	2.5
2+426	87.70	69.00	60.43	5.75	0.544	49.52	2008.81	5.55	13.87	6	1	2	1	1
2+449	86.95	69.00	60.43	5.75	0.542	49.58	2008.81	5.55	13.87	6	1	2	1	1
2+469	72.90	69.00	60.43	5.75	0.495	50.81	2008.81	5.55	13.87	6	1	2	1	1
2+547	21.20	77.50	58.00	1.29	0.338	59.52	2327.17	7.41	15.59	12	1.5	3	1	2.5
2+561	13.10	77.50	58.00	1.29	0.301	61.80	2327.17	7.41	15.59	12	1.5	3	1	2.5
Zon. Erg. Road Left Tunnel 2														
2+873	12.05	40.00	53.20	0.23	0.364	58.67	7256.21	10.77	8.42	18	3	2	0.7	10
2+893	18.64	40.00	53.20	0.23	0.386	56.81	7256.21	10.77	8.42	18	3	2	0.7	10
2+911	22.07	40.00	53.20	0.23	0.398	56.01	7256.21	10.77	8.42	18	3	2	0.7	10
2+927	26.00	21.63	47.71	0.12	0.127	44.19	5525.11	3.17	5.53	18	3	2	0.7	10
2+947	36.67	21.63	42.71	0.17	0.131	39.47	4047.85	3.17	5.53	18	4	2	0.7	10
2+963	35.92	21.63	45.71	0.38	0.142	40.93	4865.66	3.17	5.53	8	4	2	0.7	10
2+981	36.65	21.63	45.71	0.38	0.143	40.78	4865.66	3.17	5.53	8	4	2	0.7	10
3+003	36.95	21.63	42.71	0.38	0.132	39.41	4047.85	3.17	5.53	8	4	2	0.7	10
3+277	89.59	29.37	38.42	0.16	0.316	40.80	5555.35	5.74	6.68	9	1.5	4	0.66	5
3+301,	85.41	29.37	38.42	0.16	0.306	41.17	5555.35	5.74	6.68	9	1.5	4	0.66	5
3+328	77.09	29.37	38.42	0.16	0.222	33.92	5555.35	5.74	6.68	9	1.5	4	0.66	5

Table C.1. Continued

3+351	73.40	29.37	38.42	0.16	0.216	34.33	5555.35	5.74	6.68	9	1.5	4	0.66	5
3+378	71.02	29.37	38.42	0.16	0.212	34.54	5555.35	5.74	6.68	9	1.5	4	0.66	5
4+225	42.62	59.62	56.04	3.94	0.378	46.00	13861.52	6.50	12.03	12	3	1	0.66	2.5
4+242	32.17	59.62	56.04	3.94	0.353	47.72	13861.52	6.50	12.03	12	3	1	0.66	2.5
4+264	26.17	59.62	56.04	3.94	0.338	48.90	13861.52	6.50	12.03	12	3	1	0.66	2.5
4+298	13.94	59.62	56.04	3.94	0.309	52.04	13861.52	6.50	12.03	12	3	1	0.66	2.5
48+788	32.41	43.36	37.77	0.06	0.085	31.73	722.12	3.25	9.01	24	1.5	4	0.66	7.5
48+839	38.44	11.05	37.74	0.01	0.123	34.21	909.97	4.92	4.15	12	1	6	0.66	10
48+840	40.41	11.05	37.74	0.01	0.126	33.85	909.97	4.92	4.15	12	1	6	0.66	10
48+903	46.67	11.05	37.74	0.01	0.135	32.80	909.97	4.92	4.15	12	1	6	0.66	10
48+904	43.44	11.05	37.74	0.01	0.130	33.32	909.97	4.92	4.15	12	1	6	0.66	10
48+951	43.13	13.83	35.74	0.01	0.078	26.39	374.84	2.58	4.49	12	1	6	0.66	10
49+025	53.88	13.83	35.74	0.01	0.088	24.86	374.84	2.58	4.49	12	1	6	0.66	10
49+044	58.99	13.83	37.57	0.05	0.098	25.06	411.62	2.58	4.49	12	1.5	3	0.66	7.5
49+343	41.59	68.55	45.45	0.09	0.154	35.67	788.92	4.16	13.78	12	1	6	1	10
49+345	39.69	68.55	45.45	0.09	0.152	36.01	788.92	4.16	13.78	12	1	6	1	10
49+350	36.01	68.55	42.95	0.02	0.131	35.69	676.74	4.16	13.78	20	1	10	0.66	10
49+357	32.86	68.55	42.95	0.02	0.126	36.34	676.74	4.16	13.78	20	1	10	0.66	10
49+390	39.77	68.55	42.95	0.02	0.136	34.97	676.74	4.16	13.78	20	1	10	0.66	10
49+400	33.00	68.55	42.95	0.02	0.126	36.31	676.74	4.16	13.78	20	1	10	0.66	10
49+417	54.38	68.55	51.95	1.14	0.227	36.20	1200.25	4.16	13.78	6	1.5	3	1	5
49+970	117.36	45.67	51.62	0.91	0.258	27.98	1794.29	3.20	9.42	12	3	3	0.66	2.5
49+977	136.82	45.67	51.62	0.91	0.278	26.88	1794.29	3.20	9.42	12	3	3	0.66	2.5
50+024	122.60	45.67	36.62	0.03	0.294	34.93	726.62	3.20	9.42	15	1	6	0.66	10
50+777	90.40	30.25	45.30	0.50	0.336	44.44	2054.19	6.48	6.82	12	1	2	1	2.5
50+825	82.12	30.25	45.30	0.50	0.318	45.16	2054.19	6.48	6.82	12	1	2	1	2.5

Caglayan Tunnel

50+880	72.67	3.94	30.94	0.005	0.095	22.71	148.35	3.07	3.37	12	1	6	1	10
50+886	72.16	3.94	30.94	0.005	0.095	22.75	148.35	3.07	3.37	12	1	6	1	10
50+886	72.22	3.94	30.94	0.005	0.095	22.75	148.35	3.07	3.37	12	1	6	1	10
50+890	72.16	3.94	30.94	0.005	0.095	22.75	148.35	3.07	3.37	12	1	6	1	10
50+906	69.66	3.94	30.94	0.005	0.093	22.98	148.35	3.07	3.37	12	1	6	1	10
50+918	63.49	3.94	30.94	0.005	0.088	23.58	148.35	3.07	3.37	12	1	6	1	10
51+148	44.25	31.44	40.71	0.05	0.226	50.31	1440.66	5.70	7.01	12	1.5	8	1	10
51+166	49.62	31.44	40.71	0.05	0.2430	49.48	1440.66	5.70	7.01	12	1.5	8	1	10
51+195	32.93	31.44	40.71	0.02	0.188	52.38	1440.66	5.70	7.01	24	1.5	8	1	10
51+242	32.42	32.80	39.67	0.02	0.165	49.72	667.15	4.44	7.22	24	1.5	8	1	10
Puren Tunnel														
71+010	6.00	53.44	28.88	0.10	0.025	42.27	76.45	3.03	10.85	20	1.5	4	1	10
71+368	136.47	70.72	46.13	2.35	0.255	26.92	1595.54	2.912	14.22	3	1	2	1	5
71+921	356.54	42.27	33.37	0.70	0.283	15.28	685.40	2.55	8.82	6	1	2	1	5
71+925	360.25	42.27	33.37	0.70	0.285	15.22	685.40	2.55	8.82	6	1	2	1	5
71+968	378.84	42.27	33.37	0.70	0.294	14.97	685.40	2.55	8.82	6	1	2	1	5
71+983	381.35	42.27	33.37	0.70	0.295	14.93	685.40	2.55	8.82	6	1	2	1	5
71+998	387.72	42.27	33.37	0.70	0.297	14.85	685.40	2.55	8.82	6	1	2	1	5
71+999	387.72	42.27	33.37	0.70	0.297	14.85	685.40	2.55	8.82	6	1	2	1	5
72+270	466.72	42.27	33.37	0.70	0.331	13.94	685.40	2.55	8.82	6	1	2	1	5
72+985	384.21	72.84	49.92	2.42	0.831	29.79	3758.22	4.27	14.65	3	1	2	1	5
73+512	74.51	72.84	56.92	2.73	0.334	35.33	5937.93	4.27	14.65	4	1.5	2	1	5
73+513	74.51	72.84	56.92	2.73	0.334	35.33	5937.93	4.27	14.65	4	1.5	2	1	5
73+560	56.24	72.84	60.92	2.73	0.376	38.43	7636.35	4.27	14.65	4	1.5	2	1	5
73+572	53.82	72.84	60.92	2.73	0.373	38.71	7636.35	4.27	14.65	4	1.5	2	1	5
73+593	48.88	72.84	55.92	1.82	0.279	37.91	5566.27	4.27	14.65	6	1.5	2	1	5

CURRICULUM VITAE

PERSONAL INFORMATION

Surname, Name: Satıcı, Özgür
Nationality: Turkish (TC)
Date and Place of Birth: 07 October 1974, Ankara
Marital Status: Married, two children
Phone: +90 312 449 83 61
email: osatici@gmail.com

EDUCATION

Ph.D.: METU, Department of Geological Engineering, Graduation 2018
M.Sc.: HU, Department of Mining Engineering, Graduation 2007
M.Sc.: AU, Department of Business Administration, Graduation 2001
B.Sc.: HU, Department of Geological Engineering, Graduation 1997

WORK EXPERIENCE

2017- : Ankara University, Department of Business Administration,
Risk Management and Its Application graduate course,
Part Time Instructor
2015- : General Directorate of Highways (GDH), Internal Audit Unit,
Internal Auditor
2011-2015: GDH, Research and Development Department,
Geological Surveys Chief
2001-2011: GDH, Research and Development Department,
Geological Survey Engineer
1998-2001: GDH, 4th Division Directorate, Engineering Geology Engineer

FOREIGN LANGUAGES

Advanced English

PUBLICATIONS

THESIS

1. Satıcı, O., 2002, Kültürün Ülkemiz Kamu Çalışanlarının Performansına ve Kamu Örgütlerinin İşleyişine Etkileri, Master of Science Thesis, Ankara University
2. Satıcı, O., 2007, Kavak Merzifon Yolu Küçükbelvar Tüneli Stabilite Analizi, Master of Science Thesis, Hacettepe University

INTERNATIONAL JOURNALS

1. Satıcı, O., Unver, B., Assessment of Tunnel Portal Stability at Jointed Rock Mass: A Comparative Case Study, Computers and Geotechnics, 2015, v64, p.72–82

NATIONAL JOURNALS

1. Satıcı, O., Topal, T., 2015, Evaluation of Tunnel Excavation Methods in Accordance with Engineering Geology and Rock Mass Classification Systems, Journal of Geological Engineering, v39, p.45-57
2. Akış, E., Satıcı O., 2017, Underground Structures, Rock Structures and Rock Mechanics from Ancient Era to the Modern Age, Journal of Geological Engineering, v41, p.155-172

INTERNATIONAL SYMPOSIUM and CONGRESS

1. Satıcı, O., Gungor A.G., 2015, Effects Of Paleo-Rock Landslide and Heavy Rainfalls to Tunnel Excavation, ITA-WTC 2015, Promoting Tunneling in South East European Region, Dubrovnik, Croatia

NATIONAL SYMPOSIUM and CONGRESS

1. Satıcı, O., 2016, Tünel Yapım Çalışmalarında Risk Modellemesi, Ulusal Tünelcilik ve Yeraltı Yapıları Kongresi, KGM, Ankara, p.797